PhD Program in Neuroscience

Instituto de Neurociencias (CSIC-UMH)

# Microenvironmental Snail1 drives melanoma progression

---

Doctoral Thesis presented by

**Marta Arumí Planas**

Thesis Director

Dr. Berta López Sánchez-Laorden

---

Universidad Miguel Hernández de Elche

- 2025 -

The doctoral thesis, entitled “Microenvironmental Snail1 drives melanoma progression” is presented **under the modality of a compendium of publications**, and includes the following work:

- **Arumi-Planas, M.,** Rodriguez-Baena, F. J., Cabello-Torres, F., Gracia, F., Lopez-Blau, C., Nieto, M. A., & Sanchez-Laorden, B. Microenvironmental Snail1-induced immunosuppression promotes melanoma growth. Oncogene 42, 2659–2672 (2023). Doi: 10.1038/s41388-023-02793-5

Sant Joan d'Alacant, 7th November 2025

Dr. Berta López Sánchez-Laorden, director of the doctoral thesis entitled **"Microenvironmental Snail1 drives melanoma progression".**

**REPORTS:**

That Ms. Marta Arumí Planas has carried out, under my supervision, the work entitled "Microenvironmental Snail1 drives melanoma progression" in accordance with the terms and conditions defined in her Research Plan and in accordance with the Code of Good Practice of the University Miguel Hernández of Elche, satisfactory fulfilling the objectives foreseen for its public defence as a doctoral thesis.

I sign for appropriate purposes, at Sant Joan d'Alacant, 7th November 2025.

Thesis director

Dr. Berta López Sánchez-Laorden

Sant Joan d'Alacant, 7th November 2025

Ms. María Cruz Morenilla Palao, Coordinator of the Neuroscience PhD Program at the Institute of Neurosciences in Alicante, a joint centre of Miguel Hernández University (UMH) and the Spanish National Research Council (CSIC).

**REPORTS:**

That Ms. Marta Arumí Planas has carried out under the supervision of our PhD Program the work entitled "Microenvironmental Snail1 drives melanoma progression" in accordance with the terms and conditions defined in her Research Plan and in accordance with the Code of Good Practice of the University Miguel Hernández of Elche, satisfactory fulfilling the objectives foreseen for its public defence as a doctoral thesis.

Which I sign for the appropiate purposes, in Sant Joan d'Alacant, 7th November 2025.

Dr. María Cruz Morenilla Palao

Coordinator of the PhD Program in Neuroscience




Funding/Grants/Scholarship:

The realization of this Doctoral Thesis has been carried out thanks to a “Formación de Personal Investigador (FPI)” pre-doctoral scholarship financed by the AEI, Ministerio de Economía, Industria y Competitividad, with reference BES-2017-080854 (2018-2022), and a contract of a higher degree in technical and professional activities funded by the National R&D Plan project with reference: PID2019-106852-RB100 (2022-2023).

The research has been funded by the following research projects: SAF2016-75702R, PID2019-106852-RB100 (MCIN-AEI), the Prometeo Program for Groups of Excellence (CIPROM/2021/045) from Generalitat Valenciana, Melanoma Research Alliance and Fero Foundation.

# Table of contents

**TABLE OF CONTENTS** ..... **1**

**ABBREVIATIONS LIST** ..... **5**

**ABSTRACT** ..... **7**

**RESUMEN** ..... **11**

**INTRODUCTION** ..... **15**

1. Melanoma ..... 17
   - 1.1. Biological and genetic features of melanoma progression ..... 17
   - 1.2. Current melanoma therapies ..... 20
2. The tumour microenvironment (TME) in melanoma ..... 21
3. EMT-TFs in cancer biology ..... 23
   - 3.1. Snail1 in cancer ..... 25
4. Cancer-associated fibroblasts (CAFs) ..... 26
   - 4.1. CAFs biology and plasticity ..... 26
   - 4.2. Tumorigenic CAFs function ..... 29
   - 4.3. Targeting CAFs in anti-cancer therapies ..... 33
5. Melanoma preclinical mouse models ..... 34
   - 5.1. Genetic models ..... 34
   - 5.2. Xenograft models ..... 35
   - 5.3. Syngeneic models ..... 36

**OBJECTIVES** ..... **39**

**MATERIAL AND METHODS** ..... **43**

1. Experimental mice ..... 45
   - 1.1. Mouse handling ..... 45
   - 1.2. Mouse transgenic lines ..... 45
   - 1.3. Genotyping ..... 47
   - 1.4. Tamoxifen administration ..... 47
2. Cell culture ..... 48
3. Treatments of cultured cells ..... 48

3.1. Transfection of plasmids and interfering RNAs ..... 48
3.2. TGFβ administration ..... 49
3.3. CYD19 drug administration ..... 49
4. Experimental melanoma mouse models ..... 49
4.1. Inducible melanoma reporter model ..... 49
4.2. Melanoma subcutaneous allografts ..... 50
4.3. Anti-PD-1 therapy experiment ..... 50
4.4. Experimental lung metastasis assay ..... 51
5. Histology ..... 51
6. Staining and imaging in tissues and cells ..... 52
6.1. Hematoxylin and Eosin staining ..... 52
6.2. Immunofluorescence in tissue sections ..... 52
6.3. Immunofluorescence in cultured cells ..... 53
7. Sample preparation and immunolabelling for FACS analysis ..... 55
7.1. Tissue processing for FACS analysis ..... 55
7.2. Immunolabelling techniques and cell sorting ..... 55
8. Molecular methods ..... 56
8.1. Total RNA extraction, cDNA synthesis and RT-qPCR analysis ..... 56
8.2. Chromatin immunoprecipitation (ChIP) assay ..... 57
9. Morpholino oligomer and *in vivo* treatment ..... 57
10. Quantification of images ..... 59
10.1. Quantification of KI-67 and Cleaved CASPASE-3 ..... 59
10.2. Quantification of metastatic burden ..... 59
11. *In silico* analyses ..... 59
11.1. RNA-seq ..... 59
11.2. Analysis of publicly available transcriptomic datasets ..... 60
11.3. Statistical analysis ..... 61

**RESULTS ..... 63**

1. Snail1 expression in murine melanomas ..... 65
2. Snail1$^{ME}$ contribution to melanoma growth and progression ..... 68
2.1. Generation and validation of Snail1 conditional knockout mice ..... 68
2.2. Snail1 reactivation in the tumour microenvironment promotes melanoma growth ..... 69

2.3. Snail1 is reactivated in melanoma-associated fibroblasts within the TME……72

2.4. Snail1 reactivation in CAFs promotes melanoma growth..... 75

3. Mechanisms underlying the regulatory function of Snail1$^{ME}$ in melanoma growth... ..... 78

3.1. Snail1 expression is associated to immunosuppressive gene signatures in melanoma-associated fibroblasts..... 78

3.2. Snail1 expression is associated to immunosuppressive gene signatures in CAFs from additional mouse and patient´s tumours..... 83

3.3. Snail1 in melanoma-associated fibroblasts regulates anti-tumour immune responses..... 84

3.4. Snail1 correlates with poor clinical outcomes in melanoma patients..... 86

3.5. Snail1$^{ME}$ targeting phenocopies the effects of anti-PD-1 therapy in melanoma..... 87

4. Snail1 regulates Fap expression in fibroblasts..... 89

5. Snail1 as a therapeutic target in melanoma..... 94

5.1. Snail1 is reactivated in the metastatic niche microenvironment..... 94

5.2. Snail1$^{ME}$ targeting reduces metastatic burden and improves mice survival..... 96

5.3. Systemic targeting of Snail1 *in vivo* as a potential therapeutic strategy for melanoma..... 102

**DISCUSSION.....105**

**CONCLUSIONS.....115**

**CONCLUSIONES .....119**

**BIBLIOGRAPHY.....123**

**APPENDIX.....147**

**ACKNOWLEDGMENTS .....173**

# Abbreviations list

| | |
|---|---|
| **4-HT** | 4-Hydroxytamoxifen |
| **AKT** | Protein kinase B |
| **APC** | Allophycocyanin |
| **apCAF** | Antigen-presenting CAF |
| **ARG1** | Arginase 1 |
| **BLI** | Bioluminescence imaging |
| **BRAF** | v-Raf murine sarcoma viral oncogene homolog B |
| **BS** | Binding site |
| **BSA** | Bovine serum albumin |
| **CAFs** | Cancer-associated fibroblasts |
| **CAR-T** | Chimeric antigen receptor T-cell |
| **CBP** | CREB-binding protein |
| **CCL2** | C-C Motif chemokine ligand 2 |
| **CCL5** | C-C Motif chemokine ligand 5 |
| **CDK** | Cyclin-dependent kinase |
| **CDKN2A** | Cyclin-dependent kinase inhibitor 2A |
| **ChIP** | Chromatin immunoprecipitation |
| **Control-MO** | Control-morpholino |
| **CTLA-4** | Cytotoxic T-lymphocyte-associated protein 4 |
| **CXCL12** | C-X-C motif chemokine ligand 12 |
| **CXCR4** | C-X-C chemokine receptor type 4 |
| **DAPI** | 4’,6-diamidino-2-phenylindole |
| **DC** | Dendritic cell |
| **DEGs** | Differentially expressed genes |
| **dH2O** | Distilled water |
| **DMEM** | Dulbecco’s modified eagle medium |
| **DMSO** | Dimethyl sulfoxide |
| **dpi** | Days post injection |
| **ECM** | Extracellular matrix |
| **EDTA** | Etheylenediaminetetraacetic acid |
| **EMT** | Epithelial to mesenchymal transition |
| **ERK** | Extracellular signal-regulated kinase |
| **F12** | Ham's F-12 nutrient mixture |
| **FACS** | Fluorescence-activated cell sorting |
| **FAP** | Fibroblast activation protein |
| **FBS** | Fetal bovine serum |
| **FGF2** | Fibroblast growth factor 2 |
| **FITC** | Fluorescein isothiocyanate |
| **FOXP3** | Forkhead box P3 |
| **FSP-1** | Fibroblast-specific protein-1 |
| **GEMMs** | Genetic engineered mouse models |
| **GFP** | Green fluorescent protein |
| **GO** | Gene ontology |
| **GSEA** | Gene set enrichment analysis |
| **H&E** | Hematoxylin and Eosin |
| **HEPES** | 4-(2-hydroxyethyl)-1-piperazineethanesulfonic acid |
| **HGF** | Hepatocyte growth factor |
| **iCAF** | Inflammatory CAF |
| **IF** | Immunofluorescence |
| **IL-1** | Interleukin-1 |
| **IL-2** | Interleukin-2 |
| **IL-6** | Interleukin-6 |
| **IL-8** | Interleukin-8 |
| **IVIS** | *In vivo* imaging system |
| **KO** | Knockout |

| | |
|---|---|
| **LAG-3** | Lymphocyte-activation gene 3 |
| **Luc** | Luciferase |
| **MAPK** | Mitogen-activated protein kinase |
| **MCP-1** | Monocyte chemoattractant protein-1 |
| **M-CSF1** | Colony-stimulating factor 1 |
| **MDSC** | Myeloid-derived suppressor cells |
| **MMPs** | Matrix metalloproteinases |
| **MO** | Morpholino oligomer |
| **mRNA** | Messenger RNA |
| **myCAF** | Myofibroblastic CAF |
| **NC** | Negative control region |
| **NF1** | Neurofibromin 1 |
| **NGS** | Normal goat serum |
| **NK** | Natural killer |
| **NRAS** | v-Ras neuroblastoma viral oncogene homolog |
| **O/N** | Overnight |
| **OCT** | Optimal cutting temperature medium |
| **OS** | Overall survival |
| **p/s/cm2/sr** | Photons per second per square centimeter per steradian |
| **PBS** | Phosphate-buffered saline |
| **PD-1** | Programmed death-1 |
| **PDAC** | Pancreatic ductal adenocarcinoma |
| **PDGFRα** | Platelet-derived growth factor receptor alpha |
| **PDGFRβ** | Platelet-derived growth factor receptor beta |
| **PD-L1** | Programmed death-ligand 1 |
| **PDPN** | Podoplanin |
| **PDX** | Patient-derived xenograft |
| **PFA** | Paraformaldehyde |
| **PGE2** | Prostaglandin E2 |
| **PI3K** | Phosphoinositide 3-kinase |
| **PTEN** | Phosphatase and tensin homolog |
| **qPCR** | quantitative PCR |
| **RGP** | Radial growth phase |
| **RhoA** | Ras Homolog Family Member A |
| **RNA** | Ribonucleic acid |
| **RNA-seq** | RNA sequencing |
| **RT** | Room temperature |
| **RT-PCR** | Reverse-transcription polymerase chain reaction |
| **scRNA-seq** | Single-cell RNA sequencing |
| **SEM** | Standard error of estimate of mean value |
| **SiRNA** | Short interfering RNA |
| **Snail1$^{ME}$** | Microenvironmental Snail1 |
| **Snail1-MO** | Snail1-morpholino |
| **TAM** | Tamoxifen |
| **TAMs** | Tumour-associated macrophages |
| **TCGA** | The Cancer Genome Atlas |
| **TF** | Transcription factor |
| **TGFβ** | Transforming growth factor-beta |
| **Thy-1** | Thymocyte differentiation antigen 1 |
| **TILs** | Tumour infiltrating lymphocytes |
| **TME** | Tumour microenvironment |
| **TNFα** | Tumour necrosis factor alpha |
| **T-regs** | Regulatory T cells |
| **UBC** | Ubiquitin C |
| **UV** | Ultraviolet |
| **VEGF** | Vascular endothelial growth factor |
| **VGP** | Vertical growth phase |
| **VM** | *Vivo*-morpholino |
| **WT** | Wild type |
| **YFP** | Yellow fluorescent protein |
| **α-SMA** | α-Smooth muscle actin |

# ABSTRACT

# Abstract

Melanoma is an aggressive form of skin cancer, primarily due to its high metastatic abilities and resistance to existing therapeutic strategies. The behaviour and progression of melanoma are significantly influenced by its highly heterogeneous tumour microenvironment (TME). This TME not only provides a scaffold but also acts as an active participant in cancer progression. Snail1 is a transcription factor responsible for inducing the epithelial to mesenchymal transition, a vital process during embryonic development that is reactivated in pathological conditions, including cancer and fibrosis. Snail1 plays a critical role in carcinoma progression, promoting invasion and metastasis when expressed in epithelial cells but also in cells from the stroma. Nonetheless, the specific contribution of Snail1 to non-epithelial malignancies, such as melanoma, remained to be clarified.

In this study, we have uncovered a novel regulatory function of Snail1 within the melanoma microenvironment. We have shown that Snail1 expression is reactivated in the melanoma stroma, predominantly in fibroblasts. We have used BRAF-driven melanomas generated in mice engineered to conditionally deplete Snail1 in the stroma and, systemic Snail1 targeting to show that stromal Snail1 blockade significantly attenuates melanoma growth, reduces lung metastatic burden, and extends mice survival. Transcriptomic analysis of melanoma-associated fibroblasts, analyses of tumour samples and fibroblasts in culture, indicate that stromal Snail1 regulates FAP expression and promotes melanoma progression by fostering an immunosuppressive environment, thus attenuating anti-tumour immune responses. These findings unveil a novel role of stromal Snail1 in melanoma biology and support its potential as a therapeutic target, which could enhance the efficacy of existing treatments. This research also emphasizes the need to further investigate the components of the TME to improve melanoma treatments.

# RESUMEN

# Resumen

El melanoma es una forma muy agresiva de cáncer de piel, principalmente debido a sus altas capacidades metastásicas y su resistencia a las estrategias terapéuticas existentes. El comportamiento y la progresión del melanoma están significativamente influenciados por su microambiente tumoral que es muy heterogéneo. El microambiente tumoral no solo proporciona un soporte a los tumores, sino que también actúa como un regulador en la progresión del cáncer. Snail1 es un factor de transcripción responsable de inducir la transición epitelio-mesenquimal, un proceso vital durante el desarrollo embrionario que se reactiva en condiciones patológicas, incluyendo cáncer y fibrosis. Snail1 juega un papel fundamental en la progresión de los carcinomas, promoviendo la invasión y metástasis no solo cuando se expresa en células epiteliales, sino también en las células del estroma. No obstante, la contribución específica de Snail1 a las neoplasias no epiteliales, como el melanoma, no está bien caracterizada.

En este estudio, hemos descubierto una nueva función reguladora de Snail1 dentro del microambiente del melanoma. Hemos demostrado que la expresión de Snail1 se reactiva en el estroma del melanoma, predominantemente en los fibroblastos. Para ello, hemos generado modelos de melanoma en ratones que permiten eliminar condicionalmente la expresión de Snail1 en el estroma. Además, hemos utilizado estrategias de inhibición sistémica de Snail1 para demostrar que el bloqueo de Snail1 en el estroma atenúa el crecimiento del melanoma, reduce la carga metastásica pulmonar y extiende la supervivencia de los ratones. Mecanísticamente, mostramos que la expresión de Snail1 en el estroma regula la expresión de FAP y promueve la progresión del melanoma al fomentar un entorno inmunosupresor, atenuando así las respuestas inmunitarias antitumorales. Estos hallazgos revelan una nueva función de Snail1 en el microambiente tumoral y en la biología del melanoma y respaldan su potencial como objetivo terapéutico, lo cual podría mejorar la eficacia de los tratamientos existentes. Además, este trabajo respalda la necesidad de profundizar en el estudio de los componentes del microambiente tumoral para mejorar las estrategias terapéuticas contra el melanoma.

# INTRODUCTION

# 1. Melanoma

Over the last two decades, while the overall incidence of cancer has declined, the rate of melanoma diagnosis has risen 3% annually (Siegel et al., 2023). This rising trend is particularly pronounced in Europe, North America, and Oceania, where fair-skinned populations are more susceptible to ultraviolet (UV) radiation exposure, a major risk factor for melanoma (Carr et al., 2020; Sung et al., 2021). Additional contributing factors to this aggressive skin cancer include family history (Ford et al., 1995), the presence of numerous melanocytic nevi (Gandini et al., 2005), a history of childhood sunburns (Rastrelli et al., 2014), immunosuppressive conditions or treatments (Rizvi et al., 2017), and specific skin, hair and eye colour phenotypes (Rastrelli et al., 2014).

Melanoma is an aggressive form of skin cancer that originates from melanocytes, the pigment-producing cells in the skin that develop from the neural crest during embryonic development (Kanitakis, 2020). This cancer is characterised by its high metastatic potential and its resistance to conventional therapies (Rossi et al., 2019). Early diagnosis is crucial, as melanoma can be successfully removed through surgery if detected early. However, once the cancer spreads to other organs, treatment options become significantly more limited (Davis et al., 2019). Specifically, cutaneous malignant melanoma is the deadliest form of skin cancer, responsible for nearly 90% of skin cancer-related deaths, even though it represents less than 3% of all skin cancer cases (Garbe et al., 2022).

## 1.1. Biological and genetic features of melanoma progression

Melanoma arises from the malignant transformation of melanocytes, which are found in different anatomical locations, with cutaneous melanoma being the most prevalent form. The malignant transformation of melanocytes into metastatic melanoma results from a complex interplay of external and internal triggers, tumour-specific factors, and immune-related mechanisms (Schadendorf et al., 2018).

Similar to other types of cancer, the progression of melanocytic lesions to malignant melanoma involves a series of mutations and alterations (Shain & Bastian, 2016). In 1984, Clark and colleagues (Clark et al., 1984) presented a simplified five-stage model for melanoma progression (**Figure 1**). The acquisition of nevi, whether congenital or acquired, often results from somatic mutations in the v-Ras neuroblastoma viral oncogene homolog (NRAS) (Bauer et al., 2007) or v-Raf murine sarcoma viral oncogene

homolog B (BRAF) (Pollock et al., 2003) genes, resulting in abnormal activation of the mitogen-activated protein kinase (MAPK) signalling pathway (Omholt et al., 2003). Nevi may progress to melanoma through genetic and epigenetic alterations, including additional mutations in tumour suppressor genes such as CDKN2A (Melnikova et al., 2004) or the phosphatase and tensin homolog (PTEN) (Dankort et al., 2009). The radial growth phase (RGP) involves horizontal melanoma cell proliferation at the epidermal level (Miller & Mihm, 2006) . The vertical growth phase (VGP) is characterized by vertical proliferation into the dermis, involving significant molecular changes (Haqq et al., 2005), which alter the microenvironment and facilitate immune evasion (Itakura et al., 2011). During the metastatic phase, melanoma cells detach from the primary site and spread to other organs, often initially colonizing sentinel lymph nodes (Thompson et al., 1995). This process is facilitated by the loss of cell adhesion molecules, such as E-cadherin (Gottardi et al., 2001; Haass et al., 2005).

Although the Clark model provides an initial framework for understanding melanoma progression, only 20-30% of melanomas arise from pre-existing nevi, and not all stages are necessarily involved in melanoma development (J. K. Rivers, 2004). Thus, a more comprehensive classification system that integrates pathological and genetic criteria is now used for the diagnosis and treatment of melanoma patients.

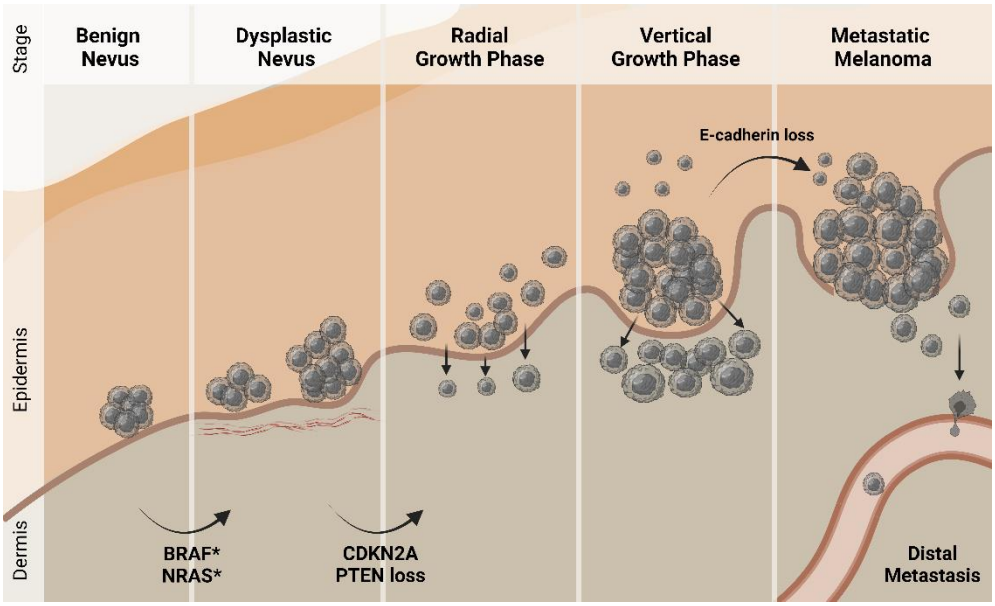


**Figure 1| Stages of melanoma progression.** Different stages from benign nevus to metastatic melanoma according to the Clark model. The most common and characteristic molecular lesions are shown at each stage. Created with BioRender.com.

Extensive studies have explored the genetic mutations of melanoma, which has the highest mutation rate among cancers (Hayward et al., 2017; Lawrence et al., 2013). The MAPK pathway is the most commonly activated pathway in melanoma, and its hyperactivation occurs in 90% of cases (Fecher et al., 2008). In 2015, The Cancer Genome Atlas (TCGA) network conducted a comprehensive analysis of cutaneous melanoma, classifying it based on the prevalence of commonly mutated genes (**Figure 2**). The most common subtype, found in 50-60% of cases, is characterized by BRAF mutations, with the V600E (valine-to-glutamic acid mutation at residue 600; $BRAF^{V600E}$) mutation being the most prevalent. The second major subtype, constituting approximately 25% of cases, is defined by RAS mutations, primarily involving NRAS mutations at codon Q61 (glutamine-to-arginine; $NRAS^{Q61R}$) (Gutiérrez-Castañeda et al., 2020). Interestingly, NRAS and BRAF mutations are mutually exclusive, and co-mutations rarely occur (Schadendorf et al., 2018; Sensi et al., 2006). A third subtype, observed in 15% of the cases, is associated with mutations in the Neurofibromin 1 (NF1) gene (Cirenajwis et al., 2017). The remaining subtype, referred to as triple Wild-Type, lacks these genetic alterations (TCGA, 2015). Despite these genomic classifications, there is limited correlation between these genetic subtypes and clinical outcomes in melanoma (Gutiérrez-Castañeda et al., 2020; TCGA, 2015).

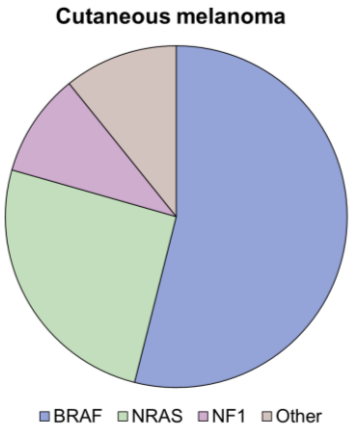


**Figure 2| Distribution of activating mutations in cutaneous melanoma.** Adapted from Schadendorf et al., 2018.

The genetic features of melanoma, particularly the mutations leading the hyperactivation of the MAPK pathway, play a crucial role in the development of the disease and represent key targets for therapeutic interventions (Sosman et al., 2012). Additional genetic events and transcriptional plasticity also contribute to melanoma progression, highlighting the complexity of the disease and the need for further

investigation into potential therapeutic strategies (Arozarena & Wellbrock, 2019; Karras et al., 2022).

## 1.2. Current melanoma therapies

Traditional treatments for melanoma, such as dacarbazine-based chemotherapy (Eggermont & Kirkwood, 2004) and IL-2 immunotherapy (Atkins et al., 1999), have demonstrated limited effectiveness, resulting in a median overall survival of only 9 months for patients (Jenkins & Fisher, 2021). However, the identification of specific genetic mutations in melanoma, coupled with a deeper understanding of its biology, has enabled the development of more effective therapies, including targeted therapies and immunotherapies (Boutros et al., 2024). Notably, immunotherapies exploit the melanoma microenvironment, which plays a crucial role in its progression and treatment response (Postovit et al., 2006). Despite the significant improvements in melanoma treatment offered by these new therapeutic strategies, not all patients respond to these treatments, and many who initially benefit eventually develop resistance after a relatively short period of disease control (Davis et al., 2019; J. Zhang et al., 2024).

Targeted therapies specifically address mutations in melanoma, particularly through BRAF inhibitors such as vemurafenib and dabrafenib, which have been shown to improve survival rates (Chapman et al., 2011; Menzies et al., 2012). Although initially successful, their long-term effectiveness is limited due to acquired resistance (Kozar et al., 2019). To address this challenge, MEK inhibitors such as trametinib are combined with BRAF inhibitors (Eroglu & Ribas, 2016). Nonetheless, resistance to this combined therapy also develops within months, highlighting the need for ongoing research to overcome resistance mechanisms (Brighton et al., 2018; Xue et al., 2018).

Immunotherapy aims to enhance the immune system anti-tumour response, mainly by activating its cytotoxic activity. The development of immune checkpoint inhibitors, such as relatlimab targeting lymphocyte-activation gene 3 (LAG-3) (Su et al., 2023), ipilimumab targeting cytotoxic T-lymphocyte antigen 4 (CTLA) (Wolchok et al., 2013), and nivolumab and pembrolizumab targeting programmed cell death-1 (PD-1) receptor, as well as atezolizumab targeting its ligand PD-L1 (Hamid et al., 2019; J. Zhang et al., 2024), represents a significant breakthrough in melanoma treatment. These therapies have demonstrated significant efficacy in enhancing anti-tumour immunity (Leonardi et al., 2020). Despite these advancements, a significant number of patients show minimal or no initial response. Even when combining CTLA-4 and PD-1 inhibitors, many patients

either fail to respond or eventually develop treatment resistance (Hodi et al., 2018). This variability in patient responses to immunotherapies underscores the incomplete understanding of the mechanisms driving treatment outcomes (Lim et al., 2023). Moreover, mutations and alterations within the tumour microenvironment may contribute to the lack of response, highlighting the need to elucidate these mechanisms for more effective therapies. Consequently, current research efforts are focused on addressing these limitations by developing second-generation immunotherapies, combinatorial treatments and identifying predictive biomarkers (Jenkins et al., 2018).

## 2. The tumour microenvironment (TME) in melanoma

Tumours are not isolated entities, but rather exist in the context of a host tissue containing a heterogeneous population of local and recruited cells, collectively referred to as tumour microenvironment (TME) or tumour stroma. In addition to cancer cells, the TME comprises a variety of cells including endothelial cells, pericytes, cancer-associated fibroblasts (CAFs) and immune cells. Additionally, the TME includes extracellular components such as the extracellular matrix (ECM) and an array of secreted-signalling molecules, like cytokines, chemokines, growth factors and hormones (**Figure 3**) (Junttila & De Sauvage, 2013; Whiteside, 2008).

The interaction among these TME components constitutes a tightly regulated network that plays a significant role in determining the tumour fate in a context-dependent manner. For instance, this intricate interplay between cancer cells and the TME can promote tumour growth, survival, immune evasion, metabolic reprogramming, and metastases (Davidson et al., 2020; Visser & Joyce, 2023). The cells within the TME and their secreted molecules play a critical role in cancer pathogenesis, which make them attractive targets for therapeutic strategies. Targeting the TME is particularly promising in overcoming treatment resistance and immunosuppression, both of which are critical factors affecting clinical outcomes in cancer patients (Baghban et al., 2020).

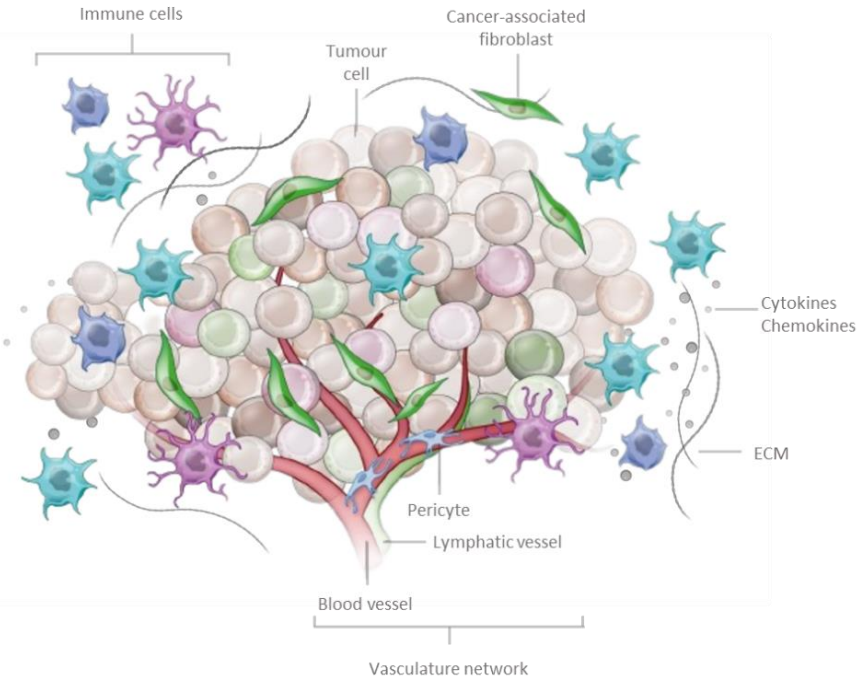


**Figure 3| Components of the TME**. The TME consists of both cellular and extracellular components. The cellular components include immune cells, cancer-associated fibroblasts (CAFs), endothelial cells and pericytes. The extracellular components comprise the ECM and soluble factors, such as cytokines and chemokines. Adapted from Junttila & De Sauvage, 2013.

Melanoma, a complex cancer significantly influenced by its microenvironment, demonstrates how these stromal components play crucial roles in both the progression and resistance to treatment. While melanoma cells express antigens that can be recognized by T-cells (Boon et al., 2006), they also employ several mechanisms to evade immunosurveillance. For instance, they express ligands such as PD-L1 to modulate T-cell function (Hino et al., 2010). Moreover, melanoma cells recruit immunosuppressive cells like myeloid-derived suppressor cells (MDSCs), macrophages, and regulatory T cells (T-regs), which inhibit T-cell activation and proliferation (Filipazzi et al., 2007; Miracco et al., 2007). Notably, PD-L1 has been used as a prognostic marker for melanoma progression (Hino et al., 2010). The efficacy of immunotherapies for melanoma largely depends on the presence of tumour infiltrating lymphocytes (TILs) and melanoma antigens. However, the inhibitory effects of immunomodulatory ligands and immunosuppressive cell populations can compromise the effectiveness of such therapies (Waldman et al., 2020). Therefore, identifying additional targets within the melanoma microenvironment beyond TILs density is essential to enhance the effectiveness and safety of melanoma treatments.

In addition to adaptive immune cells, innate immune cells significantly regulate the melanoma microenvironment. For example, tumour-associated macrophages (TAMs) are recruited through MCP-1 and subsequently produce IL-8 and VEGF, which stimulate vessel growth and thus support tumour expansion and invasion (Gazzaniga et al., 2007; Varney et al., 2005). Furthermore, TAMs secrete TNFα that contributes to melanoma growth and promotes resistance to targeted therapies (Smith et al., 2014).

Interestingly, it has been recently shown that GABAergic signalling between resident keratinocytes and melanocytes also promotes melanoma initiation, providing a novel mechanism by which the TME regulates melanoma biology (Tagore et al., 2023).

Furthermore, dermal fibroblasts can also interact with melanoma cells and modulate their behaviour throughout the progression of the disease (Flach et al., 2011). In the early stages, these fibroblasts can inhibit tumour growth by releasing anti-tumour factors. However, in later stages, they may acquire pro-tumour characteristics, supporting the proliferation of metastatic cells. The mechanisms underlying this switch are not yet fully understood (Tiago et al., 2014; Zhou et al., 2015). In addition to promoting melanoma metastasis by secreting different matrix metalloproteinases (MMPs) enzymes and other matrix proteins that lead to ECM remodelling (Kääriäinen et al., 2006; Wandel et al., 2000), fibroblasts also play a critical role in the development of resistance to targeted therapy in melanoma, emphasizing their importance in this context (Straussman et al., 2012; Tiago et al., 2014).

Consequently, elucidating the interactions between fibroblasts and other stromal cells, including immune cells, within the melanoma microenvironment may reveal novel targets for improving treatment outcomes and overcoming resistance to therapy. Understanding these interactions can provide insights into new therapeutic strategies aimed at targeting the TME to enhance the efficacy of melanoma treatments.

## 3. EMT-TFs in cancer biology

Epithelial to mesenchymal transition (EMT) is a fundamental biological process in which epithelial cells undergo significant phenotypic changes, losing their polarity and adhesion while acquiring mesenchymal features, including increased mobility and invasiveness (Nieto, 2013; Nieto et al., 2016). This transformation is crucial during embryonic development, facilitating cell migration and organ formation (Dongre &

Weinberg, 2019; Youssef & Nieto, 2024). However, EMT can be aberrantly activated in pathological conditions such as cancer and organ fibrosis (Grande et al., 2015; Thiery et al., 2009; Youssef & Nieto, 2024).

The regulation of EMT is controlled by a complex network of transcription factors (TFs), known as EMT-TFs. These key inducers include members of the Snail, Zeb, Twist, and Prrx families (Nieto et al., 2016). By binding to specific DNA sequences, EMT-TFs downregulate epithelial genes and activate mesenchymal ones, allowing epithelial cells to migrate and disseminate (Nieto, 2017; Nieto et al., 2016). EMT-TFs respond to different extracellular signals, such as growth factors, cytokines, hypoxic conditions, and inflammation. These stimuli influence intracellular signaling pathways that regulate the transcription of different EMT-TFs. Thus, understanding the molecular mechanisms underlying EMT regulation could offer new therapeutic strategies for treating multiple diseases (Dongre & Weinberg, 2019; Nieto & Cano, 2012; Peinado et al., 2007).

In cancer, the reactivation of EMT grants tumour cells invasive and migratory capabilities (Hanahan, 2022; Lu & Kang, 2019). This process enables cancer cells to detach from the primary tumour, invade surrounding tissues, and metastasize to distant organs (Brabletz et al., 2018). EMT also leads to the development of stem-cell like traits, such as the attenuation of the cell cycle and the ability to self-renew, contributing to therapy resistance and tumour progression (Nieto et al., 2016; Vega et al., 2004). The aberrant reactivation of different EMT-TFs in cancer has been frequently correlated with a worse prognosis and an elevated risk of metastases (Thiery et al., 2009) and different studies have shown their crucial role in epithelial-derived carcinomas, particularly when expressed in tumour cells (Dongre et al., 2017; Dongre & Weinberg, 2019; Nieto et al., 2016), but also in non-epithelial stromal cells (Blanco-Gomez et al., 2020; Cortés et al., 2017).

Interestingly, beyond its role in carcinomas, EMT-related processes and the expression of EMT-TFs extend to non-epithelial cancers such as glioblastoma, myeloma, leukaemia, and melanoma (Dongre & Weinberg, 2019). In these diseases, a mesenchymal-like phenotypic switch is also linked to metastatic abilities, survival and treatment resistance. For instance, melanoma exploits developmental pathways similar to neural crest cell fate specification to achieve more aggressive and resistant states, involving the reprogramming of different EMT-TFs, including Zeb1/2, Twist, and Snail2 (Caramel et al., 2013; Pedri et al., 2022).

## 3.1. Snail1 in cancer

Snail1, a zinc-finger transcription factor, is a master regulator of the EMT (Nieto et al. 1994, Nieto et al 1992). Besides its importance in embryonic development, research has demonstrated the importance of this transcription factor in cancer (Batlle et al., 2000; Brenot et al., 2018; Kudo-Saito et al., 2009) and organ fibrosis (Grande et al., 2015). The pathological reactivation of Snail1 in cancer strongly correlates with increased malignancy and worse prognosis, as it alters cellular adhesion and motility (Barrallo-Gimeno & Nieto, 2005). As a potent repressor, Snail1 downregulates E-cadherin expression, thus disrupting cell-cell adhesion and allowing cancer cells to detach from the primary tumour and invade into surrounding tissues (Batlle et al., 2000; Cano et al., 2000). Additionally, Snail1 has been associated with chemotherapy resistance by modulating survival pathways and interfering with cell cycle to prevent apoptosis. Specifically, Snail1 targets crucial survival proteins such as p53 and caspases, and interferes with signalling pathways like ERK and PI3K (Barrallo-Gimeno & Nieto, 2005; Peinado et al., 2007), contributing to cancer cell survival and malignancy. It also supresses essential cell cycle regulators, including cyclin-dependent kinase (CDK) and cyclins, leading to cell cycle arrest (Vega et al., 2004). Consequently, this arrest enables a shift in cancer cell activity from proliferation to invasion and migration, further contributing to cancer progression. As a potent survival effector of cancer cells, Snail1 represses apoptosis triggered by TGFβ signalling pathway, thus altering its role from tumour-suppressive to tumour-promoting (Franco et al., 2010).

Although Snail1 is predominantly recognized as a transcriptional repressor (Cano et al., 2000), it can also act as an activator under specific conditions, notably when interacting with other factors like Twist (Rembold et al., 2014) or CREB-binding protein (CBP) (Hsu et al., 2014). By acetylating Snail1, CBP enhances its stability and allows Snail1 to activate the expression of CCL2 and CCL5, which are cytokines that are involved in the recruitment of TAMs and contribute to cancer progression (Hsu et al., 2014). Snail1 can activate Zeb1 expression, which in turn induces tumorigenic properties during cancer progression and metastases (Ye et al., 2015).The tumour-promoting functions of Snail1 are not limited to epithelial cancers. Previous studies have investigated the impact of Snail1-induced EMT in melanoma cells (Brenot et al., 2018; Kudo-Saito et al., 2009), showing that it contributes to the malignant transformation of melanocytes *in vitro* (Poser et al., 2001), enhances invasive capabilities, or promotes immunosuppression (Brenot et al., 2018; Kudo-Saito et al., 2009).

In addition, stromal Snail1 expression in cancer has predominantly been observed in fibroblasts (Alba-Castellón et al., 2016; K.-W. Lee et al., 2022; Stanisavljevic et al., 2015), where it promotes their activation and contributes to tumour progression and invasion. Specifically, Snail1 induces the transformation of fibroblasts into CAFs, enhancing their ability to secrete pro-tumorigenic factors and remodel the ECM (Alba-Castellón et al., 2016). Compared to normal fibroblasts, Snail1-expressing CAFs are associated with increased migration and invasion of epithelial cells in colorectal xenograft models. Additionally, Snail1-postive CAFs modify the TME by increasing ECM stiffness and promoting anisotropic fibre orientation through the RhoA/α-SMA-dependent pathway. This remodelling facilitates colorectal cancer cell invasion and promotes EMT in tumour cells (A. Herrera et al., 2014; Stanisavljevic et al., 2015). Collectively, these studies underscore the critical role of stromal Snail1 in fibroblast activation and its impact on cancer progression. However, the underlying mechanisms by which Snail1 activates fibroblasts remain unclear, and its specific functions in CAFs, particularly in melanoma, have yet to be fully elucidated.

# 4. Cancer-associated fibroblasts (CAFs)

As mentioned above, among the cellular components of the TME, fibroblasts are one of the most abundant and crucial stromal cells in many tumours, playing a significant role in tumour progression (Lavie et al., 2022; Östman & Augsten, 2009; Sahai et al., 2020). Under regular conditions, fibroblasts preserve tissue homeostasis and support proper cellular interactions and functionality. However, in response to different factors secreted by cancer or immune cells, fibroblasts can become activated, adopting a different phenotype and functional properties that distinguish them from their quiescent counterparts in healthy tissues (Kuzet & Gaggioli, 2016). These activated fibroblasts, known as CAFs, display an enormous degree of heterogeneity and plasticity in their origin, marker expression and function (Sahai et al., 2020).

## 4.1. CAFs biology and plasticity

CAFs can arise from different sources, including resident tissue fibroblasts, bone-marrow derived mesenchymal stem cells, adipocyte-derived precursor cells, endothelial cells, mesothelial cells, or pericytes (**Figure 4a, b**). This diversity in origin contributes to

the observed heterogeneity in CAF subtypes, each with unique phenotypic and functional characteristics (Elyada et al., 2019; Lavie et al., 2022).

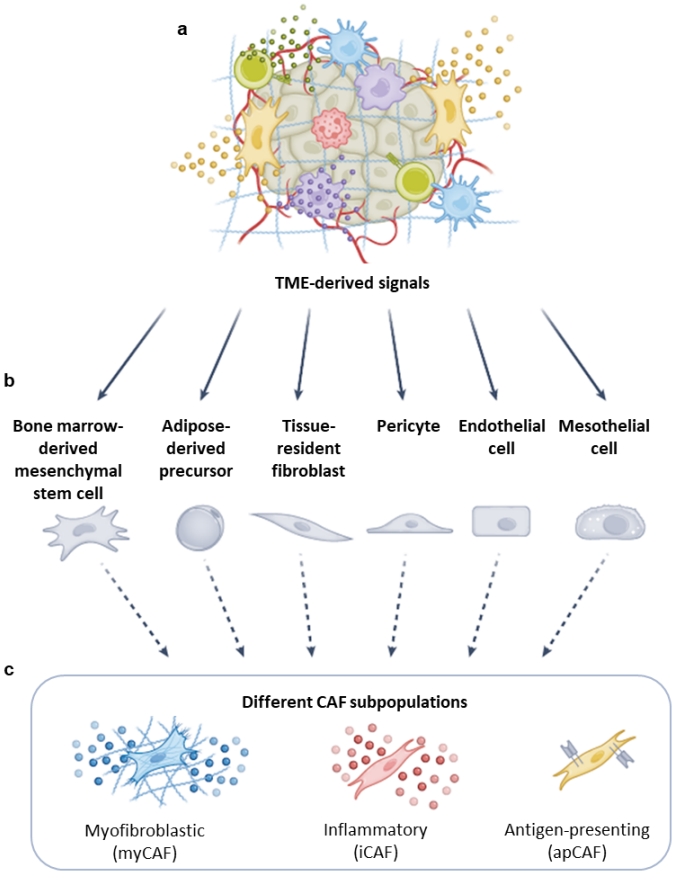


**Figure 4| Origins and main subsets of CAFs.** Signals from the TME **(a)** reprogram surrounding healthy cells **(b)** into CAFs. The major CAF subpopulations can be classified into three main groups **(c)** including myCAF, iCAF and apCAF distinguished by their primary roles in cancer progression.

CAFs achieve different functions by releasing different signalling molecules, including growth factors, cytokines, chemokines, MMPs, and ECM components that affect the behaviour of both tumour and immune cells (Kalluri & Zeisberg, 2006). Consequently, CAFs have emerged as a promising target for cancer treatment (Monteran & Erez, 2019). However, the heterogeneity and diversity of CAFs in the different types of cancer make their identification and characterization challenging.

Identifying CAFs accurately remains challenging due to the lack of a pan-specific marker to differentiate them from the tumour stroma (Sahai et al., 2020). Several markers, such as fibroblast activation protein (FAP), fibroblast-specific protein-1 (FSP-1), platelet-derived growth factor receptors alpha (PDGFRα) and beta (PDGFRβ), thymocyte differentiation antigen 1 (Thy-1), podoplanin (PDPN) and alpha-smooth

muscle actin (α-SMA), have been linked to fibroblasts. However, these markers do not consistently label all CAFs subtypes (Augsten, 2014; Cortez et al., 2014; Monteran & Erez, 2019). This barrier has led to conflicting evidence regarding the role of CAFs subpopulations in tumour progression, as different CAFs subpopulations present different functional properties that can either promote or inhibit tumour growth (Feig et al., 2013; Özdemir et al., 2014).

Advancements in single-cell RNA sequencing (scRNA-seq) technologies have enhanced our understanding of CAFs heterogeneity across different tumour types. Recent transcriptome studies suggest that there are three to seven major fibroblast subtypes (**Figure 4c**), with overlapping features and variability depending on the specific context (Davidson et al., 2020; Lavie et al., 2022; Luo et al., 2022).

Research on the characterization of CAFs subtypes at a single cell level has primarily focused on human pancreatic cancer (Biffi et al., 2019; Elyada et al., 2019), although other cancers like lung (Lambrechts et al., 2018), breast (Bartoschek et al., 2018), prostate (S. Chen et al., 2021; Vickman et al., 2020), head and neck (Puram et al., 2017) and colorectal (H. Li et al., 2017) have also been studied. In human pancreatic cancer, major CAFs subsets, including myofibroblastic (myCAF), inflammatory (iCAF), and antigen-presenting (apCAF), have been identified (Elyada et al., 2019). These subsets have also been observed in mouse models of pancreatic cancer by scRNA-seq (Biffi et al., 2019; Elyada et al., 2019; Öhlund et al., 2017). In triple-negative breast cancer, four different CAF subtypes have been identified based on the differential expression of six CAF markers, including FAP, integrin β1/CD29, α-SMA, S100A4/FSP1, PDGFRβ, and caveolin-1. In this scenario, the CAF-S1 subset, characterized by high expression levels of FAP compared to the other CAF subsets, demonstrated a remarkable capacity to promote an immunosuppressive environment by inducing T-reg differentiation (Costa et al., 2018; Kieffer et al., 2020).

Recently, in a murine melanoma model, three key CAF subsets known as S1 (immune), S2 (desmoplastic), and S3 (contractile) were identified (Davidson et al., 2020). The S1 subset ($Pdpn^{high}$ $Pdgfr\alpha^{high}$ $Cd34^{high}$) attracts and activate immune cells; the S2 subset ($Pdpn^{high}$ $Pdgfr\alpha^{high}$ $Cd34^{low}$) is involved in ECM stiffness and angiogenesis; and the S3 subset ($Acta2^{high}$) participates in the cytoskeleton organization. Interestingly, the presence of these subsets changes over the disease course, with early-stage tumours primarily containing S1 and S2 cells, while mid- and late-stage tumours mainly consist of S2 and S3 cells. However, the roles of these subpopulations in melanoma require

further research to elucidate their molecular mechanisms and therapeutic implications (Davidson et al., 2020).

In conclusion, the functional heterogeneity of CAFs highlights the importance of understanding the different roles of each subtype within the TME to develop more effective treatment strategies. Further research is needed to elucidate the complex interactions between CAFs subtypes, their specific functions in the TME, and their implications for cancer therapy.

## 4.2. Tumorigenic CAFs function

CAFs play a complex role within the TME, contributing significantly to disease progression (**Figure 5**) (Kalluri, 2016; Sahai et al., 2020).

### 4.2.1. ECM remodelling

The extracellular matrix (ECM) is crucial for providing structural and biochemical support to cells and tissues. During cancer progression, alterations in the ECM composition and organization occur, impacting its stiffness and interactions with cells. CAFs play a central role in these transformations, promoting tumour growth by secreting ECM components and enzymes that increase its density and stiffness (Winkler et al., 2020). They also release proteases, cytokines and chemokines that enhance tumour growth, migration, and invasion (Erdogan & Webb, 2017).

Beyond enzymatic modifications, CAFs generate mechanical forces through their contractile cytoskeleton and integrin-mediated adhesion, altering ECM properties and activating mechanotransduction signals in cancer cells. For example, CAFs facilitate cancer cell movement by aligning fibronectin fibres (Erdogan et al., 2017). Culturing epithelial cells in a CAF-synthesized matrix induces a mesenchymal phenotype (Dumont et al., 2013). These changes significantly impact tumour growth, invasion, metastasis, immune infiltration and treatment response (Chakraborty et al., 2021; Kuczek et al., 2019; Taufalele et al., 2023).

### 4.2.2. Angiogenesis

Angiogenesis, which refers to the formation of new blood vessels from pre-existing ones, is essential in sustaining tumour growth. CAFs contribute to this process by secreting multiple pro-angiogenic factors (Kalluri & Zeisberg, 2006; Podar et al., 2012). Among these factors, vascular endothelial growth factor (VEGF) is the main stimulator

of angiogenesis and it is not only produced by tumour cells but also by CAFs when exposed to tumour-conditioned media (Guo et al., 2008) or hypoxic conditions (Hlatky et al., 1994). To further support angiogenesis, CAFs recruit endothelial cells and mobilize monocytes from the bone marrow through the CXCL12-CXCR4 signalling pathway (Kalluri, 2016; Orimo et al., 2005). In the context of melanoma, aged CAFs secrete the WNT antagonist SFRP2, enhancing the angiogenic and malignant properties of tumours in elderly individuals (Kaur et al., 2016). CAFs expressing FAP modulate angiogenesis by balancing pro- and anti-angiogenic mediators (Patsouras et al., 2015; Santos et al., 2009). Other factors secreted by CAFs, such as fibroblast growth factor 2 (FGF2) and osteopontin, further contribute to angiogenesis (Fabris et al., 2010).

Interestingly, the pro-angiogenic pathways activated by CAFs not only stimulate blood vessel formation but also indirectly influence tumour immunity. These angiogenic mechanisms allow the trans-endothelial migration of immune cells, which in turn contributes to the establishment of an immunosuppressive environment (Kalluri, 2016).

### 4.2.3. Modulation of the immune response

Among the different components of the TME, CAFs have emerged as critical players in shaping the immune landscape of tumours (J. Chen et al., 2022). They release a range of molecules that influence both the innate and adaptive immune cells, primarily fostering an immunosuppressive environment, thus compromising the efficacy of immunotherapy approaches and promoting tumour growth (Harper & Sainson, 2014; Sahai et al., 2020).

Generally, CAFs regulate the immune cell infiltration by secreting pro-inflammatory cytokines such as IL-1 (Erez et al., 2010) and IL-6 (Flint et al., 2016), and expressing ligands such as CXCL12 (Feig et al., 2013) that drive an immunosuppressive signalling. CXCL12 specifically recruits immunosuppressive cells, promotes tumour survival, and enhances angiogenesis. In this context, FAP-expressing CAFs are a primary source of CXCL12 and block T-cell infiltration through the CXCL12-CXCR4 axis in many cancers, including pancreatic ductal adenocarcinoma (PDAC) and lung carcinoma models (Feig et al., 2013; Joyce & Fearon, 2015). Blocking the CXCL12-CXCR4 interaction has been shown to induce cancer regression and improve the efficacy of checkpoint inhibitors in preclinical models (I. X. Chen et al., 2019; Feig et al., 2013).

Furthermore, CAFs impair T-cell function by indirectly recruiting and modulating the activity of suppressive myeloid cells, such as monocytes and macrophages (Cohen et al., 2017), neutrophils (Yu et al., 2017) and MDSCs (Yang et al., 2016). In this context,

CAFs secrete chemokines such as CCL2, which is one of the most studied mediators for immune cell recruitment in different types of cancer, including lymphoma and breast cancer (Ksiazkiewicz et al., 2010; Yang et al., 2016). Reducing the levels of factors like CCL2 leads to increased T-cell infiltration and reduced tumour growth (Yang et al., 2016). In addition, CAFs impair the infiltration and function of $CD8^+$ cytotoxic T cells by secreting TGFβ (Mariathasan et al., 2018; Tauriello et al., 2018) and CXCL12 (Orimo et al., 2005), compromising the effectiveness of anti-PD-L1 therapies and overall anti-tumour responses (Feig et al., 2013).

CAFs with elevated FAP expression promote the recruitment and survival of FOXP3+ regulatory T cells, leading to immunosuppression and poor patient outcomes in cancers like triple-negative breast cancer (Costa et al., 2018; Kieffer et al., 2020). This is in line with the observed tumour rejection after FAP-positive fibroblast elimination in experimental models (Kraman et al., 2010b). Moreover, the coexistence of regulatory T cells and CAFs in the TME is linked to reduced anti-tumour immunity and lower survival rates in many cancers, although the underlying crosstalk mechanisms remain elusive (Kinoshita et al., 2013).

Besides modulating T-cell activity indirectly, CAFs can directly induce antigen-specific cytotoxic T-cell death by acting as antigen-presenting cells themselves (Lakins et al., 2018). Moreover, CAFs may also induce immune evasion through mechanisms that are independent of lymphocyte activity. They also impair the function of Natural Killer (NK) cells, which are well-known innate effector cells (Balsamo et al., 2009), through the release of Prostaglandin E2 (PGE2) and indoleamine-2,3-dioxygenase (IDO), thereby reducing their cytotoxic activity against cancer cells (Balsamo et al., 2009; T. Li et al., 2012, 2013; Ziani et al., 2017). Additionally, in hepatocellular carcinoma CAFs have been shown to transform dendritic cells (DC), which are crucial for activating cytotoxic T cells, into regulatory DCs, reducing their anti-tumour efficacy via the IL-6 mediated STAT3 pathway (J. T. Cheng et al., 2016).

Additionally, CAFs influence macrophage infiltration and polarization towards a tumour-promoting M2 phenotype (M. Herrera et al., 2013) by secreting cytokines such as macrophage colony-stimulating factor-1 (M-CSF1) or IL-6 (Mace et al., 2013). These M2 macrophages activate CAFs through IL-6 and CXCL12, establishing a feedback loop that promotes disease progression (Comito et al., 2014; M. Herrera et al., 2013).

Understanding the complex roles of CAFs in modulating immune responses is vital for developing effective targeted immunotherapies.

### 4.2.4. Resistance to therapy in cancer treatment

CAFs are central mediators of therapy resistance in cancer treatment through multiple mechanisms. One key mechanism is the ECM produced by CAFs, which acts as a physical barrier, impairing effective drug delivery to cancer cells and allowing them to evade apoptosis (Hazlehurst et al., 2000; Park et al., 2008). For example, in BRAF-mutant melanomas, CAFs create a fibronectin-rich ECM, contributing to resistance against BRAF inhibitors (Hirata et al., 2015).

Moreover, CAFs secrete soluble factors such as TGFβ, IL-6 and HGF (Mueller et al., 2012), which modify transcriptional and non-transcriptional processes in cancer cells, leading to apoptosis inhibition and cell cycle arrest (Kumari et al., 2016; Meads et al., 2009; Mueller et al., 2012). TGFβ can induce mesenchymal programmes in cancer cells, which enhance their adhesion to the ECM, and IL-6 reduces the efficacy of chemotherapies by activating pro-survival signalling pathways (Kumari et al., 2016; Qiao et al., 2018). Similarly, HGF has been identified as a contributor to resistance in preclinical models treated with BRAF inhibitors (Straussman et al., 2012). Furthermore, CAFs undergo behavioural changes upon exposure to conventional chemotherapies, radiotherapy, and targeted therapies, leading to the release of proteins, including WNT16B, and specific cytokines that drive resistance and promote a more aggressive cancer phenotype (Sun et al., 2013).

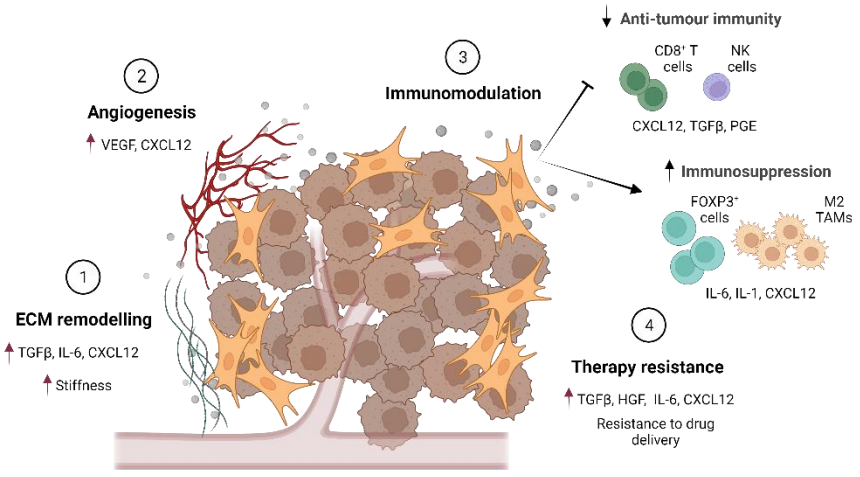


**Figure 5| Overview of the predominant mechanisms through which CAFs contribute to tumour progression.** These processes include **(1)** ECM remodelling, **(2)** angiogenesis, **(3)** alteration of the immune response including the activation of immunosuppressive cells and the suppression of anti-tumour immune cells, and **(4)** resistance to therapies. Created with BioRender.com.

Importantly, CAFs also restrict the effectiveness of immunotherapies by limiting T-cell mobility within tumours through the secretion of factors like TGFβ and CXCL12. Targeting these factors, along with the PD-1/PD-L1 axis, improves T-cell infiltration and overall anti-tumour activity (Feig et al., 2013; Tauriello et al., 2018). This underscores the need for further investigation of CAFs to better understand their role in therapeutic resistance and to identify new strategies for improving anticancer therapy efficacy.

## 4.3. Targeting CAFs in anti-cancer therapies

The multiple roles of CAFs in promoting tumour growth across different cancer types highlight their potential as therapeutic targets. There are many ongoing clinical trials exploring the use of CAF-specific agents together with existing treatments (Sahai et al., 2020). These trials generally aim to ablate CAFs, neutralize their tumour-promoting functions, or induce a dormant state (X. Chen & Song, 2019).

Interestingly, therapies designed to remove fibroblasts often focus on FAP expression. Strategies include anti-FAP antibodies engineered to deliver cell division inhibitors and immunotoxins designed to target FAP (Fang et al., 2016; Hofheinz et al., 2003; Ostermann et al., 2008). For instance, the anti-FAP-PE39 immunotoxin has effectively suppressed the growth of mammary tumours and promotes lymphocyte infiltration (Fang et al., 2016). Other approaches aim to enhance immune responses against FAP-expressing cells, such as using dendritic cell vaccines transfected with FAP mRNA (J. Lee et al., 2005) and adoptive therapy with chimeric antigen receptor (CAR)-T cells, which have shown promising anti-tumour effects (L. C. S. Wang et al., 2014). However, the depletion of FAP-positive cells can cause adverse effects like bone marrow toxicity (Roberts et al., 2013).

Alternative strategies focus on reverting the activated CAFs state to a dormant state, inhibiting their tumour-promoting functions. Targeting the vitamin D receptor in pancreatic cancer, for instance, has reverted activated stellate cells to a more dormant state, decreasing aggressiveness (Sherman et al., 2014). Interestingly, anti-fibrotic agents like Pirfenidone and TGFβ antagonists have been used to inhibit the CAFs ECM production, enhancing the efficacy of chemotherapy and anti-tumour immunity (Takai et al., 2016).

Despite promising preclinical results with minimal toxicity, translating these findings into clinical practice remains challenging. Ongoing research is investigating more selective approaches for targeting FAP or discovering new targets to improve precision and efficacy of CAF-based therapies.

Critically, as mentioned above, the biology of CAFs and whether they can be targeted in melanoma is poorly characterized.

# 5. Melanoma preclinical mouse models

Melanoma mouse models are powerful tools for studying the mechanisms driving melanoma progression, metastasis, and resistance to therapies, as well as for evaluating new therapeutic interventions. Although no single mouse model can completely replicate the heterogeneous nature of human melanoma, each offers unique advantages for studying specific aspects of melanoma biology (Becker et al., 2010).

## 5.1. Genetic models

Genetically engineered mouse models (GEMMs) are generated using techniques such as transgenic expression, viral infection, or CRISPR-Cas9 editing to introduce mutations commonly found in human melanoma, including BRAF, NRAS, PTEN and CDKN2A. These engineered mutations enable GEMMs to replicate the molecular and histological features of human melanoma, as well as its progression from benign nevi to malignant melanoma. By backcrossing these alleles into the immunologically relevant C57BL/6 strain, researchers can induce tumours and establish cell lines with genetic alterations that closely mirror the genetic profiles observed in human melanoma (Larue & Beermann, 2007).

GEMMs are particularly interesting for studying the efficacy of targeted therapies within an immunocompetent host, as they generally exhibit longer latency periods compared to syngeneic models, providing a more accurate representation of disease development (Becker et al., 2010).

A notable example of a GEMM is the metastatic melanoma model developed by Dankort and colleagues (Dankort et al., 2009), which incorporates the $BRAF^{V600E}$ mutation. This model uses the Cre-recombinase/LoxP system under the control of the tyrosinase promoter, allowing for the conditional activation of the $BRAF^{V600E}$ mutation

and the simultaneous deletion of PTEN in melanocytes. The combination of $BRAF^{V600E}$ and PTEN deletion leads to malignant melanoma that closely mirrors human metastatic disease (Goel et al., 2006; Madhunapantula et al., 2019).

Similarly, Ackermann and colleagues (Ackermann et al., 2005) demonstrated that introducing an NRAS mutation at codon 61, leads to melanoma formation in mice. When combined with the deletion of the P16INK4a and P14ARF tumour suppressor genes, this mutation also results in metastasis in mice, specifically to the lymph nodes, lungs and liver (Ackermann et al., 2005). This mouse model has been used to isolate the 1014 cell line, which has high metastatic potential, recapitulating the metastatic patterns observed in the original mouse model (Ackermann et al., 2005; Petit et al., 2019).

In addition to the 1014 cell line, other murine melanoma cell lines have been obtained from GEMMs, which are useful tools as they can be reimplanted in mice with the same genetic background with a functional immune system (Aktary et al., 2023).

## 5.2. Xenograft models

Xenograft models involve grafting human melanoma cells from primary or metastatic patient tumours into immunocompromised mice. However, these cells often have been adapted to non-physiological 2D culture conditions, compromising the reproducibility of laboratory and clinical results (Tveit & Pihl, 1981). To address this issue, researchers directly biopsy tumour pieces from patients and transplant them into immunodeficient mice, creating patient-derived xenograft (PDX) models. This technique preserves the *in vivo* cell features present in human tumours, as the cells have not been exposed to culture conditions (Madhunapantula et al., 2019; Rebecca et al., 2020).

Although xenograft models do not have a functional immune system, they are instrumental for studying the heterogeneity and behaviour of human melanoma cells. They also enable the testing of specific anti-tumour agents. However, for the investigation of the immunomodulating therapies and resistance mechanisms to immune checkpoint inhibitors, PDX models are not ideal due to the absence of a functional immune system and potential limitations in representing the TME and human immune responses to therapies (Rebecca et al., 2020). To address these limitations, laboratories in the melanoma research field have been currently developing humanized mouse tumour models. These models incorporate human immune cells into mice, providing a

more accurate platform for studying human melanoma and its interaction with the immune system (Rebecca et al., 2020).

## 5.3. Syngeneic models

Syngeneic models involve injecting murine melanoma cell lines into immunocompetent mice of the same strain. These cell lines, derived from spontaneous or induced tumours in mice, are particularly useful for studying melanoma interactions with the microenvironment and evaluating the efficacy of immunotherapies. Unlike xenograft models that use immunodeficient mice, syngeneic models maintain a fully functional immune system, providing a more accurate *in vivo* representation of tumour-immune interactions (Madhunapantula et al., 2019).

A commonly used cell line in syngeneic models is the B16F10, which originated from a spontaneous melanoma and was further passaged *in vivo* to enhance its metastatic potential (Fidler, 1973). The B16F10 line is frequently used due to its rapid growth, ease of manipulation, and well-characterized metastatic behaviour. However, it lacks common human melanoma mutations such as $BRAF^{V600E}$ and $NRAS^{Q61R}$, and it exhibits low immunogenicity and aggressive tumour growth. Although the B16F10 cell line has provided valuable insights into multiple essential processes, its limitations hinder its ability to accurately replicate the biological complexity and heterogeneity of human melanoma (Melnikova et al., 2004).

To address these limitations, in this study we primarily used cell lines derived from GEMMs carrying mutations prevalent in human melanoma, such as NRAS or BRAF. Specifically, we used the 5555 cell line, derived from a $BRAF^{V600E}$ mouse model (Dhomen et al., 2009), the YUMM1.7 cell line, derived from $Braf^{V600E}$ $Pten^{-/-}$ $Cdkn2a^{-/-}$ mouse model (Meeth et al., 2016), the 1014 cell line, derived from a $NRAS^{Q61K}$ mouse model (Petit et al., 2019), and the FCT1 cell line, isolated from a tumour arising in a $Braf^{V600E}$/$Pten^{loxP}$/tdTomato transgenic mouse generated in our laboratory. These GEMM-derived cell lines harbour clinically relevant mutations and exhibit tumour behaviours similar to human melanoma, including responsiveness to targeted therapies and immune checkpoint inhibitors (Kuzu et al., 2015).

The use of these cell lines allows the study of melanoma within the context of an intact immune system and native tumour microenvironment, providing a reliable framework for investigating melanoma biology and therapeutic response in immunocompetent hosts. However, despite their enhanced translational relevance, GEMM-derived syngeneic models introduce increased complexity due to tumour heterogeneity, which can lead to more variable experimental outcomes (Madhunapantula et al., 2019).

# OBJECTIVES

Despite the established function of Snail1 in carcinomas and fibrosis, its role in non-epithelial cells has not been thoroughly characterized. Stromal Snail1 has been shown to influence carcinoma biology and our preliminary results indicated that Snail1 is highly expressed in the melanoma microenvironment. Given the high relevance of the TME in the regulation of melanoma biology, the main aim of this thesis is to elucidate whether microenvironmental Snail1 contributes to melanoma progression and if this is the case, to investigate the underlying mechanisms and explore whether Snail1 targeting could constitute an effective therapeutic strategy. This understanding could reveal new strategies to address the significant challenges of advanced melanoma.

## General objective

This thesis aims to understand the contribution of microenvironmental Snail1 to melanoma biology *in vivo* using preclinical mouse models.

## Specific objectives

1. To characterize the expression of Snail1 in melanoma mouse models.

2. To investigate the functional role of Snail1 in the melanoma microenvironment and its impact on melanoma progression.

3. To assess the potential of targeting microenvironmental Snail1 as a novel therapeutic approach in melanoma.

# MATERIAL AND METHODS

# 1. Experimental mice

## 1.1. Mouse handling

All experiments involving animals were performed in accordance with the European Community Council Directive (2010/63/EU) and Spanish legislation. The protocols were approved by the CSIC and UMH Ethical Committee and the Animal Welfare Committee at the Institute of Neurosciences CSIC-UMH. Mice were hosted in a pathogen-free facility under controlled temperature and humidity, with a 12 h light/dark cycle. Both male and female C57BL/6 mice, aged 7-8 weeks, were used in all experiments.

## 1.2. Mouse transgenic lines

The following mouse lines were used during this thesis.

**Tg(UBC-cre/ERT2)$^{1Ejb}$, Gt(ROSA)26Sor$^{tm9(CAG-tdTomato)Hze}$, 129S6-Snai1$^{tm1.1St}$**

Abbreviated as UBC-CreERT2-tdTomato-Snail1$^{fl/fl}$ (Snail1$^{ME}$-KO); UBC-CreERT2-tdTomato-Snail1$^{+/+}$ (Snail1$^{ME}$-WT).

To generate this transgenic line, the UBC-CreERT2 mice (Ruzankina et al., 2007) (RRID:IMSR_JAX:008085) were crossed with the tdTomato reporter mice (RRID:IMSR_JAX:007909) and the *Snai1$^{fl/fl}$* mice (Rowe et al., 2009). The UBC-CreERT2 mice carry the Cre recombinase fused to the human estrogen receptor ligand binding domain together with the ubiquitin C (UBC) promoter. This allows for a tamoxifen inducible Cre activity in all tissue types, providing a temporal control of recombination. The tdTomato reporter mice contain the tdTomato gene inserted into the Rosa26 locus with a STOP cassette flanked by loxP sites, which prevents tdTomato transcription. When the UBC-CreERT2 mice express the Cre recombinase, the STOP cassette is removed, leading to tdTomato protein expression in all tissues. In addition to the tdTomato allele, the transgenic mice used in this thesis also carry the Snail1$^{fl/fl}$ allele, which has LoxP sites flanking exon 3 of the *Snail1* gene. This enabled the study of Snail1 in the TME by silencing this TF and tracing cells with the tdTomato protein in a time-dependent manner following tamoxifen administration.

**129P2(Cg)-Cx3cr1$^{tm2.1(cre/ERT2)Litt}$**

Abbreviated as Cx3cr1CreERT2-YFP.

To examine myeloid populations in tumours, Cx3cr1CreERT2-YFP mice (RRID: IMSR_JAX:021160) were used. This mouse model is a knock-in strain that expresses the Cre-ERT2 protein under the control of the chemokine receptor 1 (Cx3cr1) promoter, followed by an internal ribosome entry site (IRES) and an enhanced yellow fluorescent protein (YFP). The resulting mouse model enables the analysis of myeloid populations through the expression of the YFP reporter protein (Jung et al., 2000). Mice were kindly given by Jose Lopez-Atalaya from the Instituto de Neurociencias CSIC-UMH.

**Cg-Tg(Tyr-cre/ERT2)13Bos, *Braf$^{tm1Mmcm}$, Pten$^{tm1Hw}$, Gt(ROSA)26Sor$^{tm9(CAG-tdTomato)Hze}$***

Abbreviated as Braf$^{V600E}$/Pten$^{loxP}$/tdTomato.

In this study, the Braf$^{V600E}$/Pten$^{loxP}$/tdTomato mouse model was used to validate our data with inducible transgenic melanomas. This model was generated by crossing the BRAF-driven mouse melanoma model Braf$^{CA}$,Pten$^{loxP}$,Tyr::CreERT2 (Braf$^{V600E}$/Pten$^{loxP}$) (Dankort et al., 2009) (RRID:IMSR_JAX:013590), which expresses a constitutively active BRAF$^{V600E}$ mutant protein and lacks PTEN function, with the tdTomato reporter line (RRID:IMSR_JAX:007909). The Tyr::CreERT2 transgene, active in melanoblasts and melanocytes, expresses an inducible form of Cre recombinase upon 4-hydroxytamoxifen (4-HT) administration, under the control of the Tyr promoter. In the absence of Cre recombinase activity, the BRAF$^{CA}$ model expresses the WT BRAF protein. Upon Cre-mediated recombination, the mutated Braf$^{V600E}$ allele becomes active. Additionally, the Pten$^{loxP}$ model has loxP sites flanking exon 5 of the *Pten* gene, which leads to PTEN protein loss of function when recombination occurs. Thus, the administration of 4-HT induces simultaneous expression of BRAF$^{V600E}$ and PTEN loss in melanocytes, triggering the development of melanomas wherein the melanocytes express the tdTomato fluorescence.

**129S-PDGFRα$^{tm1.1(cre/ERT2)Blh}$, Gt(ROSA)26Sor$^{tm9(CAG-tdTomato)Hze}$, 129S6-Snai1$^{tm1.1St}$**

Abbreviated as PDGFRα-CreERT2-tdTomato-Snail1$^{fl/fl}$

In order to analyse Snail1 in fibroblasts, PDGFRα-CreERT2 (L. E. Rivers et al., 2008) mice were crossed with the tdTomato reporter mice and the *Snai1$^{fl/fl}$* mice, previously described. PDGFRα-CreERT2 mice have the Cre/ERT2 fusion gene inserted at the start

codon of the platelet derived growth factor receptor alpha polypeptide (PDGFRα) gene. Therefore, upon tamoxifen administration, recombination leads to the deletion of Snail1 in PDGFRα-expressing cells, and expression of tdTomato in these cells. This mouse model enabled the investigation of Snail1 in PDGFRα cells, which primarily consist of fibroblasts in melanomas. PDGFRα-CreERT2 mice was kindly given by Isabel Perez-Otaño from the Instituto de Neurociencias CSIC-UMH.

## 1.3. Genotyping

The genotyping of the animals used was performed through collection of distal tail or ear tissue followed by NaOH (50 mM) DNA isolation. The PCRs were carried out using the primers listed in **Table 1**.

| Allele | Primer Sequence (5'→3') | Amplicon length |
|---|---|---|
| UBC-CreERT2 | Fw: GCGCTCTGGCAGTAAAAACTATC<br>Rv: GTGAAACAGCATTGCTGTCACTT | UBC-CreERT2 allele: 100bp |
| tdTomato | Fw: AAGGGAGCTGCAGTGGAGTA<br>Rv: CCGAAAATCTGTGGGAAGTC<br>Fw: GGC ATTAAA GCA GCG TATCC<br>Rv: CTG TTC CTGTACGGCATGG | WT allele: 297 bp<br>tdTomato allele: 196 bp |
| Snail1$^{fl/fl}$ | Fw: CTGCCAGGTGGGAAGGACT<br>Rv: CAA GGACATGCGGGAGAAGGT | WT allele: 324 bp<br>Snail1 Flox allele: 424 bp |
| Cx3cr1-CreERT2 | Fw: AAGACTCACGTGGACCTGCT<br>Rv Mutant: CGGTTATTCAACTTGCACCA<br>Rv WT: AGGATGTTGACTTCCGAGTTG | Cx3cr1-CreERT2: 300 bp |
| PDGFRα-CreERT2 | Fw: TCGATGCAACGAGTGATGAG<br>Rv: TTCGGCTATACGTAACAGGG | PDGFRα-CreERT2: 480 pb |
| Braf$^{CA}$ | Fw: TGAGTATTTTTGTGGCAACTGC<br>Rv: CTCTGCTGGGAAAGCGGC | WT allele: 185 pb<br>Mutant allele: 308 pb |
| Pten$^{loxP}$ | Fw: CAAGCACTCTGCGAACTGAG<br>Rv: AAGTTTTTGAAGGCAAGATGC | WT allele: 156 pb<br>Mutant allele: 328 pb |
| Tyr::CreERT2 | Fw: GGAGCAAACAGTAGCTTCAC<br>Rv: AGCTTCGATGATGGGCTTAC | Tyr::CreERT2: 201 pb |

**Table 1| Primers used to genotype mouse transgenic lines.**

## 1.4. Tamoxifen administration

To obtain a tamoxifen solution, tamoxifen (Sigma) was dissolved in a mixture of corn oil and ethanol (90:10 v/v). This solution was administered intraperitoneally to adult mice at a dose of 100mg/kg body weight. The injection schedule of tamoxifen consisted of one injection every two days for the first four doses, followed by two weekly injections.

# 2. Cell culture

Murine melanoma cell line $Braf^{V600E}$-5555 (Dhomen et al., 2009; Hirata et al., 2015) was originally obtained from Richard Marais´ laboratory and luciferase-expressing $Braf^{V600E}$-5555 (5555-Luc) were kindly given by Imanol Arozarena´s lab (NavarraBiomed). The $Braf^{WT}Nras^{WT}$-B16F10 (CRL-6475) and $Braf^{V600E}$-YUMM1.7 (CRL-3362) cell lines were obtained from ATCC. The $Nras^{Q61K}$ -1014 cell line was kindly provided by Prof Lionel Larue at INSERM, France. The FCT1 cell line was isolated in our laboratory from a tumour arising in a $Braf^{V600E}/Pten^{loxP}$/tdTomato transgenic mouse. Additionally, NIH3T3 mouse fibroblasts (CRL-1658) were purchased from ATCC.

All cell lines, except $Nras^{Q61K}$-1014, were cultured in DMEM medium (Sigma) supplemented with 10% fetal bovine serum (FBS) and 1% penicillin/streptomycin (Sigma). The $Nras^{Q61K}$-1014 cell line was maintained in F12 (Biowest) medium, also supplemented with 10% FBS and 1% penicillin/streptomycin (Sigma). Cells were kept at 37ºC in a humidified atmosphere with 5% $CO_2$, and the medium was replaced every 2/3 days. Melanoma cells were passaged at 80% confluency at a ratio 1:10 every 72 h, while NIH3T3 cells were passaged at 60-70% confluency 1:20 every 72 h. Cells were discarded after up to seven consecutive passages and replaced with fresh stocks. All cell lines were tested for mycoplasma contamination every month at the host institution, and only mycoplasma-negative cells were used in the experiments.

# 3. Treatments of cultured cells

## 3.1. Transfection of plasmids and interfering RNAs

For Snail1-silencing experiments, NIH3T3 cells were transfected with siRNA targeting mouse *Snail1* using RNAi MAX (Invitrogen). As a control, a fluorescent oligonucleotide reagent, Block-it™ (Invitrogen), was used. The siRNAs used for RNA interference were obtained from Silencer® predesigned siRNA (Ambion) and specifically targeted *Snail1* (Snail1 siRNA (antisense): AUAUUUGCAGUUGAAGAUCtt). Prior to transfection, 100,000 NIH3T3 cells were seeded on 6-well plates and allowed to adhere for 24 h. Post transfection with either siRNA against *Snail1* or Block-it™, cells were treated with 2 ng/ml TGFβ (TGFβ1, Millipore, USA). The cells were then collected at 48 and 72 h post transfection to identify the most effective time point for reducing Snail1

mRNA levels for subsequent analysis. Cell lysis and RNA extraction were performed using the Illustra RNAspin Mini Isolation Kit (GE healthcare).

For the Snail1-overexpression experiments, NIH3T3 cells were transfected with a Snail1-Myc plasmid. Cells were initially seeded in 10 cm culture dish plates 24 h prior to transfection. Transfection was performed using Lipofectamine 3000 (Invitrogen), following the manufacturer's instructions, at 70% confluency. After 48 h, cells were harvested and used for ChIP assays (see below).

### 3.2. TGFβ administration

For Snail1-upregulation experiments, a total of 100,000 NIH3T3 cells were seeded on 6-well plates for 24 h prior to TGFβ (2ng/ml) administration. Cells were collected at 48 and 72 h post-TGFβ administration and the most effective time point for Snail1 upregulation was chosen for further experiments. The collected cells were then processed for RNA extraction using the Illustra RNAspin Mini Isolation Kit (GE healthcare).

### 3.3. CYD19 drug administration

NIH3T3 cells were first treated with TGFβ (2ng/ml) for 24 h. Subsequently, the cells were exposed to either a vehicle control or 5nM of CYD19 (Cat#AOB11460, Aobious) in the presence of TGFβ for an additional 48 h. After this treatment period, cells were analysed either by immunofluorescence or for gene expression levels.

## 4. Experimental melanoma mouse models

### 4.1. Inducible melanoma reporter model

Tumours were topically induced in 6-8 weeks $Braf^{V600E}$/$Pten^{loxP}$/tdTomato mice. Treatment with 1.5 µl 4-HT (Sigma) (8 mg/ml), dissolved in ethanol:DMSO (80:20), was applied on the shaved skin of the back. Mice were immobilised until 4-HT solution had completely dried. Tumours were collected once they reached the predetermined limit size of 1000-1200 $mm^3$, which was calculated using the formula: Tumour volume= length x width x depth x 0.562.

## 4.2. Melanoma subcutaneous allografts

To assess the impact of Snail1 on melanoma progression, 5 x $10^6$ $Braf^{V600E}$-5555 melanoma cells suspended in 100ul of sterile phosphate-buffered saline (PBS) were subcutaneously injected into the right flank of 7-to-8-weeks old $Snail1^{ME}$-WT or $Snail1^{ME}$-KO mice on day 0. Mice were monitored daily until tumour became palpable (70-80 $mm^3$), typically around day 9 post injection (9dpi). Tamoxifen was then administered intraperitoneally three times a week on alternate days until the end of the experiment. Tumour volumes were measured every 2 days with a calliper and calculated using the formula: Tumour volume= length x width x depth x 0.562 (mm). Mice were euthanized once tumours reached the predetermined limit size of 1000-1200 $mm^3$, and when possible, based on tumour size, samples were divided for histological analysis and/or RNA extraction.

The same experimental approach was used to evaluate the impact of Snail1-silencing specifically in PDGFRα-positive cells to melanoma progression in PDGFRα-CreERT2-$Snail1^{fl/fl}$ mice.

To investigate myeloid populations within melanomas, Cx3cr1CreERT2-YFP mice were used. These mice were subcutaneously injected with 5 x $10^6$ $Braf^{V600E}$-5555 melanoma cells as previously described, and tumours were subjected to immunofluorescence analyses.

In order to understand the effect of Snail1 on melanoma tumour establishment, tamoxifen administration began a week prior to 5 x $10^6$ $Braf^{V600E}$-5555 cells subcutaneous injection. Tumour volume was monitored every two days and mice were euthanized when tumours reached the predetermined limit size.

## 4.3. Anti-PD-1 therapy experiment

To investigate the combined effects of Snail1 silencing and immunotherapy with anti-PD-1, 7-to-8-weeks old $Snail1^{ME}$-WT and $Snail1^{ME}$-KO mice were subcutaneously injected with 5 x $10^6$ $Braf^{V600E}$-5555 melanoma cells on day 0. Mice were monitored daily until tumours became palpable. Animals were subsequently divided into four treatment groups: (1) The $Snail1^{ME}$-WT control group, which received intraperitoneally tamoxifen injections every two days, starting on 7 dpi until reaching the experimental endpoint. (2) The $Snail1^{ME}$-WT with PD-1 group, which was subjected to 10mg/kg body weight intraperitoneal injections of anti-PD-1 (BioxCell, PD-1 CD279, BE0273) starting on 8 dpi,

with subsequent doses administered every 3 days for a total of five doses, together with tamoxifen administration. (3) The Snail1$^{ME}$-KO control group, which received intraperitoneally tamoxifen injections every two days, starting on 7 dpi until the endpoint. (4) The Snail1$^{ME}$-KO with PD-1, which was subjected to 10mg/kg body weight intraperitoneal injections of anti-PD-1 (BioxCell, PD-1 CD279, BE0273) starting on 8 dpi, with subsequent doses administered every 3 days for a total of five doses, together with tamoxifen administration.

## 4.4. Experimental lung metastasis assay

To evaluate the impact of Snail1 in metastatic establishment and progression *in vivo*, 1 x $10^4$ 5555-Luc cells in 100 ul of sterile PBS were intravenously injected into the lateral tail vein, using a 27-gauge needle. Lung colonisation was analysed *in vivo* and *ex vivo* by bioluminescence imaging (BLI). For imaging, anaesthetized mice (isoflurane) were injected intraperitoneally with D-luciferin (Perkin Elmer) (150 mg/kg body weight in sterile PBS $Ca^{2+}Mg^{2}$-free) and imaged with an *in vivo* imaging system (IVIS) Lumina XR imaging system (PerkinElmer). The lung bioluminescence intensity signal of each mouse was quantified using Living Image software (PerkinElmer). Tamoxifen was administered three days a week until the end of the experiment. Mice were sacrificed 3 weeks post injection, and lungs were collected for histological analysis.

In order to investigate the role of Snail1 to metastases establishment, tamoxifen treatment started one week prior to tail vein injection of 5555-Luc cells. To assess the impact of Snail1 to metastases progression, tamoxifen administration began once experimental metastases were already established and detected by BLI.

# 5. Histology

Sample fixation protocols were optimized according to sample size to achieve the best quality for immunohistochemical stainings. Tumour pieces were fixed at 4ºC for 4 h with 4% paraformaldehyde (PFA), while whole lungs were fixed at 4ºC overnight (O/N) with 4% PFA. After fixation, samples were thoroughly washed with PBS for one day. Subsequently, the samples were incubated at 4ºC for three days in a 30% sucrose solution. Next, the samples were embedded in the desired orientation in optimal cutting

temperature (OCT) medium, and they were kept in dry ice until transferred to -80ºC for sectioning.

The samples were sectioned at 8 µm thickness using a cryostat (Leica). Subsequently, samples were dried for 2 h at RT before being used for immunolabelling or stored at -80ºC to preserve their integrity.

# 6. Staining and imaging in tissues and cells

## 6.1. Hematoxylin and Eosin staining

In order to perform Hematoxylin and Eosin (H&E) staining of 8 µm frozen sections, slides were firstly dried for several hours at RT. Then, sections were immersed in Hematoxylin (Sigma; diluted 1:1 in $dH_2O$) solution for 30 seconds, rinsed with tap water until the colorant was cleared, and then stained with Eosin (Sigma; diluted 1:1 in $dH_2O$) for 4 minutes. The samples were thoroughly washed with $dH_2O$ until residual dye was removed. Subsequently, samples were dehydrated through a series of ethanol-water solutions (25%, 50%, 75% and 100%) for 2 seconds each. Following dehydration, samples were treated with two changes of xylene 100% for 10 minutes each. Then, slides were mounted with rapid mounting medium for microscopy Entellan™ (Sigma) and dried overnight in a fume hood at RT. Finally, stained sections were subjected to quantification analyses.

## 6.2. Immunofluorescence in tissue sections

For immunofluorescence (IF) staining, tissue sections obtained from the cryostat were extensively washed with PBS and then incubated with blocking solution (5% normal goat serum (NGS), 1% bovine serum albumin (BSA) and 0.1% Triton x-100 in PBS) for 1 at RT. After blocking, sections were incubated with the primary antibodies (see **Table 2**) O/N at 4ºC in the same blocking solution. Next day, after extensive washing in PBS with 0,1% Tween, slices were incubated with the secondary antibodies (see **Table 3**) diluted in blocking solution for 1 h at RT. Finally, sections were washed with PBS 0,1% Tween several times, stained with DAPI (Sigma; 1 µg/ml) and mounted in Dako Fluorescence Mounting Medium (Dako).

Finally, imaging was performed using an Olympus FV1200 confocal microscope (Olympus) with 20x or 40x objectives and analysed using ImageJ software.

## 6.3. Immunofluorescence in cultured cells

In order to obtain samples of cultured fibroblasts isolated by FACS-sorting for immunofluorescence staining, sorted fibroblasts were seeded onto glass coverslips in 12-well plates at 37ºC in a 5% $CO_2$ humidified incubator. Coverslips were pre-treated with poly-lysine (Sigma) to promote cell adhesion.

For immunolabelling, cells were fixed with 4% PFA for 15 minutes at RT, washed three times with PBS, and incubated with permeabilization solution (0.1% Triton x-100 in PBS) for 15 min. Subsequently, cells were incubated with blocking solution (0.1% Triton x-100 and 1% BSA in PBS) for 1 h at RT. Cells were then incubated with the primary antibodies (see **Table 2**) O/N at 4ºC in blocking solution and the following day for 30 minutes at RT. After washing three times with PBS, cells were incubated with the appropriate secondary antibody (see **Table 3**) diluted in blocking solution for 1 h at RT, counterstained with DAPI (Sigma; 1 µg/ml) and mounted with Dako. Finally, samples were imaged with an Olympus FV1200 confocal microscope and analysed with ImageJ software.

| Antibody | Host | Dilution | Application | Provider | Cat. no. |
|---|---|---|---|---|---|
| Myc-tag | Goat | 1:500 | ChIP | Abcam | ab9132 |
| IgG | Rabbit | 1:500 | ChIP | Thermo Fisher kit | 1862739 |
| Snail1 | Rabbit | 1:50 | IF | Cell Signalling | 3879 |
| GFP | Chicken | 1:500 | IF | Aveslab | GFP-1020 |
| PDGFRα | Rat | 1:100 | IF | Invitrogen | 14-1401-82 |
| KI-67 | Rabbit | 1:1000 | IF | Abcam | ab15580 |
| Cleaved-CASPASE 3 | Rabbit | 1:500 | IF | Cell signalling | 9664 |
| α-SMA | Mouse | 1:1000 | IF | Sigma | A2547 |
| CD45 | Rat | 1:350 | IF | BD Pharmingen™ | 550539 |
| PDGFRα-APC | Rat | 1:50 | FACS | Biolegend | 135908 |
| CD11b-APC | Rat | 1:50 | FACS | Biolegend | 101211 |
| Ly6C-FITC | Rat | 1:50 | FACS | Biolegend | 128005 |
| Ly6G-APC/Fire | Rat | 1:50 | FACS | Biolegend | 127651 |
| CD3-APC | Rat | 1:50 | FACS | Biolegend | 100235 |
| CD4-APC/Fire | Rat | 1:50 | FACS | Biolenged | 100459 |
| CD8a-FITC | Rat | 1:50 | FACS | Biolegend | 100705 |
| CD45-APC | Rat | 1:50 | FACS | Biolegend | 103112 |
| CD11c-APC/Fire | Armenian Hamster | 1:50 | FACS | Biolegend | 117352 |
| CD22-FITC | Rat | 1:50 | FACS | Biolegend | 126106 |
| CD335-FITC | Rat | 1:50 | FACS | Biolegend | 137606 |
| FOXP3-AF488 | Rat | 1:50 | FACS | Biolegend | 126406 |

**Table 2| List of primary antibodies.** ChIP, Chromatin immunoprecipitation; IF, Immunofluorescence; FACS, Fluorescence-activated cell sorting.

| Antibody | Host | Dilution | Application | Provider | Cat. no. |
|---|---|---|---|---|---|
| Alexa Fluor® 488 anti-rabbit | Goat | 1:500 | IF | Invitrogen | A11008 |
| Alexa Fluor® 488 anti-chicken | Goat | 1:500 | IF | Life Technologies | A11039 |
| Alexa Fluor® 488 anti-rat | Goat | 1:500 | IF | Invitrogen | A11006 |
| Alexa Fluor® 647 anti-rabbit | Goat | 1:500 | IF | Life Technologies | A27040 |
| Alexa Fluor® 647 anti-rat | Goat | 1:500 | IF | Invitrogen | A21247 |
| Alexa Fluor® 647 anti-mouse | Donkey | 1:500 | IF | Invitrogen | A31571 |

**Table 3| List of secondary antibodies.** IF, Immunofluorescence.

# 7. Sample preparation and immunolabelling for FACS analysis

## 7.1. Tissue processing for FACS analysis

To prepare single-cell suspensions suitable for fluorescence-activated cell sorting (FACS) analysis, mechanical disruption was performed using a scalpel to process subcutaneous tumours or lungs. The samples were then subjected to a cold and slow enzymatic digestion (2.5 mg/ml Collagenase A and 0.2 mg/ml DNAse I) (both from Roche) in PBS at 4ºC for 1 h while being gently agitated. The resulting cell suspension was filtered through a 40µm cell strainer using a 3 ml syringe plunger to facilitate the process. The filtered suspension was then centrifuged (5 minutes at 350 g followed by 1 minute at 10.000 rpm) and the cell pellets were resuspended in 1 ml of RBC lysis buffer (Biolegend, #420302) for 4 minutes at RT to lyse red blood cells. After centrifugation, the cells were resuspended in FACS buffer (2,5 mM EDTA and 24,5 mM HEPES in PBS) for subsequent immunolabelling or sorting.

## 7.2. Immunolabelling techniques and cell sorting

The single-cell suspension solution was subjected to immunolabelling for FACS analysis. Initially, the samples were blocked with Fc-block CD16/CD32 (Biolegend, #101320, 1:50) in FACS buffer for 10 minutes on ice to prevent nonspecific binding. For cell surface staining, cells were resuspended in the appropriate cocktail of fluorescent-labelled antibodies (see **Table 2**) and incubated for 30 minutes on ice, protected from light, in FACS buffer. If intracellular staining was required, cells underwent centrifugation for 5 minutes at 350 g after surface marker staining, then were fixed, permeabilized, and stained for transcription factors using the True-Nuclear Transcription Factor Buffer Set

(Biolegend, #424401), following the manufacturer's instructions. Cell viability was assessed using DAPI staining.

To isolate fibroblasts cells from melanomas, PDGFRα$^{+}$ GFP$^{-}$ tdTomato$^{+}$ cells were selected and sorted directly into an Eppendorf tube containing lysis solution from Arcturus PicoPure RNA Isolation Kit (Thermofisher). To validate the isolated melanoma-associated fibroblasts, the sorted cells were seeded onto glass coverslips treated with poly-L-lysine (Sigma, # P4707) and analysed for different fibroblast markers through immunofluorescence, as mentioned above (see **Table 2**).

To characterize the immune cell profile of the samples, flow cytometry analysis was performed by analysing 50.000 live singlets per sample. The fluorescent data collected were analysed using BD FACSDiva Software (BD Bioscience).

# 8. Molecular methods

## 8.1. Total RNA extraction, cDNA synthesis and RT-qPCR analysis

For gene expression analyses, RNA was extracted using two different kits according to the sample type. The Illustra RNAspin Mini Isolation Kit (GE healthcare) was used for tissues and cell culture samples, following manufacturer's instructions. For FACS-isolated samples, the Arcturus PicoPure RNA Isolation Kit (Thermo Fisher) was employed following manufacturer's instructions. In this case, the total RNA was eluted in 15 µl of elution buffer and 1 µl was used for RNA quantification and quality control using the Bioanalyzer High Sensitivity RNA chip.

Reverse transcription was carried out using the Maxima First Strand cDNA Synthesis Kit (Thermo Fisher), and RT-qPCR was performed using the Fast SYBR Green Mastermix (Applied Biosystems) in a Step One Plus machine (Applied Biosystems) with the primers listed in **Table 4**. To ensure accuracy, all primers were tested by generating a standard curve with serial dilutions of the sample of interest; only primers demonstrating efficacy between 90% and 110% were used. The relative levels of expression were calculated using the comparative Ct method normalized to the TBP housekeeping gene and then experimental samples were normalised to their respective controls:

$$\Delta Ct = Ct\ (gene\ of\ interest) - Ct\ (housekeeping)$$

$$\Delta\Delta Ct = \Delta Ct\ (experimental\ sample) - \Delta Ct\ (control\ sample)$$

$$Fold\ change = 2^{-\Delta\Delta Ct}$$

## 8.2. Chromatin immunoprecipitation (ChIP) assay

For ChIP assays, NIH3T3 cells transfected with Snail-Myc were used. Cells at 80% confluence from a 10 cm culture dish were fixed with 1% PFA for 10 minutes at RT. The fixation was stopped by adding glycine solution to a final concentration of 0.125M and incubated for an additional 5 minutes at RT. Cells were then harvested and pooled from 4 plates, and chromatin was isolated using the Pierce™ Magnetic ChIP Kit (Thermo Fisher), following the manufacturer's instructions. Sonication was carried out in a Bioruptor® Pico sonication device (Diagenode) in 15 cycles of 30-second on/off intervals. Immunoprecipitation and DNA isolation were performed using the same Pierce™ Magnetic ChIP Kit and the anti-Myc antibody listed in **Table 2**. Finally, the isolated DNA was used for direct qPCR assays.

# 9. Morpholino oligomer and *in vivo* treatment

In order to target Snail1 expression systemically *in vivo*, a morpholino oligomer (MO) strategy was used. A Snail1-specific vivo-morpholino (Snail1-MO) designed against the boundary sequences of the intron 1 and exon 2 of the *Snail1* gene (5′-TGAACTCTGCGGGAAGAGAAGAGAC-3′) and a standard control morpholino (Control-MO) that targets the human β-globin intron mutation (5′-CCTCTTACCTCATTACAATTTATA-3′) were designed by Gene Tools. C57BL/6 mice, aged 7 weeks, were intravenously injected with 5555-Luc cells into the tail vein. After 10 dpi, a solution containing either Snail1-MO or Control-MO in saline (100 µl; 6 mg MO per kg) was administered through tail vein injections in the corresponding mice every other day. After a 20-day treatment period, mice were sacrificed, and their lungs were collected for histological analysis to assess the efficacy of the treatment.

| Gene | Primer Sequence (5'→3') | Orientation |
|---|---|---|
| mTBP Fw | CCTTGTACCCTTCACCAATGAC | Sense |
| mTBP Rv | ACAGCCAAGATTCACGGTAGA | Antisense |
| mSnail1 Fw | CAGCTGCTTCGAGCCATAGA | Sense |
| mSnail1 Rv | TGAGGGAGGTAGGGAAGTGG | Antisense |
| mSnail1-e2 Fw (VM experiment) | CACGCTGCCTTGTGTCT | Sense |
| mSnail1-e3 Rv (VM experiment) | GAATGGCTTCTCACCAGTGT | Antisense |
| mSnail1-exon1 Fw (RT-PCR) | AGTTGACTACCGACCTTGCG | Sense |
| mSnail1-exon3 Rv (RT-PCR) | TGGTATCTCTTCACATCCGAG | Antisense |
| mFAP Fw | GGCTGGGGCTAAGAATCCG | Sense |
| mFAP Rv | GCATACTCGTTCACTGGACAC | Antisense |
| mPDGFRα Fw | GGCACAGGTCACCACGAT | Sense |
| mPDGFRα Rv | GCGAGTTTAATGTTTATGCCTTG | Antisense |
| mCD3 Fw | CAGTCAAGAGCTTCAGACAAG | Sense |
| mCD3 Rv | GATGGCTGTACTGGTCATATTC | Antisense |
| mArg1 Fw | CCGATTCACCTGAGCTTTGA | Sense |
| mArg1 Rv | AAAGGAGCCCTGTCTTGTAAAT | Antisense |
| mCD8 Fw | CCATGAGGGACACGAATAATAA | Sense |
| mCD8 Rv | GAGTTCACTTTCTGAAGGACTG | Antisense |
| mFOXP3 Fw | CAATAGTTCCTTCCCAGAGTTC | Sense |
| mFOXP3 Rv | TCGGATAAGGGTGGCATAG | Antisense |
| mVim Fw | CGGCTGCGAGAGAAATTGC | Sense |
| mVim Rv | CCACTTTCCGTTCAAGGTCAAG | Antisense |
| BS1 Fw (ChIP) | GCGCTTGCTTTAGTGGTGAT | Sense |
| BS1 Fw (ChIP) | TTTGGAAAATAGGCACTTAGGA | Antisense |
| BS2 Fw (ChIP) | ATTTGGCTCCACTGTTCTTCC | Sense |
| BS2 Fw (ChIP) | CCGTTTTATTTCACCTTTTTGTT | Antisense |
| BS3 Fw (ChIP) | TGGAGACACCATATTCTAGCAAC | Sense |
| BS3 Fw (ChIP) | TTCATTTTGGCTAAGTCCACATA | Antisense |
| BS4 Fw (ChIP) | TTTCTCTCGGATTGACGCCT | Sense |
| BS4 Rv (ChIP) | CAAATTGAAGCAGTACCAGGCA | Antisense |
| BS5 Fw (ChIP) | TGGATCAATGTCATTCTGTCTG | Sense |
| BS5 Fw (ChIP) | TCTTGGAGCTCCTGCTGAGT | Antisense |
| NC Fw (ChIP) | ATTTTGTGCTGCATAACCTCCT | Sense |
| NC Rv (ChIP) | TAGCAACATCCTAAGCTGGACA | Antisense |

**Table 4| List of qPCR primers used.** VM, *Vivo*-morpholino. ChIP, Chromatin immunoprecipitation.

# 10. Quantification of images

## 10.1. Quantification of KI-67 and Cleaved CASPASE-3

To assess proliferation and apoptosis in subcutaneous tumours and experimental lung metastases, sections were stained with KI-67 and Cleaved CASP-3 antibodies to specifically label proliferating and apoptotic cells, respectively. The stained sections were then imaged using an Olympus FV1200 confocal microscope and the images were analysed using ImageJ software. Proliferation and apoptosis within melanomas were quantified by counting cells in three random fields at the tumour invasive front, tumour centre, and tumour edge in each section. The same number of pictures was taken for each tumour, with four different tumours analysed per condition. For experimental lung metastases, representative images of different metastases were taken from each lung section, with four different lungs examined per condition. The number of proliferating and apoptotic cells was quantified as the density of apoptotic or proliferating tumour cells per square millimetre (cells/ $mm^2$).

## 10.2. Quantification of metastatic burden

Quantification of lung metastatic burden was conducted by collecting nine serial H&E-stained sections at intervals of 150 µm, covering a total depth of 1,200 µm of lung tissue. These sections were imaged using a Leica DFC700T digital camera. The total metastases burden (metastasis area/total lung area *100), number of metastases (number of metastases/ lung) and metastases size (total metastatic area/ number of metastases) were calculated using Image J software.

# 11. *In silico* analyses

## 11.1. RNA-seq

For RNA sequencing, fibroblasts were isolated from $Snail1^{ME}$ -WT and $Snail1^{ME}$ -KO tumours. Mice were initially injected with 5 x $10^6$ GFP-expressing 5555 cells and once tumours reached a volume of 80-100 $mm^3$ four doses of tamoxifen were injected intraperitoneally on alternate days. Finally, mice were sacrificed, and tumours were digested and subjected to RNA extraction using the Arcturus PicoPure RNA Isolation Kit (Thermo Fisher) as previously described.

The integrity and purity of RNA were assessed using the RNA Nano 6000 Assay on the Bioanalyzer 2100 (Agilent). Samples were sent to Novogene Co., where sequencing libraries were prepared using the NEBNext® Single Cell/Low Input RNA Library Prep Kit for Illumina (NEB) following the manufacturer's recommendations. Sequencing was performed using a cBot Cluster Generation Sequencing using PE Cluster Kit cBot-HS (Illumina) according to the manufacturer's instructions. After cluster generation, the library preparations were sequenced on an Illumina platform and 250 bp paired-end reads were generated.

Raw data (raw reads) of FASTQ format were mapped to a mouse reference transcriptome (Mus_musculus.GRCm38.cdna.all.fa) built with Kallisto v.0.46.1. Read quantification to reference transcriptome was performed with Kallisto as well. The following steps were performed using R and RStudio. Tximport was used to import abundance.tsv files to R environment. EdgeR was used for differential expression analysis to obtain DEGlist objects and normalisation. The MatrixStats package was used to determine the statistics on the data. Data was filtered by choosing transcripts with at least 10 reads and later, at least 1 CPM in at least 3 samples. Normalisation factor TMM (trimmed mean of M-values) was applied. Limma and edgeR were used to obtain a final DEG list, which was adjusted by BH (Benjamini-Hochberg) and sorted by p.value<0,05 and LFC >1. Finally, the graphical constructs of the RNA-seq data were performed using gplots, plotly, gprofiler2, clusterprofiler and GSEABase (Mootha et al., 2003; Subramanian et al., 2005).

## 11.2. Analysis of publicly available transcriptomic datasets

To explore the heterogeneity in our RNA-seq samples of CAFs, we conducted a comparative analysis by aligning our transcriptomic data with publicly available datasets detailing different CAF subpopulations across different cancer contexts. Specifically, single-cell RNA sequencing (scRNA-seq) data from a murine melanoma model, reported by Davidson et al. (Davidson et al., 2020) were downloaded from the supplementary information and ArrayExpress database (accession number: E-MTAB-742). Additionally, to enrich this comparative analysis, RNA-seq data from sorted fibroblasts in human breast cancer (Costa et al., 2018) were accessed from the repository EGAS00001002508. Custom gene sets based on differentially expressed genes (DEGs) that define these CAF subpopulations were generated, and Gene Set Enrichment

Analysis (GSEA) was conducted to compare these sets with our dataset (Mootha et al., 2003; Subramanian et al., 2005).

Additionally, to investigate the relationship between *Fap* and *Snail1* gene expression across different cancer types, The Cancer Genome Atlas (TCGA) database was used (The TCGA Research Network: http://www.cancer.gov/tcga). A Pearson correlation analysis was performed using the TCGA database, which encompasses all cancer types, and a significance threshold was established at a p-value <0,05.

## 11.3. Statistical analysis

All statistical tests were carried out using Prism (GraphPad software, version 8.0). For quantitative PCR, tumour burden and cell counting, treatments were compared to their corresponding controls using two tailed Student's t- test. Mice survival was analysed using Kaplan-Meier survival curves, and the log-rank (Mantel-Cox) test was used to compare survival curves using GraphPad Prism. All bar graphs in the study represent Mean ± SEM (Standard Error of the Mean). The levels of statistical significance were indicated as follows: ns = not significant, *= p≤0.05, ** = p≤0.01, *** = p≤0.001, and **** = p≤0.0001.

# RESULTS

## 1. Snail1 expression in murine melanomas

Snail1 is an EMT-TF whose expression has been previously identified in both epithelial (Brenot et al., 2018; Cano et al., 2000) and stromal cells (Alba-Castellón et al., 2016; Stanisavljevic et al., 2015) from carcinomas. In addition, previous studies have explored the impact of Snail1 overexpression in melanoma cells (Kudo-Saito et al., 2009; Liu et al., 2011). However, the expression and contribution of Snail1 to melanoma biology in an *in vivo* context had not been investigated.

With this in mind, we decided to focus our research towards understanding Snail1 expression and function in mouse melanoma models. To this end, we performed a detailed characterization of Snail1 expression in different murine melanoma models to identify which specific cell types within melanomas express this transcription factor.

We first analysed Snail1 expression in tumour samples from a melanoma reporter mouse model available in our laboratory. This model was generated by crossing a BRAF-driven mouse melanoma model $Braf^{CA}$,$Pten^{loxP}$,Tyr::CreERT2 ($Braf^{V600E}$/$Pten^{loxP}$) (Dankort et al., 2009) with Rosa-LSL-tdTomato mice ($Braf^{V600E}$/$Pten^{loxP}$/tdTomato). In this model, treatment with 4-HT induces melanoma development with a short latency (Dankort et al., 2009) and leads to the expression of the tdTomato fluorescent protein in melanocytes and melanoma cells (**Figure 6a**). Immunofluorescence analysis confirmed that SNAIL1 expression was specifically present in tdTomato-negative cells within the $Braf^{V600E}$/$Pten^{loxP}$/tdTomato tumours and absent in the normal skin of these mice, indicating a reactivation of SNAIL1 in the stromal cells but not in the melanoma cells (**Figure 6b**).

To investigate the specific role of Snail1 within the melanoma stroma, we next generated a syngeneic melanoma model in which $Braf^{V600E}$-5555 cells (Dhomen et al., 2009; Hirata et al., 2015) were injected into UBC-Cre-ERT2 mice (Ruzankina et al., 2007) crossed with Rosa-LSL-tdTomato (tdTomato) mice. This model allows the ubiquitous expression of the Tomato fluorescent protein upon tamoxifen administration, facilitating the tracking of red-labelled stromal cells within the allografts, thereby distinguishing them from melanoma cells (**Figure 6c**). Immunofluorescence analysis demonstrated SNAIL1 expression in recombined tdTomato-positive cells within the melanoma microenvironment of $Braf^{V600E}$-tumours, which was not present in the normal skin (**Figure 6d**).

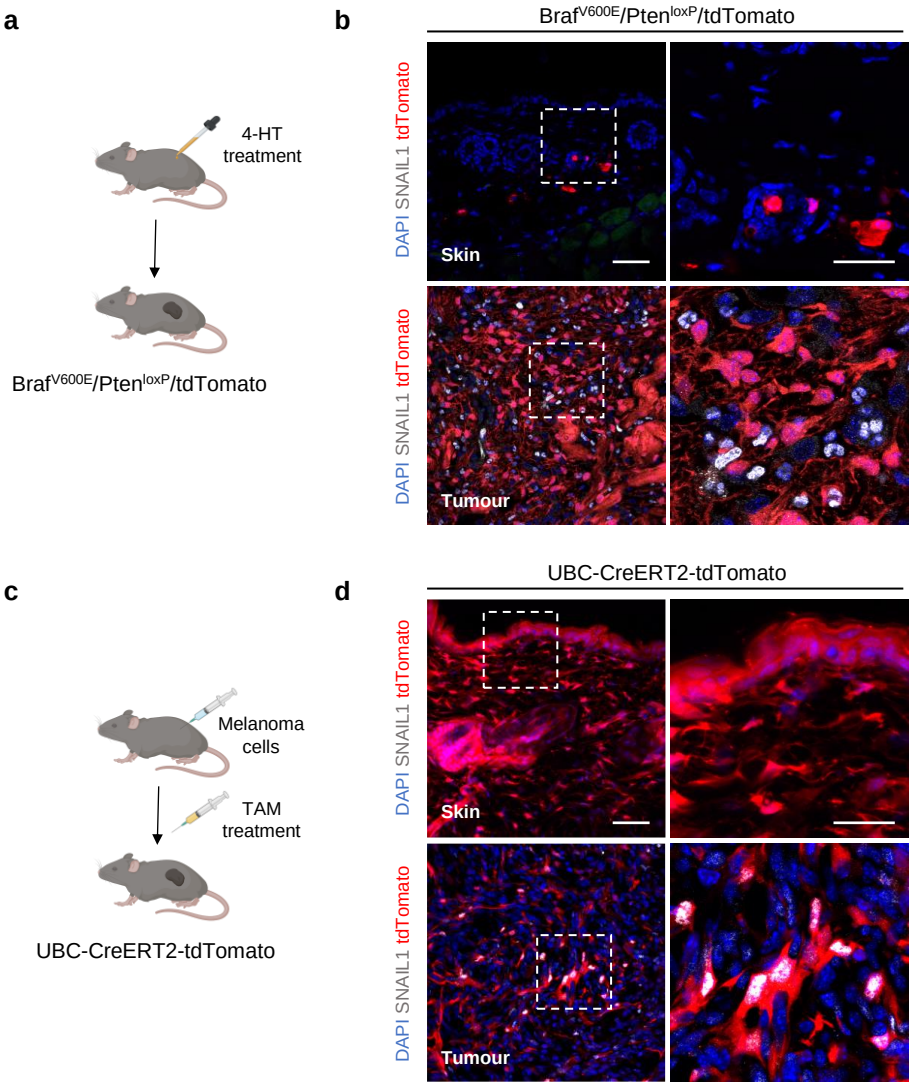


**Figure 6| SNAIL1 is reactivated in the melanoma microenvironment. (a)** Schematic representation of the strategy used to characterize Snail1 expression in Braf$^{CA}$,Pten$^{loxP}$,tdTomato,Tyr::CreERT2 transgenic inducible melanomas. Created with BioRender.com. **(b)** Representative images of immunolabelling for SNAIL1 (white) in control skin (upper panel) and tumours (lower panel) from Braf$^{V600E}$/Pten$^{loxP}$/tdTomato mice. Melanoma cells are labelled in red (tdTomato). **(c)** Schematic representation of the strategy used to investigate Snail1 expression in UBC-CreERT2-tdTomato melanomas. Created with BioRender.com. **(d)** Representative images of immunolabelling for SNAIL1 (white) in control skin (upper panel) and Braf$^{V600E}$-5555 tumours (lower panel) from UBC-CreERT2-tdTomato. Stromal cells are labelled in red (tdTomato). Scale bars: 50µm and 25µm for higher magnification pictures.

To investigate the reactivation of microenvironmental Snail1 (Snail1$^{ME}$) on melanoma, and to determine whether this could be found in different melanoma subtypes, we expanded our study to include additional syngeneic melanoma models. These models were characterized by oncogenic mutations in BRAF*, NRAS*, or WT variants of both (BRAF$^{WT}$/NRAS$^{WT}$), allowing us to assess Snail1 expression across tumours with different oncogenic origins.

To clearly differentiate between melanoma cells and stromal cells within melanomas, we performed subcutaneous injections of GFP-expressing melanoma cells into UBC-CreERT2-tdTomato mice. These melanoma cells harboured specific mutations, including $Braf^{V600E}$ (5555), $Braf^{V600E}Pten^{loxP}$ (FCT1) and $Braf^{V600E}$- $Pten^{loxP}$ $Cdkn2a^{-/-}$ (YUMM1.7). Tamoxifen administration was then initiated to trigger the recombination of the tdTomato protein, leading to the expression of tdTomato in stromal cells. This allowed us to distinguish the red-labelled stromal cells from the GFP-expressing melanoma cells (**Figure 7a**). Through immunofluorescence analyses, we confirmed the reactivation of SNAIL1 within the stromal cells of these BRAF-mutated tumours (**Figure 7b**).

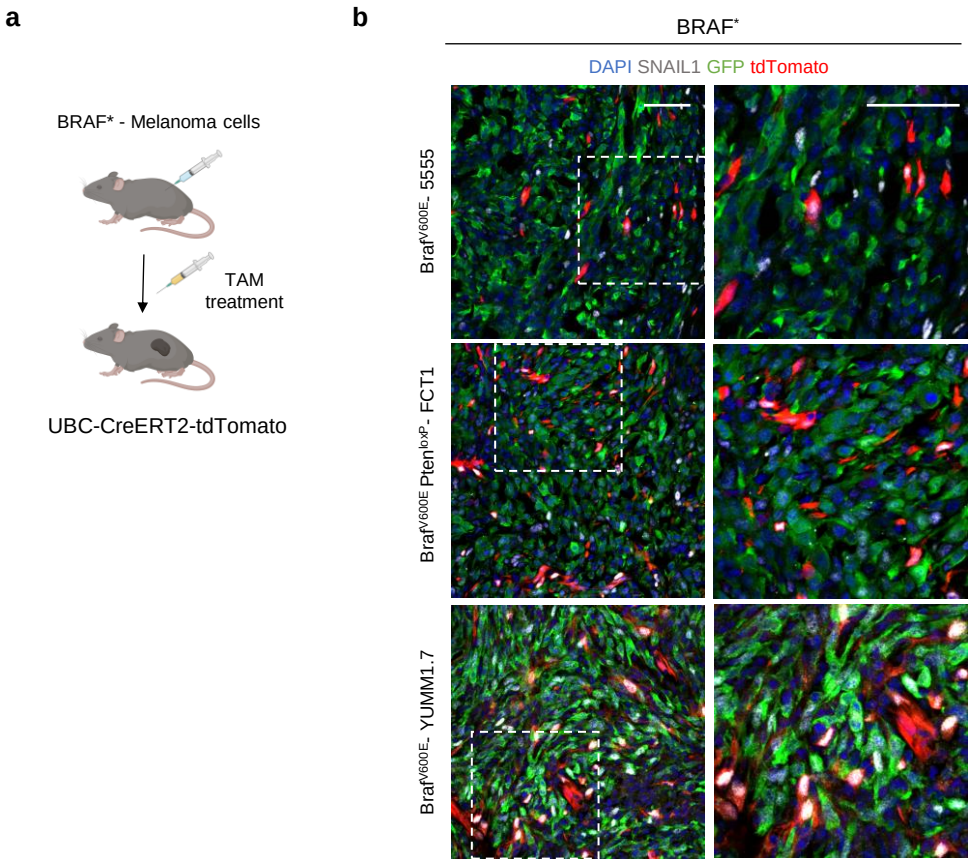


**Figure 7| SNAIL1 is reactivated in different syngeneic melanoma models with oncogenic BRAF mutations. (a)** Schematic representation of the strategy used to study SNAIL1 expression in different BRAF-mutated melanoma cell lines. Created with BioRender.com. **(b)** Representative images of double immunolabeling for SNAIL1 (white), tdTomato (stromal cells) and GFP (green, melanoma cells) in subcutaneous tumours from (a) upon injection of different mouse melanoma cell lines tagged with GFP: 5555 ($Braf^{V600E}$); FCT1 ($Braf^{V600E}Pten^{flox/+}$); YUMM1.7 ($Braf^{V600E}Pten^{flox/flox}Cdkn2a^{-/-}$). Scale bars: 50µm.

Additionally, we carried out subcutaneous injections using $Nras^{Q61K}$ -1014 and $Braf^{WT}Nras^{WT}$-B16F10 GFP-expressing melanoma cells into UBC-CreERT2-tdTomato mice (**Figure 8a**). Upon tamoxifen administration, we confirmed the expression of

SNAIL1 in the stromal cells across these different tumour types (**Figure 8b,c**). These findings suggest that Snail1$^{ME}$ may have a significant impact on melanomas arising from different genetic backgrounds, indicating its broad regulatory potential within the TME.

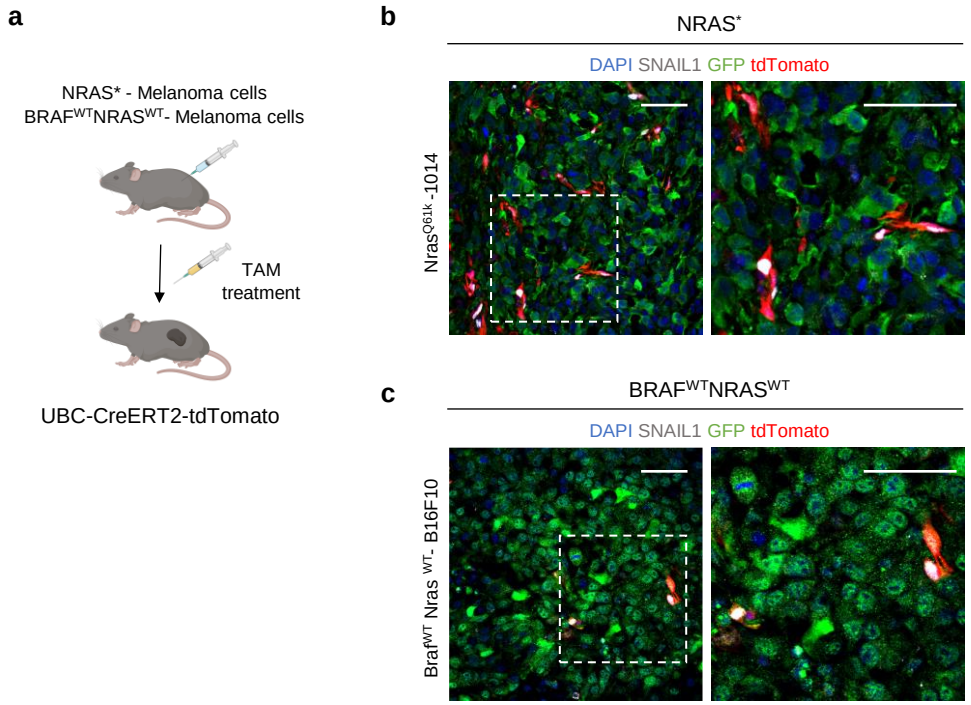


**Figure 8| SNAIL1 is reactivated in syngeneic melanoma models driven by a NRAS oncogenic mutation and in Braf$^{WT}$ Nras$^{WT}$-B16F10 melanomas. (a)** Schematic representation of the strategy used to study SNAIL1 expression in different melanoma cell lines. Created with BioRender.com. **(b, c)** Representative images of double immunolabeling for SNAIL1 (white), tdTomato (stromal cells) and GFP (green, melanoma cells) in subcutaneous tumours from (a) upon injection of 1014 (Nras$^{Q61K}$) and B16F10 (Braf$^{WT}$Nras$^{WT}$), respectively. Scale bars: 50µm.

# 2. Snail1$^{ME}$ contribution to melanoma growth and progression

## 2.1. Generation and validation of Snail1 conditional knockout mice

After identifying that the transcription factor Snail1 is predominantly found in stromal cells within the microenvironment of different melanoma subtypes, we sought to investigate its functional role in melanoma progression. To achieve this, we generated a genetically engineered mouse model by crossbreeding UBC-Cre-ERT2-tdTomato mice with Snail1$^{fl/fl}$ mice (Rowe et al., 2009). This breeding strategy resulted in a mouse model that enabled us to precisely block Snail1 reactivation in the stromal cells (**Figure 9a,b**). Melanomas were generated by subcutaneously injecting Braf$^{V600E}$-5555 cells into UBC-Cre-ERT2-tdTomato-Snail1$^{+/+}$ mice, referred to as Snail1$^{ME}$-WT, and UBC-Cre-ERT2-

tdTomato-Snail1$^{fl/fl}$ mice, referred to as Snail1$^{ME}$-KO (**Figure 9b**). To block Snail1 expression in stromal cells, tamoxifen was administered either prior to the subcutaneous injections or once tumours became detectable and palpable, depending on the experimental aim. Subsequently, melanoma growth was monitored. As expected, immunofluorescence analyses revealed the absence of Snail1 in tdTomato-recombined stromal cells in Snail1$^{ME}$-KO mice, validating both the successful generation of the model and the efficiency of Snail1 deletion (**Figure 9c,d**).

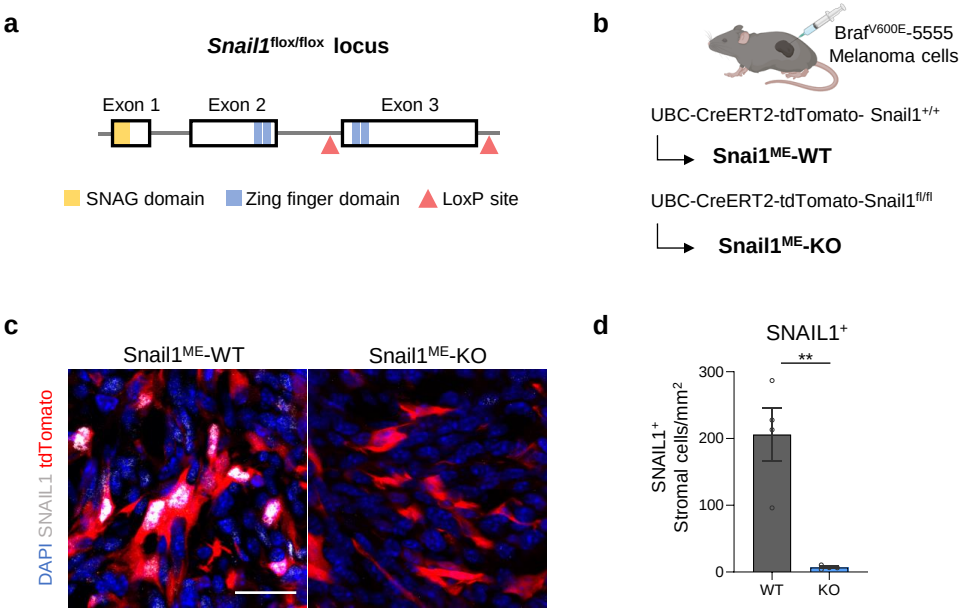


**Figure 9| Validation of a conditional knockout mouse model to address the impact of microenvironmental Snail1 in melanoma progression. (a)** Schematic illustration of the *Snail1* gene. The floxed allele has loxP sites flanking exon 3. **(b)** Mouse models used for the evaluation of Snail1 on the melanoma microenvironment with temporal control of *Snail1* loss of function and tdTomato fluorescence as a recombination reporter. Created with BioRender.com. **(c)** Representative image of immunolabelling for Snail1 (white) in Snail1$^{ME}$-WT (left) and Snail1$^{ME}$-KO (right) tumours upon tamoxifen administration. Stromal cells are labelled in red (tdTomato). **(d)** Quantification of Snail1$^{+}$ stromal cells (n=4 per condition) from Snail1$^{ME}$-WT and Snail1$^{ME}$-KO tumours after tamoxifen administration. Data are represented by Mean±SEM and statistically significant differences are tested by unpaired two-tailed Student t-test. Each dot represents one animal (**=p<0.01).

## 2.2. Snail1 reactivation in the tumour microenvironment promotes melanoma growth

Next, we assessed the impact of Snail1$^{ME}$ on melanoma growth. To do this, we first administered tamoxifen to effectively block stromal Snail1 expression, after which we performed subcutaneous injections of Braf$^{V600E}$-5555 cells into the mice (**Figure 10a**).

Tumour monitoring revealed a trend towards smaller initial tumour sizes in Snail1$^{ME}$-KO mice, which was accompanied by a decreased tumour growth over time (**Figure 10b**).

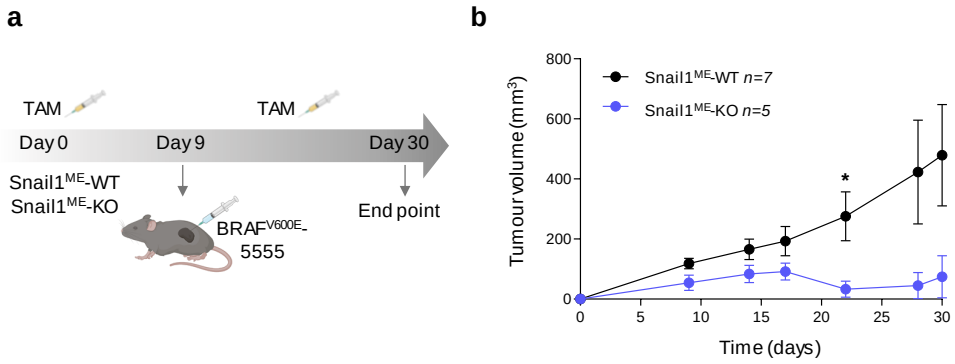


**Figure 10| Snail1$^{ME}$ ablation reduces melanoma establishment and growth. (a)** Schematic representation of the protocol used to evaluate the role of Snail1 to melanoma formation and progression. Created with BioRender.com. **(b)** Braf$^{V600E}$-5555 tumour growth curves comparing Snail1$^{ME}$-WT and Snail1$^{ME}$-KO (n= 7 Snail1$^{ME}$-WT and n= 5 Snail1$^{ME}$-KO). Data are represented by Mean±SEM and statistically significant differences are tested by unpaired two-tailed Student t-test. Each dot represents one animal (*=p<0.05).

This observation led us to investigate further into the contribution of Snail1 during melanoma progression. For that purpose, we designed an experimental approach that recapitulates better the situation in the clinic, where treatment begins upon melanoma detection. Accordingly, Braf$^{V600E}$-5555 cells were subcutaneously injected, and tamoxifen treatment began once melanomas became detected and palpable (**Figure 11a**). Importantly, we found a significant reduction of melanoma growth in Snail1$^{ME}$-KO mice, particularly evident after 13dpi, compared to Snail1$^{ME}$-WT mice, in which tumours continued to grow throughout the experiment (**Figure 11b,c**). These results support the critical role of Snail1 in the melanoma microenvironment in promoting melanoma growth.

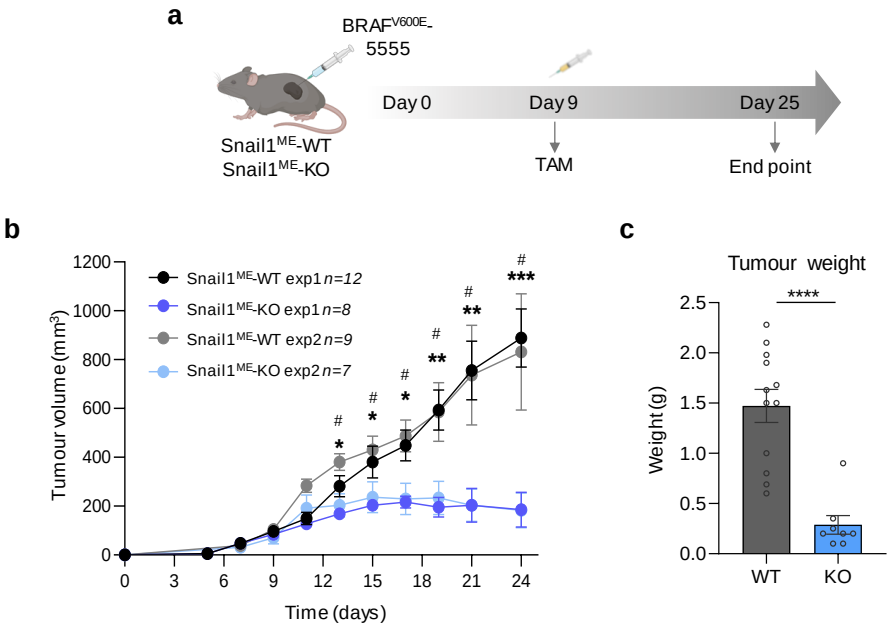


**Figure 11| Snail1$^{ME}$ ablation reduces melanoma growth. (a)** Schematic representation of the protocol used to evaluate the role of Snail1 in melanoma growth. Created with BioRender.com. **(b)** Braf$^{V600E}$-5555 tumour growth curves comparing Snail1$^{ME}$-WT and Snail1$^{ME}$-KO mice assessed in two independent experiments combined in this graph (exp1 n=12 Snail1$^{ME}$-WT and n=8 Snail1$^{ME}$-KO; exp2 n=9 Snail1$^{ME}$-WT and n=7 Snail1$^{ME}$-KO). **(c)** Final weight after collection of tumours from Snail1$^{ME}$-WT (n=12) and Snail1$^{ME}$-KO (n=8) mice. Data are represented by Mean±SEM and statistically significant differences are tested by unpaired two-tailed Student t-test. Each dot represents one animal (*=p<0.05, **=p<0.01, ***p<0.001, ****p<0.0001 and #=p<0.05 for experiment 2). WT=Snail1$^{ME}$-WT and KO= Snail1$^{ME}$-KO.

To explore the mechanisms underlying the observed reductions in tumour size following Snail1$^{ME}$ inhibition, we conducted immunofluorescence analyses to assess tumour cell proliferation and apoptosis (**Figure 12a**). We observed an increased proliferation of melanoma cells in Snail1$^{ME}$-WT tumours, as evidenced by a higher number of KI-67 positive tumour cells compared to Snail1$^{ME}$-KO tumours, which correlated with their larger size (**Figure 12b,c**). In contrast, Snail1$^{ME}$-KO tumours exhibited a greater number of apoptotic melanoma cells, as indicated by an increase in Cleaved CASP-3 positive tumour cells (**Figure 12d,e**). These findings indicate that Snail1 reactivation in the melanoma microenvironment is necessary for melanoma growth, as it plays a protective role in preventing cell death in melanoma cells.

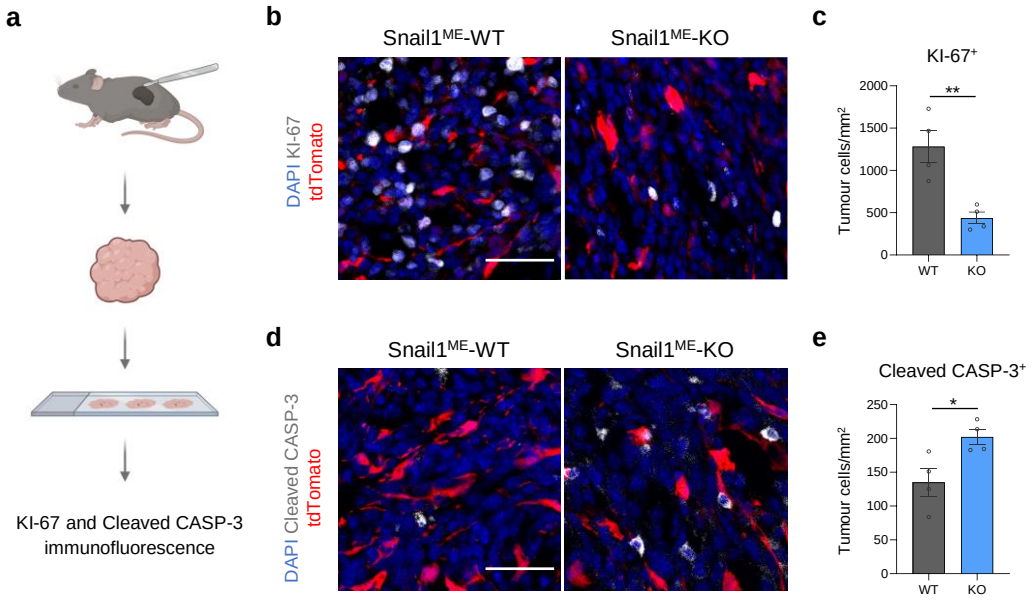


**Figure 12| Snail1$^{ME}$ ablation reduces proliferation and promotes melanoma cell apoptosis. (a)** Schematic representation of the strategy used to evaluate the proliferation and apoptosis of Snail1$^{ME}$-WT and Snail1$^{ME}$-KO tumours. Created with BioRender.com. **(b)** Representative images of immunolabelling for KI-67(white) in tumours from Snail1$^{ME}$-WT (left) and Snail1$^{ME}$-KO (right) mice. Stromal cells are labelled in red (tdTomato). (c) Quantification of KI-67 (white) tumour nuclei-positive cells in images from (b) (n=4). **(d)** Representative images of immunolabelling for Cleaved CASP-3 (white) in Snail1$^{ME}$-WT and Snail1$^{ME}$-KO tumours. Stromal cells are labelled in red (tdTomato). **(e)** Quantification of images from (d) (n=4). Data are represented by Mean±SEM and statistically significant differences are tested by unpaired two-tailed Student t-test. Each dot represents one animal (*=p<0.05, **=p<0.01). WT=Snail1$^{ME}$-WT and KO= Snail1$^{ME}$-KO. Scale bars: 50µm.

## 2.3. Snail1 is reactivated in melanoma-associated fibroblasts within the TME

Upon confirming Snail1 reactivation in the melanoma stroma and its impact in modulating tumour growth, we aimed to further characterize its functional role. For this purpose, Snail1 expression was first assessed by immunofluorescence in the main stromal cells present in tumours (**Figure 13**, **Figure *14***).

Previous studies have shown the expression of Snail1 and other EMT-TFs in macrophages (Cortés et al., 2017) and CAFs (Alba-Castellón et al., 2016; Blanco-Gomez et al., 2020; K.-W. Lee et al., 2022; Stanisavljevic et al., 2015) in epithelial-derived tumours.

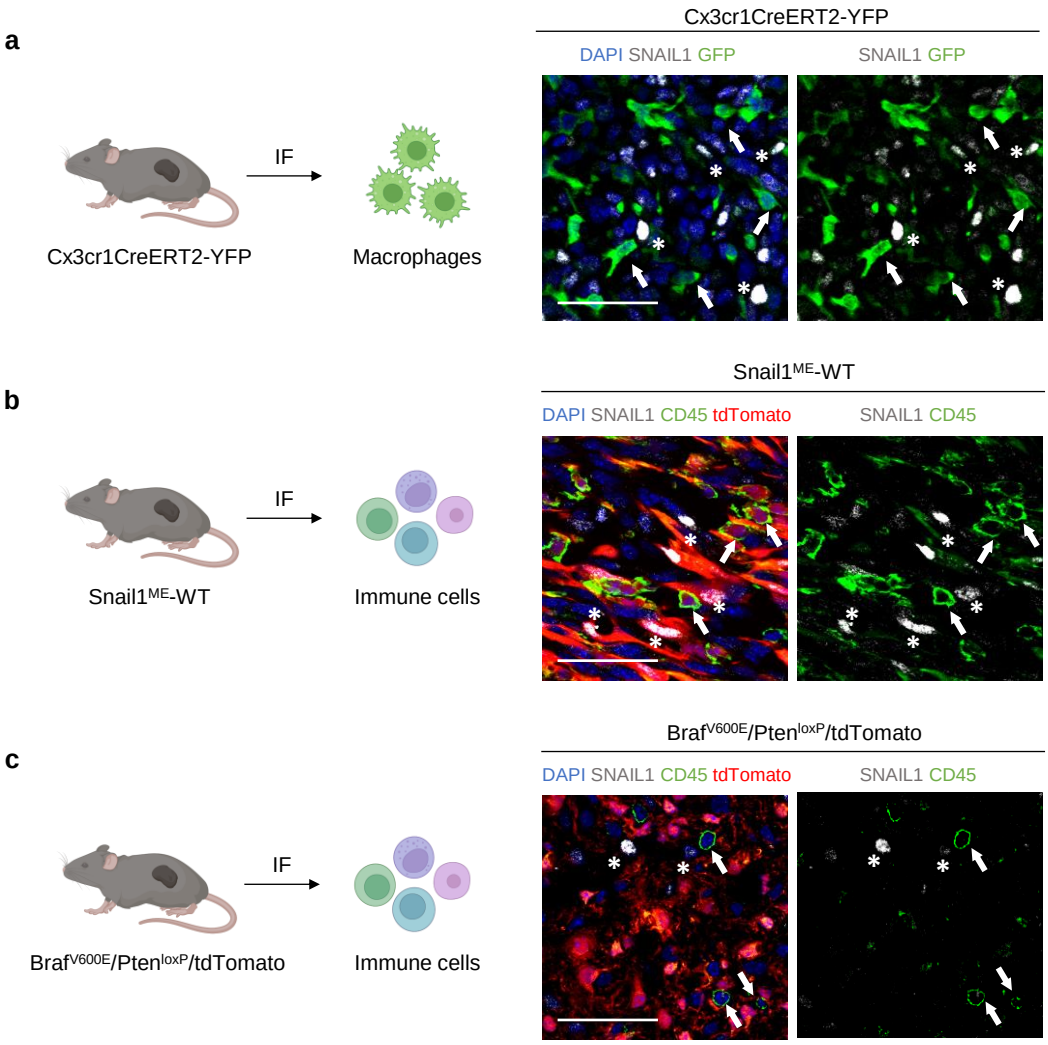


**Figure 13| SNAIL1 is not expressed in the immune microenvironment of melanomas. (a)** Representative images of immunolabelling for SNAIL1 (white) and myeloid cells (green) in a section of a Braf$^{V600E}$-5555 melanoma grown in Cx3cr1CreERT2-YFP mice. Arrows indicate macrophages, asterisks indicate SNAIL1$^{+}$ cells. **(b)** Representative images of immunolabelling for SNAIL1 (white) and CD45 (green, immune cells) in melanomas from Snail1$^{ME}$-WT mice. Stromal cells are labelled in red (tdTomato). Arrows indicate double-positive tdTomato$^{+}$CD45$^{+}$ immune cells, asterisks indicate SNAIL1$^{+}$ cells. **(c)** Representative images of double immunolabeling for SNAIL1 (white) and CD45 (green, immune cells) in Braf$^{V600E}$/Pten$^{loxP}$/tdTomato melanoma model. tdTomato indicates melanoma cells (red). Arrows indicate immune cells, asterisks highlight SNAIL1$^{+}$ stromal cells. Scale bars: 50µm. IF, immunofluorescence. Created with BioRender.com.

To investigate Snail1 expression in these cell populations in melanoma, we first analysed Braf$^{V600E}$-5555 tumours grown in Cx3cr1CreERT2-YFP reporter mice. These mice are characterised by constitutive YFP expression in the myeloid lineage (Geissmann et al., 2003; Jung et al., 2000), including both monocytes and macrophages. Immunofluorescence analysis revealed that SNAIL1 was not expressed in Cx3cr1-positive cell populations in our tumour samples (**Figure 13a**).

We extended our analysis to include additional immune subsets by using CD45 staining as a marker for the immune cells. Consistently, our results demonstrated an absence of SNAIL1 expression in CD45-positive immune cells in Snail1$^{ME}$-WT (**Figure 13b**). This finding was further confirmed in the Braf$^{V600E}$/Pten$^{loxP}$/tdTomato melanoma transgenic model (**Figure 13c**).

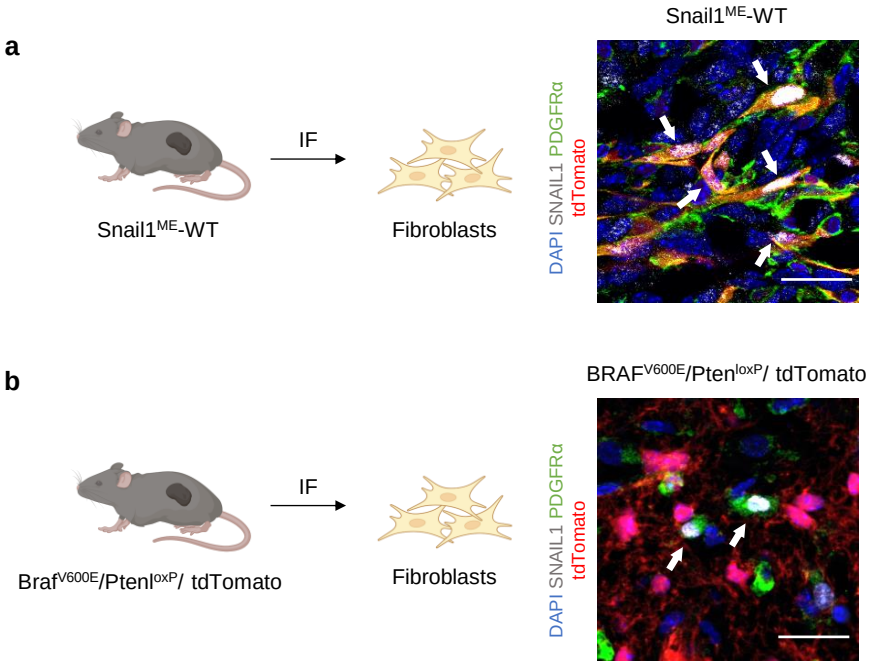


**Figure 14| SNAIL1 is predominantly reactivated in melanoma-associated fibroblasts. (a)** Representative image of immunolabelling for SNAIL1 (white) and PDGFRα (green) in Braf$^{V600E}$-5555 tumours from Snail1$^{ME}$-WT mice. Stromal cells are labelled in red (tdTomato). Arrows indicate fibroblasts (triple-positive for SNAIL1$^{+}$PDGFRα$^{+}$tdTomato$^{+}$). **(b)** Representative image of immunolabelling for SNAIL1 (white) and PDGFRα (green) in Braf$^{V600E}$/PtenI$^{oxP}$/ tdTomato melanomas in which tumour cells are labelled in red (tdTomato). Arrows indicate fibroblasts (SNAIL1$^{+}$PDGFRα$^{+}$tdTomato$^{-}$). Scale bars: 25µm. IF, immunofluorescence. Created with BioRender.com.

In contrast, SNAIL1 expression was detected in melanoma-associated fibroblasts, as indicated by double staining for PDGFRα and tdTomato in Snail1$^{ME}$-WT tumours (**Figure 14a**). This result was further confirmed in the melanoma transgenic Braf$^{V600E}$/Pten$^{loxP}$/tdTomato model, where SNAIL1 was also found in PDGFRα$^{+}$tdTomato$^{-}$ melanoma-associated fibroblasts (**Figure 14b**). Altogether, these results indicate that Snail1 is mainly expressed in CAFs and is absent in immune cell populations.

## 2.4. Snail1 reactivation in CAFs promotes melanoma growth

Given our previous findings indicating that SNAIL1 is predominantly expressed in CAFs from the melanoma microenvironment, we sought to determine whether the observed reduction in tumour growth could be specifically attributed to this fibroblast population.

In order to explore the functional relevance of SNAIL1 in regulating tumour growth within the CAF population, we used a PDGFRα-CreERT2-tdTomato reporter mouse model crossed with Snail1$^{fl/fl}$ (Rowe et al., 2009) mice. This model allowed us to temporally control *Snail1* loss-of-function specifically in PDGFRα-positive fibroblasts. Melanomas were induced by subcutaneous injections of Braf$^{V600E}$-5555 cells into PDGFRα-CreERT2-tdTomato reporter mice, referred to as PDGFRα-Snail1 WT, and into PDGFRα-CreERT2-tdTomato-Snail1$^{fl/fl}$ mice, referred to as PDGFRα-Snail1 KO mice (**Figure 15a**).

Our immunofluorescence analyses confirmed SNAIL1 reactivation in PDGFRα$^{+}$-tdTomato labelled cells, consistent with our previous results from the Snail1$^{ME}$-WT mouse model. Additionally, we confirmed that SNAIL1 expression was successfully blocked following tamoxifen administration, thus validating the effectiveness of this mouse model (**Figure 15b**).

Notably, our studies revealed that blocking Snail1 expression in PDGFRα$^{+}$ CAFs prior to melanoma cells injection (**Figure 15c**) resulted in reduced tumour growth (**Figure 15d**) and improved survival rates in mice (**Figure 15e**). To extend our understanding, we also assessed the impact of blocking Snail1 activity in PDGFRα-positive fibroblasts on already established tumours (**Figure 16a**). The results showed a significant decrease in melanoma growth compared to the control group (**Figure 16b,c**).

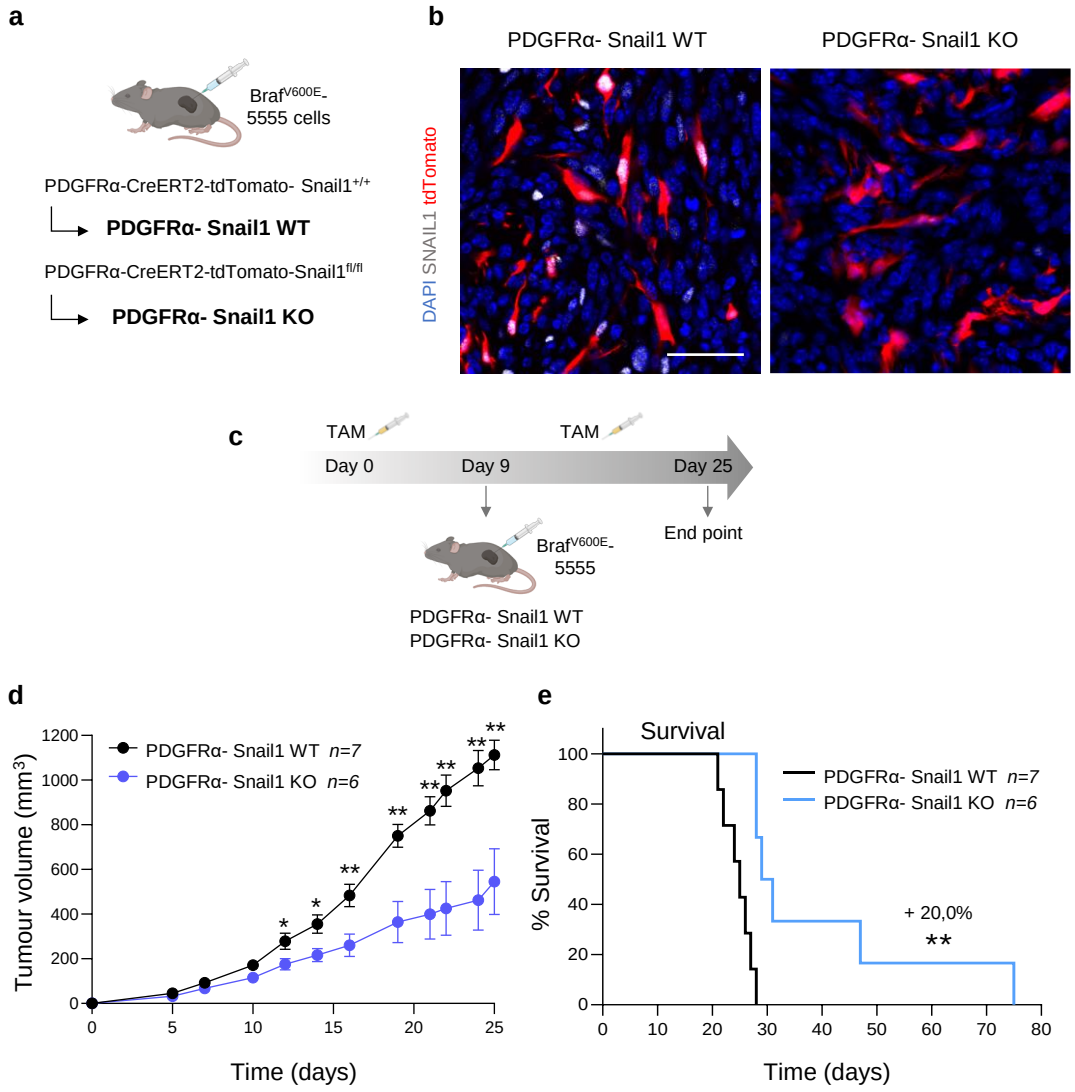


**Figure 15| Snail1 ablation in PDGFRα⁺ fibroblasts reduces melanoma growth and improves mice survival. (a)** Mouse models used for the evaluation of Snail1 impact on melanoma-associated fibroblasts (PDGFRα⁺). Created with BioRender.com. **(b)** Representative images of immunolabelling for SNAIL1 (white) in PDGFRα-CreERT2-tdTomato (PDGFRα-Snail1 WT) (left) and PDGFRα-CreERT2-tdTomato-Snail1$^{fl/fl}$ (PDGFRα-Snail1 KO) (right) tumours upon tamoxifen administration. tdTomato indicates PDGFRα+ cells (red). **(c)** Schematic representation of the protocol used to evaluate the role of Snail1 in PDGFRα⁺-fibroblasts to melanoma formation and progression. Created with BioRender.com. **(d)** Braf$^{V600E}$-5555 tumour growth curves comparing PDGFRα- Snail1 WT and PDGFRα- Snail1 KO mice after tamoxifen administration (n=7 WT and n=6 KO). **(e)** Overall survival of PDGFRα- Snail1 WT and PDGFRα- Snail1 KO mice with Braf$^{V600E}$-5555 melanomas after Snail1-silencing compared to controls (n=7 WT and n=6 KO). Data are represented by Mean±SEM and statistically significant differences are tested by unpaired two-tailed Student t-test (*=p<0.05 and **=p<0.01). Scale bar: 50µm.

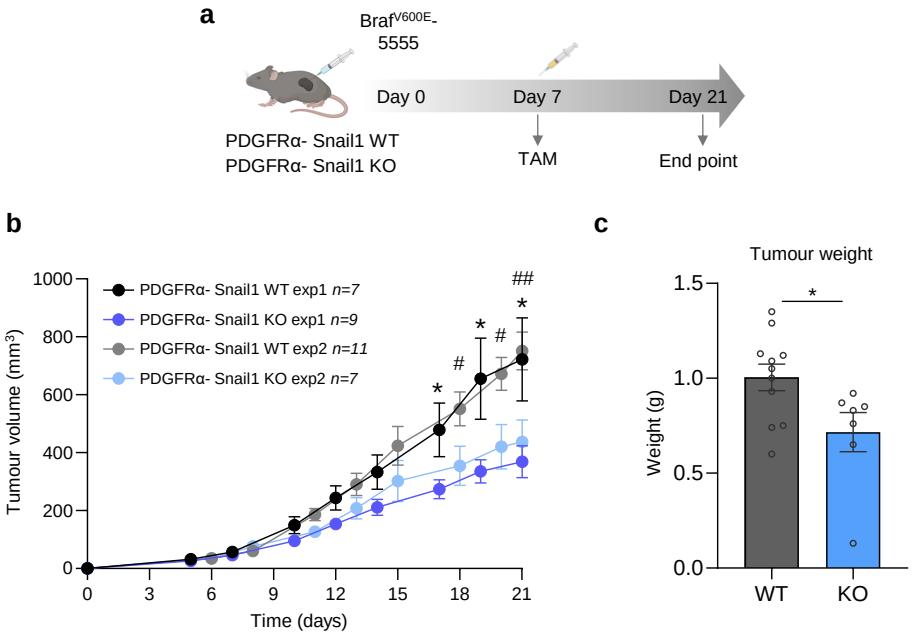


**Figure 16| Snail1 ablation in PDGFRα-positive fibroblasts reduces melanoma growth. (a)** Schematic representation of the protocol used to evaluate the role of Snail1 in PDGFRα$^{+}$-fibroblasts to melanoma progression. Created with BioRender.com. **(b)** Braf$^{V600E}$-5555 tumour growth curves comparing PDGFRα- Snail1 WT and PDGFRα- Snail1 KO mice assessed in two independent experiments combined in this graph (exp1 n=7 WT and n=9 KO; exp2 n=11 WT and n=7 KO). **(c)** Final weight after collection of tumours from (a) PDGFRα- Snail1 WT (n=11) and PDGFRα- Snail1 KO mice (n=7). Data are represented by Mean±SEM and statistically significant differences are tested by unpaired two-tailed Student t-test. Each dot represents one animal (*=p<0.05 and #=p<0.05, ##=p<0.01 for experiment 2). WT= PDGFRα- Snail1 and KO= PDGFRα- Snail1.

Altogether, these findings highlight the crucial role that Snail1$^{+}$ melanoma-associated fibroblasts in driving tumour growth.

# 3. Mechanisms underlying the regulatory function of Snail1$^{ME}$ in melanoma growth

Upon establishing that Snail1 is predominantly expressed in CAFs and that its targeting in these cells leads to reduced melanoma growth, we aimed to elucidate the underlying mechanisms. To identify Snail1 downstream targets in fibroblasts, we performed a transcriptomic analysis comparing Snail1-WT and Snail1-KO fibroblasts, isolated from Snail1$^{ME}$-WT and Snail1$^{ME}$-KO tumours, respectively.

## 3.1. Snail1 expression is associated to immunosuppressive gene signatures in melanoma-associated fibroblasts.

First, to isolate fibroblasts, we used melanomas from Snail1$^{ME}$-WT and Snail1$^{ME}$-KO mice, generated by injecting GFP-expressing Braf$^{V600E}$-5555 cells. These mice were treated with tamoxifen until tumours were dissected and digested using a cold enzymatic solution. Fibroblasts were then labelled with an APC-conjugated anti-PDGFRα antibody and sorted by FACS as PDGFRα$^{+}$tdTomato$^{+}$GFP$^{-}$ cells (**Figure 17a**). We strategically selected an early time point for tumour sample collection, when considerable tumour size differences were already evident between both groups but Snail1-KO tumours had not yet fully regressed (**Figure 17b**).

Before proceeding with RNA sequencing, we confirmed the integrity and specificity of the isolated cell population through RT-qPCR and immunofluorescence analyses. As expected, we found an enrichment of *Pdgfrα* levels in the sorted samples compared to the non-sorted controls by RT-qPCR (**Figure 17c**). Additionally, we confirmed *Snail1* downregulation in PDGFRα$^{+}$tdTomato$^{+}$ cells from Snail1-KO mice at the chosen time point (**Figure 17c**). Further validation at the protein level corroborated that the isolated cells were positive for PDGFRα, SNAIL1, and α-SMA, another marker commonly associated with CAFs (**Figure 17d,e**). These results demonstrated the successful isolation of a highly specific fibroblast population for further analyses.

Subsequently, we performed transcriptomic analysis on the isolated Snail1-WT and Snail1-KO fibroblasts samples, each consisting of PDGFRα$^{+}$tdTomato$^{+}$GFP$^{-}$ cells pooled from three mice of the same genotype. Differential gene expression analysis was performed, and hierarchical clustering revealed that samples from the same group clustered together (**Figure 18**). Notably, among the 520 differentially expressed genes (DEGs) detected upon Snail1 targeting, 323 were upregulated and 197 were

downregulated, which is consistent with Snail1 role as a transcriptional repressor (Cano et al., 2000).

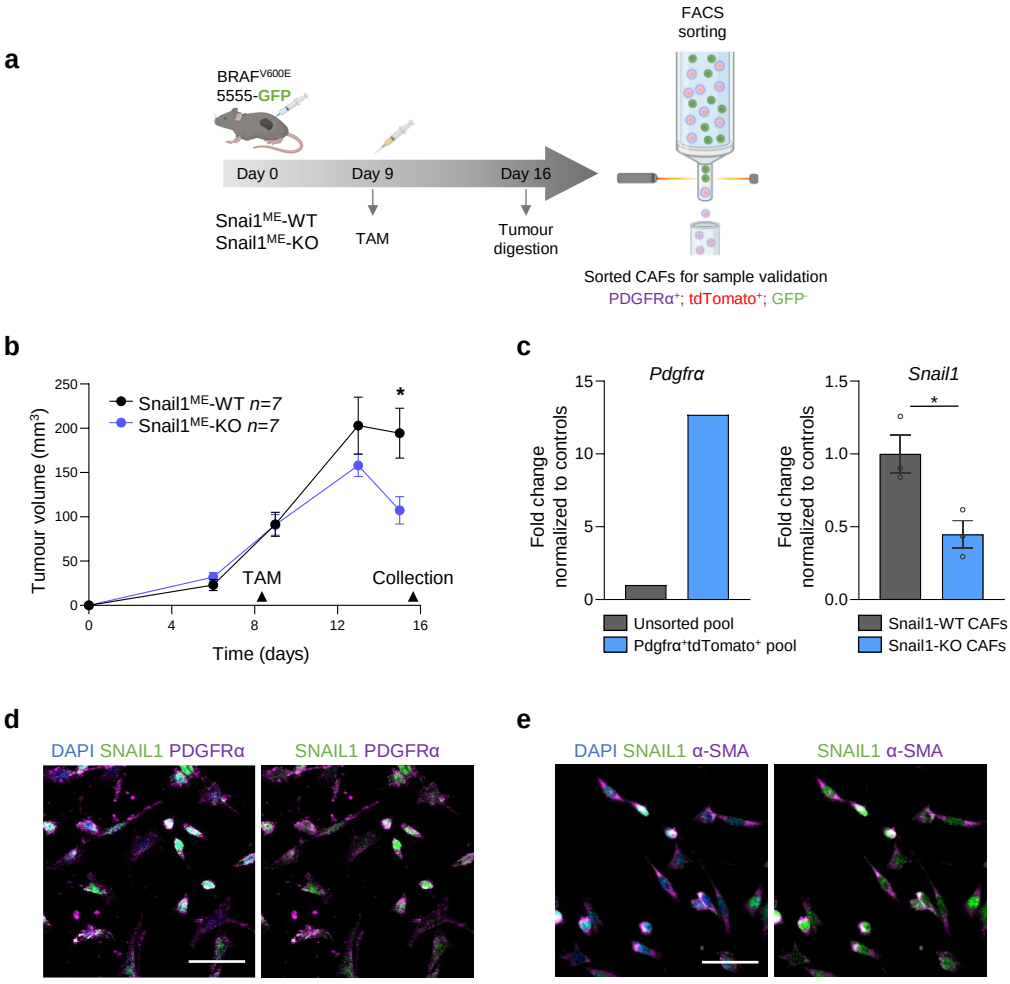


**Figure 17| Strategy for the isolation and validation of fibroblasts from Snail1$^{ME}$-WT and Snail1$^{ME}$-KO tumours. (a)** Schematic representation of the strategy used to isolate fibroblastrs from Braf$^{V600E}$-5555 melanomas grown subcutaneously in Snail1$^{ME}$-WT and Snail1$^{ME}$-KO mice. Created with BioRender.com. **(b)** Tumour growth graph of a representative experiment showing the selected time point for CAFs isolation (Snail1$^{ME}$-WT=7 and Snail1$^{ME}$-KO=7). **(c)** *Pdgfrα* and *Snail1* mRNA levels assessed by RT-qPCR to validate the fibroblasts population isolated by FACS (Pdgfrα$^{+}$tdTomato$^{+}$GFP$^{-}$) from tumours in (a) (samples from 3 animals with the same genotype were pooled for each condition). **(d,e)** Representative images of double immunolabeling for SNAIL1 (green) and different CAFs markers (magenta), specifically PDGFRα in the right panel and α-SMA in the left panel, magenta), in cells isolated from tumours in (a) after FACS-sorting (Pdgfrα$^{+}$tdTomato$^{+}$GFP$^{-}$). Scale bars: 50µm. Data are represented by Mean±SEM and statistically significant differences are tested by unpaired two-tailed Student t-test (*=p<0.05).

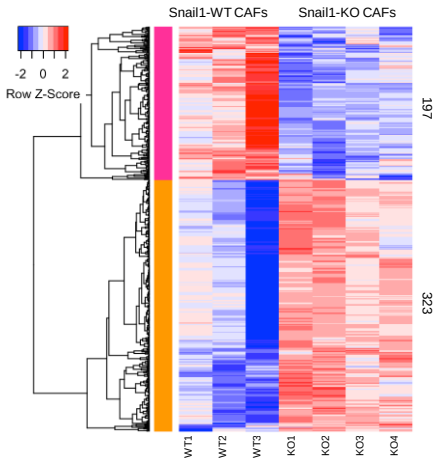


**Figure 18| Differential gene expression in Snail1-WT and Snail1-KO sorted fibroblasts.** Cluster analysis heatmap from the differentially expressed genes (DEGs) with a -2–2 Z score scale. It presents filtered and normalized counts per million data from DEGs, comparing Snail1-WT and Snail1-KO CAFs. Each column represents a different sample, each comprising three animals of the same genotype: WT n=3 and KO n=4.

With the aim of identifying the molecular mechanism underlying Snail1 function in the CAFs, we next performed a gene ontology enrichment analysis on the DEGs in Snail1-KO fibroblasts (**Figure 19**). Our analysis indicated a significant enrichment of biological processes associated with morphogenesis and differentiation among the upregulated genes upon Snail1 silencing (**Figure 19a**), which is consistent with the well-established role of Snail1 in embryonic development (Carver et al., 2001; Nieto et al., 1992).

In contrast, analysis of the downregulated genes demonstrated a significant association with immune system processes. Notably, 11 of the 15 most enriched biological processes were associated with immune system functions (**Figure 19b**). These findings strongly suggest that Snail1 may play a crucial role in shaping the immunological landscape within the TME, potentially through mechanisms such as the regulation of cytokine secretion or the alteration of immune cell infiltration patterns.

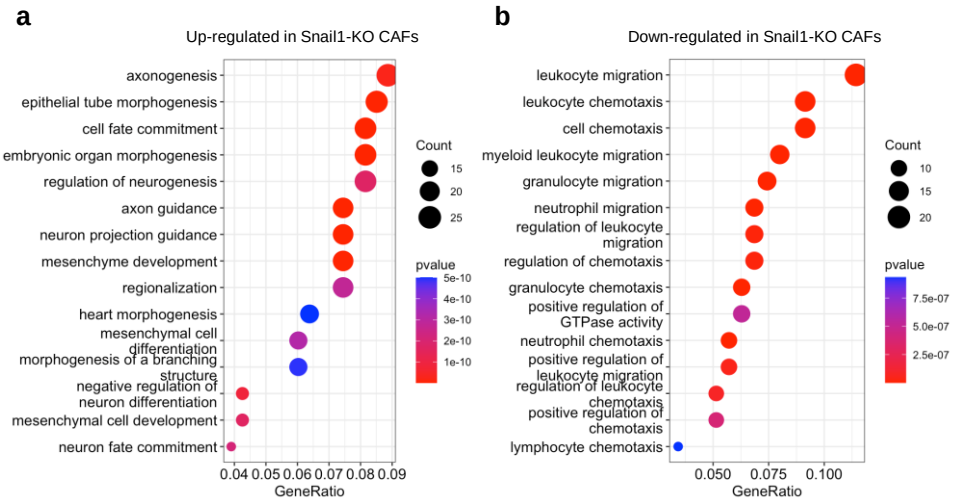


**Figure 19| Gene ontology enrichment analysis of the differentially expressed genes. (a)** Dot plot of the 15 most significant GO terms of the up-regulated genes. **(b)** Dot plot of the 15 most significant GO terms of the down-regulated genes. Dot size and colour indicate the number and significance of genes within each set, respectively.

Further exploration using GSEA (Subramanian et al., 2005) analysis indicated that melanoma-associated fibroblasts were characterized by an enrichment of pathways related to TGFβ signalling, EMT, fibroblasts activation in carcinomas, and pathways linked to both immunosuppression and pro-inflammatory responses (Erez et al., 2010). Notably, this enrichment was diminished in Snail1-KO fibroblasts (**Figure 20a**). Given the downregulation of genes and pathways predominantly associated with immunosuppression in Snail1-KO fibroblasts, we performed a DEG analysis focused on immunosuppressive genes (**Figure 20b**). Specifically, key immunosuppressive genes such as *Ccl1*, *Ccl22*, *Cxcl13*, *Fap* or *Ccr7,* which have been previously associated with suppressing anti-tumour immune activity (Kuehnemuth et al., 2018; Martinenaite et al., 2016; Ren et al., 2022; Weber et al., 2020; Wiedemann et al., 2016; Yang et al., 2016), were significantly downregulated in Snail1-KO fibroblasts (**Figure 20b,c,d**). These results suggest a potential enrichment of the anti-tumour immune response in tumours lacking Snail1$^{ME}$.

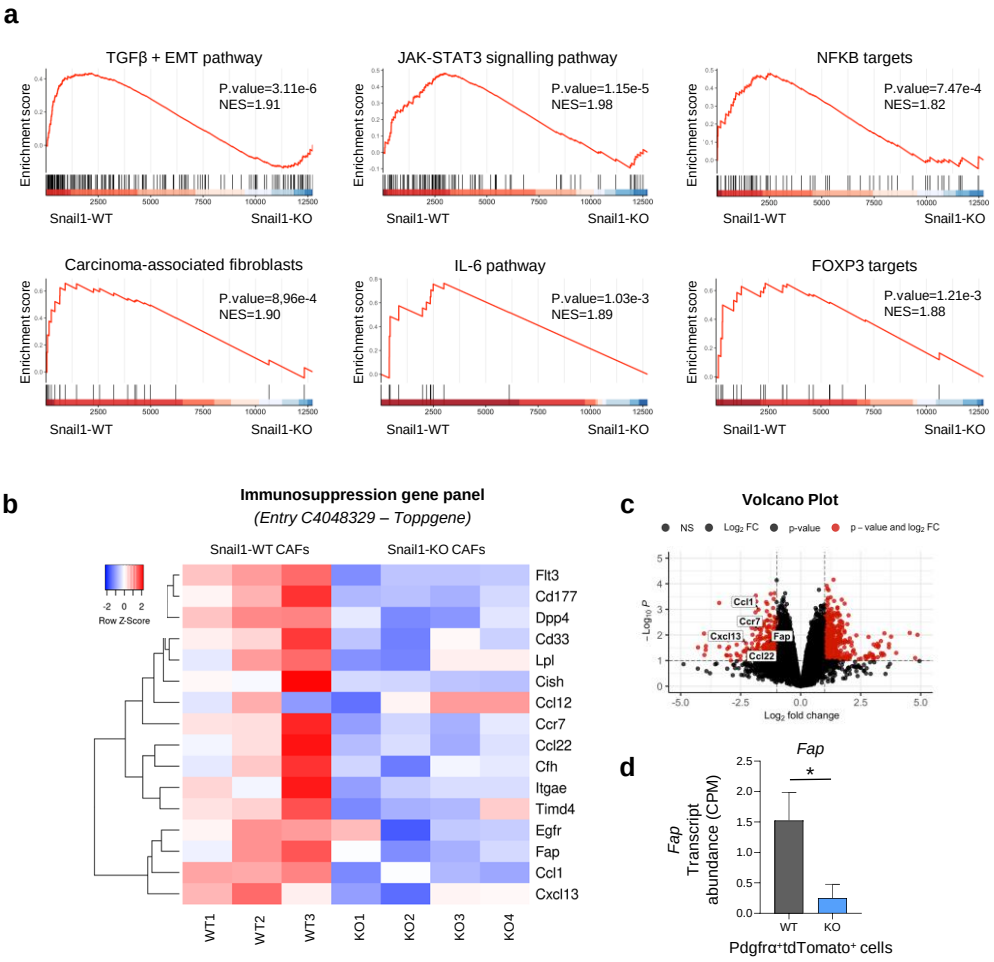


**Figure 20| Snail1 in PDGFRα-positive CAFs is associated with fibroblasts activation and immunosuppressive signatures. (a)** Gene set enrichment analysis (GSEA) of DEGs genes ranked by log2 ratios, revealing the enrichment of the indicating signatures in Snail1-WT CAFs. Normalised enrichment score (NES) and corresponding p-values are represented. **(b)** Heatmap panel showing the expression of genes associated with immunosuppression from entry C4048329 in the TopGene and DisGeNet databases. **(c)** Volcano plot of Log2 fold change of DEGs from Snail1-WT and Snail1-KO fibroblast samples. The red dots on the right represent the upregulated genes and the red dots on the left the downregulated genes. **(d)** *Fap* transcript quantification in Pdgfrα$^{+}$tdTomato$^{+}$ fibroblasts from RNA-seq analysis (CPM, counts per million) of melanomas grown in Snail1-WT (WT) and Snail1-KO (KO) mice.

## 3.2. Snail1 expression is associated to immunosuppressive gene signatures in CAFs from additional mouse and patient´s tumours

To better understand the role of Snail1 in CAFs, we took advantage of publicly available transcriptomic datasets of fibroblasts populations (**Figure 21**). Interestingly, aligning our transcriptomic data with melanoma stromal scRNA-seq data (Davidson et al., 2020), we observed that Pdgfrα$^{+}$tdTomato$^{+}$ fibroblasts from Snail1$^{ME}$-WT tumours were significantly enriched in signatures corresponding to S1 (“immune”) and S2 (“desmoplastic”) CAF subpopulations. Importantly, the most significant differential signature between our Pdgfrα$^{+}$tdTomato$^{+}$ cells from Snail1$^{ME}$-WT and Snail1$^{ME}$-KO tumours was linked to the S1 (“immune”) subpopulation (**Figure 21a**), which is characterized by an elevated expression of immunomodulatory factors (Davidson et al., 2020).

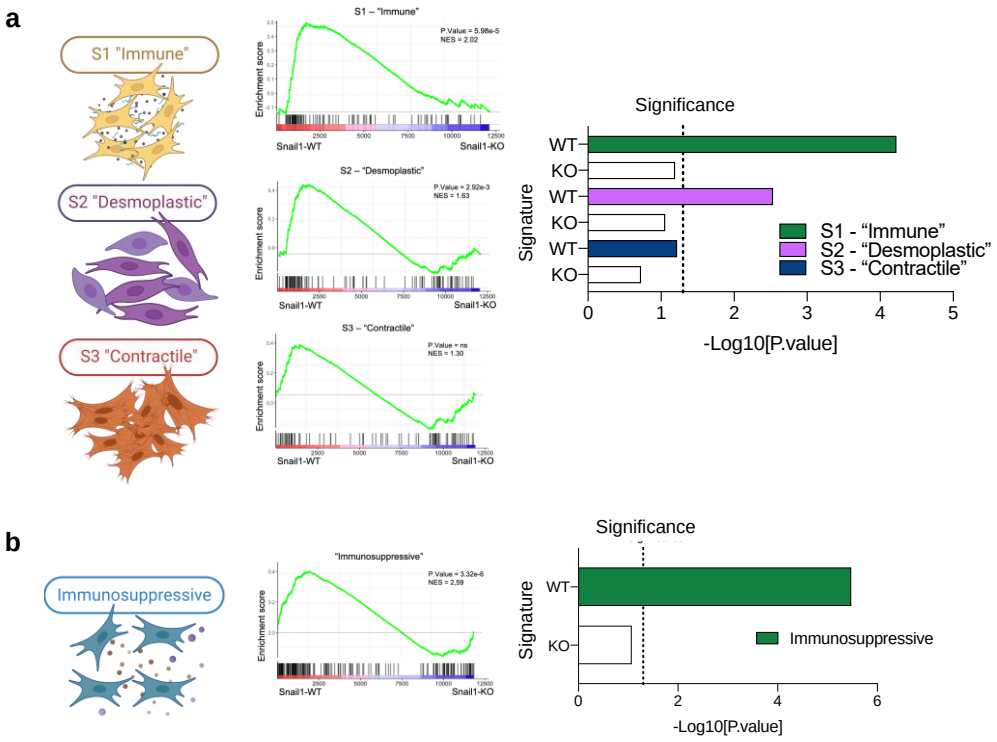


**Figure 21| Comparative analysis of Snail1-WT and Snail1-KO fibroblasts with additional transcriptomic datasets. (a)** GSEA analysis of custom gene sets derived from DEGs in the S1 “immune”, S2 “desmoplastic”, and S3 “contractile” CAFs subpopulations as defined by (Davidson et al., 2020). **(b)** GSEA analysis of marker gene sets in the immunosuppressive breast CAF subpopulation, as defined by (Costa et al., 2018). Normalized enrichment score (NES) and corresponding p-values are represented. Ns, not significant. Created with BioRender.com.

To further corroborate these findings, we conducted an additional analysis by comparing our transcriptomic data with an independent dataset obtained from human breast cancer CAFs (**Figure 21b**), previously identified as immunosuppressive (Costa et al., 2018). Together, these results confirm the potential role of Snail1 in promoting immunosuppression when expressed in CAFs.

## 3.3. Snail1 in melanoma-associated fibroblasts regulates anti-tumour immune responses

Our transcriptomic analyses strongly suggested that the anti-tumour effects observed upon Snail1 targeting in the melanoma microenvironment were closely associated with the immunoregulatory functions of CAFs. To determine whether these transcriptional alterations corresponded to changes in immune cell infiltration, we next performed flow cytometry analysis on $Braf^{V600E}$-5555 melanomas grown in $Snail1^{ME}$-WT and $Snail1^{ME}$-KO mice (**Figure 22a**).

Strikingly, consistent with the impaired melanoma growth, we observed a higher percentage of tumour-infiltrating cytotoxic T cells ($CD8a^{+}$) in $Snail1^{ME}$-KO tumours compared to $Snail1^{ME}$-WT tumours (**Figure 22b**). Additionally, we detected a significant decrease of regulatory T cells ($FOXP3^{+}$) within $Snail1^{ME}$-KO tumours (**Figure 22c**). Further analysis revealed an increased presence of B cells and Natural Killer cells in tumours from $Snail1^{ME}$-KO mice (**Figure 22d**), while the populations of dendritic and myeloid cells remained constant (**Figure 22e,f**). However, we detected increased levels of *Arginase 1* (*Arg1*) in melanomas from $Snail1^{ME}$-WT mice (**Figure 22g**), a marker for M2-like macrophages with known immunosuppressive and protumorigenic functions (Movahedi et al., 2010).

Collectively, these results provide evidence that $Snail1^{ME}$ acts as an inhibitor of the anti-tumour immune responses, thus promoting melanoma progression.

.

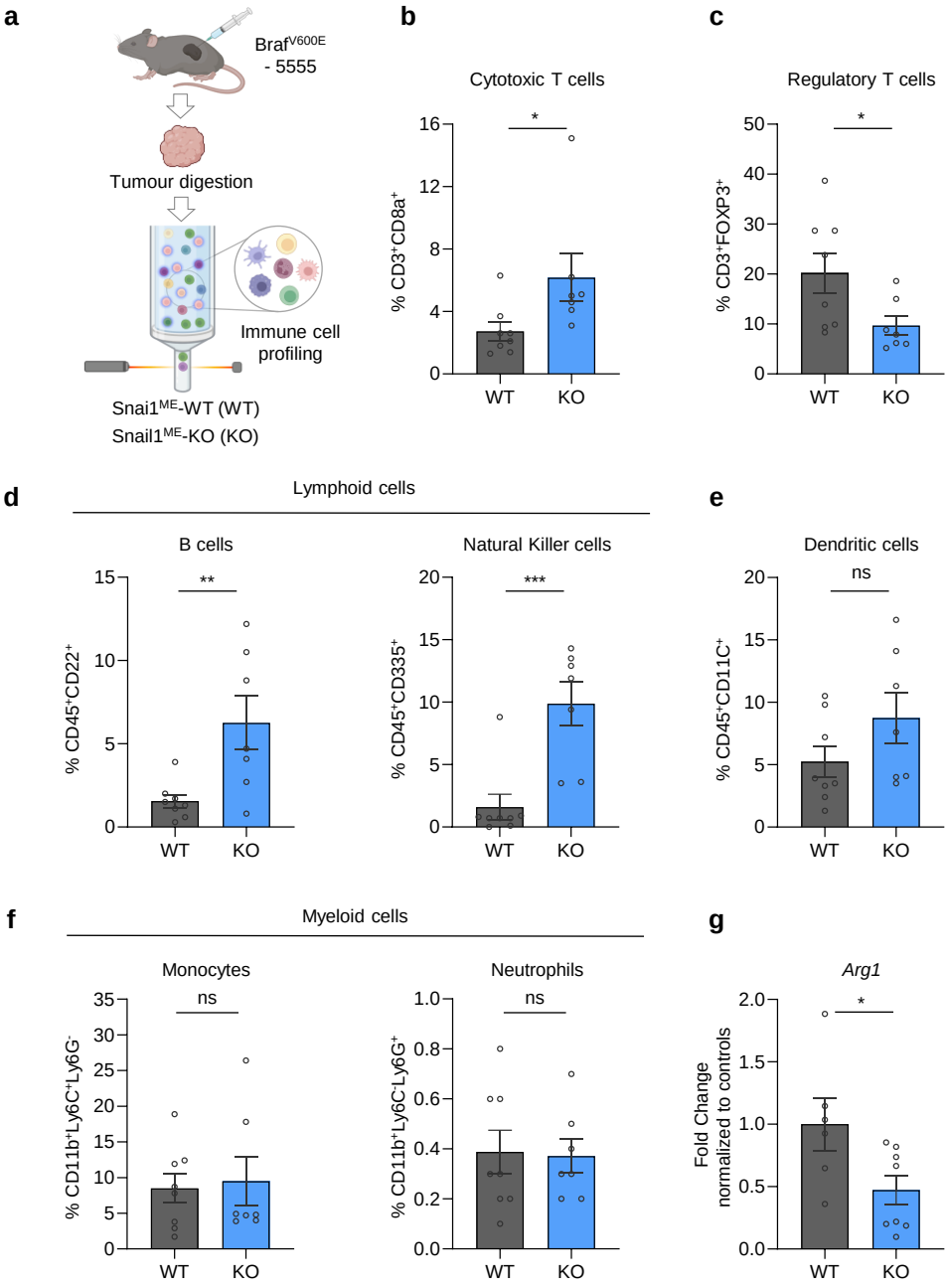


**Figure 22| Snail1$^{ME}$ targeting induces an anti-tumour immune response in melanoma. (a)** Schematic representation of the strategy used to characterize the immune cell profiling by flow cytometry analysis in Braf$^{V600E}$-5555 melanomas from Snail1$^{ME}$-WT (WT, n= 8) and Snail1$^{ME}$-KO (KO, n= 7) mice. **(b, c)** Graphs showing percentages of Cytotoxic T cells (CD3$^+$CD8a$^+$) and Regulatory T cells (CD3$^+$FOXP3$^+$) in tumours from (a). **(d)** Graphs showing percentages of lymphoid cells from (a); B cells (CD45$^+$CD22$^+$) and natural killer cells (CD45$^+$CD335$^+$). **(e)** Graph showing percentage of dendritic cells (CD45$^+$CD11c$^+$) in tumours from (a). **(f)** Graphs showing percentages of myeloid cells in tumours from (a); monocytes (CD11b$^+$Ly6C$^+$Ly6G$^-$) and neutrophils (CD11b$^+$Ly6C$^-$Ly6G$^+$), are represented. **(g)** Arg1 mRNA levels detected by RT-qPCR in tumour samples from Snail1$^{ME}$-WT and Snail1$^{ME}$-KO mice (n= 6 WT and n= 8 KO). Data are represented by Mean ± SEM and statistically significant differences are tested by unpaired two-tailed Student t-test. Each dot represents one animal (ns= not significant, *=p< 0.05, **=p< 0.01, ***p< 0.001).

## 3.4. Snail1 correlates with poor clinical outcomes in melanoma patients

Given our findings indicating the immunosuppressive activity of Snail1 in experimental models and the established association between immunosuppression and resistance to immunotherapy (Jenkins et al., 2018), we sought to explore the relationship between Snail1 expression levels and clinical outcomes in melanoma patients treated with immune checkpoints inhibitors. Through the analysis of transcriptomic datasets (Kovács & Győrffy, 2022) of Kaplan-Meier Plotter (Lánczky & Győrffy, 2021), we found that elevated Snail1 expression either pre-treatment or during treatment with anti-programmed death-1 (anti-PD-1) correlated with a lower overall survival rates in melanoma patients (**Figure 23**).

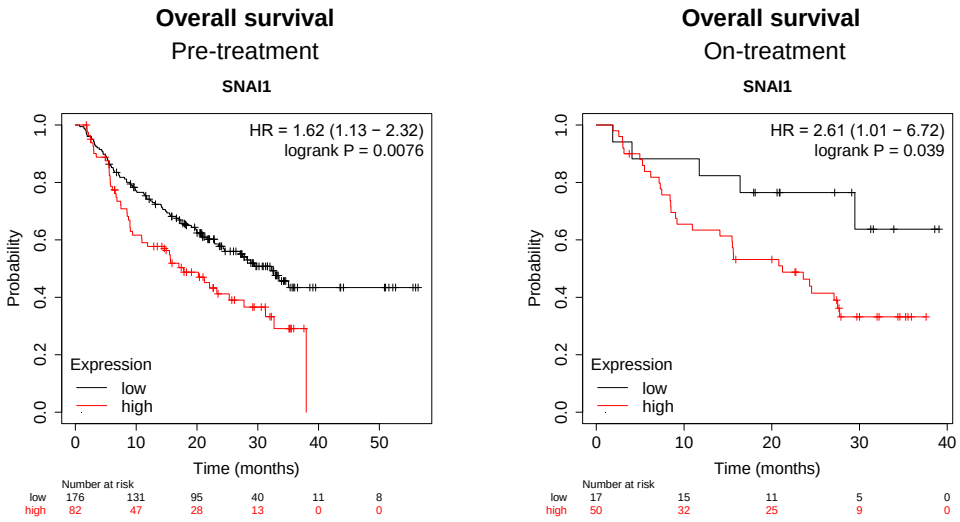


**Figure 23| Prognostic value of SNAIL1 expression in melanoma patients receiving anti-PD-1 therapy. (a)** Overall survival analysis of melanoma patients before anti-PD-1 therapy (n=258). **(b)** Overall survival analysis of melanoma patients on-treatment with anti-PD-1 therapy (n=67). Data was analysed using Kaplan-Meier Plotter. Survival curves for patients with SNAIL1 expression above the median are represented in red, and for those below the median in black. HR, hazard ratio.

## 3.5. Snail1$^{ME}$ targeting phenocopies the effects of anti-PD-1 therapy in melanoma

Given the demonstrated correlation between elevated Snail1 levels and reduced overall survival rates in melanoma patients treated with anti-PD-1 therapy, we sought to evaluate the potential therapeutic implications of Snail1 depletion on the efficacy of anti-PD-1 immune checkpoint therapy *in vivo*. To this end, Braf$^{V600E}$-5555 melanomas were grown in both Snail1$^{ME}$-WT and Snail1$^{ME}$-KO mice. Once tumours were established, mice were divided into four different groups. All mice received tamoxifen treatment; however, two groups (Snail1$^{ME}$-WT TAM and Snail1$^{ME}$-KO TAM) were treated exclusively with tamoxifen, while the other two groups (Snail1$^{ME}$-WT TAM + aPD1 and Snail1$^{ME}$-KO TAM + aPD1) received both tamoxifen and anti-PD- 1 therapy (**Figure 24a**). This experimental design enabled a direct comparison of tumour growth across different conditions, evaluating the effects of Snail1 depletion alone, immune checkpoint inhibition, and their combined impact.

Our results revealed that Snail1$^{ME}$-WT mice exhibited a significant reduction in tumour growth upon anti-PD-1 treatment, confirming the sensitivity of Braf$^{V600E}$-5555 melanomas to this therapy. As expected, in the absence of anti-PD-1 treatment, Snail1$^{ME}$-KO mice presented smaller tumours than those from Snail1$^{ME}$-WT mice, which kept growing over time. Intriguingly, the administration of anti-PD-1 therapy to Snail1$^{ME}$-KO mice did not result in a further reduction in tumour size (**Figure 24b**).

Taken together, these findings suggest that the tumour-suppressive effects of targeting Snail1 are comparable to those of anti-PD-1 therapy in Snail1$^{ME}$-WT mice. However, additional studies are required to corroborate these observations and to elucidate the mechanisms underlying these effects.

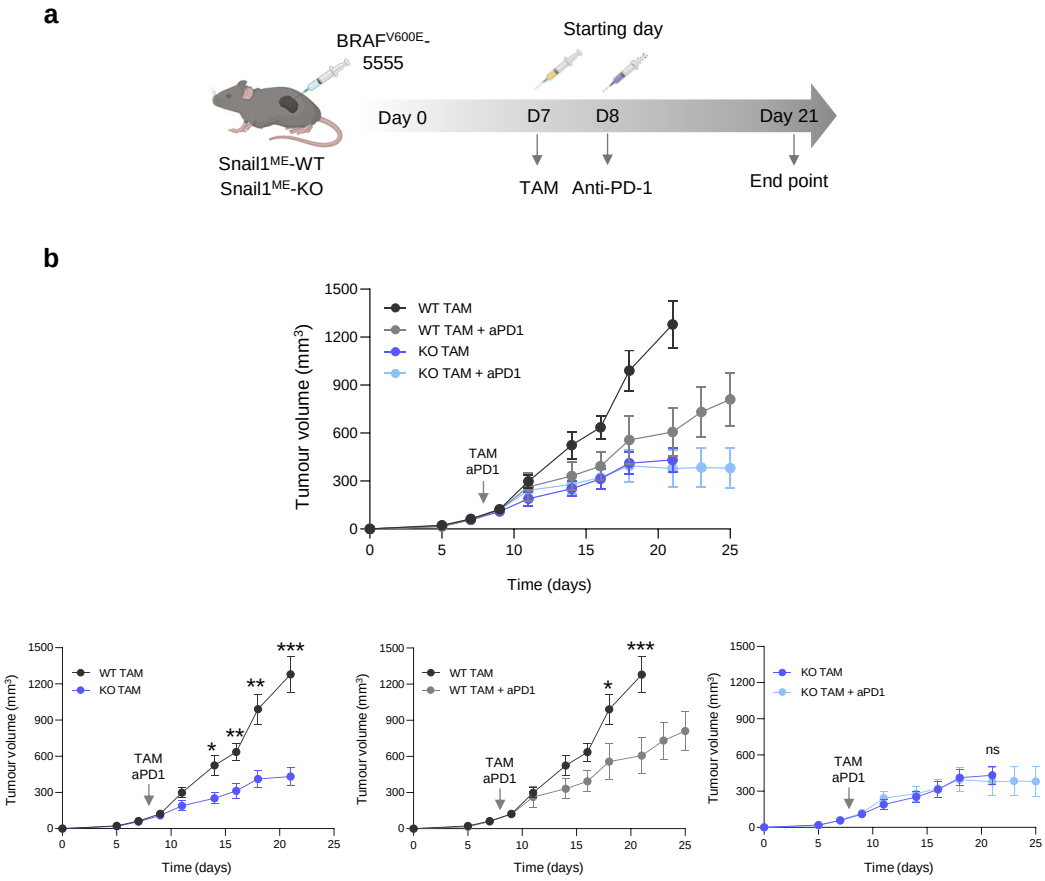


**Figure 24| Snail1$^{ME}$ targeting phenocopies anti-PD-1 therapy. (a)** Schematic representation of the strategy used to investigate the impact of silencing Snail1 in combination with anti-PD-1 therapy *in vivo*. **(b)** Tumour volume at the indicated days post injection in Snail1$^{ME}$-WT and Snail1$^{ME}$-KO treated with tamoxifen or tamoxifen with anti-PD-1 (10 mg/kg, every 3 days) starting at 8dpi. Different groups (upper panel) are indicated in the horizontal axis (n= 9 Snail1$^{ME}$-WT with TAM, n= 9 Snail1$^{ME}$-WT with anti-PD-1 + TAM, n= 7 Snail1$^{ME}$-KO with TAM, n= 6 Snail1$^{ME}$-KO with anti-PD-1 + TAM). Comparison between relevant conditions are indicated (lower panel). Data are represented by Mean ± SEM and statistically significant differences are tested by unpaired two-tailed Student t-test. Each dot represents one animal (ns= not significant, *=p< 0.05, **=p< 0.01, ***p< 0.001).

## 4. Snail1 regulates Fap expression in fibroblasts

Considering that Snail1 acts primarily as a transcription factor and performs its function by regulating gene expression, we next aimed to identify Snail1 downstream targets that could be implicated in immunomodulation. Analysis of our RNA-seq data revealed that *Fap* was one of the most significantly downregulated genes following Snail1 inhibition in fibroblasts isolated from Snail1$^{ME}$-KO tumours (**Figure 20b,c,d**).

Interestingly, recent studies using syngeneic carcinoma models indicate that FAP-expressing CAFs contribute to tumour progression by promoting immune-evasion within an immunosuppressive environment (Cohen et al., 2017; Costa et al., 2018; Cremasco et al., 2018; Takahashi et al., 2015; Yang et al., 2016; Y. Zhang & Ertl, 2016). Based on this, we aimed to further explore the relationship between Snail1 and Fap.

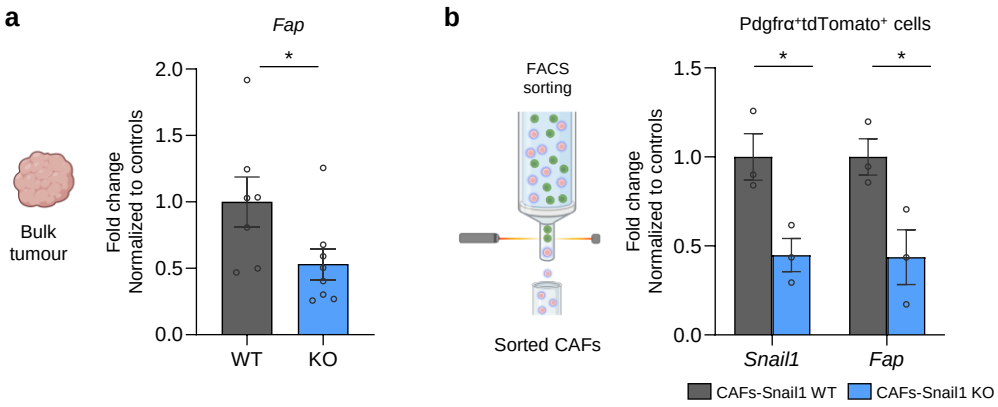


**Figure 25| Fap is a downstream target of Snail1 in melanoma-associated fibroblasts. (a)** *Fap* mRNA levels detected by RT-qPCR in Braf$^{V600E}$-5555 bulk tumour samples from Snail1$^{ME}$-WT (WT) and Snail1$^{ME}$-KO (KO) mice (n=7 WT and n=8 KO). **(b)** *Snail1* and *Fap* mRNA levels detected by RT-qPCR in Snail1-WT and Snail1-KO Pdgfra$^{+}$tdTomato$^{+}$ sorted fibroblasts from Snail1$^{ME}$-WT and Snail1$^{ME}$-KO subcutaneous tumours (n=3 WT and n=3 KO, with samples from 3 animals of the same genotype pooled for each condition). Data are represented by Mean ± SEM and statistically significant differences are tested by unpaired two-tailed Student t-test. Each dot represents one animal (*=p< 0.05).

We first focused on evaluating the effect of *Snail1* on *Fap* expression in our experimental models. Supporting our previous RNA-seq data (**Figure 20**), we observed significantly lower mRNA levels of *Fap* in Snail1$^{ME}$-KO tumours compared to Snail1$^{ME}$-WT tumours (**Figure 25a**). Further validation in sorted Pdgfrα$^{+}$tdTomato$^{+}$ fibroblasts from Snail1$^{ME}$-KO tumours confirmed reduced *Fap* expression (**Figure 25b**).

To elucidate the regulatory role of Snail1 at the molecular level, we manipulated its expression in NIH3T3 fibroblasts cells (**Figure 26a**). Consistent with our previous results, *Fap* expression was decreased when *Snail1* was downregulated using siRNA (**Figure 26b**). Conversely, TGFβ treatment, which upregulates *Snail1* levels, resulted in increased *Fap* expression (**Figure 26c**). To further validate these findings, we used CYD19 (H. M. Li et al., 2020), a novel drug designed to induce Snail1 degradation. We assessed the efficacy of CYD19 in degrading Snail1 at both gene and protein levels (**Figure 26d**). Additionally, *Vimentin* was used as a functional readout of Snail1 capabilities to induce EMT in fibroblasts. Interestingly, CYD19 treatment led to a decrease in *Fap* levels in NIH3T3 fibroblasts, reinforcing the role of *Snail1* in regulating *Fap* expression (**Figure 26d**).

Supporting these findings, analysis of The Cancer Genome Atlas (TCGA) data from different cancers revealed a positive correlation between *Snail1* and *Fap* expression in 28 tumour types, including melanoma (**Figure 27**).

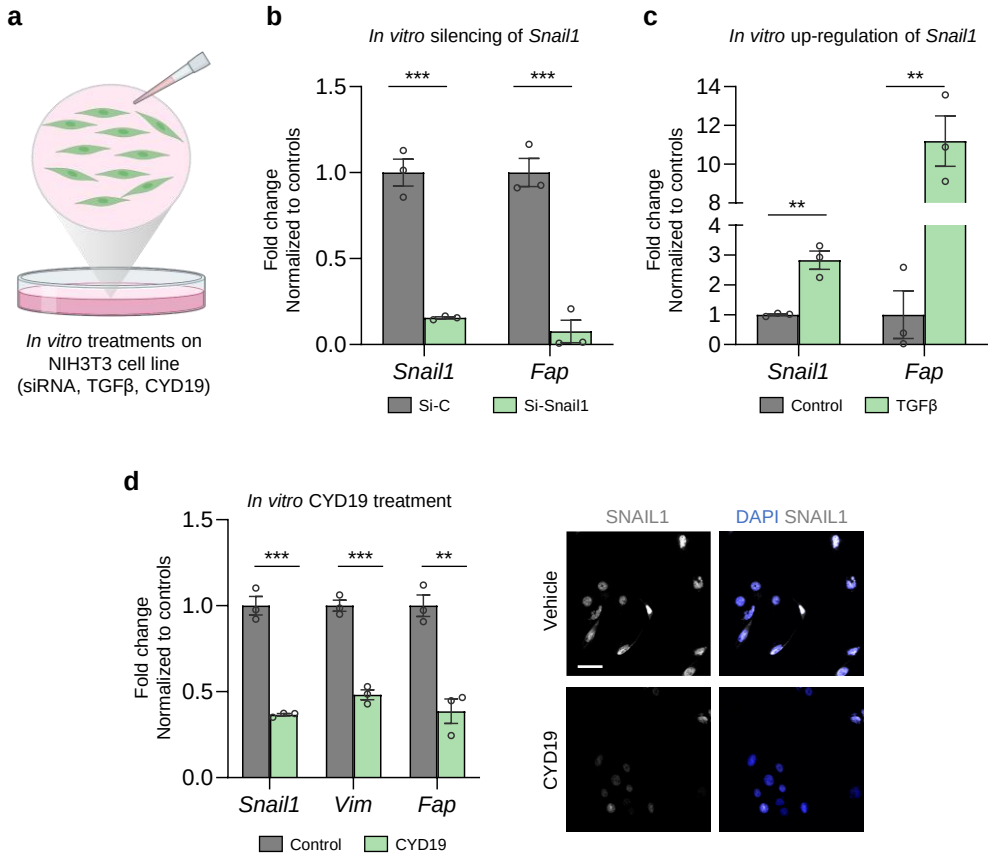


**Figure 26| Validation of *Fap* as direct target of *Snail1* in NIH3T3 cell line under different *in vitro* conditions. (a)** Schematic representation of the in vitro treatments applied to NIH3T3 cells to investigate the relationship between *Snail1* and *Fap*. **(b)** *Snail1* and *Fap* mRNA levels decrease detected by RT-qPCR upon *Snail1*-silencing using a siRNA in TGFβ-treated NIH3T3 cells. Cells were collected 48 h post-transfection (n= 3). **(c)** *Snail1* and *Fap* mRNA levels increase detected by RT-qPCR upon TGFβ treatment in NIH3T3 cells. Cells were collected 48 h post TGFβ treatment (n= 3). **(d)** *Snail1*, *Vimentin* and *Fap* mRNA levels detected by RT-qPCR in NIH3T3 cells treated with TGFβ (2 ng/ml) for 24 h, followed by treatment with either vehicle or CYD19 (5 nM) in the presence of TGFβ for an additional 48 h (left panel). Representative IF of SNAIL1 (white) in cells from (d). Scale bar: 50 μm (right panel). Data are represented by Mean ± SEM and statistically significant differences are tested by unpaired two-tailed Student t-test. Each dot represents one animal (**=p< 0.01, ***p< 0.001).

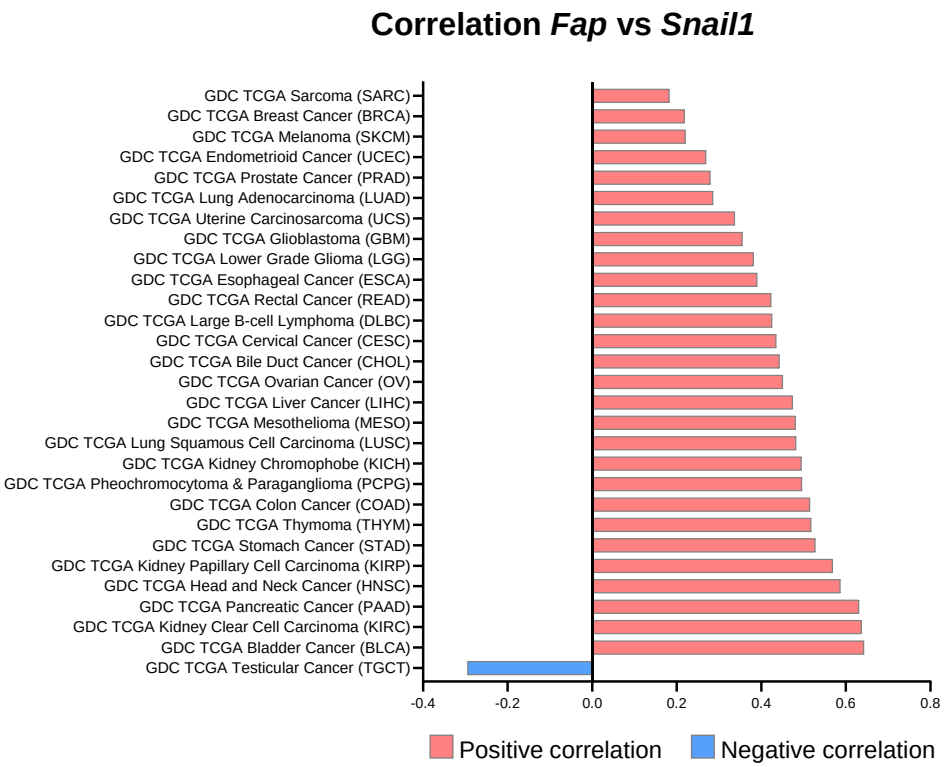


**Figure 27| Correlation analysis of *Fap* and *Snail1* across cancer types.** Pearson correlation analysis results for the expression levels of Fap and Snail1, using all cancer types data from The Cancer Genome Atlas program (TCGA) database. The graph includes cancer types with statistically significant correlations ($p<0.05$), with positive correlations represented in red and negative correlations in blue.

Considering the observed downregulation of *Fap* when *Snail1* levels are diminished, and its upregulation upon Snail1 overexpression, we hypothesized that Snail1 may directly bind to the regulatory regions of the *Fap* promoter to regulate its expression in fibroblasts. To test this hypothesis, we conducted chromatin immunoprecipitation (ChIP) assays using NIH3T3 cells transiently overexpressing Snail1 tagged with a Myc epitope (**Figure 28a**).

Using the SnapGene® software, we identified multiple Snail1 consensus E-boxes (CANNTG) near the transcription start sites of both murine and human *Fap* promoters (Villarejo et al., 2014). Regions containing two or more E-box motifs were considered as predicted Snail1 binding sites (BS), and we found several within the mouse *Fap* promoter (BS1, BS2, BS3, BS4 and BS5). An intergenic region lacking SNAIL1 binding sites (He et al., 2012) was used as a negative control (NC) (**Figure 28b**).

Subsequent ChIP analysis on NIH3T3 cells transfected with Snail1-Myc (**Figure 28c**) demonstrated significant enrichment of Snail1 at BS1, BS2 and BS3, when compared to the IgG control. These results indicated that SNAIL1 can directly activate *Fap* expression in fibroblasts (**Figure 28d**). Altogether, these data strongly indicate that Snail1 regulates Fap expression in fibroblasts.

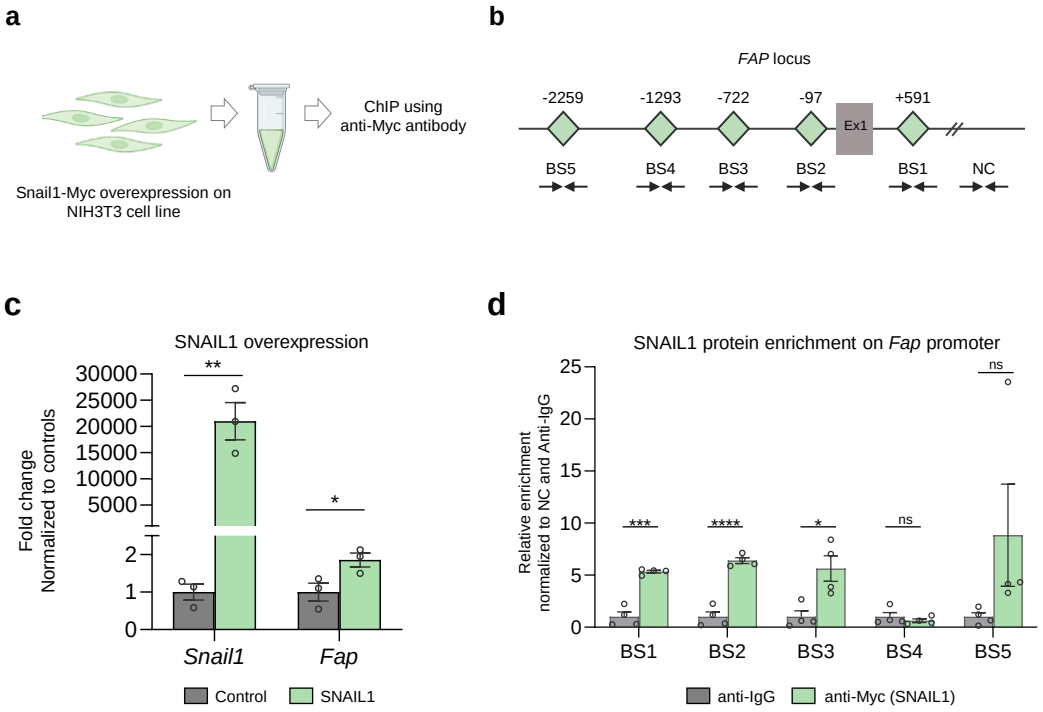


**Figure 28| Snail1 directly regulates Fap in fibroblasts binding to its promoter. (a)** Schematic representation of the strategy used to investigate the SNAI enrichment on the *Fap* promotor by ChIP assay in NIH3T3 cells, using an anti-Myc antibody (for SNAI-Myc overexpression). Created with BioRender.com. **(b)** Representation of the mouse *Fap* locus. SNAIL1 potential binding sites (E-boxes; CANNTG) on *Fap* promoter are represented as green diamonds (BS1: +591 bp, BS2: −97bp, BS3: −722bp, BS4: −1293bp, BS5 −2259bp). An intergenic region without SNAIL1 binding sites was used as a negative control (NC). Ex1: Snail1 exon 1. **(c)** Validation of *Snail1* and *Fap* mRNA levels increase detected by RT-qPCR after Snail1 transfection in NIH3T3 cells (n= 3). **(d)** Relative enrichment of SNAIL1 binding to the five potential sites, normalised to the NC region and the anti-IgG controls (n= 4). Data are represented by Mean ± SEM and statistically significant differences are tested by unpaired two-tailed Student t-test. Each dot represents one independent experiments (ns= not significant, * = p< 0.05, ** = p< 0.01, ***p< 0.001, ****p< 0.0001).

# 5. Snail1 as a therapeutic target in melanoma

Therapeutic management of melanoma patients usually begins when the cells have disseminated to the lymph nodes or distant organs. Given our previous results showing that Snail$^{ME}$ targeting blocks subcutaneous melanoma growth, we next investigated the potential role of targeting Snail1 in the metastatic niche microenvironment.

## 5.1. Snail1 is reactivated in the metastatic niche microenvironment

To elucidate the contribution of this transcription factor to the metastatic niche microenvironment, we injected luciferase-expressing Braf$^{V600E}$-5555 melanoma cells into the tail vein of Snail1$^{ME}$-WT and Snai1$^{ME}$-KO mice (**Figure 29a**).

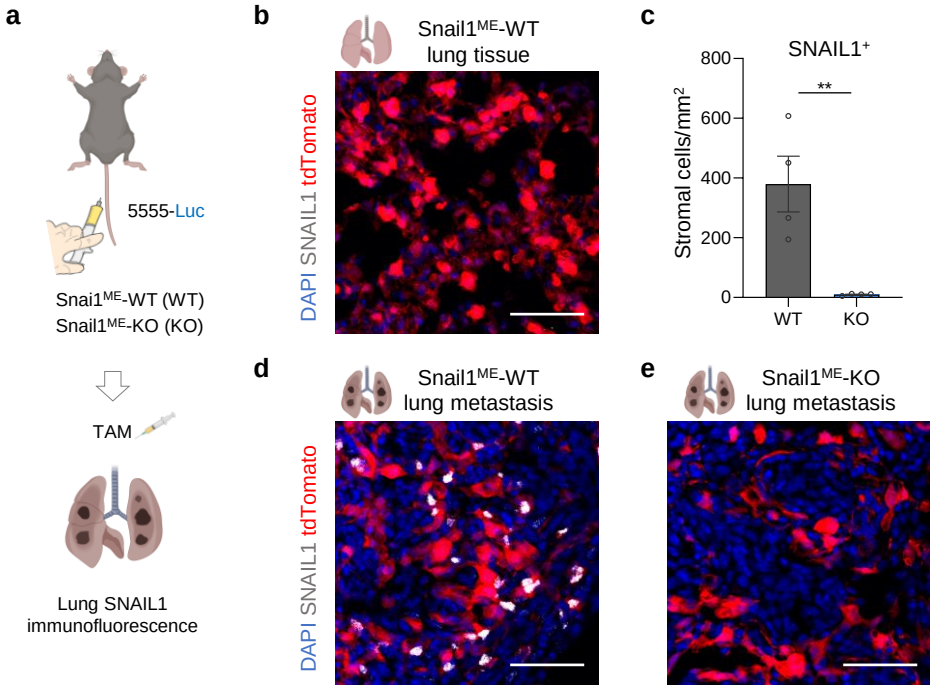


**Figure 29| Snail1 is reactivated in the lung metastatic niche. (a)** Schematic illustration of the experimental approach used to assess SNAIL1 expression in melanoma lung metastases and confirm its depletion post-tamoxifen treatment. Created with BioRender.com. **(b)** Representative image of immunolabelling for SNAIL1 (white) in control lung tissue after tamoxifen administration. **(c)** SNAIL1 quantification post-tamoxifen administration in Braf$^{V600E}$-5555 lung metastases, comparing Snail1$^{ME}$-WT (n=4) and Snail1$^{ME}$-KO (n=4) mice. **(d,e)** Representative images of immunolabelling for SNAI (white) in Braf$^{V600E}$-5555 lung metastases from Snail1$^{ME}$-WT and Snail1$^{ME}$-KO samples described in (c)**.** Stromal cells are labelled in red (tdTomato). Data are represented by Mean±SEM and statistically significant differences are tested by unpaired two-tailed Student t-test. Each dot represents one animal (**=p<0.01). WT=Snail1$^{ME}$-WT and KO= Snail1$^{ME}$-KO. Scale bars: 50µm.

Initial validation confirmed the absence of SNAIL1 in control lungs (**Figure 29b**). Interestingly, Snail1 reactivation was observed in the metastatic microenvironment of Snail1$^{ME}$-WT mice (**Figure 29c,d**), suggesting that Snail1 could have an impact in regulating melanoma metastases. In contrast, tamoxifen administration effectively suppressed Snail1 expression in Snail1$^{ME}$-KO mice, confirming the efficacy of this model for studying the implications of this transcription factor in melanoma lung metastases (**Figure 29e**).

Using a similar approach, we further detected SNAIL1 expression in PDGFRα-positive CAFs from melanoma lung metastases in Snail1$^{ME}$-WT mice (**Figure 30a**). This result was corroborated by identifying SNAIL1 expression in PDGFRα$^{+}$-positive CAFs in lung metastases obtained from Braf$^{V600E}$/Pten$^{loxP}$/tdTomato mice (**Figure 30b**).

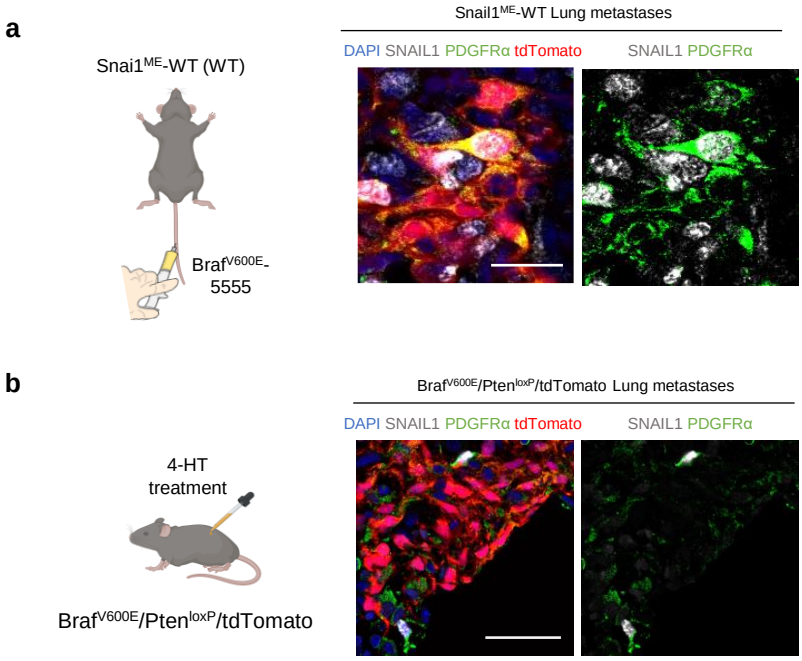


**Figure 30| Snail1 is reactivated in PDGFRα-positive fibroblasts within melanoma lung metastases.** **(a)** Representative images of double immunolabelling of SNAIL1 (white) and PDGFRα (green, fibroblasts) in Braf$^{V600E}$-5555 lung metastases from Snail1$^{ME}$-WT. Stromal cells are labelled in red (tdTomato). Scale bar: 25µm**. (b)** Representative images of double immunolabelling of SNAI (white) and PDGFRα (green, fibroblasts) in Braf$^{V600E}$-5555 lung metastases from Braf$^{V600E}$/Pten$^{loxP}$/tdTomato mice after 4-HT treatment. Tumour cells are labelled in red (tdTomato). Scale bar: 50µm. Created with BioRender.com.

## 5.2. Snail1$^{ME}$ targeting reduces metastatic burden and improves mice survival

To elucidate the contribution of Snail1$^{ME}$ to melanoma lung metastases colonization, we initially administered tamoxifen to block Snail1 activity in the lung microenvironment. We then injected luciferase-expressing Braf$^{V600E}$-5555 melanoma cells into the tail vein of Snail1$^{ME}$-WT and Snail1$^{ME}$-KO mice. The progression of metastases was monitored using BLI in an IVIS until the end of the experiment (**Figure 31a**). Interestingly, a reduced BLI signal was observed in Snail1$^{ME}$-KO mice, pointing towards a decreased metastatic burden (¡Error! No se encuentra el origen de la referencia.**b**). At the end of the experiment, lung tissues were weighted, with those from Snail1$^{ME}$-KO group showing a significant reduction in weight (-46.7%) (**Figure 31c**). These observations were further corroborated by histological analyses (**Figure 31d**), which revealed a significant decrease in the metastatic burden (-90.4%), a reduction in the number of metastasis (-73.7%), and a significant shrinkage in the size of individual metastases (-70.7%) in the Snail1$^{ME}$-KO mice (**Figure 31d,e**).

In a parallel experiment, we wanted to assess the impact of Snail1$^{ME}$ on the progression of pre-established melanoma lung metastases. In this approach, luciferase-expressing Braf$^{V600E}$-5555 melanoma cells were initially injected into the tail vein of mice. Following the visual confirmation of metastases using the IVIS, tamoxifen was administered to block Snail1 expression (**Figure 32a**). Over the course of the experiment, Snail1$^{ME}$-KO mice exhibited a reduction in BLI signal in the lungs (**Figure 32b**), indicating decreased metastatic growth. *Ex vivo* BLI analyses of the lungs confirmed these observations, showing a reduced BLI signal in Snail1$^{ME}$-KO lungs (**Figure 32c**). Additionally, lung tissue weights were significantly reduced (-37.5%) in Snail1$^{ME}$-KO (**Figure 32d**). Histological quantification of the lungs (**Figure 32e**) further supported these results, showing a significant reduction in the metastatic burden (-82.9%), fewer metastases number (-47.6%), and smaller metastases size (-77.5%) in the Snail1$^{ME}$-KO group (**Figure 32f**).

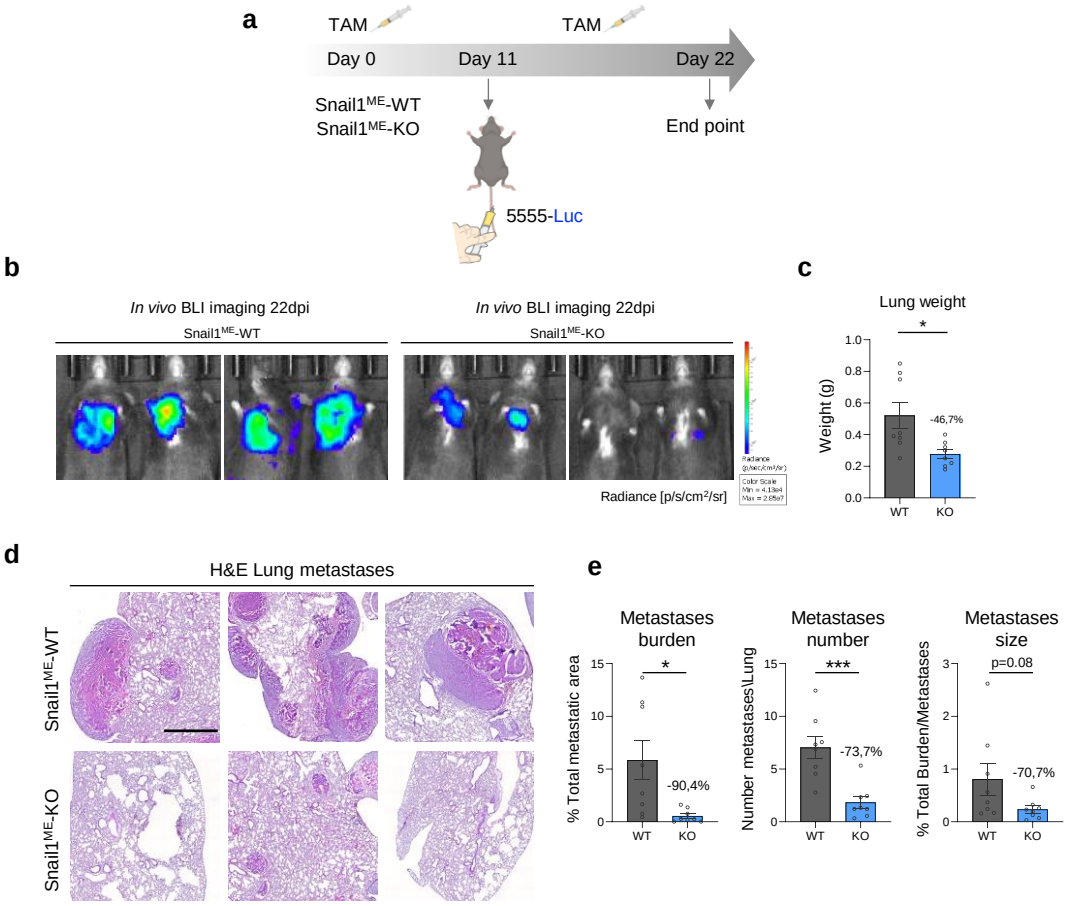


**Figure 31| Snail1$^{ME}$ depletion reduces melanoma lung metastases colonization. (a)** Experimental set-up of the in vivo strategy used design to study the contribution of microenvironmental Snail1 to lung metastases formation in Snail1$^{ME}$-WT (WT) and Snail1$^{ME}$-KO (KO) mice following tamoxifen administration. Created with BioRender.com. **(b)** Representative in vivo BLI signal images from mice in (a) at 22dpi. The BLI scale is represented next to the panel. Measurement units: p/s/cm$^2$/sr. **(c)** Lung weight from Snail1$^{ME}$-WT and Snail1$^{ME}$-KO mice described in (a). (d) Representative H&E-stained lung sections at 22dpi. Scale bar: 2mm. **(e)** Metastases burden, metastases number and metastases size quantification from lungs in (a) (n= 8 WT and n= 8 KO). Data are represented by Mean±SEM and statistically significant differences are tested by unpaired two-tailed Student t-test. Each dot represents one animal (*=p<0.05, ***p<0.001).

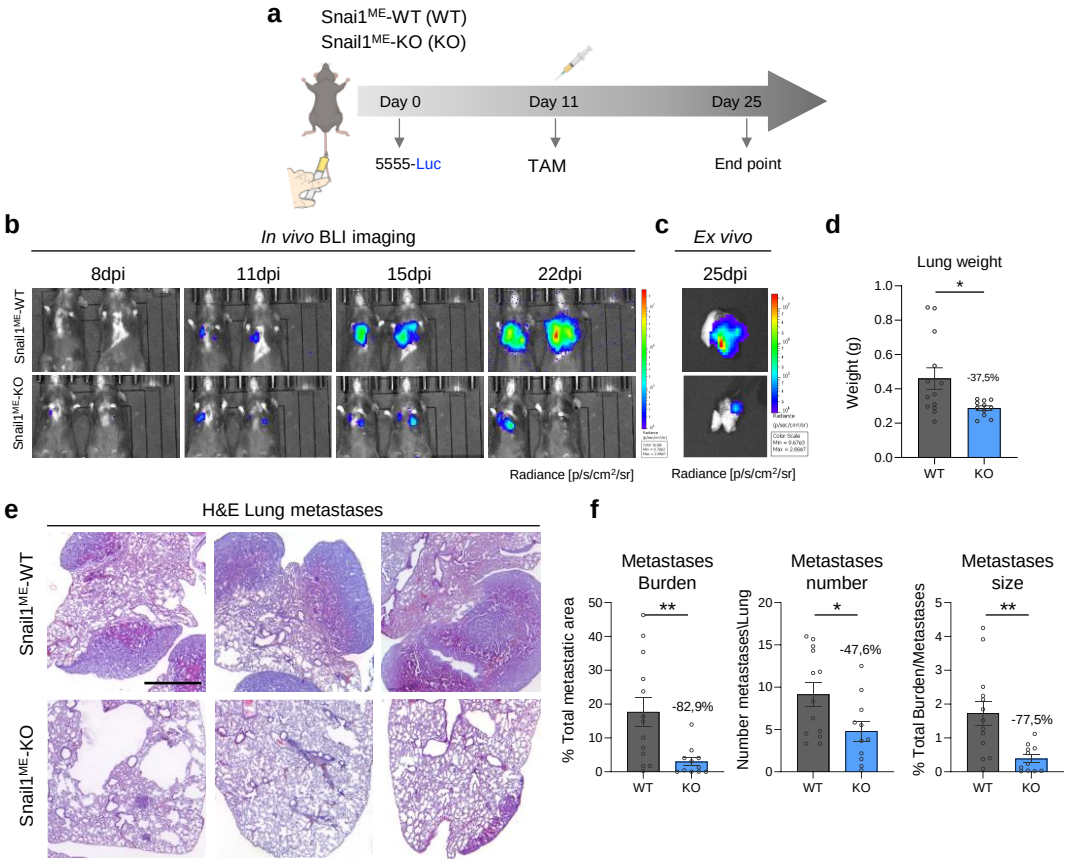


**Figure 32| Snail1$^{ME}$ depletion reduce melanoma lung metastases progression. (a)** Experimental set-up of the in vivo strategy used design to study the contribution of microenvironmental Snail1 to lung metastases progression in Snail1$^{ME}$-WT (WT) and Snail1$^{ME}$-KO (KO) mice. Created with BioRender.com. **(b, c)** Representative *in vivo* and *ex vivo* BLI signal images from mice in (a). The BLI scale is represented next to the panel. Measurement units: p/s/cm$^2$/sr. **(d)** Lung weight from Snail1$^{ME}$-WT and Snail1$^{ME}$-KO mice at 25dpi. **(e)** Representative H&E-stained lung sections at 25dpi. Scale bar: 2mm**. (f)** Metastases burden, metastases number and metastases size quantification from lungs in (a) (n= 13 WT and n= 11 KO). Data are represented by Mean±SEM and statistically significant differences are tested by unpaired two-tailed Student t-test. Each dot represents one animal (*=p<0.05, **p<0.01).

Further, we investigated the potential impact of Snail1$^{ME}$ inhibition on overall mice survival (**Figure 33a**). Kaplan-Meier survival analysis demonstrated an almost 30% increase in the lifespan of Snail1$^{ME}$-KO mice compared to Snail1$^{ME}$-WT counterparts, as assessed by long-rank test ($X^2$=6.92, p<0.01) (**Figure 33b**). Additionally, lung weight measurements corroborated this finding, revealing a reduction in lung weight (-42,1%), which indicates a decreased metastatic burden in the Snail1$^{ME}$-KO group (**Figure 33c**).

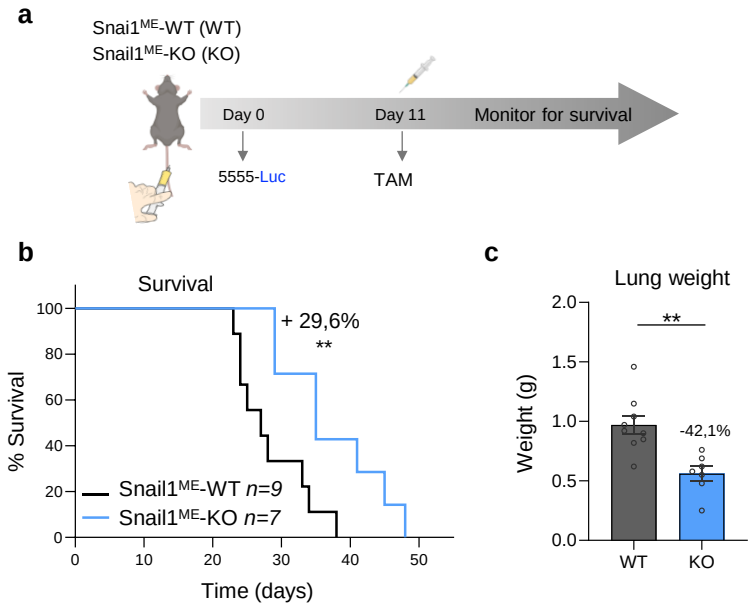


**Figure 33| Snail1$^{ME}$ ablation in melanoma lung metastases improves survival in mice. (a)** Schematic representation of the experimental approach used to evaluate how microenvironmental Snail1 in lung metastases impacts mice survival. **(b)** Overall survival of Snail1$^{ME}$-WT and Snail1$^{ME}$-KO with melanoma lung metastases after Snail1-silencing (n= 9 WT and n= 7 KO). Survival curves compared using the log-rank (Mantel-Cox) test. **(c)** Lung weight from Snail1$^{ME}$-WT and Snail1$^{ME}$-KO mice in (b). Data are represented by Mean±SEM and statistically significant differences are tested by unpaired two-tailed Student t-test. Each dot represents one animal (**p<0.01). WT= Snail1$^{ME}$-WT and KO= Snail1$^{ME}$-KO.

Importantly, as in the subcutaneous tumours, we conducted a detailed analysis of the lung metastases from Snail1$^{ME}$-KO mice (**Figure 34a**). Immunofluorescence analyses were performed to assess melanoma cell proliferation and apoptosis. The results demonstrated that Snail1$^{ME}$-KO metastases showed a significant decrease in proliferation, as indicated by fewer KI-67-positive melanoma cells (**Figure 34b,c**), and a significant increase in apoptosis, reflected by higher Cleaved-CASP3-positive melanoma cells (**Figure 34d,e**). These findings are consistent with the reduced metastatic burden and are in line with our prior results from the subcutaneous tumours.

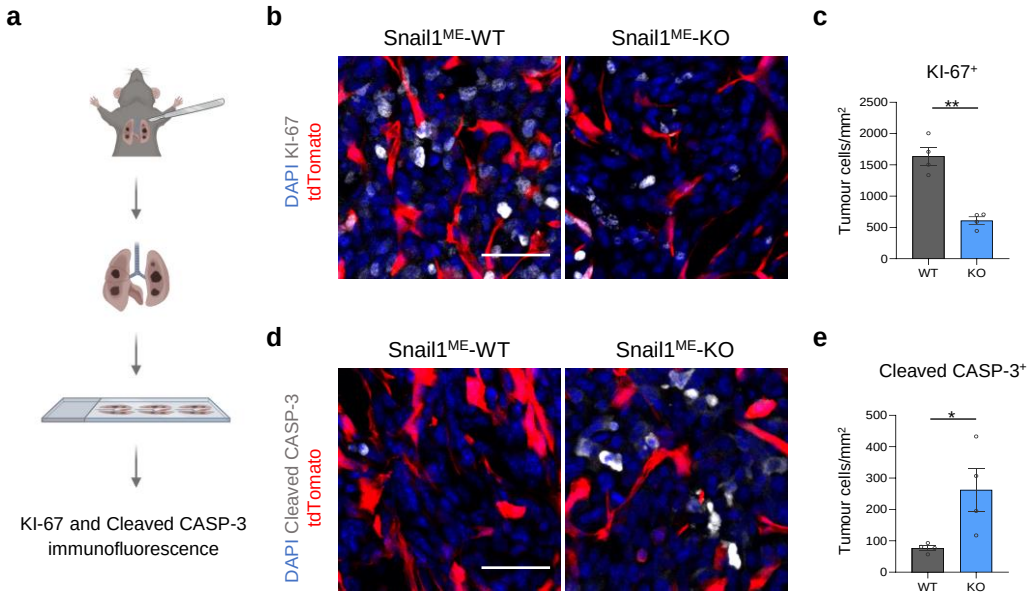


**Figure 34| Snail1$^{ME}$ ablation reduces proliferation and promotes melanoma cell apoptosis at the metastatic niche. (a)** Schematic representation of the strategy used to evaluate the proliferation and apoptosis of Snail1$^{ME}$-WT and Snail1$^{ME}$-KO experimental lung metastases. Created with BioRender.com. **(b)** Representative images of immunolabelling for KI-67(white) in lungs from Snail1$^{ME}$-WT (left) and Snail1$^{ME}$-KO (right) mice. Stromal cells are labelled in red (tdTomato). **(c)** Quantification of KI-67 (white) tumour nuclei-positive cells in images from (b) (n=4). **(d)** Representative images of immunolabelling for Cleaved CASP-3 (white) in Snail1$^{ME}$-WT and Snail1$^{ME}$-KO experimental lung metastases. Stromal cells are labelled in red (tdTomato). **(e)** Quantification of images from (d) (n=4). Data are represented by Mean±SEM and statistically significant differences are tested by unpaired two-tailed Student t-test. Each dot represents one animal (*=p<0.05, **=p<0.01). WT=Snail1$^{ME}$-WT and KO= Snail1$^{ME}$-KO. Scale bars: 50µm.

Subsequent evaluation of the immune infiltrate in the lungs by flow cytometry (**Figure 35a**) revealed that metastases from Snail1$^{ME}$-KO mice had an increased number of cytotoxic T cells (CD8a$^{+}$) (**Figure 35b**) and a lower infiltration of regulatory T cells (FOXP3$^{+}$) compared to those from Snail1$^{ME}$-WT mice (**Figure 35c**). Interestingly, the populations of lymphoid, dendritic and myeloid cells remained unchanged (**Figure 35d,e,f**) . Furthermore, reduction in *Fap* mRNA levels was detected in lung metastases from Snail1$^{ME}$-KO mice (**Figure 35g**), further supporting our previous findings.

Taken together, these findings strongly suggest that genetic inhibition of Snail1 within the TME leads to a reduction in metastatic growth. This outcome is consistent with our prior results, showing a less immunosuppressive microenvironment and an enhanced anti-tumour immune response upon Snail1 silencing.

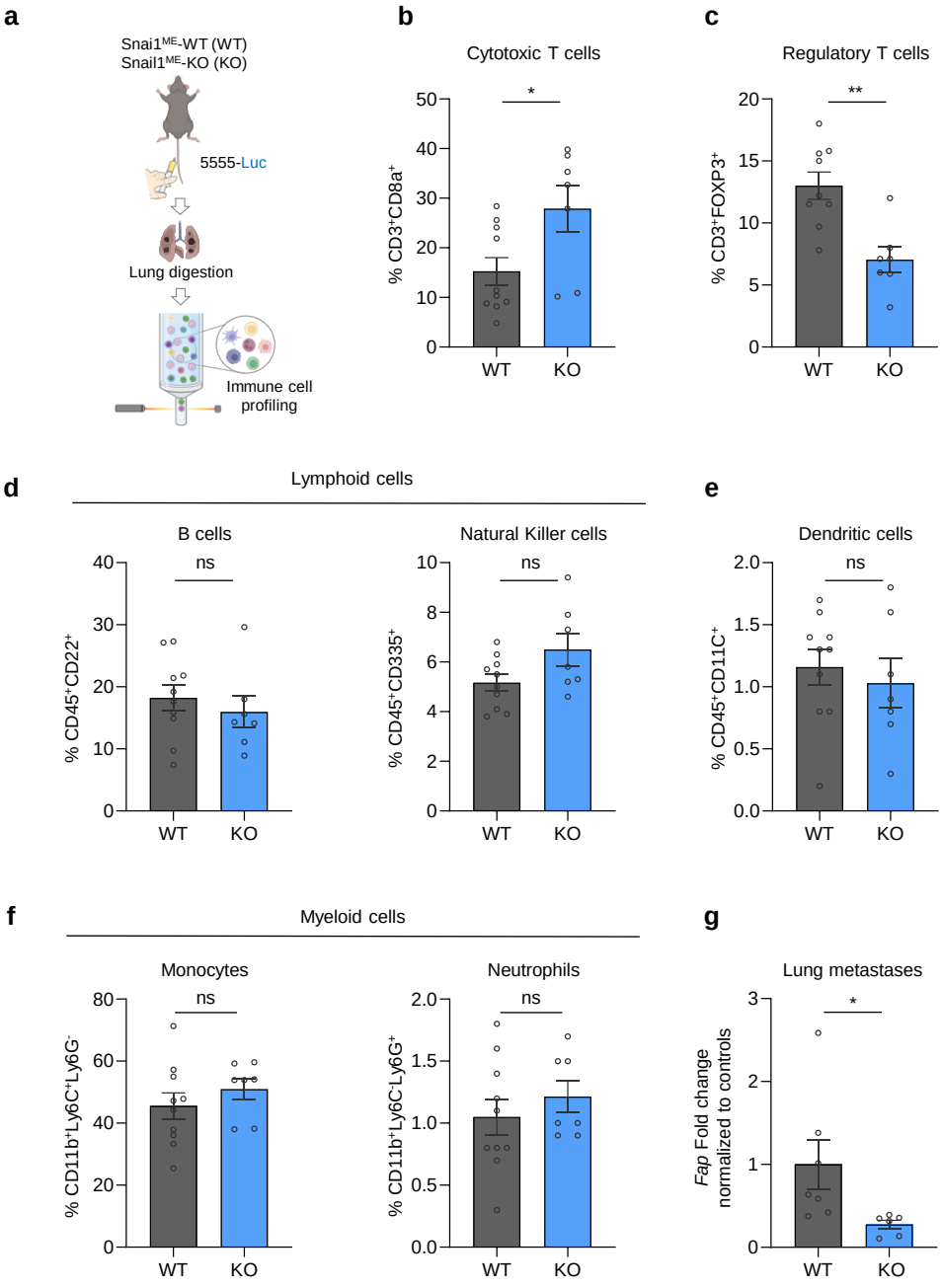


**Figure 35| Snail1$^{ME}$ targeting in melanoma lung metastases leads an anti-tumour immune response. (a)** Schematic representation of the strategy used to characterize the immune cell profiling by flow cytometry analysis in Braf$^{V600E}$-5555 melanoma lung metastases from Snail1$^{ME}$-WT (WT, n= 10) and Snail1$^{ME}$-KO (KO, n= 7) mice. **(b, c)** Graphs showing percentages of Cytotoxic T cells (CD3$^+$CD8a$^+$) and Regulatory T cells (CD3$^+$FOXP3$^+$) in tumours from (a). **(d)** Graphs showing percentages of lymphoid cells from (a); B cells (CD45$^+$CD22$^+$) and natural killer cells (CD45$^+$CD335$^+$). **(e)** Graph showing percentage of dendritic cells (CD45$^+$CD11c$^+$) in tumours from (a). **(f)** Graphs showing percentages of myeloid cells in tumours from (a); monocytes (CD11b$^+$Ly6C$^+$Ly6G$^-$) and neutrophils (CD11b$^+$Ly6C$^-$Ly6G$^+$), are represented (n= 8 WT and n= 7 KO). **(g)** *Fap* mRNA levels detected by RT-qPCR in experimental lung metastases samples from Snail1$^{ME}$-WT and Snail1$^{ME}$-KO mice (n= 7 WT and n= 6 KO). Data are represented by Mean ± SEM and statistically significant differences are tested by unpaired two-tailed Student t-test. Each dot represents one animal (ns= not significant, *=p< 0.05, **=p< 0.01).

## 5.3. Systemic targeting of Snail1 *in vivo* as a potential therapeutic strategy for melanoma

Previous work in the laboratory demonstrated the therapeutic potential of targeting Snail1 with antisense oligonucleotides in renal fibrosis (Grande et al., 2015). To explore the applicability of this strategy in melanoma, we employed a similar strategy by administering a VIVO-morpholino (VI-MO) that targets a specific splicing site in the *Snail1* mRNA (referred to as Snail1-MO) (Grande et al., 2015). This VI-MO was injected into the tail vein of C57BL/6 mice with established luciferase-expressing $Braf^{V600E}$-5555 lung metastases. After confirming the presence of lung metastases by BLI imaging, mice were subjected to VI-MOs treatments, and metastatic progression was continuously monitored using the IVIS system (**Figure 36a**). Results from both *in vivo* (**Figure 36b**) and *ex vivo* (**Figure 36c**) BLI analyses demonstrated a significant reduction in signal intensity and metastatic burden Snail1-MO treated mice. At the end of the experiment, histological examination of the lungs revealed significant reductions in lung tissue weight (56.7%) (**Figure 36d**), metastatic burden (55.9%), and the number of metastases (37.4%), compared to the Control-MO treated group (**Figure 36e,f**).

To validate the effectiveness of Snail1-MO in supressing Snail1 expression, we conducted protein and gene expression analyses in the lung metastases of treated mice (**Figure 37a,b**). Immunofluorescence analyses showed a significant decrease in SNAIL1-positive cells in the lung metastases of Snail1-MO treated mice, compared to the Control-MO treated mice and untreated healthy controls (**Figure 37a**). This reduction in SNAIL1 protein levels was supported by RT-qPCR analyses, which revealed decreased *Snail1* expression levels in lungs from Snail1-MO treated mice. This downregulation was concomitant with a reduction in *Fap* mRNA levels (**Figure 37b**), thus corroborating our previous findings that Snail1 regulates *Fap*.

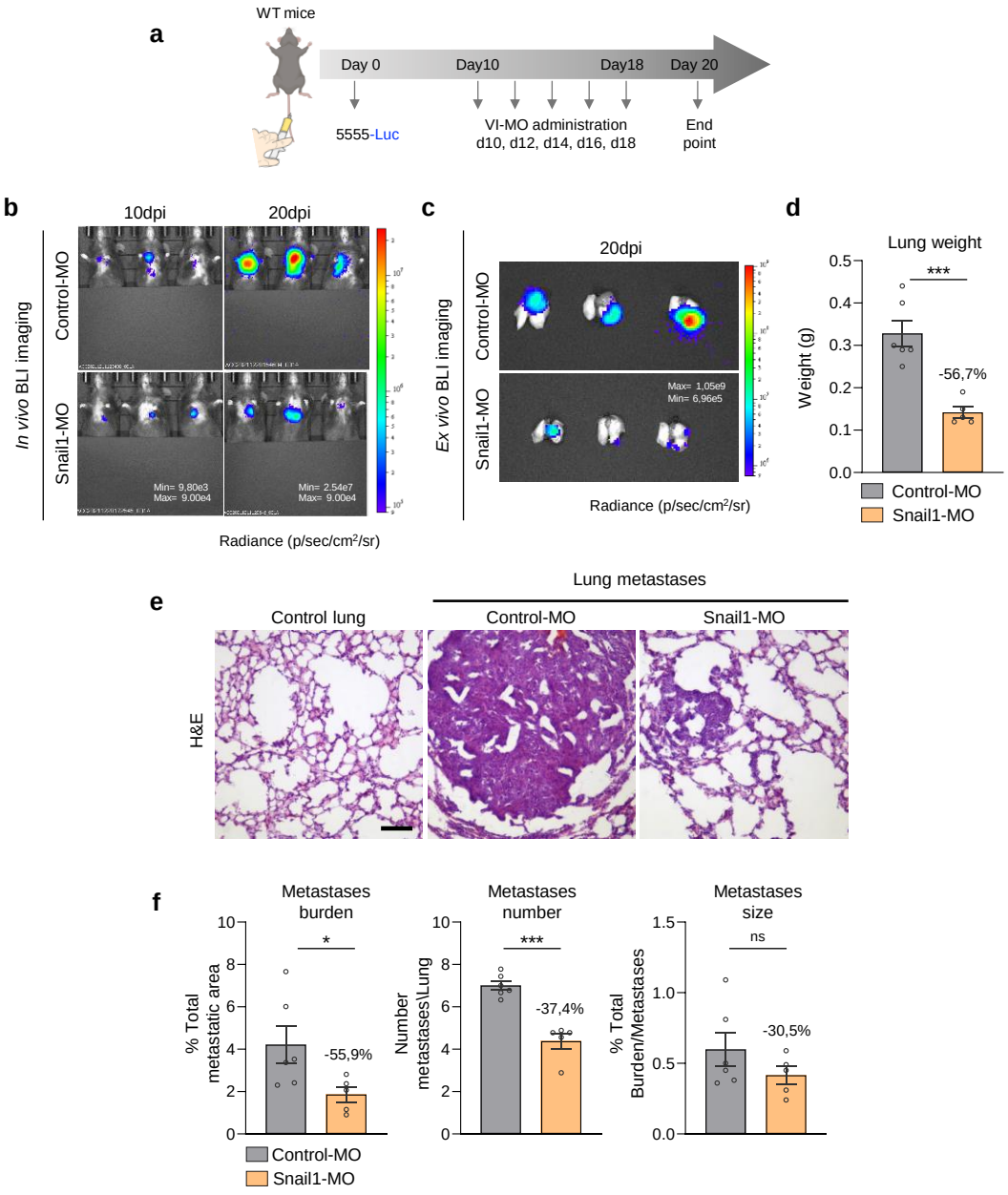


**Figure 36| Snail1 systemic targeting significantly reduces melanoma lung metastases in mice. (a)** Schematic representation of the experimental approach. Nine days after tail vein injection of $Braf^{V600E}$-5555 cells, C57BL/6 mice were injected with vivo-morpholino (VI-MO) control (Control-MO, n=6) or Snail1 morpholino (Snail1-MO, n=5) every other day. Created with BioRender.com. **(b)** Representative in vivo BLI signal images from mice in (a) at 10 and 20dpi. **(c)** Representative ex vivo BLI signal images of lungs from mice in (a) at 20dpi. The BLI scale is represented in each panel. Measurement units: p/s/cm$^2$/sr. **(d)** Final weight after collection of lungs from mice treated with Control-MO or Snail1-MO. **(e)** Representative H&E-stained lung sections after VI-MO treatment. Scale bar: 100µm. **(f)** Metastasis burden, metastasis number and metastasis size quantification from mice treated with Control-MO or Snail1-MO. Data are represented by Mean±SEM and statistically significant differences are tested by unpaired two-tailed Student t-test. Each dot represents one animal (ns= not significant, *=p<0.05, ***p<0.001).

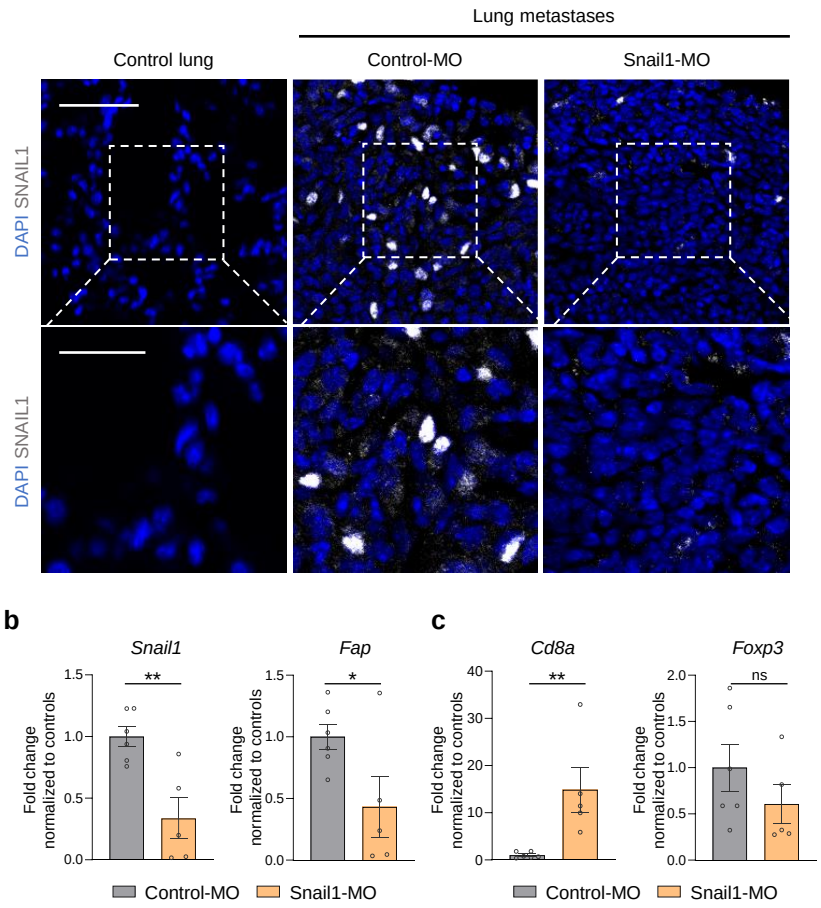


**Figure 37| Snail1 systemic targeting with VM enhances anti-tumour immunity at the metastatic nivhe. (a)** Representative images of immunolabelling for SNAIL1 (white) in lungs tissue sections after VI-MOs treatment. **(b)** *Snail1* and *Fap* mRNA levels assessed by RT-qPCR in lung metastases samples from mice treated with Control-MO (n=6) or Snail1-MO (n=5). **(c)** *Cd8a* and *Foxp3* mRNA levels assessed by RT-qPCR in lung metastases samples from mice treated with Control-MO (n=6) or Snail1-MO (n=5). Data are represented by Mean±SEM and statistically significant differences are tested by unpaired two-tailed Student t-test. Each dot represents one animal (ns= not significant, *=p<0.05, **p<0.01). Scale bars: 50µm and 25µm for higher magnification pictures.

Additionally, we assessed the impact of Snail1-MO treatment on the immune profile of the lungs. Notably, we observed a significant increase in *Cd8a* expression levels, along with a trend towards decreased *Foxp3* expression (**Figure 37c**). These findings indicate that systemic inhibition of Snail1 induce an anti-tumour immune response and reduces metastatic burden in melanoma, consistent with the effects observed in our Snail1$^{ME}$-KO mice.

# DISCUSSION

Snail1 is a crucial EMT-TF during embryonic development, but it is generally not expressed in healthy adult tissues. Its reactivation in epithelial cells is involved in fibrosis and the progression of several cancer types (Boutet et al., 2006; Nieto et al., 2016). Snail1-induced EMT provides carcinoma cells with migratory and invasive traits promoting metastasis (Nieto et al., 2016). Although previous studies have shown that Snail1 overexpression in melanoma cells *in vitro* promotes invasion and metastasis (Kudo-Saito et al., 2009), the contribution to melanoma biology in an *in vivo* context had not been defined. In this study, we identify a novel immunoregulatory role for Snail1 in melanoma when it is expressed in the TME.

Interestingly, the modulation of the immune response within the TME is crucial for determining clinical outcomes in cancer patients. Recent research underscores the importance of the TME in fostering anti-cancer immunity and affecting the effectiveness of immunotherapies. These findings suggest that targeting TME components could be a good strategy to improve treatment outcomes. Therefore, a thorough understanding of the TME is essential for predicting patient responses and identifying new therapeutic strategies (J. Chen et al., 2022).

By analysing mouse melanomas from different genetic backgrounds, we consistently identified the reactivation of Snail1 in the TME across all samples, that included inducible melanomas from GEMMs and subcutaneous and lung melanomas from allografts. This finding highlights the ubiquitous expression of Snail1$^{ME}$ and its potential as a key therapeutic target in tumours and metastasis from different genetic backgrounds. We specifically focused on investigating the contribution of Snail1 to BRAF-driven melanoma models, given the high prevalence of this mutation in this type of cancer (Rebecca et al., 2020). For this, we generated a mouse model that enables Snail1 ablation within an undisturbed immunocompetent environment, allowing us to investigate the contribution of Snail1$^{ME}$ to melanoma in an *in vivo* context. We demonstrate that blocking Snail1$^{ME}$, either prior to tumour and metastases establishment or after they are detectable, blocks melanoma growth. This is associated with increased apoptosis and reduced proliferation of melanoma cells upon Snail1$^{ME}$ targeting, leading to smaller tumours and metastases.

Characterization of melanomas from these models reveals that Snail1 is reactivated particularly in CAFs. Previous studies had identified Snail1 in the stroma of different carcinomas, particularly within the fibroblasts of breast and colorectal cancers (Francí et al., 2009; Stanisavljevic et al., 2015). As previously described, CAFs are a prominent component of the TME and are known to significantly contribute to tumour growth,

invasion and metastases (Lavie et al., 2022). The implication of Snail1 in CAFs from carcinomas has been linked to malignant phenotypes, leading to worse patient outcomes (Francí et al., 2009; A. Herrera et al., 2014; Stanisavljevic et al., 2015). However, the specific cellular and molecular mechanisms by which Snail1 impacts CAFs function, especially in melanoma, remained largely unexplored. Previous findings showed that Snail1 expression in CAFs from breast or colorectal cancer promotes tumour cell invasion through paracrine signalling (Alba-Castellón et al., 2016). However, we found that in melanoma Snail1 reactivation in CAFs leads to tumour growth. To elucidate the molecular mechanisms by which Snail1$^{+}$CAFs support melanoma growth, we conducted a transcriptomic analysis comparing fibroblasts isolated from tumours in Snail1$^{ME}$-WT and Snail1$^{ME}$-KO mice. Gene Ontology enrichment analysis revealed that differentially down-regulated genes in Snail1-KO fibroblasts are predominantly associated with the regulation and recruitment of immune cells. Although the contribution of stromal Snail1 to the regulation of the immune response in melanoma had not been previously described, these results are consistent with those obtained upon Snail1 transduction in melanoma cells reported previously. Particularly, this study indicated that silencing Snail1-induced EMT in melanoma cells improves systemic immune responses (Kudo-Saito et al., 2009).

Recently, single-cell RNA sequencing studies to investigate CAF heterogeneity and functionality across different tumour types have shed light into the understanding of their features that can be harnessed to design better cancer therapies (Costa et al., 2018; Lavie et al., 2022; Luo et al., 2022). While extensive characterization of CAF subsets in pancreas and breast cancer has been conducted (Lavie et al., 2022), less is known about CAFs biology in melanoma biology. Our results reveal that ablation of Snail1 leads to a decrease in pathways related to the activation of carcinoma-associated fibroblasts. This finding aligns with previous studies demonstrating that Snail1 expression in fibroblasts is necessary for their activation in different carcinoma models (Alba-Castellón et al., 2016), suggesting that this is also the case in melanoma. In addition, previous studies from the laboratory indicated that Snail1 is reactivated in renal fibrosis, promoting a profibrotic inflammatory environment by sustaining TGFβ signalling and cytokines production (Grande et al., 2015). Our results reveal a similar pattern in melanoma, where Snail1 depletion in CAFs affects TGFβ signalling and inflammation, impacting into the recruitment and activation of immune cells.

Interestingly, three different melanoma CAFs subsets have been recently identified in a syngeneic B16 melanoma model (Davidson et al., 2020). Notably, PDGFRα expression was widely found in the populations enriched at early stages of melanoma progression, which is the time point at which we performed the CAFs transcriptomic analysis. Two of the three populations described, associated with early melanoma stages, and exhibiting high levels of PDGFRα, were linked to immunomodulation. Subset S1 plays a direct role in the recruitment and regulation of immune cells, while subset S2 is associated with the modulation of the ECM remodelling, including different collagens members associated with a fibrotic phenotype (Bonnans et al., 2014), which is, in turn, implicated in immune exclusion (Davidson et al., 2020). Interestingly, our transcriptomic analysis show that CAFs in our melanoma BRAF-driven model are particularly enriched in the signatures corresponding to the S1 and S2 subpopulations, and that the bigger difference between CAFs upon Snail1 targeting corresponds to the immunoregulatory S1 signature. Therefore, all these results support that Snail1 is implicated in fostering an immunosuppressive environment, which, in turn, diminishes the anti-tumour immune responses. This is supported by our results showing that in subcutaneous tumours and metastases, Snail1$^{ME}$-targeting is associated with enhanced anti-tumour immune responses, evidenced by increased infiltration of CD8$^{+}$-T lymphocytes and decreased FOXP3$^{+}$-T lymphocytes.

Critically, we find that one of the most differentially expressed genes between fibroblasts from Snail1$^{ME}$-WT and Snail1$^{ME}$-KO tumours is *Fap*, which is highly expressed in Snail1$^{+}$CAFs and downregulated upon Snail1 targeting. Previous research indicated that targeting Fap can supress tumour growth in murine models. Nevertheless, the majority of these studies have primarily concentrated on the effects of Fap on tumour cell biology and tumour-associated angiogenesis in immunocompromised mice using xenograft models (J. D. Cheng et al., 2002; Lo et al., 2015). However, additional research had established an association between FAP-expressing CAF populations and immunosuppressive characteristics (Costa et al., 2018; Cremasco et al., 2018; Y. Zhang & Ertl, 2016). Interestingly, the suppression of FAP$^{+}$ stromal cells has been shown to promote anti-tumour responses mediated by T cells in an immunocompetent pancreatic mouse model (Kraman et al., 2010a) and FAP$^{+}$CAFs can induce an immunosuppressive phenotype by recruiting MDSCs through CCL2 signalling (Yang et al., 2016). Furthermore, elevated FAP expression in CAFs through the JAK-STAT3 signalling pathway contributes to a pro-tumorigenic immune response, leading to increased production of anti-inflammatory cytokines such as IL-10 and TGFβ (Yang et al., 2016).

Consistent with these evidences, our RNA-sequencing data shows downregulation of the JAK-STAT3 signalling pathway, among other pro-tumorigenic pathways, when Snail1 is blocked. These results align with the decreased *Fap* levels found in Snail1-KO CAFs, which are associated with anti-tumour immunity and reduced tumour growth. Indeed, we found that Snail1$^{ME}$-KO tumours exhibited a higher infiltration of CD8$^{+}$ cytotoxic T cells, B cells and NK cells, and a lower infiltration of FOXP3$^{+}$ regulatory T cells, which correlates with impaired melanoma growth. Further, FAP-expressing CAFs have been associated with the recruitment and differentiation of immunosuppressive cells such as regulatory FOXP3$^{+}$T lymphocytes, MDSCs, and TAMs (Y. Zhang & Ertl, 2016). In agreement with this, we find that the decrease in regulatory T cells found in the TME of tumours from Snail1$^{ME}$-KO mice favours an anti-tumorigenic phenotype. In addition, we find a statistically significant increase in *Arg1* mRNA levels in Snail1$^{ME}$-WT tumours. This enrichment is associated with the so-called M2 macrophage phenotype, known for its immunosuppressive properties and its role in supporting cancer progression (Hao et al., 2012).

Given these evidences indicating that FAP-expressing CAFs promote an immunosuppressive phenotype (Costa et al., 2018; Yang et al., 2016; Y. Zhang & Ertl, 2016) as well as tumour growth, invasion, and metastases (H. Wang et al., 2014; Wen et al., 2017), we further explored SNAIL1-FAP relationship. Notably, as mentioned above, *Fap* is among the most downregulated genes in our transcriptomic analysis of fibroblasts from Snail1$^{ME}$-KO mice. Our *in vitro* data, involving the overexpression or silencing of Snail1, indicate that Snail1 can regulate *Fap*. Although Snail1 is primarily recognized as a potent transcriptional repressor and was the first E-cadherin repressor identified (Batlle et al., 2000; Cano et al., 2000), Snail1 can shift its function to an activator through different mechanisms, such as interacting with CBP, which involves lysine residue acetylation (Hsu et al., 2014; Rembold et al., 2014), or by binding to the p65 subunit (Stanisavljevic et al., 2011). These interactions enable Snail1 to induce the expression of mesenchymal genes or promote immune modulation. In addition, in carcinoma cells, Snail1 directly activates cytokine transcription implicated in the recruitment of tumour-associated macrophages inducing changes in the TME (Hsu et al., 2014). Interestingly, in this study we used the drug CYD19 on fibroblast *in vitro* to specifically target Snail1. CYD19 drug has the ability to block Snail1-CBP/p300 interactions by disrupting the acetylation and stabilization of Snail1, which leads to its degradation and subsequently reduces the expression of its target genes (H. M. Li et al., 2020). Our findings suggest that the activation of Fap mediated by Snail1 might be due

to a potential interaction with CBP. This is evidenced by a significant decrease in *Fap* mRNA levels upon CYD19 treatment, concomitant with a reduction in Snail1 protein and mRNA levels. Interestingly, the pharmacological inhibition of Snail1 by CYD19 in carcinomas has been shown to impair tumour growth and metastases *in vitro* and *in vivo* (H. M. Li et al., 2020).

Previous studies have demonstrated that FAP is expressed in stromal fibroblasts of most epithelial cancers (Scanlan et al., 1994) and we show that *Snail1* expression is positively correlated with *Fap* expression across most cancer types, including melanoma. Critically, we have analysed *Fap* promoter region in different species, and found Snail1 binding sites in the *Fap* promoter. Furthermore, we demonstrate that SNAIL1 directly binds to the *Fap* promoter, indicating that Snail1 can induce *Fap* expression in fibroblasts. This induction might contribute to the immunosuppressive microenvironment in Snail1$^{ME}$-WT tumours, promoting a pro-tumorigenic response and resulting in larger tumours compared to those from Snail1$^{ME}$-KO mice.

Moreover, our work reveals that the ablation of Snail1$^{ME}$ in melanoma also impairs the colonization and progression of experimental lung metastases *in vivo*, indicating that blocking Snail1 reactivation in the melanoma microenvironment affects not only the subcutaneous compartment but also extends its influence to the metastatic niche. The results from the experimental lung metastases assays, where Snail1$^{ME}$ is abolished before and after tumour cell injections, reveals that blocking Snail1 not only impairs metastases growth but also decreases the number of metastases, indicating that Snail1$^{ME}$ plays a role in the colonization of melanoma cells. This finding suggests that targeting Snail1$^{ME}$ could be an effective therapeutic strategy to prevent early-stage metastatic dissemination in melanoma. Furthermore, we show that decreased *Fap* levels and anti-tumour immune responses in the metastatic niche upon Snail1 silencing recapitulate those occurring in the subcutaneous compartment. This suggests that despite the heterogeneity of CAFs, Snail1 is expressed in this population in an organ-independent manner to promote immunosuppression and tumour growth. Therefore, targeting Snail1$^{ME}$ could be a promising approach to enhance anti-tumour immunity and inhibit melanoma progression across different organs.

Immunosuppression in the TME is associated with poor patient outcomes and worst responses to immunotherapies, and therefore understanding the mechanisms driving immunosuppression is very relevant for cancer treatment (Rouse, 2007; Waldman et al., 2020). Immune checkpoint inhibitors have significantly improved melanoma therapies.

However, despite these advancements, their effectiveness is still limited, with a response rate of approximately 50% (Carlino et al., 2021). Current research efforts to enhance the efficacy of immune checkpoint inhibitors are focused on investigating the mechanisms that regulate immunosuppression (Jenkins et al., 2018) and identifying biomarkers to predict patient responses. Our findings indicate that Snail1 expression is associated with worse clinical outcomes in melanoma patients receiving anti-PD-1 therapy. This is consistent with the fact that Snail1$^{ME}$ promotes immunosuppression, as an immune-deprived tumour is likely to be less responsive to anti-PD-1 therapy, which relies on the activation of immune system to target and eliminate cancer (Gellrich et al., 2020). This highlights the potential to target Snail1 to improve response to anti-PD-1 therapy. However, our preliminary *in vivo* experiments show that the combination of anti-PD-1 therapy and Snail1$^{ME}$ loss does not significantly reduce tumour growth, suggesting that responses driven by targeting Snail1$^{ME}$ may share some of the antitumour immunity mechanisms elicited by PD-1 blockade. However, further experiments are needed to properly assess the effect of targeting Snail1 in combination with anti-PD-1 therapy in melanoma progression, including its impact on the metastatic niche.

Critically, previous attempts at targeting CAFs in cancer have included systemic inhibition of FAP, however this led to unexpected side effects, such as cachexia (Roberts et al., 2013). In this work, we demonstrate that *in vivo* systemic targeting with a Snail1 morpholino reduces metastatic burden in mice, extending their survival with no adverse effects. Moreover, as Snail1 was previously associated with increased metastasis by favouring immune evasion by an EMT-dependent mechanism in melanoma cells (Kudo-Saito et al., 2009), our data further support the Snail1 potential as a promising therapeutic target in melanoma. Snail1 has classically considered undruggable, however CYD19, has proved efficient in impairing tumour growth in mouse models of breast cancer (H. M. Li et al., 2020). In this study we show that this compound not only blocks Snail1 expression but also decreases *Fap* levels in fibroblasts and considering that Snail1 expression is almost absent in healthy tissues (Boutet et al., 2006), its inhibition in melanoma patients should be safe and lack major adverse effects.

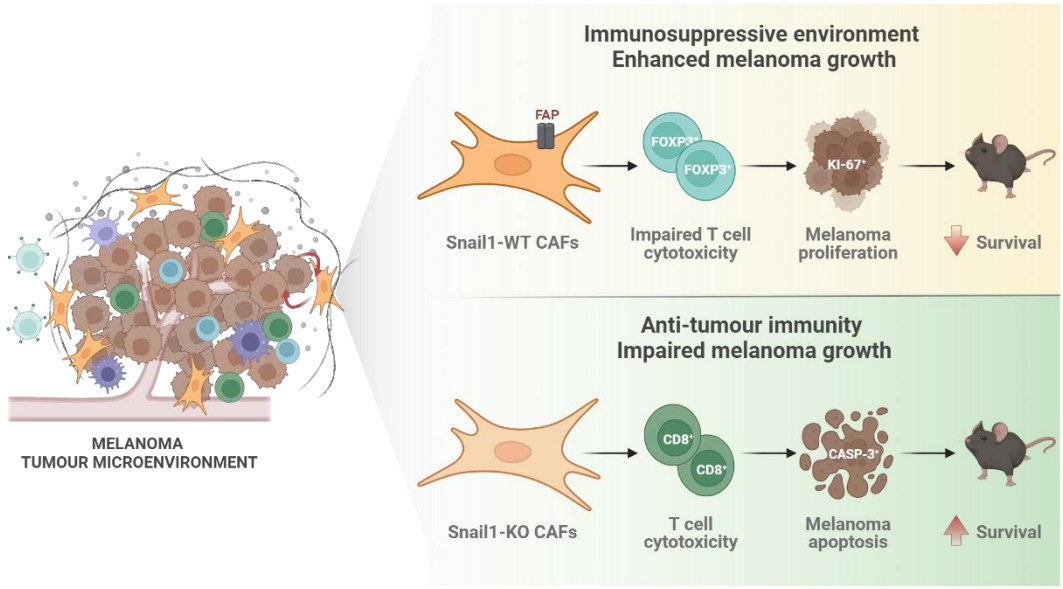


**Figure 38| Schematic illustration of the key findings on the regulatory role of Snail1$^{ME}$ in melanoma growth.** Briefly, Fap expression in fibroblasts is regulated by Snail1, leading to an immunosuppressive phenotype in the melanoma microenvironment. This process is partly driven by cytotoxic T cell dysfunction and regulatory T cell enrichment, thus promoting melanoma growth. Conversely, in the absence of Snail1 in the TME, Fap expression is downregulated in CAFs, resulting in a shift towards an anti-tumour immune response. These changes are directly linked to increased melanoma cell apoptosis, decreased tumour growth, reduced metastatic burden, and improved mice survival. Created with BioRender.com.

In this study, we demonstrate the crucial role of Snail1$^{ME}$ in shaping the TME and its significant impact on melanoma growth. Snail1$^{ME}$ acts as a driver of CAF-induced immunosuppression, reducing anti-tumour immunity and promoting melanoma progression (**Figure 38**). Furthermore, Snail1 expression correlates with reduced efficacy to immune checkpoint inhibitors. Therefore, our findings suggest that Snail1$^{ME}$ represents a promising therapeutic target for reactivating the immune system against melanoma. Targeting Snail1$^{ME}$ could enhance the efficacy of existing treatments and improve patient outcomes. Additionally, this research broadens our understanding of the complex interactions within the TME in cancer and provides a foundation for further studies on therapeutic strategies that may inhibit Snail1. Such interventions may offer new and effective avenues for combating this aggressive cancer.

# CONCLUSIONS

1. **Snail1 is reactivated in the melanoma microenvironment** across different mouse models, particularly in cancer-associated fibroblasts in subcutaneous tumours and at the metastatic niche.

2. **Snail1 expression in the microenvironment contributes to melanoma growth**. Snail1$^{ME}$ ablation blocks melanoma growth and promotes tumour cell apoptosis in subcutaneous tumours and metastases.

3. **Snail1 expression in CAFs is associated with fibroblast activation and immunosuppressive signatures**. Transcriptomic analysis of melanoma-associated fibroblasts upon Snail1$^{ME}$ silencing, and CAFs subsets in patient´s samples, indicates that Snail1 induces immunosuppression.

4. **Snail1 expression correlates with poor clinical outcomes in melanoma patients.** Immunosuppression contributes to reduced responses to immunotherapy, and there is an inverse correlation between Snail1 levels, and the effectiveness of anti-PD-1 therapy, supporting the immunosuppressive role of Snail 1 in melanoma.

5. **Snail1 targeting induces anti-tumour immune responses in melanoma.** Consistent with the identified immunosuppressive role of Snail1$^{ME}$, its depletion leads to increased infiltration of cytotoxic T cells, B cells, and NK cells, and decreased infiltration of regulatory T cells in subcutaneous tumours and metastasis, correlating with impaired melanoma growth.

6. **Snail1 induces Fap expression in fibroblasts.** Experiments in cultured fibroblasts indicate that FAP, a CAF marker previously associated with immunosuppression, is a direct target of Snail1. Analyses of available data from patient´s samples indicate a positive correlation between Snail1 and Fap expression.

7. **Systemic targeting of Snail1 *in vivo* reduces melanoma growth.** The use of VI-MO to block Snail1 is associated with a lower metastatic burden, reduced FAP levels and increased Cd8a levels, supporting enhanced anti-tumour immunity and highlighting the potential of Snail1 as a therapeutic strategy in melanoma treatment.

8. Altogether, these results indicate that **Snail1 is a driver of CAF-induced immunosuppression,** which reduces anti-tumour immunity and promotes melanoma growth.

# CONCLUSIONES

1. **Snail1 se reactiva en el microambiente del melanoma** en diferentes modelos de ratón, especialmente en los fibroblastos asociados al cáncer, tanto en tumores subcutáneos como en el nicho metastásico.

2. **La expresión de Snail1 en el microambiente favorece el crecimiento del melanoma.** La eliminación de Snail1 en el estroma detiene el crecimiento del melanoma y promueve la apoptosis de las células tumorales en melanomas subcutáneos y metástasis.

3. **La expresión de Snail1 en fibroblastos asociados al cáncer está relacionada con su activación y con características inmunosupresoras.** El análisis transcriptómico de fibroblastos asociados al melanoma, tras el silenciamiento de Snail1 en el microambiente, así como el estudio de las subpoblaciones de CAF en muestras de pacientes, indican que Snail1 promueve inmunosupresión.

4. **La expresión de Snail1 se asocia con resultados clínicos más desfavorables en pacientes con melanoma.** La inmunosupresión está relacionada con respuestas deficientes a la inmunoterapia, y la expresión de Snail1 muestra una correlación inversa con las respuestas a la terapia anti-PD-1, lo que respalda el papel inmunosupresor de Snail1 en el melanoma.

5. **La inhibición sistémica de Snail1 induce respuestas inmunitarias antitumorales en el melanoma**. Consistente con la identificación de su papel inmunosupresor en el estroma, la depleción de Snail1 provoca a una mayor infiltración de células T citotóxicas, células B y células NK, y a una reducción de la infiltración de células T reguladoras en tumores subcutáneos y metástasis, lo que se asocia con una disminución del crecimiento melanoma.

6. **Snail1 induce la expresión de Fap en fibroblastos.** Experimentos en fibroblastos cultivados indican que FAP, un marcador de CAF previamente asociado con la inmunosupresión está directamente regulado por Snail1. Los análisis de datos de muestras de pacientes indican una correlación positiva entre la expresión de Snail1 y Fap.

7. **El bloqueo sistémico de Snail1 *in vivo* reduce el crecimiento del melanoma.** El uso de VI-MO para bloquear Snail1 se asocia con una menor carga metastásica, niveles reducidos de FAP y niveles incrementados de Cd8a, lo que respalda una mayor inmunidad antitumoral y destaca el potencial de Snail1 como una estrategia terapéutica en el tratamiento del melanoma.

8. En conjunto, estos resultados indican que **Snail1 es un elemento clave en la inmunosupresión inducida por los CAF**, lo que disminuye la inmunidad antitumoral y favorece el crecimiento del melanoma

# BIBLIOGRAPHY

Ackermann, J., Frutschi, M., Kaloulis, K., McKee, T., Trumpp, A., & Beermann, F. (2005). Metastasizing melanoma formation caused by expression of activated N-RasQ61K on an INK4a-deficient background. *Cancer Research*, *65*(10), 4005–4011. https://doi.org/10.1158/0008-5472.CAN-04-2970

Aktary, Z., Raymond, J. H., Pouteaux, M., Delmas, V., Petit, V., & Larue, L. (2023). Derivation and Use of Cell Lines from Mouse Models of Melanoma. *Journal of Investigative Dermatology*, *143*(4), 538-544.e2. https://doi.org/10.1016/j.jid.2023.01.005

Alba-Castellón, L., Olivera-Salguero, R., Mestre-Farrera, A., Peña, R., Herrera, M., Bonilla, F., Casal, J. I., Baulida, J., Peña, C., & De Herreros, A. G. (2016). Snail1-dependent activation of cancer-associated fibroblast controls epithelial tumor cell invasion and metastasis. *Cancer Research*, *76*(21), 6205–6217. https://doi.org/10.1158/0008-5472.CAN-16-0176

Arozarena, I., & Wellbrock, C. (2019). Phenotype plasticity as enabler of melanoma progression and therapy resistance. *Nature Reviews Cancer*, *19*(7), 377–391. https://doi.org/10.1038/s41568-019-0154-4

Atkins, M. B., Lotze, M. T., Dutcher, J. P., Fisher, R. I., Weiss, G., Margolin, K., Abrams, J., Sznol, M., Parkinson, D., Hawkins, M., Paradise, C., Kunkel, L., & Rosenberg, S. A. (1999). High-dose recombinant interleukin 2 therapy for patients with metastatic melanoma: Analysis of 270 patients treated between 1985 and 1993. *Journal of Clinical Oncology*, *17*(7), 2105–2116. https://doi.org/10.1200/jco.1999.17.7.2105

Augsten, M. (2014). Cancer-associated fibroblasts as another polarized cell type of the tumor microenvironment. *Frontiers in Oncology*, *4 MAR*(March), 1–8. https://doi.org/10.3389/fonc.2014.00062

Baghban, R., Roshangar, L., Jahanban-esfahlan, R., Seidi, K., Ebrahimi-kalan, A., Jaymand, M., Kolahian, S., Javaheri, T., & Zare, P. (2020). Tumor microenvironment complexity and therapeutic implications at a glance. *Cell Communication and Signaling*, *18*, 1–19.

Balsamo, M., Scordamaglia, F., Pietra, G., Manzini, C., Cantoni, C., Boitano, M., Queirolo, P., Vermi, W., Facchetti, F., Moretta, A., Moretta, L., Mingari, M. C., & Vitale, M. (2009). Melanoma-associated fibroblasts modulate NK cell phenotype and antitumor cytotoxicity. *Proceedings of the National Academy of Sciences of the United States of America*, *106*(49), 20847–20852. https://doi.org/10.1073/pnas.0906481106

Barrallo-Gimeno, A., & Nieto, M. A. (2005). The Snail genes as inducers of cell movement and survival: Implications in development and cancer. *Development*, *132*(14), 3151–3161. https://doi.org/10.1242/dev.01907

Bartoschek, M., Oskolkov, N., Bocci, M., Lövrot, J., Larsson, C., Sommarin, M., Madsen, C. D., Lindgren, D., Pekar, G., Karlsson, G., Ringnér, M., Bergh, J., Björklund, Å., & Pietras, K. (2018). Spatially and functionally distinct subclasses of breast cancer-associated fibroblasts revealed by single cell RNA sequencing. *Nature Communications*, *9*(1). https://doi.org/10.1038/s41467-018-07582-3

Batlle, E., Sancho, E., Francí, C., Domínguez, D., Monfar, M., Baulida, J., & De Herreros, A. G. (2000). The transcription factor Snail is a repressor of E-cadherin gene expression in epithelial tumour cells. *Nature Cell Biology*, *2*(2), 84–89. https://doi.org/10.1038/35000034

Bauer, J., Curtin, J. A., Pinkel, D., & Bastian, B. C. (2007). Congenital Melanocytic Nevi Frequently Harbor NRAS Mutations but no BRAF Mutations. *Journal of Investigative Dermatology*, *127*, 179–182. https://doi.org/10.1038/sj.jid.5700490

Becker, J. C., Houben, R., Schrama, D., Voigt, H., Ugurel, S., & Reisfeld, R. A. (2010). Mouse models for melanoma: A personal perspective. *Experimental Dermatology*, *19*(2), 157–164. https://doi.org/10.1111/j.1600-0625.2009.00986.x

Biffi, G., Oni, T. E., Spielman, B., Hao, Y., Elyada, E., Preall, J., & Tuveson, D. A. (2019). IL-1-induced JAK/STAT signaling is antagonized by TGF-β to shape CAF heterogeneity in pancreatic ductal adenocarcinoma. *Cancer Discovery*, *9*(2), 282–301. https://doi.org/10.1158/2159-8290.CD-18-0710.IL-1-induced

Blanco-Gomez, A., Hontecillas-Prieto, L., Corchado-Cobos, R., García-Sancha, N., Salvador, N., Castellanos-Martín, A., Saez-Freire, M. D. M., Mendiburu-Eliçabe, M., Alonso-Lopez, D., De Las Rivas, J., Lorente, M., García-Casas, A., Del Carmen, S., Abad-Hernandez, M. D. M., Cruz-Hernandez, J. J., Rodríguez-Sanchez, C. A., Claros-Ampuero, J., García-Cenador, B., García-Criado, J., … Castillo-Lluva, S. (2020). Stromal SNAI2 is required for ERBB2 breast cancer progression. *Cancer Research*, *80*(23), 5216–5230. https://doi.org/10.1158/0008-5472.CAN-20-0278

Bonnans, C., Chou, J., & Werb, Z. (2014). Remodelling the extracellular matrix in development and disease. *Nature Reviews Molecular Cell Biology*, *15*(12), 786–801. https://doi.org/10.1038/nrm3904

Boon, T., Coulie, P. G., Van Den Eynde, B. J., & Van Der Bruggen, P. (2006). Human T cell responses against melanoma. *Annual Review of Immunology*, *24*, 175–208. https://doi.org/10.1146/annurev.immunol.24.021605.090733

Boutet, A., De Frutos, C. A., Maxwell, P. H., Mayol, M. J., Romero, J., & Nieto, M. A. (2006). Snail activation disrupts tissue homeostasis and induces fibrosis in the adult kidney. *EMBO Journal*, *25*(23), 5603–5613. https://doi.org/10.1038/sj.emboj.7601421

Boutros, A., Croce, E., Ferrari, M., Gili, R., Massaro, G., Marconcini, R., Arecco, L., Tanda, E. T., & Spagnolo, F. (2024). The treatment of advanced melanoma: Current approaches and new challenges. *Critical Reviews in Oncology/Hematology*, *196*(September 2023), 104276. https://doi.org/10.1016/j.critrevonc.2024.104276

Brabletz, T., Kalluri, R., Nieto, M. A., & Weinberg, R. A. (2018). EMT in cancer. *Nature Reviews Cancer*, *18*(2), 128–134. https://doi.org/10.1038/nrc.2017.118

Brenot, A., Knolhoff, B. L., Denardo, D. G., & Longmore, G. D. (2018). SNAIL1 action in tumor cells influences macrophage polarization and metastasis in breast cancer through altered GM-CSF secretion. *Oncogenesis*, *7*(32). https://doi.org/10.1038/s41389-018-0042-x

Brighton, H. E., Angus, S. P., Bo, T., Roques, J., Tagliatela, A. C., Darr, D. B., Karagoz, K., Sciaky, N., Gatza, M. L., Sharpless, N. E., Johnson, G. L., & Bear, J. E. (2018). New mechanisms of resistance to MEK inhibitors in melanoma revealed by intravital imaging. *Cancer Research*, *78*(2), 542–557. https://doi.org/10.1158/0008-5472.CAN-17-1653

Cano, A., Pérez-Moreno, M. A., Rodrigo, I., Locascio, A., Blanco, M. J., Del Barrio, M. G., Portillo, F., & Nieto, M. A. (2000). The transcription factor Snail controls epithelial-mesenchymal transitions by repressing E-cadherin expression. *Nature Cell Biology*, *2*(2), 76–83. https://doi.org/10.1038/35000025

Caramel, J., Papadogeorgakis, E., Hill, L., Browne, G. J., Richard, G., Wierinckx, A., Saldanha, G., sborne, J., Hutchinson, P., Tse, G., Lachuer, J., Puisieux, A., Pringle, J. H., Ansieau, S., & Tulchinsky, E. (2013). A Switch in the Expression of Embryonic EMT-Inducers Drives the Development of Malignant Melanoma. *Cancer Cell*, *24*(4), 466–480. https://doi.org/10.1016/j.ccr.2013.08.018

Carlino, M. S., Larkin, J., & Long, G. V. (2021). Immune checkpoint inhibitors in melanoma. *The Lancet*, *398*(10304), 1002–1014. https://doi.org/10.1016/S0140-6736(21)01206-X

Carr, S., Smith, C., & Wernberg, J. (2020). Epidemiology and Risk Factors of Melanoma. *Surgical Clinics of North America*, *100*(1), 1–12. https://doi.org/10.1016/j.suc.2019.09.005

Carver, E. A., Jiang, R., Lan, Y., Oram, K. F., & Gridley, T. (2001). The Mouse Snail Gene Encodes a Key Regulator of the Epithelial-Mesenchymal Transition. *Molecular and Cellular Biology*, *21*(23), 8184–8188. https://doi.org/10.1128/mcb.21.23.8184-8188.2001

Chakraborty, M., Chu, K., Shrestha, A., Revelo, X. S., Zhang, X., Gold, M. J., Khan, S., Lee, M., Huang, C., Akbari, M., Barrow, F., Chan, Y. T., Lei, H., Kotoulas, N. K., Jovel, J., Pastrello, C., Kotlyar, M., Goh, C., Michelakis, E., … Winer, D. A. (2021). Mechanical Stiffness Controls Dendritic Cell Metabolism and Function. *Cell Reports*, *34*(2), 108609. https://doi.org/10.1016/j.celrep.2020.108609

Chapman, P. B., Hauschild, A., Robert, C., Haanen, J. B., Ascierto, P., Larkin, J., Dummer, R., Garbe, C., Testori, A., Maio, M., Hogg, D., Lorigan, P., Lebbe, C., Jouary, T., Schadendorf, D., Ribas, A., O'Day, S. J., Sosman, J. A., Kirkwood, J. M., … McArthur, G. A. (2011). Improved Survival with Vemurafenib in Melanoma with BRAF V600E Mutation. *New England Journal of Medicine*, *364*(26), 2507–2516. https://doi.org/10.1056/nejmoa1103782

Chen, I. X., Chauhan, V. P., Posada, J., Ng, M. R., Wu, M. W., Adstamongkonkul, P., Huang, P., Lindeman, N., Langer, R., & Jain, R. K. (2019). Blocking CXCR4 alleviates desmoplasia, increases T-lymphocyte infiltration, and improves immunotherapy in metastatic breast cancer. *Proceedings of the National Academy of Sciences of the United States of America*, *116*(10), 4558–4566. https://doi.org/10.1073/pnas.1815515116

Chen, J., Hu, S., Wang, H., Zhao, T., Song, Y., Zhong, X., Luo, Q., Xu, M., He, L., Chen, Q., Du, B., Xiao, J., & Wang, K. (2022). Integrated analysis reveals the pivotal interactions between immune cells in the melanoma tumor microenvironment. *Scientific Reports*, *12*(1), 1–16. https://doi.org/10.1038/s41598-022-14319-2

Chen, S., Zhu, G., Yang, Y., Wang, F., Xiao, Y. T., Zhang, N., Bian, X., Zhu, Y., Yu, Y., Liu, F., Dong, K., Mariscal, J., Liu, Y., Soares, F., Loo Yau, H., Zhang, B., Chen, W., Wang, C., Chen, D., … Ren, S. (2021). Single-cell analysis reveals transcriptomic remodellings in distinct cell types that contribute to human prostate cancer progression. *Nature Cell Biology*, *23*(1), 87–98. https://doi.org/10.1038/s41556-020-00613-6

Chen, X., & Song, E. (2019). Turning foes to friends: targeting cancer-associated fibroblasts. *Nature Reviews Drug Discovery*, *18*(2), 99–115. https://doi.org/10.1038/s41573-018-0004-1

Cheng, J. D., Dunbrack, R. L., Valianou, M., Rogatko, A., Alpaugh, R. K., & Weiner, L. M. (2002). Promotion of tumor growth by murine fibroblast activation protein, a serine protease, in an animal model. *Cancer Research*, *62*(16), 4767–4772.

Cheng, J. T., Deng, Y. N., Yi, H. M., Wang, G. Y., Fu, B. S., Chen, W. J., Liu, W., Tai, Y., Peng, Y. W., & Zhang, Q. (2016). Hepatic carcinoma-associated fibroblasts induce ido-producing regulatory dendritic cells through il-6-mediated stat3 activation. *Oncogenesis*, *5*(2). https://doi.org/10.1038/oncsis.2016.7

Cirenajwis, H., Lauss, M., Ekedahl, H., Torngren, T., Kvist, A., Saal1, L. H., Olsson, H., Staaf, J., Carneiro, A., Ingvar, C., Harbst, K., Hayward, N. K., & Jonsson, G. (2017). NF1 -mutated melanoma tumors harbor distinct clinical and biological characteristics. *Molecular Oncology*, *11*, 438–451. https://doi.org/10.1002/1878-0261.12050

Clark, W. H., Elder, D. E., Guerry, D., Epstein, M. N., Greene, M. H., & Van Horn, M. (1984). A Study of Tumor Progression : The Precursor Lesions of Superficial Spreading and Nodular Melanoma. *Human Pathology*, *15*(12), 1147–1165. https://doi.org/10.1016/S0046-8177(84)80310-X

Cohen, N., Shani, O., Raz, Y., Sharon, Y., Hoffman, D., Abramovitz, L., & Erez, N. (2017). Fibroblasts drive an immunosuppressive and growth-promoting microenvironment in breast cancer via secretion of Chitinase 3-like 1. *Oncogene*, *36*(31), 4457–4468. https://doi.org/10.1038/onc.2017.65

Comito, G., Giannoni, E., Segura, C. P., Barcellos-De-Souza, P., Raspollini, M. R., Baroni, G., Lanciotti, M., Serni, S., & Chiarugi, P. (2014). Cancer-associated fibroblasts and M2-polarized macrophages synergize during prostate carcinoma progression. *Oncogene*, *33*(19), 2423–2431. https://doi.org/10.1038/onc.2013.191

Cortés, M., Sanchez-Moral, L., de Barrios, O., Fernández-Aceñero, M. J., Martínez-Campanario, M., Esteve-Codina, A., Darling, D. S., Győrffy, B., Lawrence, T., Dean, D. C., & Postigo, A. (2017). Tumor-associated macrophages (TAMs) depend on ZEB1 for their cancer-promoting roles. *The EMBO Journal*, *36*(22), 3336–3355. https://doi.org/10.15252/embj.201797345

Cortez, E., Roswall, P., & Pietras, K. (2014). Functional subsets of mesenchymal cell types in the tumor microenvironment. *Seminars in Cancer Biology*, *25*, 3–9. https://doi.org/10.1016/j.semcancer.2013.12.010

Costa, A., Kieffer, Y., Scholer-Dahirel, A., Pelon, F., Bourachot, B., Cardon, M., Sirven, P., Magagna, I., Fuhrmann, L., Bernard, C., Bonneau, C., Kondratova, M., Kuperstein, I., Zinovyev, A., Givel, A. M., Parrini, M. C., Soumelis, V., Vincent-Salomon, A., & Mechta-Grigoriou, F. (2018). Fibroblast Heterogeneity and Immunosuppressive Environment in Human Breast Cancer. *Cancer Cell*, *33*(3), 463-479.e10. https://doi.org/10.1016/j.ccell.2018.01.011

Cremasco, V., Astarita, J. L., Grauel, A. L., Keerthivasan, S., MacIsaac, K., Woodruff, M. C., Wu, M., Spel, L., Santoro, S., Amoozgar, Z., Laszewski, T., Migoni, S. C., Knoblich, K., Fletcher, A. L., LaFleur, M., Wucherpfennig, K. W., Pure, E., Dranoff, G., Carroll, M. C., & Turley, S. J. (2018). FAP delineates heterogeneous and functionally divergent stromal cells in immune-excluded breast tumors. *Cancer Immunology Research*, *6*(12), 1472–1485. https://doi.org/10.1158/2326-6066.CIR-18-0098

Dankort, D., Curley, D. P., Cartlidge, R. A., Nelson, B., Karnezis, A. N., Damsky, W. E., You, M. J., DePinho, R. A., McMahon, M., & Bosenberg, M. (2009). BrafV600E cooperates with Pten loss to induce metastatic melanoma. *Nature Genetics*, *41*(5), 544–552. https://doi.org/10.1038/ng.356

Davidson, S., Efremova, M., Riedel, A., Mahata, B., Pramanik, J., Huuhtanen, J., Kar, G., Vento-Tormo, R., Hagai, T., Chen, X., Haniffa, M. A., Shields, J. D., & Teichmann, S. A. (2020). Single-Cell RNA Sequencing Reveals a Dynamic Stromal Niche That Supports Tumor Growth. *Cell Reports*, *31*(7), 107628. https://doi.org/10.1016/j.celrep.2020.107628

Davis, L. E., Shalin, S. C., & Tackett, A. J. (2019). Current state of melanoma diagnosis and treatment. *Cancer Biology and Therapy*, *20*(11), 1366–1379. https://doi.org/10.1080/15384047.2019.1640032

Dhomen, N., Reis-filho, J. S., Dias, R., Hayward, R., Savage, K., Delmas, V., Larue, L., Pritchard, C., & Marais, R. (2009). Oncogenic Braf Induces Melanocyte Senescence and Melanoma in Mice. *Cancer Cell*, *15*(4), 294–303. https://doi.org/10.1016/j.ccr.2009.02.022

Dongre, A., Rashidian, M., Reinhardt, F., Bagnato, A., Keckesova, Z., Ploegh, H. L., & Weinberg, R. A. (2017). Epithelial-to-mesenchymal Transition contributes to Immunosuppression in Breast Carcinomas. *Cancer Research*, *77*, 3982–3989. https://doi.org/10.1158/0008-5472.CAN-16-3292.Epithelial-to-mesenchymal

Dongre, A., & Weinberg, R. A. (2019). New insights into the mechanisms of epithelial–mesenchymal transition and implications for cancer. *Nature Reviews Molecular Cell Biology*, *20*(2), 69–84. https://doi.org/10.1038/s41580-018-0080-4

Dumont, N., Liu, B., Defilippis, R. A., Chang, H., Rabban, J. T., Karnezis, A. N., Tjoe, J. A., Marx, J., Parvin, B., & Tlsty, T. D. (2013). Breast fibroblasts modulate early dissemination, tumorigenesis, and metastasis through alteration of extracellular matrix characteristics. *Neoplasia (United States)*, *15*(3), 249–262. https://doi.org/10.1593/neo.121950

Eggermont, A. M. M., & Kirkwood, J. M. (2004). Re-evaluating the role of dacarbazine in metastatic melanoma: What have we learned in 30 years? *European Journal of Cancer*, *40*(12), 1825–1836. https://doi.org/10.1016/j.ejca.2004.04.030

Elyada, E., Bolisetty, M., Laise, P., Flynn, W. F., Elise, T., Burkhart, R. A., Teinor, J. A., Belleau, P., Biffi, G., Lucito, M. S., Sivajothi, S., Armstrong, T. D., Engle, D. D., Yu, K. H., Hao, Y., Wolfgang, C. L., Park, Y., & Preall, J. (2019). Cross-species single-cell analysis of pancreatic ductal adenocarcinoma reveals antigen-presenting cancer-associated fibroblasts Ela. *Cancer Discovery*, *9*(8), 1102–1123. https://doi.org/10.1158/2159-8290.CD-19-0094.Cross-species

Erdogan, B., Ao, M., White, L. M., Means, A. L., Brewer, B. M., Yang, L., Washington, M. K., Shi, C., Franco, O. E., Weaver, A. M., Hayward, S. W., Li, D., & Webb, D. J. (2017). Cancer-associated fibroblasts promote directional cancer cell migration by aligning fibronectin. *Journal of Cell Biology*, *216*(11), 3799–3816. https://doi.org/10.1083/jcb.201704053

Erdogan, B., & Webb, D. J. (2017). Cancer-associated fibroblasts modulate growth factor signaling and extracellular matrix remodeling to regulate tumor metastasis. *Biochemical Society Transactions*, *45*(1), 229–236. https://doi.org/10.1053/j.gastro.2016.08.014.CagY

Erez, N., Truitt, M., Olson, P., & Hanahan, D. (2010). Cancer-Associated Fibroblasts Are Activated in Incipient Neoplasia to Orchestrate Tumor-Promoting Inflammation in an NF-κB-Dependent Manner. *Cancer Cell*, *17*(2), 135–147. https://doi.org/10.1016/j.ccr.2009.12.041

Eroglu, Z., & Ribas, A. (2016). Combination therapy with BRAF and MEK inhibitors for melanoma: Latest evidence and place in therapy. *Therapeutic Advances in Medical Oncology*, *8*(1), 48–56. https://doi.org/10.1177/1758834015616934

Fabris, V. T., Sahores, A., Vanzulli, S. I., Colombo, L., Molinolo, A. A., Lanari, C., & Lamb, C. A. (2010). Inoculated mammary carcinoma-associated fibroblasts : contribution to hormone independent tumor growth. *BMC Cancer*, *10*.

Fang, J., Liang Xiao, Joo, K.-I., Liu, Y., Zhang, C., Liu, S., Conti, P. S., Li, Z., & Wanga, P. (2016). A Potent Immunotoxin Targeting Fibroblast Activation Protein for Treatment of Breast Cancer in Mice Jinxu. *International Journal of Cancer*, *138*(4), 1013–1023. https://doi.org/10.1002/ijc.29831.A

Fecher, L. A., Amaravadi, R. K., & Flaherty, K. T. (2008). *The MAPK pathway in melanoma*.

Feig, C., Jones, J. O., Kraman, M., Wells, R. J. B., Deonarine, A., Chan, D. S., Connell, C. M., Roberts, E. W., Zhao, Q., Caballero, O. L., Teichmann, S. A., Janowitz, T., Jodrell, D. I., Tuveson, D. A., & Fearon, D. T. (2013). Targeting CXCL12 from FAP-expressing carcinoma-associated fibroblasts synergizes with anti-PD-L1 immunotherapy in pancreatic cancer. *Proceedings of the National Academy of Sciences of the United States of America*, *110*(50), 20212–20217. https://doi.org/10.1073/pnas.1320318110

Fidler, I. J. (1973). Selection of successive tumour lines for metastasis. *Nat. New Biol*, *241*, 20.

Filipazzi, P., Valenti, R., Huber, V., Pilla, L., Canese, P., Iero, M., Castelli, C., Mariani, L., Parmiani, G., & Rivoltini, L. (2007). Identification of a new subset of myeloid suppressor cells in peripheral blood of melanoma patients with modulation by a granulocyte-macrophage colony-stimulation factor-based antitumor vaccine. *Journal of Clinical Oncology*, *25*(18), 2546–2553. https://doi.org/10.1200/JCO.2006.08.5829

Flach, E. H., Rebecca, V. W., Herlyn, M., Smalley, K. S. M., & Anderson, A. R. A. (2011). Fibroblasts contribute to melanoma tumor growth and drug resistance. *Molecular Pharmaceutics*, *8*(6), 2039–2049. https://doi.org/10.1021/mp200421k

Flint, T. R., Janowitz, T., Connell, C. M., Roberts, E. W., Denton, A. E., Coll, A. P., Jodrell, D. I., & Fearon, D. T. (2016). Tumor-Induced IL-6 Reprograms Host Metabolism to Suppress Anti-tumor Immunity. *Cell Metabolism*, *24*(5), 672–684. https://doi.org/10.1016/j.cmet.2016.10.010

Ford, D., Bliss, J. M., Swerdlow, A. J., Armstrong, B. K., Franceschi, S., Green, A., Holly, E. A., Mack, T., Mackie, R. M., Østerlind, A., Walter, S. D., Peto, J., & Easton, D. F. (1995). Risk of cutaneous melanoma associated with a family history of the disease. *International Journal of Cancer*, *62*(4), 377–381. https://doi.org/10.1002/ijc.2910620403

Francí, C., Gallén, M., Alameda, F., Baró, T., Iglesias, M., Virtanen, I., & de Herreros, A. G. (2009). Snail1 protein in the stroma as a new putative prognosis marker for colon tumours. *PLoS ONE*, *4*(5), 1–7. https://doi.org/10.1371/journal.pone.0005595

Franco, D. L., Mainez, J., Vega, S., Sancho, P., Murillo, M. M., De Frutos, C. A., Del Castillo, G., López-Blau, C., Fabregat, I., & Nieto, M. A. (2010). Snail1 suppresses TGF-β-induced apoptosis and is sufficient to trigger EMT in hepatocytes. *Journal of Cell Science*, *123*(20), 3467–3477. https://doi.org/10.1242/jcs.068692

Gandini, S., Sera, F., Cattaruzza, M. S., Pasquini, P., Abeni, D., Boyle, P., & Melchi, C. F. (2005). Meta-analysis of risk factors for cutaneous melanoma: I. Common and atypical naevi. *European Journal of Cancer*, *41*(1), 28–44. https://doi.org/10.1016/j.ejca.2004.10.015

Garbe, C., Amaral, T., Peris, K., Hauschild, A., Arenberger, P., Basset-Seguin, N., Bastholt, L., Bataille, V., del Marmol, V., Dréno, B., Fargnoli, M. C., Forsea, A. M., Grob, J. J., Höller, C., Kaufmann, R., Kelleners-Smeets, N., Lallas, A., Lebbé, C., Lytvynenko, B., … Lorigan, P. (2022). European consensus-based interdisciplinary guideline for melanoma. Part 1: Diagnostics: Update 2022. *European Journal of Cancer*, *170*, 236–255. https://doi.org/10.1016/j.ejca.2022.03.008

Gazzaniga, S., Bravo, A. I., Guglielmotti, A., Van Rooijen, N., Maschi, F., Vecchi, A., Mantovani, A., Mordoh, J., & Wainstok, R. (2007). Targeting tumor-associated macrophages and inhibition of MCP-1 reduce angiogenesis and tumor growth in a human melanoma xenograft. *Journal of Investigative Dermatology*, *127*(8), 2031–2041. https://doi.org/10.1038/sj.jid.5700827

Geissmann, F., Jung, S., & Littman, D. R. (2003). Blood monocytes consist of two principal subsets with distinct migratory properties. *Immunity*, *19*(1), 71–82. https://doi.org/10.1016/S1074-7613(03)00174-2

Gellrich, F. F., Schmitz, M., Beissert, S., & Meier, F. (2020). Anti-PD-1 and novel combinations in the treatment of melanoma—an update. *Journal of Clinical Medicine*, *9*(1), 1–17. https://doi.org/10.3390/jcm9010223

Goel, V. K., Lazar, A. J. F., Warneke, C. L., Redston, M. S., & Haluska, F. G. (2006). Examination of mutations in BRAF, NRAS, and PTEN in primary cutaneous melanoma. *Journal of Investigative Dermatology*, *126*(1), 154–160. https://doi.org/10.1038/sj.jid.5700026

Gottardi, C. J., Wong, E., & Gumbiner, B. M. (2001). E-Cadherin Suppresses Cellular Transformation by Inhibiting b-Catenin Signaling in an Adhesion-independent Manner. *The Journal of Cell Biology*, *153*(5), 1049–1059.

Grande, M. T., Sánchez-Laorden, B., López-Blau, C., De Frutos, C. A., Boutet, A., Arévalo, M., Rowe, R. G., Weiss, S. J., López-Novoa, J. M., & Nieto, M. A. (2015). Snail1-induced partial epithelial-to-mesenchymal transition drives renal fibrosis in mice and can be targeted to reverse established disease. *Nature Medicine*, *21*(9), 989–997. https://doi.org/10.1038/nm.3901

Guo, X., Oshima, H., Kitmura, T., Taketo, M. M., & Oshima, M. (2008). Stromal Fibroblasts Activated by Tumor Cells Promote Angiogenesis in Mouse Gastric Cancer. *Journal of Biological Chemistry*, *283*(28), 19864–19871. https://doi.org/10.1074/jbc.M800798200

Gutiérrez-Castañeda, L. D., Nova, J. A., & Tovar-Parra, J. D. (2020). Frequency of mutations in BRAF, NRAS, and KIT in different populations and histological subtypes of melanoma: A systemic review. *Melanoma Research*, 62–70. https://doi.org/10.1097/CMR.0000000000000628

Haass, N. K., Smalley, K. S. M., & Li, L. (2005). Adhesion , migration and communication in melanocytes and melanoma. *Pigment Cell Melanoma Res.*, *18*, 150–159. https://doi.org/10.1111/j.1600-0749.2005.00235.x

Hamid, O., Robert, C., Daud, A., Hodi, F. S., Hwu, W. J., Kefford, R., Wolchok, J. D., Hersey, P., Joseph, R., Weber, J. S., Dronca, R., Mitchell, T. C., Patnaik, A., Zarour, H. M., Joshua, A. M., Zhao, Q., Jensen, E., Ahsan, S., Ibrahim, N., & Ribas, A. (2019). Five-year survival outcomes for patients with advanced melanoma treated with pembrolizumab in KEYNOTE-001. *Annals of Oncology*, *30*(4), 582–588. https://doi.org/10.1093/annonc/mdz011

Hanahan, D. (2022). Hallmarks of Cancer: New Dimensions. *Cancer Discovery*, *12*(1), 31–46. https://doi.org/10.1158/2159-8290.CD-21-1059

Hao, N. B., Lü, M. H., Fan, Y. H., Cao, Y. L., Zhang, Z. R., & Yang, S. M. (2012). Macrophages in tumor microenvironments and the progression of tumors. *Clinical and Developmental Immunology*, *2012*. https://doi.org/10.1155/2012/948098

Haqq, C., Nosrati, M., Sudilovsky, D., Crothers, J., Khodabakhsh, D., Pulliam, B. L., Federman, S., Iii, J. R. M., Allen, R. E., Singer, M. I., Leong, S. P. L., Ljung, B., Sagebiel, R. W., & Kashani-sabet, M. (2005). The gene expression signatures of melanoma progression. *PNAS*, *102*(17), 6092–6097. https://doi.org/10.1073/pnas.0501564102

Harper, J., & Sainson, R. C. A. (2014). Regulation of the anti-tumour immune response by cancer-associated fibroblasts. *Seminars in Cancer Biology*, *25*, 69–77. https://doi.org/10.1016/j.semcancer.2013.12.005

Hayward, N. K., Wilmott, J. S., Waddell, N., Johansson, P. A., Field, M. A., Nones, K., Patch, A.-M., Kakavand, H., Alexandrov, L. B., Burke, H., Jakrot, V., Kazakoff, S., Holmes, O., Leonard, C., Sabarinathan, R., Mularoni, L., Wood, S., Xu, Q., Waddell, N., … Mann, G. J. (2017). Whole-genome landscapes of major melanoma subtypes. *Nature*, *545*. https://doi.org/10.1038/nature22071

Hazlehurst, L. A., Damiano, J. S., Buyuksal, I., Pledger, W. J., & Dalton, W. S. (2000). Adhesion to fibronectin via β1 integrins regulates p27(kip1) levels and contributes to cell adhesion mediated drug resistance (CAM-DR). *Oncogene*, *19*(38), 4319–4327. https://doi.org/10.1038/sj.onc.1203782

He, A., Shen, X., Ma, Q., Cao, J., von Gise, A., Zhou, P., Wang, G., Marquez, V. E., Orkin, S. H., & Pu, W. T. (2012). PRC2 directly methylates GATA4 and represses its transcriptional activity. *Genes and Development*, *26*(1), 37–42. https://doi.org/10.1101/gad.173930.111

Herrera, A., Herrera, M., Alba-Castellon, L., Silva, J., García, V., Loubat-Casanovas, J., Álvarez-Cienfuegos, A., Miguel García, J., Rodriguez, R., Gil, B., Jesús Citores, M., Jesús Larriba, M., Ignacio Casal, J., De Herreros, A. G., Bonilla, F., & Peña, C. (2014). Protumorigenic effects of Snail-expression fibroblasts on colon cancer cells. *International Journal of Cancer*, *134*(12), 2984–2990. https://doi.org/10.1002/ijc.28613

Herrera, M., Herrera, A., Domínguez, G., Silva, J., García, V., García, J. M., Gómez, I., Soldevilla, B., Muñoz, C., Provencio, M., Campos-Martin, Y., García de Herreros, A., Casal, I., Bonilla, F., & Peña, C. (2013). Cancer-associated fibroblast and M2 macrophage markers together predict outcome in colorectal cancer patients. *Cancer Science*, *104*(4), 437–444. https://doi.org/10.1111/cas.12096

Hino, R., Kabashima, K., Kato, Y., Yagi, H., Nakamura, M., Honjo, T., Okazaki, T., & Tokura, Y. (2010). Tumor cell expression of programmed cell death-1 ligand 1 is a prognostic factor for malignant melanoma. *Cancer*, *116*(7), 1757–1766. https://doi.org/10.1002/cncr.24899

Hirata, E., Girotti, M. R., Viros, A., Hooper, S., Spencer-Dene, B., Matsuda, M., Larkin, J., Marais, R., & Sahai, E. (2015). Intravital imaging reveals how BRAF inhibition generates drug-tolerant microenvironments with high integrin β1/FAK Signaling. *Cancer Cell*, *27*(4), 574–588. https://doi.org/10.1016/j.ccell.2015.03.008

Hlatky, L., Tsionou, C., Hahnfeldt, P., & Coleman, C. N. (1994). Mammary Fibroblasts May Influence Breast Tumor Angiogenesis via Hypoxia-induced Up-Regulation and Protein Expression. *Cancer Research*, *54*, 6083–6086.

Hodi, F. S., Chiarion-Sileni, V., Gonzalez, R., Grob, J. J., Rutkowski, P., Cowey, C. L., Lao, C. D., Schadendorf, D., Wagstaff, J., Dummer, R., Ferrucci, P. F., Smylie, M., Hill, A., Hogg, D., Marquez-Rodas, I., Jiang, J., Rizzo, J., Larkin, J., & Wolchok, J. D. (2018). Nivolumab plus ipilimumab or nivolumab alone versus ipilimumab alone in advanced melanoma (CheckMate 067): 4-year outcomes of a multicentre, randomised, phase 3 trial. *The Lancet Oncology*, *19*(11), 1480–1492. https://doi.org/10.1016/S1470-2045(18)30700-9

Hofheinz, R. D., Al-Batran, S. E., Hartmann, F., Hartung, G., Jäger, D., Renner, C., Tanswell, P., Kunz, U., Amelsberg, A., Kuthan, H., & Stehle, G. (2003). Stromal antigen targeting by a humanised monoclonal antibody: An early phase II trial of sibrotuzumab in patients with metastatic colorectal cancer. *Onkologie*, *26*(1), 44–48. https://doi.org/10.1159/000069863

Hsu, D. S. S., Wang, H. J., Tai, S. K., Chou, C. H., Hsieh, C. H., Chiu, P. H., Chen, N. J., & Yang, M. H. (2014). Acetylation of snail modulates the cytokinome of cancer cells to enhance the recruitment of macrophages. *Cancer Cell*, *26*(4), 534–548. https://doi.org/10.1016/j.ccell.2014.09.002

Itakura, E., Huang, R., Wen, D., Paul, E., Cochran, A. J., Angeles, L., Angeles, L., Comprehensive, J., & Angeles, L. (2011). IL-10 expression by primary tumor cells correlates with melanoma progression from radial to vertical growth phase and development of metastatic competence. *Mod Pathol*, *24*(6), 801–809. https://doi.org/10.1038/modpathol.2011.5.IL-10

Jenkins, R. W., Barbie, D. A., & Flaherty, K. T. (2018). Mechanisms of resistance to immune checkpoint inhibitors. *British Journal of Cancer*, *118*(1), 9–16. https://doi.org/10.1038/bjc.2017.434

Jenkins, R. W., & Fisher, D. E. (2021). Treatment of Advanced Melanoma in 2020 and Beyond. *J Invest Dermatol.*, *141*(1), 23–31. https://doi.org/10.1016/j.jid.2020.03.943.Treatment

Joyce, J. A., & Fearon, D. T. (2015). T cell exclusion, immune privilege, and the tumor microenvironment. *Cancer Immunology and Immunotherapy*, *348*(6230).

Jung, S., Aliberti, J., Graemmel, P., Sunshine, M. J., Kreutzberg, G. W., Sher, A., & Littman, D. R. (2000). Analysis of Fractalkine Receptor CX 3 CR1 Function by Targeted Deletion and Green Fluorescent Protein Reporter Gene Insertion. *Molecular and Cellular Biology*, *20*(11), 4106–4114. https://doi.org/10.1128/mcb.20.11.4106-4114.2000

Junttila, M. R., & De Sauvage, F. J. (2013). Influence of tumour micro-environment heterogeneity on therapeutic response. *Nature*, *501*(7467), 346–354. https://doi.org/10.1038/nature12626

Kääriäinen, E., Nummela, P., Soikkeli, J., Yin, M., Lukk, M., Jahkola, T., Virolainen, S., Ora, A., Ukkonen, E., Saksela, O., & Höltta, E. (2006). Switch to an invasive growth phase in melanoma is associated with tenascin-C, fibronectin, and procollagen-I forming specific channel structures for invasion. *Journal of Pathology*, *210*, 181–191. https://doi.org/10.1002/path

Kalluri, R. (2016). The biology and function of fibroblasts in cancer. *Nature Reviews Cancer*, *16*(9), 582–598. https://doi.org/10.1038/nrc.2016.73

Kalluri, R., & Zeisberg, M. (2006). Fibroblasts in cancer. *Nature Reviews Cancer*, *6*(5), 392–401. https://doi.org/10.1038/nrc1877

Kanitakis, J. (2020). Anatomy , histology and immunohistochemistry of normal human skin. *European Journal of Dermatology*, *185*, 3379–3390.

Karras, P., Bordeu, I., Pozniak, J., Nowosad, A., Pazzi, C., Raemdonck, N., Landeloos, E., Herck, Y., Pedri, D., Bervoets, G., Makhzami, S., Khoo, J. H., Pavie, B., Lamote, J., Marin-bejar, O., Dewaele, M., Liang, H., Zhang, X., Hua, Y., … Marine, J. (2022). A cellular hierarchy in melanoma uncouples growth and metastasis. *Nature*, *610*, 190–198. https://doi.org/10.1038/s41586-022-05242-7

Kaur, A., Webster, M. R., Marchbank, K., Behera, R., Ndoye, A., Kugel, C. H., Dang, V. M., Appleton, J., O'Connell, M. P., Cheng, P., Valiga, A. A., Morissette, R., McDonnell, N. B., Ferrucci, L., Kossenkov, A. V., Meeth, K., Tang, H. Y., Yin, X., Wood, W. H., … Weeraratna, A. T. (2016). SFRP2 in the aged microenvironment drives melanoma metastasis and therapy resistance. *Nature*, *532*(7598), 250–254. https://doi.org/10.1038/nature17392

Kieffer, Y., Hocine, H. R., Gentric, G., Pelon, F., Bernard, C., Bourachot, B., Lameiras, S., Albergante, L., Bonneau, C., Guyard, A., Tarte, K., Zinovyev, A., Baulande, S., Zalcman, G., Vincent-Salomon, A., & Mechta-Grigoriou, F. (2020). Single-cell analysis reveals fibroblast clusters linked to immunotherapy resistance in cancer. *Cancer Discovery*, *10*(9), 1330–1351. https://doi.org/10.1158/2159-8290.CD-19-1384

Kinoshita, T., Ishii, G., Hiraoka, N., Hirayama, S., Yamauchi, C., Aokage, K., Hishida, T., Yoshida, J., Nagai, K., & Ochiai, A. (2013). Forkhead box P3 regulatory T cells coexisting with cancer associated fibroblasts are correlated with a poor outcome in lung adenocarcinoma. *Cancer Science*, *104*(4), 409–415. https://doi.org/10.1111/cas.12099

Kovács, S. A., & Győrffy, B. (2022). Transcriptomic datasets of cancer patients treated with immune-checkpoint inhibitors: a systematic review. *Journal of Translational Medicine*, *20*(1), 1–15. https://doi.org/10.1186/s12967-022-03409-4

Kozar, I., Margue, C., Rothengatter, S., Haan, C., & Kreis, S. (2019). Many ways to resistance: How melanoma cells evade targeted therapies. *Biochimica et Biophysica Acta - Reviews on Cancer*, *1871*(2), 313–322. https://doi.org/10.1016/j.bbcan.2019.02.002

Kraman, M., Bambrough, P. J., Arnold, J. N., Roberts, E. W., Magiera, L., Jones, J. O., Gopinathan, A., Tuveson, D. A., & Fearon, D. T. (2010a). Suppression of antitumor immunity by stromal cells expressing fibroblast activation protein-α. *Science*, *330*(6005), 827–830. https://doi.org/10.1126/science.1195300

Kraman, M., Bambrough, P. J., Arnold, J. N., Roberts, E. W., Magiera, L., Jones, J. O., Gopinathan, A., Tuveson, D. A., & Fearon, D. T. (2010b). Suppression of Antitumor Immunity by Stromal Cells Expressing Fibroblast Activation Protein–a. *Science*, *330*(November), 827–830.

Ksiazkiewicz, M., Gottfried, E., Kreutz, M., Mack, M., Hofstaedter, F., & Kunz-Schughart, L. A. (2010). Importance of CCL2-CCR2A/2B signaling for monocyte migration into spheroids of breast cancer-derived fibroblasts. *Immunobiology*, *215*(9–10), 737–747. https://doi.org/10.1016/j.imbio.2010.05.019

Kuczek, D. E., Larsen, A. M. H., Thorseth, M. L., Carretta, M., Kalvisa, A., Siersbæk, M. S., Simões, A. M. C., Roslind, A., Engelholm, L. H., Noessner, E., Donia, M., Svane, I. M., Straten, P. T., Grøntved, L., & Madsen, D. H. (2019). Collagen density regulates the activity of tumor-infiltrating T cells. *Journal for ImmunoTherapy of Cancer*, *7*(1), 1–15. https://doi.org/10.1186/s40425-019-0556-6

Kudo-Saito, C., Shirako, H., Takeuchi, T., & Kawakami, Y. (2009). Cancer Metastasis Is Accelerated through Immunosuppression during Snail-Induced EMT of Cancer Cells. *Cancer Cell (2009) 15(3) 195-206*. http://ac.els-cdn.com/S1535610809000324/1-s2.0-S1535610809000324-main.pdf?_tid=ee389d7c-c684-11e5-bb54-00000aacb361&acdnat=1454071174_e8bca0dd8025cf245a3948d1a9866a01

Kuehnemuth, B., Piseddu, I., Wiedemann, G. M., Lauseker, M., Kuhn, C., Hofmann, S., Schmoeckel, E., Endres, S., Mayr, D., Jeschke, U., & Anz, D. (2018). CCL1 is a major regulatory T cell attracting factor in human breast cancer. *BMC Cancer*, *18*(1), 1–6. https://doi.org/10.1186/s12885-018-5117-8

Kumari, N., Dwarakanath, B. S., Das, A., & Bhatt, A. N. (2016). Role of interleukin-6 in cancer progression and therapeutic resistance. *Tumor Biology*, *37*(9), 11553–11572. https://doi.org/10.1007/s13277-016-5098-7

Kuzet, S. E., & Gaggioli, C. (2016). Fibroblast activation in cancer: when seed fertilizes soil. *Cell and Tissue Research*, *365*(3), 607–619. https://doi.org/10.1007/s00441-016-2467-x

Kuzu, O. F., Nguyen, F. D., Noory, M. A., & Sharma, A. (2015). Current State of Animal (Mouse) Modeling in Melanoma Research. *Cancer Growth and Metastasis*, *8s1*, CGM.S21214. https://doi.org/10.4137/cgm.s21214

Lakins, M. A., Ghorani, E., Munir, H., Martins, C. P., & Shields, J. D. (2018). Cancer-associated fibroblasts induce antigen-specific deletion of CD8 + T Cells to protect tumour cells. *Nature Communications*, *9*(1), 1–9. https://doi.org/10.1038/s41467-018-03347-0

Lambrechts, D., Wauters, E., Boeckx, B., Aibar, S., Nittner, D., Burton, O., Bassez, A., Decaluwé, H., Pircher, A., Van den Eynde, K., Weynand, B., Verbeken, E., De Leyn, P., Liston, A., Vansteenkiste, J., Carmeliet, P., Aerts, S., & Thienpont, B. (2018). Phenotype molding of stromal cells in the lung tumor microenvironment. *Nature Medicine*, *24*(8), 1277–1289. https://doi.org/10.1038/s41591-018-0096-5

Lánczky, A., & Győrffy, B. (2021). Web-based survival analysis tool tailored for medical research (KMplot): Development and implementation. *Journal of Medical Internet Research*, *23*(7), 1–7. https://doi.org/10.2196/27633

Larue, L., & Beermann, F. (2007). Cutaneous melanoma in genetically modified animals. *Pigment Cell Research*, *20*(6), 485–497. https://doi.org/10.1111/j.1600-0749.2007.00411.x

Lavie, D., Ben-Shmuel, A., Erez, N., & Scherz-Shouval, R. (2022). Cancer-associated fibroblasts in the single-cell era. *Nature Cancer*, *3*(7), 793–807. https://doi.org/10.1038/s43018-022-00411-z

Lawrence, M. S., Stojanov, P., Polak, P., Kryukov, G. V., Cibulskis, K., Sivachenko, A., Carter, S. L., Stewart, C., Mermel, C. H., Roberts, S. A., Kiezun, A., Hammerman, P. S., McKenna, A., Drier, Y., Zou, L., Ramos, A. H., Pugh, T. J., Stransky, N., Helman, E., … Getz, G. (2013). Mutational heterogeneity in cancer and the search for new cancer-associated genes. *Nature*, *499*(7457), 214–218. https://doi.org/10.1038/nature12213

Lee, J., Fassnacht, M., Nair, S., Boczkowski, D., & Gilboa, E. (2005). Tumor immunotherapy targeting fibroblast activation protein, a product expressed in tumor-associated fibroblasts. *Cancer Research*, *65*(23), 11156–11163. https://doi.org/10.1158/0008-5472.CAN-05-2805

Lee, K.-W., Yeo, S.-Y., Gong, J.-R., Koo, O.-J., Sohn, I., Lee, W. Y., Kim, H. C., Yun, S. H., Cho, Y. B., Choi, M.-A., An, S., Kim, J., Sung, C. O., Cho, K.-H., & Kim, S.-H. (2022). PRRX1 is a master transcription factor of stromal fibroblasts for myofibroblastic lineage progression. *Nature Communications*, *13*(1), 1–23. https://doi.org/10.1038/s41467-022-30484-4

Leonardi, G. C., Candido, S., Falzone, L., Spandidos, D. A., & Libra, M. (2020). Cutaneous melanoma and the immunotherapy revolution (Review). *International Journal of Oncology*, *57*(3), 609–618. https://doi.org/10.3892/ijo.2020.5088

Li, H., Courtois, E. T., Sengupta, D., Tan, Y., Chen, K. H., Goh, J. J. L., Kong, S. L., Chua, C., Hon, L. K., Tan, W. S., Wong, M., Choi, P. J., Wee, L. J. K., Hillmer, A. M., Tan, I. B., Robson, P., & Prabhakar, S. (2017). Reference component analysis of single-cell transcriptomes elucidates cellular heterogeneity in human colorectal tumors. *Nature Genetics*, *49*(5), 708–718. https://doi.org/10.1038/ng.3818

Li, H. M., Bi, Y. R., Li, Y., Fu, R., Lv, W. C., Jiang, N., Xu, Y., Ren, B. X., Chen, Y. D., Xie, H., Wang, S., Lu, T., & Wu, Z. Q. (2020). A potent CBP/p300-Snail interaction inhibitor suppresses tumor growth and metastasis in wild-type p53-expressing cancer. *Science Advances*, *6*(17). https://doi.org/10.1126/sciadv.aaw8500

Li, T., Yang, Y., Hua, X., Wang, G., Liu, W., Jia, C., Tai, Y., Zhang, Q., & Chen, G. (2012). Hepatocellular carcinoma-associated fibroblasts trigger NK cell dysfunction via PGE2 and IDO. *Cancer Letters*, *318*(2), 154–161. https://doi.org/10.1016/j.canlet.2011.12.020

Li, T., Yi, S., Liu, W., Jia, C., Wang, G., Hua, X., Tai, Y., Zhang, Q., & Chen, G. (2013). Colorectal carcinoma-derived fibroblasts modulate natural killer cell phenotype and antitumor cytotoxicity. *Medical Oncology*, *30*(3). https://doi.org/10.1007/s12032-013-0663-z

Lim, S. Y., Shklovskaya, E., Lee, J. H., Pedersen, B., Stewart, A., Ming, Z., Irvine, M., Shivalingam, B., Saw, R. P. M., Menzies, A. M., Carlino, M. S., Scolyer, R. A., Long, G. V, & Rizos, H. (2023). The molecular and functional landscape of resistance to immune checkpoint blockade in melanoma. *Nature Communications*, *14*. https://doi.org/10.1038/s41467-023-36979-y

Liu, S., Kumar, S. M., Martin, J. S., Yang, R., & Xu, X. (2011). Snail1 mediates hypoxia-induced melanoma progression. *American Journal of Pathology*, *179*(6), 3020–3031. https://doi.org/10.1016/j.ajpath.2011.08.038

Lo, A., Wang, L. C. S., Scholler, J., Monslow, J., Avery, D., Newick, K., O'Brien, S., Evans, R. A., Bajor, D. J., Clendenin, C., Durham, A. C., Buza, E. L., Vonderheide, R. H., June, C. H., Albelda, S. M., & Pure, E. (2015). Tumor-promoting desmoplasia is disrupted by depleting FAP-expressing stromal cells. *Cancer Research*, *75*(14), 2800–2810. https://doi.org/10.1158/0008-5472.CAN-14-3041

Lu, W., & Kang, Y. (2019). Epithelial-Mesenchymal Plasticity in Cancer Progression and Metastasis. *Developmental Cell*, *49*(3), 361–374. https://doi.org/10.1016/j.devcel.2019.04.010

Luo, H., Xia, X., Huang, L. Bin, An, H., Cao, M., Kim, G. D., Chen, H. N., Zhang, W. H., Shu, Y., Kong, X., Ren, Z., Li, P. H., Liu, Y., Tang, H., Sun, R., Li, C., Bai, B., Jia, W., Liu, Y., … Xu, H. (2022). Pan-cancer single-cell analysis reveals the heterogeneity and plasticity of cancer-associated fibroblasts in the tumor microenvironment. *Nature Communications*, *13*, 6619. https://doi.org/10.1038/s41467-022-34395-2

Mace, T. A., Ameen, Z., Collins, A., Wojcik, S., Mair, M., Young, G. S., Fuchs, J. R., Eubank, T. D., Frankel, W. L., Bekaii-Saab, T., Bloomston, M., & Lesinski, G. B. (2013). Pancreatic cancer-associated stellate cells promote differentiation of myeloid-derived suppressor cells in a STAT3-dependent manner. *Cancer Research*, *73*(10), 3007–3018. https://doi.org/10.1158/0008-5472.CAN-12-4601

Madhunapantula, S. V., Patel, T. N., Annageldiyev, C., & Sharma, A. (2019). Animal (mouse) models of melanoma. In *Animal Models in Cancer Drug Discovery*. Elsevier Inc. https://doi.org/10.1016/B978-0-12-814704-7.00017-9

Mariathasan, S., Turley, S. J., Nickles, D., Castiglioni, A., Yuen, K., Wang, Y., Kadel, E. E., Koeppen, H., Astarita, J. L., Cubas, R., Jhunjhunwala, S., Banchereau, R., Yang, Y., Guan, Y., Chalouni, C., Ziai, J., Şenbabaoğlu, Y., Santoro, S., Sheinson, D., … Powles, T. (2018). TGFβ attenuates tumour response to PD-L1 blockade by contributing to exclusion of T cells. *Nature*, *554*(7693), 544–548. https://doi.org/10.1038/nature25501

Martinenaite, E., Munir Ahmad, S., Hansen, M., Met, Ö., Westergaard, M. W., Larsen, S. K., Klausen, T. W., Donia, M., Svane, I. M., & Andersen, M. H. (2016). CCL22-specific T Cells: Modulating the immunosuppressive tumor microenvironment. *OncoImmunology*, *5*(11). https://doi.org/10.1080/2162402X.2016.1238541

Meads, M. B., Gatenby, R. A., & Dalton, W. S. (2009). Environment-mediated drug resistance: a major contributor to minimal residual disease. *Nature Reviews*, *9*, 665–674. https://doi.org/10.1016/B978-0-12-374984-0.00951-7

Meeth, K., Wang, J. X., Micevic, G., Damsky, W., & Bosenberg, M. W. (2016). The YUMM lines: a series of congenic mouse melanoma cell lines with defined genetic alterations. *Pigment Cell and Melanoma Research*, *29*(5), 590–597. https://doi.org/10.1111/pcmr.12498

Melnikova, V. O., Bolshakov, S. V., Walker, C., & Ananthaswamy, H. N. (2004). Genomic alterations in spontaneous and carcinogen-induced murine melanoma cell lines. *Oncogene*, *23*(13), 2347–2356. https://doi.org/10.1038/sj.onc.1207405

Menzies, A. M., Long, G. V., & Murali, R. (2012). Dabrafenib and its potential for the treatment of metastatic melanoma. *Drug Design, Development and Therapy*, *6*, 391–405. https://doi.org/10.2147/DDDT.S38998

Miller, A. J., & Mihm, M. C. (2006). Melanoma. *The New England Journal of Medicine*, *355*, 51–65.

Miracco, C., Mourmouras, V., Biagioli, M., Rubegni, P., Mannucci, S., Monciatti, I., Cosci, E., Tosi, P., & Luzi, P. (2007). Utility of tumour-infiltrating CD25+FOXP3+ regulatory T cell evaluation in predicting local recurrence in vertical growth phase cutaneous melanoma. *Oncology Reports*, *18*(5), 1115–1122.

Monteran, L., & Erez, N. (2019). The dark side of fibroblasts: Cancer-associated fibroblasts as mediators of immunosuppression in the tumor microenvironment. *Frontiers in Immunology*, *10*(AUG), 1–15. https://doi.org/10.3389/fimmu.2019.01835

Mootha, V. K., Lindgren, C. M., Eriksson, K. F., Subramanian, A., Sihag, S., Lehar, J., Puigserver, P., Carlsson, E., Ridderstråle, M., Laurila, E., Houstis, N., Daly, M. J., Patterson, N., Mesirov, J. P., Golub, T. R., Tamayo, P., Spiegelman, B., Lander, E. S., Hirschhorn, J. N., … Groop, L. C. (2003). PGC-1α-responsive genes involved in oxidative phosphorylation are coordinately downregulated in human diabetes. *Nature Genetics*, *34*(3), 267–273. https://doi.org/10.1038/ng1180

Movahedi, K., Laoui, D., Gysemans, C., Baeten, M., Stangé, G., Van Bossche, J. Den, Mack, M., Pipeleers, D., In't Veld, P., De Baetselier, P., & Van Ginderachter, J. A. (2010). Different tumor microenvironments contain functionally distinct subsets of macrophages derived from Ly6C(high) monocytes. *Cancer Research*, *70*(14), 5728–5739. https://doi.org/10.1158/0008-5472.CAN-09-4672

Mueller, K. L., Madden, J. M., Zoratti, G. L., Kuperwasser, C., List, K., & Boerner, J. L. (2012). Fibroblast-secreted hepatocyte growth factor mediates epidermal growth factor receptor tyrosine kinase inhibitor resistance in triple-negative breast cancers through paracrine activation of Met. *Breast Cancer Research*, *14*(4), 1–11. https://doi.org/10.1186/bcr3224

Nieto, M. A. (2013). Epithelial plasticity: A common theme in embryonic and cancer cells. *Science*, *342*(6159). https://doi.org/10.1126/science.1234850

Nieto, M. A. (2017). Context-specific roles of EMT programmes in cancer cell dissemination. *Nature Cell Biology*, *19*(5), 416–418. https://doi.org/10.1038/ncb3520

Nieto, M. A., Bennett, M. F., Sargent, M. G., & Wilkinson, D. G. (1992). Cloning and developmental expression of Sna, a murine homologue of the Drosophila snail gene. *Development*, *116*(1), 227–237. https://doi.org/10.1242/dev.116.1.227

Nieto, M. A., & Cano, A. (2012). The epithelial-mesenchymal transition under control: Global programs to regulate epithelial plasticity. *Seminars in Cancer Biology*, *22*(5–6), 361–368. https://doi.org/10.1016/j.semcancer.2012.05.003

Nieto, M. A., Huang, R. Y. Y. J., Jackson, R. A. A., & Thiery, J. P. P. (2016). Emt: 2016. *Cell*, *166*(1), 21–45. https://doi.org/10.1016/j.cell.2016.06.028

Öhlund, D., Handly-Santana, A., Biffi, G., Elyada, E., Almeida, A. S., Ponz-Sarvise, M., Corbo, V., Oni, T. E., Hearn, S. A., Lee, E. J., Chio, I. I. C., Hwang, C. Il, Tiriac, H., Baker, L. A., Engle, D. D., Feig, C., Kultti, A., Egeblad, M., Fearon, D. T., … Tuveson, D. A. (2017). Distinct populations of inflammatory fibroblasts and myofibroblasts in pancreatic cancer. *The Journal of Experimental Medicine*, *214*(3), 579–596. https://doi.org/10.1084/jem.20162024

Omholt, K., Platz, A., Kanter, L., Ringborg, U., & Hansson, J. (2003). NRAS and BRAF Mutations Arise Early during Melanoma Pathogenesis and Are Preserved throughout Tumor Progression. *Clinical Cancer Resarch*, *9*, 6483–6488.

Orimo, A., Gupta, P. B., Sgroi, D. C., Arenzana-Seisdedos, F., Delaunay, T., Naeem, R., Carey, V. J., Richardson, A. L., & Weinberg, R. A. (2005). Stromal fibroblasts present in invasive human breast carcinomas promote tumor growth and angiogenesis through elevated SDF-1/CXCL12 secretion. *Cell*, *121*(3), 335–348. https://doi.org/10.1016/j.cell.2005.02.034

Ostermann, E., Garin-Chesa, P., Heider, K. H., Kalat, M., Lamche, H., Puri, C., Kerjaschki, D., Rettig, W. J., & Adolf, G. R. (2008). Effective immunoconjugate therapy in cancer models targeting a serine protease of tumor fibroblasts. *Clinical Cancer Research*, *14*(14), 4584–4592. https://doi.org/10.1158/1078-0432.CCR-07-5211

Östman, A., & Augsten, M. (2009). Cancer-associated fibroblasts and tumor growth - bystanders turning into key players. *Current Opinion in Genetics and Development*, *19*(1), 67–73. https://doi.org/10.1016/j.gde.2009.01.003

Özdemir, B. C., Pentcheva-Hoang, T., Carstens, J. L., Zheng, X., Wu, C. C., Simpson, T. R., Laklai, H., Sugimoto, H., Kahlert, C., Novitskiy, S. V., DeJesus-Acosta, A., Sharma, P., Heidari, P., Mahmood, U., Chin, L., Moses, H. L., Weaver, V. M., Maitra, A., Allison, J. P., … Kalluri, R. (2014). Depletion of carcinoma-associated fibroblasts and fibrosis induces immunosuppression and accelerates pancreas cancer with reduced survival. *Cancer Cell*, *25*(6), 719–734. https://doi.org/10.1016/j.ccr.2014.04.005

Park, C. C., Zhang, H. J., Yao, E. S., Park, C. J., & Bissell, M. J. (2008). B1 Integrin Inhibition Dramatically Enhances Radiotherapy Efficacy in Human Breast Cancer Xenografts. *Cancer Research*, *68*(11), 4398–4405. https://doi.org/10.1158/0008-5472.CAN-07-6390

Patsouras, D., Papaxoinis, K., Kostakis, A., Safioleas, M. C., Lazaris, A. C., & Nicolopoulou-Stamati, P. (2015). Fibroblast activation protein and its prognostic significance in correlation with vascular endothelial growth factor in pancreatic adenocarcinoma. *Molecular Medicine Reports*, *11*, 4585–4590. https://doi.org/10.3892/mmr.2015.3259

Pedri, D., Karras, P., Landeloos, E., Marine, J. C., & Rambow, F. (2022). Epithelial-to-mesenchymal-like transition events in melanoma. *FEBS Journal*, *289*(5), 1352–1368. https://doi.org/10.1111/febs.16021

Peinado, H., Olmeda, D., & Cano, A. (2007). Snail, ZEB and bHLH factors in tumour progression: An alliance against the epithelial phenotype? *Nature Reviews Cancer*, *7*(6), 415–428. https://doi.org/10.1038/nrc2131

Petit, V., Raymond, J., Alberti, C., Pouteaux, M., Gallagher, S. J., Nguyen, M. Q., Aplin, A. E., Delmas, V., & Larue, L. (2019). C57BL/6 congenic mouse NRASQ61K melanoma cell lines are highly sensitive to the combination of Mek and Akt inhibitors in vitro and in vivo. *Pigment Cell and Melanoma Research*, *32*(6), 829–841. https://doi.org/10.1111/pcmr.12807

Podar, K., Fan, F., Schimming, A., & Jaeger, D. (2012). Targeting the tumor microenvironment: Focus on angiogenesis. *Journal of Oncology*, *2012*. https://doi.org/10.1155/2012/281261

Pollock, P. M., Harper, U. L., Hansen, K. S., Yudt, L. M., Stark, M., Robbins, C. M., Moses, T. Y., Hostetter, G., Wagner, U., Kakareka, J., Salem, G., Pohida, T., Heenan, P., Duray, P., Kallioniemi, O., Hayward, N. K., Trent, J. M., & Meltzer, P. S. (2003). High frequency of BRAF mutations in nevi. *Nature Genetics*, *33*, 19–20. https://doi.org/10.1038/ng1054

Poser, I., Domínguez, D., Garcia De Herreros, A., Varnai, A., Buettner, R., & Bosserhoff, A. K. (2001). Loss of E-cadherin Expression in Melanoma Cells Involves Up-regulation of the Transcriptional Repressor Snail. *Journal of Biological Chemistry*, *276*(27), 24661–24666. https://doi.org/10.1074/jbc.M011224200

Postovit, L. M., Seftor, E. A., Seftor, R. E. B., & Hendrix, M. J. C. (2006). Influence of the microenvironment on melanoma cell fate determination and phenotype. *Cancer Research*, *66*(16), 7833–7836. https://doi.org/10.1158/0008-5472.CAN-06-0731

Puram, S. V., Tirosh, I., Parikh, A. S., Patel, A. P., Yizhak, K., Gillespie, S., Rodman, C., Luo, C. L., Mroz, E. A., Emerick, K. S., Deschler, D. G., Varvares, M. A., Mylvaganam, R., Rozenblatt-Rosen, O., Rocco, J. W., Faquin, W. C., Lin, D. T., Regev, A., & Bernstein, B. E. (2017). Single-Cell Transcriptomic Analysis of Primary and Metastatic Tumor Ecosystems in Head and Neck Cancer. *Cell*, *171*(7), 1611-1624.e24. https://doi.org/10.1016/j.cell.2017.10.044

Qiao, Y., Zhang, C., Li, A., Wang, D., Luo, Z., Ping, Y., Zhou, B., Liu, S., Li, H., Yue, D., Zhang, Z., Chen, X., Shen, Z., Lian, J., Li, Y., Wang, S., Li, F., Huang, L., Wang, L., … Zhang, Y. (2018). IL6 derived from cancer-associated fibroblasts promotes chemoresistance via CXCR7 in esophageal squamous cell carcinoma. *Oncogene*, *37*(7), 873–883. https://doi.org/10.1038/onc.2017.387

Rastrelli, M., Tropea, S., Rossi, C. R., & Alaibac, M. (2014). Melanoma: epidemiology, risk factors, pathogenesis, diagnosis and classification. *In Vivo*, *28(6):1005*, 1005–1011. https://doi.org/10.1093/med/9780199971015.003.0002

Rebecca, V. W., Somasundaram, R., & Herlyn, M. (2020). Pre-clinical modeling of cutaneous melanoma. *Nature Communications*, *11*(1), 1–9. https://doi.org/10.1038/s41467-020-15546-9

Rembold, M., Ciglar, L., Omar Yáñez-Cuna, J., Zinzen, R. P., Girardot, C., Jain, A., Welte, M. A., Stark, A., Leptin, M., & Furlong, E. E. M. (2014). A conserved role for Snail as a potentiator of active transcription. *Genes and Development*, *28*(2), 167–181. https://doi.org/10.1101/gad.230953.113

Ren, J., Lan, T., Liu, T., Liu, Y., Shao, B., Men, K., Ma, Y., Liang, X., Wei, Y., Luo, M., & Wei, X. (2022). CXCL13 as a novel immune checkpoint for regulatory B Cells and its Role in tumor metastasis. *The Journal of Immunology*, *208*, 2425–2435. https://doi.org/10.4049/jimmunol.2100341

Rivers, J. K. (2004). Is there more than one road to melanoma ? *Lancet*, *363*, 728–730.

Rivers, L. E., Young, K. M., Rizzi, M., Jamen, F., Psachoulia, K., Wade, A., Kessaris, N., & Richardson, W. D. (2008). PDGFRA/NG2 glia generate myelinating oligodendrocytes and piriform projection neurons in adult mice. *Nature Neuroscience*, *11*(12), 1392–1401. https://doi.org/10.1038/nn.2220

Rizvi, S. M. H., Aagnes, B., Holdaas, H., Gude, E., Boberg, K. M., Bjørtuft, Ø., Helsing, P., Leivestad, T., Møller, B., & Gjersvik, P. (2017). Long-term change in the risk of skin cancer after organ transplantation a population-based nationwide cohort study. *JAMA Dermatology*, *153*(12), 1270–1277. https://doi.org/10.1001/jamadermatol.2017.2984

Roberts, E. W., Deonarine, A., Jones, J. O., Denton, A. E., Feig, C., Lyons, S. K., Espeli, M., Kraman, M., McKenna, B., Wells, R. J. B., Zhao, Q., Caballero, O. L., Larder, R., Coll, A. P., O'Rahilly, S., Brindle, K. M., Teichmann, S. A., Tuveson, D. A., & Fearon, D. T. (2013). Depletion of stromal cells expressing fibroblast activation protein-α from skeletal muscle and bone marrow results in cachexia and anemia. *Journal of Experimental Medicine*, *210*(6), 1137–1151. https://doi.org/10.1084/jem.20122344

Rossi, A., Roberto, M., Panebianco, M., Botticelli, A., Mazzuca, F., & Marchetti, P. (2019). Drug resistance of BRAF-mutant melanoma: Review of up-to-date mechanisms of action and promising targeted agents. *European Journal of Pharmacology*, *862*(August). https://doi.org/10.1016/j.ejphar.2019.172621

Rouse, B. T. (2007). Regulatory T cells in health and disease. *Journal of Internal Medicine*, *262*(1), 78–95. https://doi.org/10.1111/j.1365-2796.2007.01836.x

Rowe, R. G., Li, X., Hu, Y., Saunders, T. L., Virtanen, I., Herreros, A. G. De, Becker, K., Ingvarsen, S., Engelholm, L. H., Bommer, G. T., Fearon, E. R., & Weiss, S. J. (2009). Mesenchymal cells reactivate Snail1 expression to drive three-dimensional invasion programs. *The Journal of Cell Biology*, *184*(3), 399–408. https://doi.org/10.1083/jcb.200810113

Ruzankina, Y., Pinzon-Guzman, C., Asare, A., Ong, T., Pontano, L., Cotsarelis, G., Zediak, V. P., Velez, M., Bhandoola, A., & Brown, E. J. (2007). Deletion of the Developmentally Essential Gene ATR in Adult Mice Leads to Age-Related Phenotypes and Stem Cell Loss. *Cell Stem Cell*, *1*(1), 113–126. https://doi.org/10.1016/j.stem.2007.03.002

Sahai, E., Astsaturov, I., Cukierman, E., DeNardo, D. G., Egeblad, M., Evans, R. M., Fearon, D., Greten, F. R., Hingorani, S. R., Hunter, T., Hynes, R. O., Jain, R. K., Janowitz, T., Jorgensen, C., Kimmelman, A. C., Kolonin, M. G., Maki, R. G., Powers, R. S., Puré, E., … Werb, Z. (2020). A framework for advancing our understanding of cancer-associated fibroblasts. *Nature Reviews Cancer*, *20*(3), 174–186. https://doi.org/10.1038/s41568-019-0238-1

Santos, A. M., Jung, J., Aziz, N., Kissil, J. L., & Puré, E. (2009). Targeting fibroblast activation protein inhibits tumor stromagenesis and growth in mice. *J Clin Invest*, *119*(12), 3613–3625. https://doi.org/10.1172/JCI38988.include

Scanlan, M. J., Raj, B. K. M., Calvo, B., Garin-Chesa, P., Sanz-Moncasi, M. P., Healey, J. H., Old, L. J., & Rettig, W. J. (1994). Molecular cloning of fibroblast activation protein α, a member of the serine protease family selectively expressed in stromal fibroblasts of epithelial cancers. *Proceedings of the National Academy of Sciences of the United States of America*, *91*(12), 5657–5661. https://doi.org/10.1073/pnas.91.12.5657

Schadendorf, D., van Akkooi, A. C. J., Berking, C., Griewank, K. G., Gutzmer, R., Hauschild, A., Stang, A., Roesch, A., & Ugurel, S. (2018). Melanoma. *The Lancet*, *392*(10151), 971–984. https://doi.org/10.1016/S0140-6736(18)31559-9

Sensi, M., Nicolini, G., Petti, C., Bersani, I., Lozupone, F., Molla, A., Vegetti, C., Nonaka, D., Mortarini, R., Parmiani, G., Fais, S., & Anichini, A. (2006). Mutually exclusive NRASQ61R and BRAFV600E mutations at the single-cell level in the same human melanoma. *Oncogene*, *25*(24), 3357–3364. https://doi.org/10.1038/sj.onc.1209379

Shain, A. H., & Bastian, B. C. (2016). From melanocytes to melanomas. *Nature Reviews Cancer*, *16*, 345–358. https://doi.org/10.1038/nrc.2016.37

Sherman, M. H., Yu, R. T., Engle, D. D., Ding, N., Atkins, A. R., Tiriac, H., Collisson, E. A., Connor, F., Van Dyke, T., Kozlov, S., Martin, P., Tseng, T. W., Dawson, D. W., Donahue, T. R., Masamune, A., Shimosegawa, T., Apte, M. V., Wilson, J. S., Ng, B., … Evans, R. M. (2014). Vitamin D receptor-mediated stromal reprogramming suppresses pancreatitis and enhances pancreatic cancer therapy. *Cell*, *159*(1), 80–93. https://doi.org/10.1016/j.cell.2014.08.007

Siegel, R. L., Miller, K. D., Wagle, N. S., & Jemal, A. (2023). Cancer statistics, 2023. *CA: A Cancer Journal for Clinicians*, *73*(1), 17–48. https://doi.org/10.3322/caac.21763

Smith, M. P., Sanchez-Laorden, B., O'Brien, K., Brunton, H., Ferguson, J., Young, H., Dhomen, N., Flaherty, K. T., Frederick, D. T., Cooper, Z. A., Wargo, J. A., Marais, R., & Wellbrock, C. (2014). The immune-microenvironment confers resistance to MAP kinase pathway inhibitors through macrophage-derived TNFα Michael. *Cancer Discovery*, *4*(10), 1214–1229. https://doi.org/10.1016/j.eururo.2021.01.025

Sosman, J. A., Kim, K. B., Schuchter, L., Gonzalez, R., Pavlick, A. C., Weber, J. S., McArthur, G. A., Hutson, T. E., Moschos, S. J., Flaherty, K. T., Hersey, P., Kefford, R., Lawrence, D., Puzanov, I., Lewis, K. D., Amaravadi, R. K., Chmielowski, B., Lawrence, H. J., Shyr, Y., … Ribas, A. (2012). Survival in BRAF V600–Mutant Advanced Melanoma Treated with Vemurafenib. *The New England Journal of Medicine*, 707–714.

Stanisavljevic, J., Loubat-Casanovas, J., Herrera, M., Luque, T., Peña, R., Lluch, A., Albanell, J., Bonilla, F., Rovira, A., Peña, C., Navajas, D., Rojo, F., García De Herreros, A., & Baulida, J. (2015). Snail1-expressing fibroblasts in the tumor microenvironment display mechanical properties that support metastasis. *Cancer Research*, *75*(2), 284–295. https://doi.org/10.1158/0008-5472.CAN-14-1903

Stanisavljevic, J., Porta-de-la-Riva, M., Batlle, R., de Herreros, A. G., & Baulida, J. (2011). The p65 subunit of NF-κB and PARP1 assist Snail1 in activating fibronectin transcription. *Journal of Cell Science*, *124*(24), 4161–4171. https://doi.org/10.1242/jcs.078824

Straussman, R., Morikawa, T., Shee, K., Barzily-Rokni, M., Qian, Z. R., Du, J., Davis, A., Mongare, M. M., Gould, J., Frederick, D. T., Cooper, Z. A., Chapman, P. B., Solit, D. B., Ribas, A., Lo, R. S., Flaherty, K. T., Ogino, S., Wargo, J. A., & Golub, T. R. (2012). Tumour micro-environment elicits innate resistance to RAF inhibitors through HGF secretion. *Nature*, *487*(7408), 500–504. https://doi.org/10.1038/nature11183

Su, J., Fu, Y., Cui, Z., Abidin, Z., Yuan, J., Zhang, X., Li, R., & Zhao, C. (2023). Relatlimab: a novel drug targeting immune checkpoint LAG-3 in melanoma therapy. *Frontiers in Pharmacology*, *14*(January), 1–13. https://doi.org/10.3389/fphar.2023.1349081

Subramanian, A., Tamayo, P., Mootha, V. K., Mukherjee, S., Ebert, B. L., Gillette, M. A., Paulovich, A., Pomeroy, S. L., Golub, T. R., Lander, E. S., & Mesirov, J. P. (2005). Gene set enrichment analysis: A knowledge-based approach for interpreting genome-wide expression profiles. *Proceedings of the National Academy of Sciences of the United States of America*, *102*(43), 15545–15550. https://doi.org/10.1073/pnas.0506580102

Sun, Y., Campisi, J., Higano, C., Beer, T. M., Porter, P., Coleman, I., True, L., & Nelson, P. S. (2013). Treatment-induced damage to the tumor microenvironment promotes prostate cancer therapy resistance through WNT16B. *Nature Medicine*, *18*(9), 1359–1368. https://doi.org/10.1038/nm.2890.Treatment-induced

Sung, H., Ferlay, J., Siegel, R. L., Laversanne, M., Soerjomataram, I., Jemal, A., & Bray, F. (2021). Global Cancer Statistics 2020: GLOBOCAN Estimates of Incidence and Mortality Worldwide for 36 Cancers in 185 Countries. *CA: A Cancer Journal for Clinicians*, *71*(3), 209–249. https://doi.org/10.3322/caac.21660

Tagore, M., Hergenreder, E., Perlee, S. C., Cruz, N. M., Menocal, L., Suresh, S., Chan, E., Baron, M., Melendez, S., Dave, A., Chatila, W. K., Nsengimana, J., Koche, R. P., Hollmann, T. J., Ideker, T., Studer, L., Schietinger, A., & White, R. M. (2023). GABA Regulates Electrical Activity and Tumor Initiation in Melanoma. *Cancer Discovery*, *13*(10), 2270–2291. https://doi.org/10.1158/2159-8290.CD-23-0389

Takahashi, H., Sakakura, K., Kawabata-Iwakawa, R., Rokudai, S., Toyoda, M., Nishiyama, M., & Chikamatsu, K. (2015). Immunosuppressive activity of cancer-associated fibroblasts in head and neck squamous cell carcinoma. *Cancer Immunology, Immunotherapy*, *64*(11), 1407–1417. https://doi.org/10.1007/s00262-015-1742-0

Takai, K., Le, A., Weaver, V. M., & Werb, Z. (2016). Targeting the cancer-associated fibroblasts as a treatment in triple-negative breast cancer. *Oncotarget*, *7*(50), 82889–82901. https://doi.org/10.18632/oncotarget.12658

Taufalele, P. V., Wang, W., Simmons, A. J., Southard-Smith, A. N., Chen, B., Greenlee, J. D., King, M. R., Lau, K. S., Hassane, D. C., Bordeleau, F., & Reinhart-King, C. A. (2023). Matrix stiffness enhances cancer-macrophage interactions and M2-like macrophage accumulation in the breast tumor microenvironment. *Acta Biomaterialia*, *163*, 365–377. https://doi.org/10.1016/j.actbio.2022.04.031

Tauriello, D. V. F., Palomo-Ponce, S., Stork, D., Berenguer-Llergo, A., Badia-Ramentol, J., Iglesias, M., Sevillano, M., Ibiza, S., Cañellas, A., Hernando-Momblona, X., Byrom, D., Matarin, J. A., Calon, A., Rivas, E. I., Nebreda, A. R., Riera, A., Attolini, C. S. O., & Batlle, E. (2018). TGFβ drives immune evasion in genetically reconstituted colon cancer metastasis. *Nature*, *554*(7693), 538–543. https://doi.org/10.1038/nature25492

TCGA. (2015). Genomic Classification of Cutaneous Melanoma. *Cell*, *161*, 1681–1696. https://doi.org/10.1016/j.cell.2015.05.044

Thiery, J. P., Acloque, H., Huang, R. Y. J., & Nieto, M. A. (2009). Epithelial-Mesenchymal Transitions in Development and Disease. *Cell*, *139*(5), 871–890. https://doi.org/10.1016/j.cell.2009.11.007

Thompson, J. F., McCarthy, W. H., Bosch, C. M. J., O'Brien, C. J., Quinn, M. J., Paramaesvaran, S., Crotty, K., McCarthy, S. W., Uren, R. F., & Howman-Giles, R. (1995). Setinel lymph node status as an indicator of presence of metastatic melanoma in regional lymph nodes. *Melanoma Research*, *5*, 255–260.

Tiago, M., De Oliveira, E. M., Brohem, C. A., Pennacchi, P. C., Paes, R. D., Haga, R. B., Campa, A., De Moraes Barros, S. B., Smalley, K. S., & Maria-Engler, S. S. (2014). Fibroblasts protect melanoma cells from the cytotoxic effects of doxorubicin. *Tissue Engineering - Part A*, *20*(17–18), 2412–2421. https://doi.org/10.1089/ten.tea.2013.0473

Tveit, K. M., & Pihl, A. (1981). Do cell lines in vitro reflect the properties of the tumours of origin? A study of lines derived from human melanoma xenografts. *British Journal of Cancer*, *44*(6), 775–786. https://doi.org/10.1038/bjc.1981.276

Varney, M. L., Olsen, K. J., Mosley, R. L., & Singh, R. K. (2005). Paracrine regulation of vascular endothelial growth factor-A expression during macrophage-melanoma cell interaction: Role of monocyte chemotactic protein-1 and macrophage colony-stimulating factor. *Journal of Interferon and Cytokine Research*, *25*(11), 674–683. https://doi.org/10.1089/jir.2005.25.674

Vega, S., Morales, A. V., Ocaña, O. H., Valdés, F., Fabregat, I., & Nieto, M. A. (2004). Snail blocks the cell cycle and confers resistance to cell death. *Genes and Development*, *18*(10), 1131–1143. https://doi.org/10.1101/gad.294104

Vickman, R. E., Broman, M. M., Lanman, N. A., Franco, O. E., Sudyanti, P. A. G., Ni, Y., Ji, Y., Helfand, B. T., Petkewicz, J., Paterakos, M. C., Crawford, S. E., Ratliff, T. L., & Hayward, S. W. (2020). Heterogeneity of human prostate carcinoma-associated fibroblasts implicates a role for subpopulations in myeloid cell recruitment. *Prostate*, *80*(2), 173–185. https://doi.org/10.1002/pros.23929

Villarejo, A., Cortés-Cabrera, Á., Molina-Ortíz, P., Portillo, F., & Cano, A. (2014). Differential role of snail1 and snail2 zinc fingers in E-cadherin repression and epithelial to mesenchymal transition. *Journal of Biological Chemistry*, *289*(2), 930–941. https://doi.org/10.1074/jbc.M113.528026

Visser, K. E. De, & Joyce, J. A. (2023). The evolving tumor microenvironment : From cancer initiation to metastatic outgrowth. *Cancer Cell*, *41*(3), 374–403. https://doi.org/10.1016/j.ccell.2023.02.016

Waldman, A. D., Fritz, J. M., & Lenardo, M. J. (2020). A guide to cancer immunotherapy: from T cell basic science to clinical practice. *Nature Reviews Immunology*, *20*(11), 651–668. https://doi.org/10.1038/s41577-020-0306-5

Wandel, E., Graßhoff, A., Mittag, M., Uf, H., & Fibroblasts, S. A. (2000). Fibroblasts surrounding melanoma express elevated levels of matrix metalloproteinase-1 (MMP-1) and intercellular adhesion molecule-1 (ICAM-1) in vitro. *Experimental Dermatology*, *9*, 34–41.

Wang, H., Wu, Q., Liu, Z., Luo, X., Fan, Y., Liu, Y., Zhang, Y., Hua, S., Fu, Q., Zhao, M., Chen, Y., Fang, W., & Lv, X. (2014). Downregulation of FAP suppresses cell proliferation and metastasis through PTEN/PI3K/AKT and Ras-ERK signaling in oral squamous cell carcinoma. *Cell Death and Disease*, *5*(4), 1–11. https://doi.org/10.1038/cddis.2014.122

Wang, L. C. S., Lo, A., Scholler, J., Sun, J., Majumdar, R. S., Kapoor, V., Antzis, M., Cotner, C. E., Johnson, L. A., Durham, A. C., Solomides, C. C., June, C. H., Puré, E., & Albelda, S. M. (2014). Targeting fibroblast activation protein in tumor stroma with chimeric antigen receptor T cells can inhibit tumor growth and augment host immunity without severe toxicity. *Cancer Immunology Research*, *2*(2), 154–166. https://doi.org/10.1158/2326-6066.CIR-13-0027

Weber, R., Riester, Z., Hüser, L., Sticht, C., Siebenmorgen, A., Groth, C., Hu, X., Altevogt, P., Utikal, J. S., & Umansky, V. (2020). IL-6 regulates CCR5 expression and immunosuppressive capacity of MDSC in murine melanoma. *Journal for ImmunoTherapy of Cancer*, *8*(2), 1–13. https://doi.org/10.1136/jitc-2020-000949

Wen, X., He, X., Jiao, F., Wang, C., Yang, S., Ren, X., & Li, Q. (2017). Fibroblast activation protein-α-positive fibroblasts promote gastric cancer progression and resistance to immune checkpoint blockade. *Oncology Research*, *25*(4), 629–640. https://doi.org/10.3727/096504016X14768383625385

Whiteside, T. L. (2008). The tumor microenvironment and its role in promoting tumor growth. *Oncogene*, *27*, 5904–5912. https://doi.org/10.1038/onc.2008.271

Wiedemann, G. M., Knott, M. M. L., Vetter, V. K., Rapp, M., Haubner, S., Fesseler, J.,

Kühnemuth, B., Layritz, P., Thaler, R., Kruger, S., Ormanns, S., Mayr, D., Endres, S., & Anz, D. (2016). Cancer cell-derived IL-1α induces CCL22 and the recruitment of regulatory T cells. *OncoImmunology*, *5*(9), e1175794. https://doi.org/10.1080/2162402X.2016.1175794

Winkler, J., Abisoye-Ogunniyan, A., Metcalf, K. J., & Werb, Z. (2020). Concepts of extracellular matrix remodelling in tumour progression and metastasis. *Nature Communications*, *11*(1), 1–19. https://doi.org/10.1038/s41467-020-18794-x

Wolchok, J. D., Hodi, F. S., Weber, J. S., Allison, J. P., Urba, W. J., Robert, C., O'Day, S. J., Hoos, A., Humphrey, R., Berman, D. M., Lonberg, N., & Korman, A. J. (2013). Development of ipilimumab: A novel immunotherapeutic approach for the treatment of advanced melanoma. *Annals of the New York Academy of Sciences*, *1291*(1), 1–13. https://doi.org/10.1111/nyas.12180

Xue, Z., Vis, D. J., Bruna, A., Sustic, T., Van Wageningen, S., Batra, A. S., Rueda, O. M., Bosdriesz, E., Caldas, C., Wessels, L. F. A., & Bernards, R. (2018). MAP3K1 and MAP2K4 mutations are associated with sensitivity to MEK inhibitors in multiple cancer models. *Cell Research*, *28*(7), 719–729. https://doi.org/10.1038/s41422-018-0044-4

Yang, X., Lin, Y., Shi, Y., Li, B., Liu, W., Yin, W., Dang, Y., Chu, Y., Fan, J., & He, R. (2016). FAP Promotes immunosuppression by cancer-associated fibroblasts in the tumor microenvironment via STAT3-CCL2 Signaling. *Cancer Research*, *76*(14), 4124–4135. https://doi.org/10.1158/0008-5472.CAN-15-2973

Ye, X., Tam, W. L., Shibue, T., Kaygusuz, Y., Reinhardt, F., Ng Eaton, E., & Weinberg, R. A. (2015). Distinct EMT programs control normal mammary stem cells and tumour-initiating cells. *Nature*, *525*(7568), 256–260. https://doi.org/10.1038/nature14897

Youssef, K. K., & Nieto, M. A. (2024). The epithelial- mesenchymal transition in tissue degeneration and repair. *Nature Reviews Molecular Cell Biology*.

Yu, P. F., Huang, Y., Han, Y. Y., Lin, L. Y., Sun, W. H., Rabson, A. B., Wang, Y., & Shi, Y. F. (2017). TNFα-activated mesenchymal stromal cells promote breast cancer metastasis by recruiting CXCR2+ neutrophils. *Oncogene*, *36*(4), 482–490. https://doi.org/10.1038/onc.2016.217

Zhang, J., Joshua, A. M., Li, Y., O'Meara, C. H., Morris, M. J., & Khachigian, L. M. (2024). Targeted therapy, immunotherapy, and small molecules and peptidomimetics as emerging immunoregulatory agents for melanoma. *Cancer Letters*, *586*(December 2023), 216633. https://doi.org/10.1016/j.canlet.2024.216633

Zhang, Y., & Ertl, H. C. J. (2016). Depletion of FAP+ cells reduces immunosuppressive cells and improves metabolism and functions CD8+T cells within tumors. *Oncotarget*, *7*(17), 23282–23299. https://doi.org/10.18632/oncotarget.7818

Zhou, L., Yang, K., Andl, T., Randall Wickett, R., & Zhang, Y. (2015). Perspective of targeting cancer-associated fibroblasts in melanoma. *Journal of Cancer*, *6*(8), 717–726. https://doi.org/10.7150/jca.10865

Ziani, L., Safta-Saadoun, T. Ben, Gourbeix, J., Cavalcanti, A., Robert, C., Favre, G., Chouaib, S., & Thiery, J. (2017). Melanoma-associated fibroblasts decrease tumor cell susceptibility to NK cell-mediated killing through matrix-metalloproteinases secretion. *Oncotarget*, *8*(12), 19780–19794. https://doi.org/10.18632/oncotarget.15540

# APPENDIX

ARTICLE OPEN

Check for updates

# Microenvironmental Snail1-induced immunosuppression promotes melanoma growth

Marta Arumi-Planas[1], Francisco Javier Rodriguez-Baena[1], Francisco Cabello-Torres[1], Francisco Gracia[1], Cristina Lopez-Blau[1], M. Angela Nieto[1,2] and Berta Sanchez-Laorden[1]✉



Melanoma is an aggressive form of skin cancer due to its high metastatic abilities and resistance to therapies. Melanoma cells reside in a heterogeneous tumour microenvironment that acts as a crucial regulator of its progression. Snail1 is an epithelial-to-mesenchymal transition transcription factor expressed during development and reactivated in pathological situations including fibrosis and cancer. In this work, we show that Snail1 is activated in the melanoma microenvironment, particularly in fibroblasts. Analysis of mouse models that allow stromal Snail1 depletion and therapeutic Snail1 blockade indicate that targeting Snail1 in the tumour microenvironment decreases melanoma growth and lung metastatic burden, extending mice survival. Transcriptomic analysis of melanoma-associated fibroblasts and analysis of the tumours indicate that stromal Snail1 induces melanoma growth by promoting an immunosuppressive microenvironment and a decrease in anti-tumour immunity. This study unveils a novel role of Snail1 in melanoma biology and supports its potential as a therapeutic target.

*Oncogene* (2023) 42:2659–2672; https://doi.org/10.1038/s41388-023-02793-5

**Graphical Abstract**

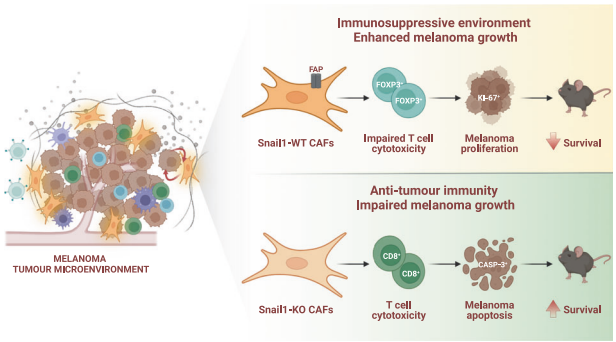


## INTRODUCTION

Melanoma is the most aggressive form of skin cancer. If found early, it can be surgically resected, but melanoma is extremely metastatic and very resistant to treatments when disseminated to other organs. Even though in recent years the landscape of melanoma treatment has greatly improved with the use of more effective targeted therapies and immunotherapies, not all patients respond to these treatments and many of the patients who respond develop resistance after a relatively short period of disease control [1]. Importantly, melanoma progression and how it responds to treatments is strongly influenced by the tumour microenvironment (TME) [2].

Epithelial to mesenchymal transition (EMT) is a developmental process that can be triggered in pathological conditions including fibrosis and cancer. Epithelial cells undergo EMT acquiring the capacity to move and disseminate [3, 4]. EMT endows cancer cells with invasive and migratory capabilities as the tumour progresses [5, 6]. The main inducers of the EMT are transcription factors (TFs) of the Snail, Twist and Zeb families. EMT-TFs coordinate the downregulation of epithelial genes and the induction of mesenchymal ones [3, 7]. EMT-TFs play an important role in the development and dissemination of epithelial-derived carcinomas, particularly when they are expressed in tumour cells [3, 8, 9] but also when their expression is associated with stromal cells, particularly cancer-associated fibroblasts (CAFs) [10–14]. CAFs, central components of the tumour stroma, are a complex and heterogeneous population of myofibroblasts whose activity associates with tumour aggressiveness. CAFs coordinate a wide array of functions including matrix remodelling, angiogenesis, and tumour-promoting immune evasion [15, 16].

[1]Instituto de Neurociencias (CSIC-UMH), Sant Joan d'Alacant, Spain. [2]CIBERER, Centro de Investigación Biomédica en Red de Enfermedades Raras, ISCIII, Madrid, Spain. ✉email: berta.lopez@umh.es

Received: 7 February 2023 Revised: 13 July 2023 Accepted: 19 July 2023
Published online: 29 July 2023

Reprogramming in the expression of different EMT-TFs, including Zeb1/2, Twist and Snail2 in melanoma cells is associated with tumour progression [17–21]. In addition, previous studies have assessed the impact of Snail1-induced EMT in melanoma cells [22–24]. However, whether Snail1 expression in the TME regulates melanoma biology has not been investigated. In this study, we use different mouse models to unveil a novel immunoregulatory role of Snail1 reactivation in the melanoma microenvironment. We show that Snail1 expression in fibroblasts regulates fibroblast activation protein alpha (Fap) expression and promotes immunosuppression. Consistent with the latter, Snail1 targeting significantly decreases tumour and metastatic burden, increasing mice survival. We also show that the effects driven by microenvironmental Snail1 targeting are associated with an increase in anti-tumour immune responses. Altogether, this indicates that stromal Snail1 has a crucial role in shaping the melanoma microenvironment to drive tumour progression.

## RESULTS

### Snail1 reactivation in the tumour microenvironment promotes melanoma growth

Snail1 expression has been previously found in epithelial and stromal cells in carcinomas [11, 25]. To characterise the expression of Snail1 in melanoma, and to distinguish tumour cells from the cells in the TME, we generated a melanoma reporter mouse model by crossing the inducible BRAF-driven mouse melanoma model $Braf^{CA}$,$Pten^{loxP}$,Tyr::CreERT2 ($Braf^{V600E}$/$Pten^{loxP}$) [26] with Rosa-LSL-tdTomato mice (tdTomato). Tamoxifen treatment of these mice results in melanoma development with a short latency [26] and the expression of the Tomato fluorescent protein in melanocytes and melanoma cells. Analysis of this model showed SNAI1 expression restricted to tdTomato-negative cells in the tumours (Fig. 1a, b) indicating that *Snail1* is reactivated in the melanoma microenvironment but not in the melanoma cells. To specifically target the stroma, we next generated a syngeneic melanoma model by injecting murine $Braf^{V600E}$-5555 cells [27, 28] in UBC-Cre-ERT2 mice [29] crossed with tdTomato mice (Fig. 1c). In this model, tamoxifen treatment promotes the ubiquitous expression of the Tomato fluorescent protein in the mouse, allowing to trace the red labelled stromal cells in the allografts. Analysis of the tumours confirmed SNAI1 expression in the recombined cells from the melanoma microenvironment that was absent in normal skin (Fig. 1d). We extended our analyses to additional oncogenic BRAF and $BRAF^{wt}$/$NRAS^{wt}$ melanoma syngeneic models and confirmed SNAI1 reactivation in the stroma of these tumours (Supplementary Fig. 1). Next, we wanted to assess the contribution of microenvironmental Snail1 ($Snail^{ME}$) to melanoma growth. For this, UBC-Cre-ERT2-tdTomato mice were bred with $Snai1^{fl/fl}$ mice [30] to prevent Snail1 reactivation in the tumour stroma. Melanomas were established by subcutaneous injection of $Braf^{V600E}$-5555 cells in UBC-Cre-ERT2-tdTomato and UBC-Cre-ERT2-tdTomato-$Snai1^{fl/fl}$ (referred as $Snail1^{ME}$-WT and $Snail1^{ME}$-KO, respectively) (Fig. 1c). When the tumours were already established, animals were treated with tamoxifen to block stromal Snail1 expression and melanoma growth was monitored (Fig. 1e). We confirmed that recombined stromal cells from $Snail1^{ME}$-KO mice lack SNAI1 expression (Fig. 1f). Importantly, melanoma growth was blocked and significantly reduced in $Snail1^{ME}$-KO compared to $Snail1^{ME}$-WT mice (Fig. 1g, h). In line with these results, we observed a decrease in the proliferation of melanoma cells from $Snail1^{ME}$-KO tumours (Fig.1i, j) and a significant increase in apoptotic melanoma cells as indicated by cleaved-Caspase 3 (Fig. 1k, l). These results show that Snail1 is expressed in the melanoma microenvironment where it is necessary for melanoma growth.

### Snail1 reactivation in melanoma-associated fibroblasts decreases anti-tumour immunity

Expression of Snail1 and other EMT-TFs have been reported in macrophages and CAFs from epithelial-derived tumours [10–14]. To investigate Snail1 expression in these cell populations in melanoma, we first analysed $Braf^{V600E}$-5555 tumours grown subcutaneously in Cx3cr1CreERT2-YFP reporter mice. These mice constitutively express YFP in the myeloid lineage including monocytes and macrophages [31, 32]. We did not detect SNAI1 on myeloid cells in our tumours (Fig. 2a) or in additional immune populations as assessed by CD45 staining (Fig. 2b, Supplementary Fig. 2a). On the contrary, we detected SNAI1 expression in melanoma-associated fibroblasts, as indicated by double tdTomato-PDGFRα positive staining (Fig. 2c). SNAI1 positive expression in melanoma-associated fibroblasts was further confirmed in the melanoma transgenic $BRAF^{V600E}$/$Pten^{loxP}$/tdTomato model (Fig. 2c). We also validated SNAI1 expression in $PDGFR\alpha^{+}$ cells by using PDGFRα-CreERT2-tdTomato reporter mice (Supplementary Fig. 2b) and confirmed that blocking SNAI1 expression in $PDGFR\alpha^{+}$ fibroblasts reduced melanoma growth (Supplementary Fig. 2c).

To determine the mechanisms implicated in Snail1 contribution to melanoma growth, we isolated $tdTomato^{+}PDGFR\alpha^{+}$ cells from $Braf^{V600E}$-5555 tumours grown in $Snail1^{ME}$-WT and $Snail1^{ME}$-KO mice after tamoxifen treatment and performed RNA sequencing (Fig. 2d, Supplementary Fig. 3a). We corroborated that isolated cells were positive for PDGFRα, SNAI1, and αSMA, an additional CAF marker (Supplementary Fig. 3b), and confirmed *Snai1* downregulation in $tdTomato^{+}PDGFR\alpha^{+}$ cells from $Snail1^{ME}$-KO mice (Supplementary Fig. 3c). Among the 520 differentially expressed genes (DEGs) detected upon Snail1 targeting, 323 were upregulated and 197 downregulated (Fig. 2e). In agreement with the role of Snail1 in embryonic development, gene ontology (GO) analysis of the upregulated genes showed an enrichment in biological processes associated with morphogenesis and differentiation (Fig. 2f) [33, 34]. On the contrary, 11 out of the 15 most enriched biological processes in the downregulated genes were associated with the immune system (Fig. 2f). In addition, gene set enrichment analysis (GSEA) [35] showed that melanoma-associated fibroblasts were enriched in signatures related to TGFβ signalling and fibroblast activation in carcinomas and this correlation was decreased upon Snail1 targeting (Fig. 2g). We also found that several of the downregulated genes including *Ccl1*, *Ccl22*, *Cxcl13* or *Ccr7* were associated with immunosuppression and decreased anti-tumour immunity [36–40] (Supplementary Fig. 3d, e). Additional GO and GSEA analyses confirmed a significant decrease in processes and genes associated with immunosuppression and pro-inflammatory pathways in Snail1 depleted melanoma-associated fibroblasts [41] (Fig. 2g, h, Supplementary Fig. 3f). Interestingly, comparison of our transcriptomic data with melanoma stromal scRNAseq data [42] showed that $tdTomato^{+}PDGFR\alpha^{+}$ cells from $Snail1^{ME}$-WT tumours were enriched in the signatures related to the S1 ("immune") and S2 ("desmoplastic") CAFs subpopulations (Fig. 2i). Critically, the most significant difference between $tdTomato^{+}PDGFR\alpha^{+}$ cells from $Snail1^{ME}$-WT and $Snail1^{ME}$-KO tumours corresponds to the signature of the S1 ("immune") population, associated to higher expression of immunomodulatory factors [42]. Further, we also compared our transcriptomic data with an additional dataset from breast cancer CAFs defined as immunosuppressive [43] and confirmed that $tdTomato^{+}PDGFR\alpha^{+}$ cells from $Snail1^{ME}$-WT were enriched in the signature associated to immunosuppression and, this correlation was decreased upon Snail1 targeting (Fig. 2j).

Altogether, our data suggest that the anti-tumour effects observed upon Snail1 targeting in the melanoma microenvironment may be related to CAFs immunoregulatory functions. To test this hypothesis, we characterised the immune infiltration in $Braf^{V600E}$-5555 melanomas upon $Snail1^{ME}$ depletion (Fig. 3a). We observed that compatible with the impaired growth of

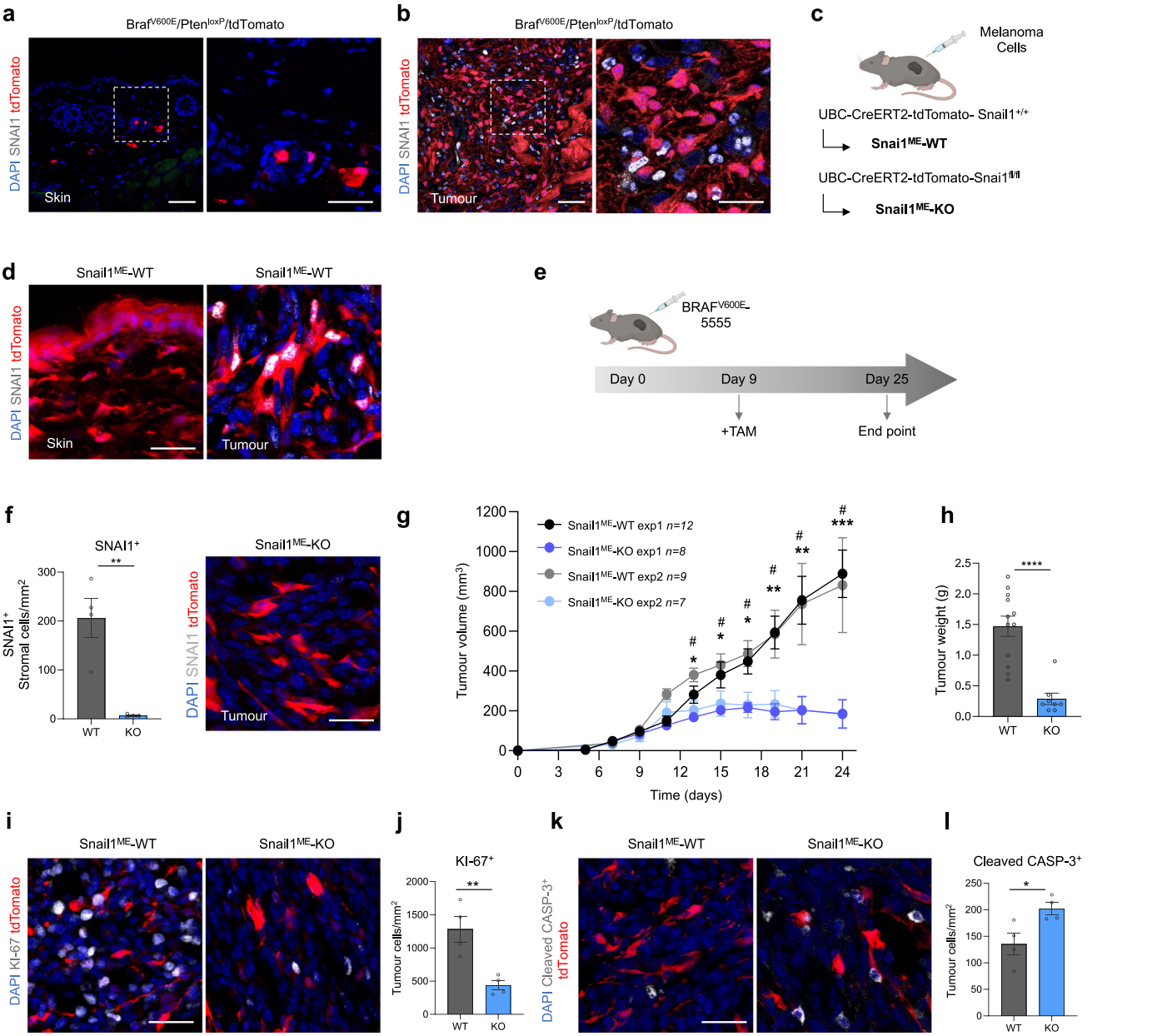


**Fig. 1 Snail1 is expressed in the melanoma microenvironment and its ablation reduces tumour growth and promotes apoptosis.** **a**, **b** Representative images of immunolabelling for SNAI1 (white) in control skin and tumours from Braf$^{CA}$, Pten$^{loxP}$, tdTomato, Tyr::CreERT2 (Braf$^{V600E}$/Pten$^{loxP}$/tdTomato) mice. Melanoma cells are labelled in red (tdTomato). **c** Mouse models generated to investigate the impact of Snail1 on the melanoma microenvironment. **d** Representative images of immunolabelling for SNAI1 (white) in control skin (left panel) and Braf$^{V600E}$-5555 tumours (right panel) from Snail1$^{ME}$-WT mice. Stromal cells are labelled in red (tdTomato). **e** Experimental set-up of the in vivo strategy design to study the contribution of Snail1 to melanoma progression. Created with BioRender.com. **f** Quantification of SNAI1$^{+}$ stromal cells ($n = 4$ per condition) (left panel) and representative image of immunolabelling for SNAI1 (white) in Snail1$^{ME}$-KO tumours upon tamoxifen administration (right panel). Stromal cells are labelled in red (tdTomato). **g** Braf$^{V600E}$-5555 tumour growth was assessed in two independent experiments combined in this graph (exp1 $n = 12$ Snail1$^{ME}$-WT and $n = 8$ Snail1$^{ME}$-KO; exp2 $n = 9$ Snail1$^{ME}$-WT and $n = 7$ Snail1$^{ME}$-KO). **h** Final weight after collection of tumours from Snail1$^{ME}$-WT (WT) and Snail1$^{ME}$-KO (KO) mice ($n = 12$ WT; $n = 8$ KO). **i** Representative images of immunolabelling for KI-67(white) in tumours from Snail1$^{ME}$-WT and Snail1$^{ME}$-KO mice. Stromal cells are labelled in red (tdTomato). **j** Quantification of KI-67 (white) tumour nuclei-positive cells in images from (**i**) ($n = 4$). **k** Representative images of immunolabelling for Cleaved-CASP3 (white) in tumours from Snail1$^{ME}$-WT and Snail1$^{ME}$-KO mice. Stromal cells are labelled in red (tdTomato). **l** Quantification of images from (**k**) ($n = 4$). Data are represented by Mean ± SEM and statistically significant differences are tested by unpaired two-tailed Student *t*-test. Each dot represents one animal (* = $p < 0.05$, ** = $p < 0.01$, *** $p < 0.001$, **** $p < 0.0001$ and # = $p < 0.05$ for experiment 2). WT = Snail1$^{ME}$-WT and KO = Snail1$^{ME}$-KO. Scale bars: 50 µm and 25 µm for higher magnification pictures.

melanomas, the percentage of tumour infiltrating cytotoxic T cells (CD8$^{+}$) was elevated in tumours from Snail1$^{ME}$-KO compared to Snail1$^{ME}$-WT mice (Fig. 3b). In addition, significantly fewer regulatory T cells (FOXP3$^{+}$) were found in Snail1$^{ME}$-KO tumours (Fig. 3c). Further analyses show an increase in B cells and Natural killer (NK) cells in tumours from Snail1$^{ME}$-KO mice, while the number of dendritic cells and myeloid cells remained constant (Fig. 3d, e). However, we detected upregulated expression of

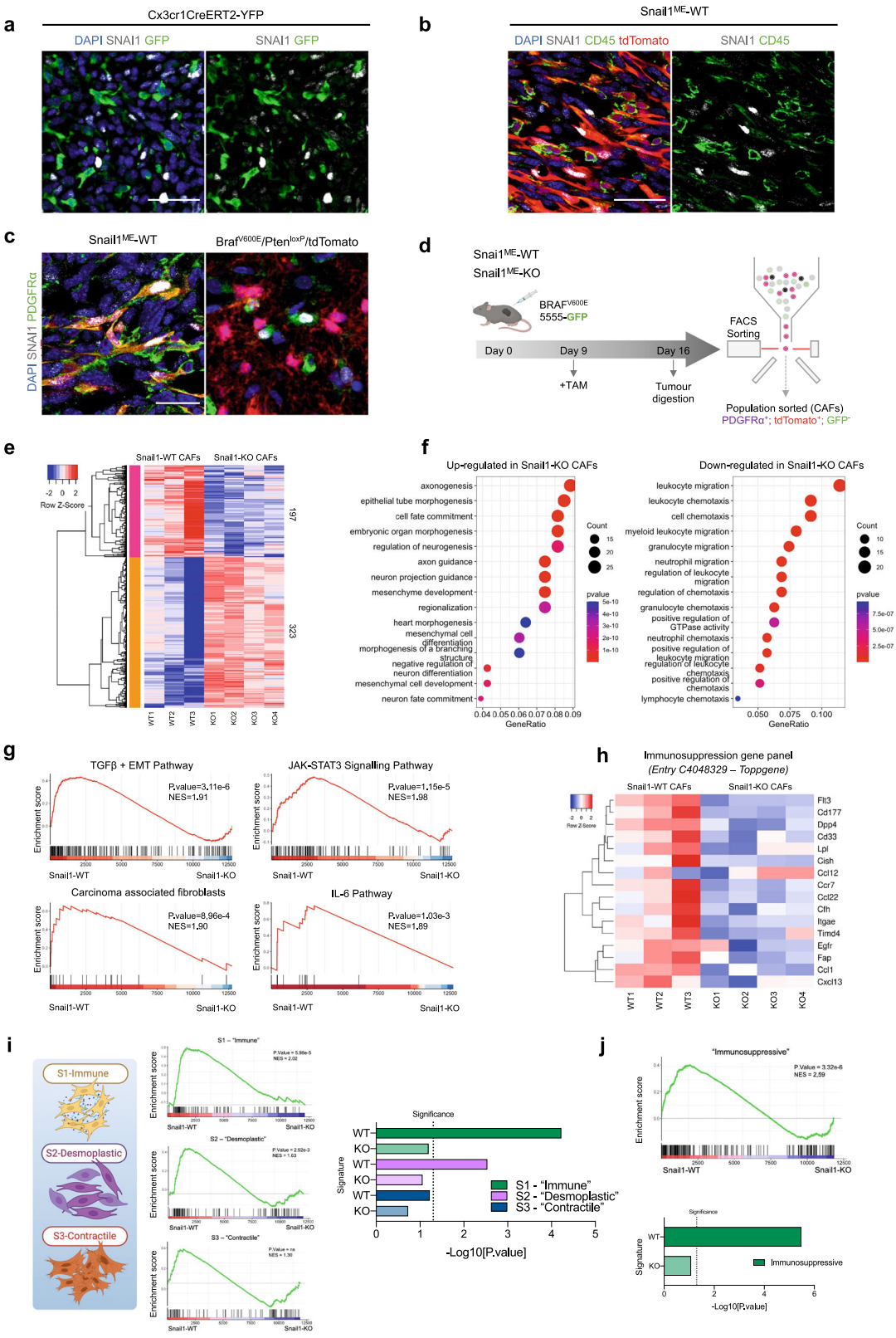


Arginase 1 (*Arg1*) (Fig. 3f) a marker associated with M2-like macrophages with immunosuppressive and pro-tumourigenic functions, in melanomas from Snail1$^{ME}$-WT compared to Snail1$^{ME}$-KO mice. Altogether, these data indicate that Snail1$^{ME}$ expression blocks anti-tumour immune responses.

Interestingly, given our results indicating that Snail1 promotes immunosuppression in our models, and the association of immunosuppression with resistance to immunotherapy [44], we sought to investigate the correlation of Snail1 levels with clinical outcomes in patients treated with immune-checkpoint inhibitors.

**Fig. 2 Snail1 expression in PDGFRα$^+$-CAFs is associated with fibroblast activation and immunosuppression signatures. a** Representative images of immunolabelling for SNAI1 (white) and myeloid cells (green) in a section of a Braf$^{V600E}$-5555 melanoma grown in Cxcr1CreERT2-YFP mice. **b** Representative images of immunolabelling for SNAI1 (white) and CD45 (green) in melanomas from Snail1$^{ME}$-WT mice. Stromal cells are labelled in red (tdTomato). **c** Representative images of immunolabelling for SNAI1 (white) and PDGFRα (green) in Braf$^{V600E}$-5555 tumours from Snail1$^{ME}$-WT mice. Stromal cells are labelled in red (tdTomato) (left panel) and in BRAF$^{V600E}$/Pten$^{loxP}$/tdTomato melanomas where melanoma cells are labelled in red (tdTomato) (right panel). Scale bar: 25 µm. **d** Schematic illustration of the strategy followed to isolate fibroblasts from Braf$^{V600E}$-5555 melanomas in Snail1$^{ME}$-WT and Snail1$^{ME}$-KO mice. Created with BioRender.com. **e** RNAseq heatmap of differentially expressed genes (DEGs). The scale bar corresponds to row Z score in a -2–2 relationship. Filtered and normalised count per million data from the DEGs has been plotted to compare Snail1-WT and Snail1-KO CAFs. Columns represent the different samples. Each sample is a pool of three different animals with the same genotype WT $n = 3$, KO $n = 4$. **f** Representation of gene ontology enrichment analysis of the 15 top GO terms as ranked by various gene set testing methods. The dot plot size and colour represent the relative number and relevance of the genes in the set, respectively. **g** Gene set enrichment analysis (GSEA) of DEGs genes (log2 ratio-ranked) shows enrichment of TGFβ + EMT, JAK-STAT3 and IL-6 pathway signatures and enrichment of Carcinoma-associated fibroblasts signature in Snail1-WT CAFs. NES (normalised enrichment score) and p-value scores are shown. **h** Panel showing expression of genes associated with immunosuppression from entry C4048329 in the Toppgene and DisGeNet databases. **i** GSEA analysis of custom gene sets generated from DEGs in the S1 "immune", S2 "desmoplastic" and S3 "contractile" CAFs populations defined in [42]. NES (normalised enrichment score) and *p* value scores are shown, ns, not significant. Created with BioRender.com. **j** GSEA analysis of marker gene sets in the immunosuppressive breast CAF population defined in [43]. NES (normalised enrichment score) and *p* value scores are shown.

Analysis from transcriptomic datasets [45] using Kaplan-Meier Plotter [46] revealed that high Snail1 expression before or on-treatment with anti-programmed death-1 (anti-PD-1) correlated with a lower overall survival in melanoma patients (Fig. 3g, h).

### Snail1 induces Fap expression in fibroblasts

Recent studies using syngeneic carcinoma models indicate that CAFs expressing FAP are responsible for immune-evasion associated with a pro-tumourigenic TME [43, 47–51]. Given our results showing that Snail1$^{ME}$ in melanoma promotes immunosuppression and that its silencing blocks tumour growth, we next investigated the potential relationship between Snail1 and Fap in fibroblasts. First, we characterised our models. Analysis of our RNAseq data showed a decrease in *Fap* expression in melanoma-associated fibroblast upon Snail1 depletion (Supplementary Fig. 3d, e). Further, we confirmed lower levels of *Fap* mRNA in tumours from Snail1$^{ME}$-KO when compared to Snail1$^{ME}$-WT mice (Fig. 4a) and in tdTomato$^+$PDGFRα$^+$ isolated fibroblasts from those tumours (Fig. 4b). In line with this, *Fap* was downregulated in NIH3T3 fibroblasts after silencing *Snai1* expression with a siRNA (Fig. 4c) and upregulated upon TGFβ treatment or *Snai1* overexpression (Fig. 4d, e). Further, we found that CYD19, an inducer of Snail1 degradation [52], reduced *Fap* expression in NIH3T3 fibroblasts (Fig. 4f) indicating that Snail1 could be regulating *Fap* expression. We also analysed TCGA (The Cancer Genome Atlas) data from different cancers and found a positive correlation between *Snai1* and *Fap* expression in 28 tumour types including melanoma (Supplementary Fig. 4). To assess whether SNAI1 could directly bind to regulatory regions of the *Fap* promoter, we next performed chromatin immunoprecipitation (ChIP) assay in *Snail1*-overexpressing NIH3T3 cells. For this, we looked for consensus Snail1 E-boxes [53] (CANNTG) within the mouse *Fap* promoter using the SnapGene® software. Both murine and human FAP promoters contain multiple Snail1 E-boxes near their transcription start site. We considered regions with 2 or more E-boxes as predicted SNAI1 binding sites (BS), and we found several within the mouse *Fap* promoter (BS1, BS2, BS3, BS4 and BS5) (Fig. 4g). Chromatin immunoprecipitation analysis confirmed that BS1, BS2 and BS3 were highly enriched in SNAI1 binding as compared with IgG control in the NIH3T3 cell line (Fig. 4h). All this together indicates that SNAI1 could directly regulate *Fap* transcription in fibroblasts.

### Snail1$^{ME}$ targeting reduces metastatic burden and increases mice survival

Our results show that targeting Snail1$^{ME}$ blocks subcutaneous melanoma growth. We next wanted to address whether Snail1 regulates the metastatic niche microenvironment. For this, we injected luciferase-expressing Braf$^{V600E}$-5555 melanoma cells in the tail vein of Snail1$^{ME}$-WT and Snail1$^{ME}$-KO mice. We confirmed that SNAI1 expression was absent in control lungs and was reactivated in the metastatic microenvironment in Snail1$^{ME}$-WT mice (Fig. 5a) and blocked in metastases from Snail1$^{ME}$-KO mice (Fig. 5a, b). We also observed SNAI1 reactivation in PDGFRα$^+$-CAFs from melanoma lung metastases in Snail1$^{ME}$-WT mice that was confirmed in Braf$^{V600E}$/Pten$^{loxP}$/tdTomato melanomas (Fig. 5c, Supplementary Fig. 5). When metastases were detected by bioluminescence in an IVIS in vivo imaging system, animals were treated with tamoxifen and metastases growth was monitored (Fig. 5d, e). Histological analysis of the lungs (Fig. 5f) showed a significant decrease in metastatic burden (−82.9%), metastases number (−47.6%) and size (−77.5%) in Snail1$^{ME}$-KO compared to Snail1$^{ME}$-WT mice (Fig. 5g). Further, we also investigated whether blocking Snail1$^{ME}$ activation could improve mice survival. Kaplan-Meier analysis showed an almost 30% increase in the survival of Snail1$^{ME}$-KO mice, compared to Snail1$^{ME}$-WT, assessed by long-rank test ($X^2 = 6.92$, $p < 0.01$) (Fig. 5h). Importantly, as in the subcutaneous tumours, these anti-tumour immune effects were associated with a decrease in proliferation and an increase in apoptosis in the melanoma cells in Snail1$^{ME}$-KO metastases (Fig. 5i, j). We then analysed the immune infiltrate in the lungs and confirmed that metastases from Snail1$^{ME}$-KO mice had an increased number of cytotoxic T cells (CD8$^+$) and a lower infiltration of regulatory T cells (FOXP3$^+$) compared to Snail1$^{ME}$-WT metastases (Fig. 5k). Gene expression analysis also showed a decrease in *Fap* mRNA levels in lung metastases from the Snail1$^{ME}$-KO mice (Fig. 5l).

The data described above indicate that genetic blockade of Snail1 activation in the TME decreases metastases growth and in line with our previous results, this is associated with a less immunosuppressive environment. We had previously shown that Snail1 targeting by injection of antisense oligonucleotides could constitute a good therapeutic strategy in renal fibrosis [54]. To investigate whether this was also the case in melanoma, we used a similar approach and injected a VIVO-morpholino (VI-MO) that targets a splicing site in the *Snai1* mRNA (Snail1-MO) [54] into the tail vein of C57BL/6 mice with established Braf$^{V600E}$-5555 lung metastases (Fig. 6a). Once lung metastases were detected by bioluminescence, the mice were treated with VI-MOs and the signal was monitored by IVIS (Fig. 6b). Histological analysis of the lungs (Fig. 6c) showed a decrease in the weight (−56.7%), metastatic burden (−55.9%) and number of metastases (−37.4%) in the Snail1-MO as compared to Control-MO treated mice (Fig. 6d). We confirmed the efficacy of the morpholino in blocking *Snail1* expression in the lung metastases (Fig. 6e, f) that was accompanied by a decrease in *Fap* levels (Fig. 6f). Further, metastases from mice treated with Snail1-MO had increased *Cd8a* compared to Control-MO treated mice (Fig. 6g). Thus, as observed in our Snail1$^{ME}$-KO mice, Snail1 systemic inhibition was associated with an anti-tumour immune response and decreased melanoma metastatic burden.

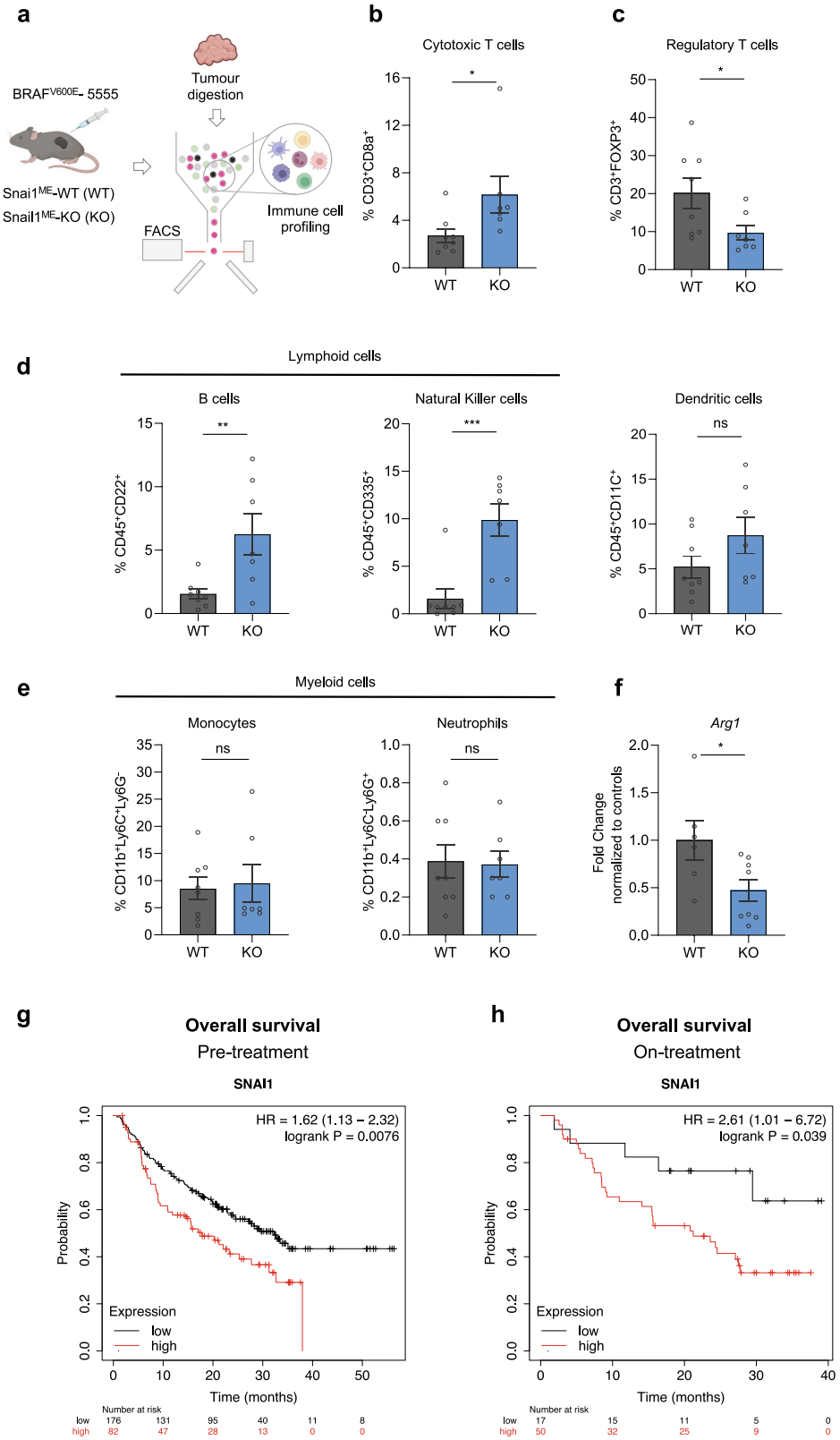


## DISCUSSION

Modulation of the immune response in the TME plays a major role in the clinical response to treatments [55]. In this study, we have identified stromal Snail1 as a driver of melanoma growth by promoting an immunosuppressive TME. Moreover, Snail1 targeting is enough to reduce melanoma metastatic burden and increase mice survival.

Snail1 is an essential TF during embryonic development whereas it is mostly absent in healthy adult tissues. Snail1 reactivation is involved in fibrosis and in the progression of several

**Fig. 3 Snail1$^{ME}$ targeting induces an anti-tumourigenic immune response in melanoma. a** Schematic representation of the strategy used to perform immune cell profiling by flow cytometry analysis of Braf$^{V600E}$-5555 melanomas in Snail1$^{ME}$-WT (WT) and Snail1$^{ME}$-KO (KO) mice. Created with BioRender.com. **b**, **c** Graphs showing percentages of Cytotoxic T cells (CD3$^+$CD8a$^+$) and Regulatory T cells (CD3$^+$FOXP3$^+$) in tumours from (a) ($n = 8$ WT and $n = 7$ KO). **d** Graphs showing percentages of lymphoid cells from (**a**); B cells (CD45$^+$CD22$^+$), natural killer cells (CD45$^+$CD335$^+$), and dendritic cells (CD45$^+$CD11c$^+$). **e** Graphs showing percentages of myeloid cells in tumours from (**a**); monocytes (CD11b$^+$Ly6C$^+$Ly6G$^-$) and neutrophils (CD11b$^+$Ly6C$^-$Ly6G$^+$), are represented ($n = 8$ WT and $n = 7$ KO). **f** *Arg1* mRNA levels detected by RT-qPCR in tumour samples from (**a**) ($n = 5$ WT and $n = 8$ KO). Data are represented by Mean ± SEM and statistically significant differences are tested by unpaired two-tailed Student *t*-test. Each dot represents one animal (ns = not significant, *=$p < 0.05$, **=$p < 0.01$, ***$p < 0.001$). **g**, **h** Prognostic value of Snail1 expression in response to anti-PD-1 therapy. Survival curves plotted for melanoma patients. *SNAI1* expression assessed before anti-PD-1 therapy ($n = 258$) or on treatment ($n = 67$). Data was analysed using Kaplan-Meier Plotter. Patients with *SNAI1* expression above the median are indicated in red line, and patients with expressions below the median in black line. HR hazard ratio.

cancer types [56], as a potent driver of the EMT process in carcinoma cells [9]. Previous studies indicated that Snail1 induction in melanoma cells promotes invasion and metastasis [22], however, Snail1 contribution to melanoma biology in an in vivo context was not defined. Our analyses of an inducible BRAF-driven melanoma reporter model reveal that SNAI1 in melanoma is reactivated in the stroma, particularly in CAFs. This is confirmed in syngeneic melanoma models where we find SNAI1 expression in CAFs in subcutaneous tumours and in lung metastases. In this study, we have generated mouse models that allow Snail1 ablation in an otherwise undisturbed immunocompetent environment to unveil the contribution of microenvironmental Snail1 to melanoma. We demonstrate that stromal Snail1 depletion blocks melanoma growth. This is associated with diminished proliferation and increased apoptosis of melanoma cells, pointing towards a non-cell autonomous role of microenvironmental Snail1 in melanoma cells. In accordance with this, Snail1 expression in CAFs from breast or colorectal cancer promotes epithelial cell invasion by paracrine signalling mediated by prostaglandinE2 [11]. Here we show that Snail1-expressing CAFs mediate a tumour-promoting phenotype in melanoma by exerting an immunoregulatory role in the tumours.

Recently, single-cell sequencing technologies have shed light into the complexity and heterogeneity of CAFs in different tumour types and a better understanding of their functions and features can be harnessed to design better therapies for cancer treatments [16, 43, 57]. Although CAFs subsets in pancreas and breast have been characterised in detail [16], less is known about CAFs modulation of melanoma biology. Recently, three different melanoma CAFs populations have been described [42] and *Pdgfra* expression was widely found in the populations enriched at early stages of melanoma progression when our CAFs transcriptomic analysis was performed. Interestingly, we find that *Fap* is highly expressed in Snail1-expressing CAFs and downregulated upon its depletion. Further, we demonstrate that SNAI1 directly binds to the *Fap* promoter indicating that Snail1 can induce FAP expression in fibroblasts. Snail1 has classically been considered a potent transcriptional repressor [25], however it can also act as a transcriptional activator [58, 59]. In carcinoma cells, Snail1 directly activates the transcription of cytokines implicated in the recruitment of tumour-associated macrophages promoting TME remodelling [58]. Moreover, we previously showed that in renal fibrosis, Snail1 reactivation in tubular epithelial cells promotes a profibrotic inflammatory microenvironment by sustaining TGFβ signalling and cytokines production [54]. We show in this study that Snail1 depletion in CAFs also impinges on pathways associated to TGFβ signalling and inflammation and into the recruitment and activation of immune cells, indicating that Snail1 has a major immunoregulatory role when expressed in the melanoma microenvironment. Further, it is known that FAP-expressing CAFs populations are associated with immunosuppressive characteristics [43, 49, 50], and that elevated FAP expression in CAFs through the JAK-STAT3 signalling pathway, contributes to a pro-tumourigenic immune response [47]. Consistently, our RNA sequencing data shows downregulation of the JAK-STAT3 signalling pathway among other pro-tumourigenic pathways when Snail1 is blocked. All these results are in line with the decrease in *Fap* levels we find in Snail1 KO-CAFs in association with anti-tumour immunity as shown by increased infiltration of cytotoxic CD8$^+$-T, B cells and NK cells, and consistent with impaired melanoma growth. FAP$^+$CAFs have also been associated with the recruitment of regulatory FOXP3$^+$-T lymphocytes [50], and in agreement with this, we find that the decrease in regulatory T cells we observe in the TME of tumours from Snail1$^{ME}$-KO mice favours an anti-tumourigenic phenotype.

Interestingly, the effects of blocking Snail1 reactivation in the melanoma microenvironment are not restricted to the subcutaneous compartment but extend to the metastatic niche. Microenvironmental Snail1 depletion impairs the progression of experimental lung metastases associated with decreased *Fap* levels and anti-tumour immune responses. This suggests that despite CAFs heterogeneity, Snail1 is expressed in this population in an organ-independent manner to promote immunosuppression and tumour growth. We also demonstrate that in vivo systemic targeting with a Snail1 morpholino reduces metastatic burden in mice, extending mice survival. Moreover, as Snail1 was previously associated with increased metastases by favouring immune evasion by an EMT-dependent mechanism in melanoma cells [22], our data further support Snail1 potential as a good therapeutic target in melanoma. Snail1 has been classically considered undruggable, however CYD19, a recently developed inhibitor of Snail1 protein-protein interactions, has proved efficient in impairing tumour growth in mouse models of breast cancer [52]. We show here that this compound not only blocks Snail1 expression but also decreases Fap levels in fibroblasts and considering that Snail1 expression is almost absent in healthy tissues [56], its inhibition in melanoma patients should be safe and lack major adverse effects.

The use of immune checkpoint inhibitors that target regulatory pathways on T cells to elicit anti-tumour responses has greatly improved the management of melanoma patients. However, only ~50% of patients respond [60]. Interestingly, Snail1-induced EMT in melanoma cells promoted resistance to immunotherapy based on intratumour injection of dendritic cells [22] and we show here that SNAI1 expression correlates with worse clinical responses to anti-PD-1 in melanoma patients. Current efforts directed to improve immune checkpoints inhibitors efficacy and the clinical management of patients include the characterisation of mechanisms regulating immunosuppression [44] and the discovery of biomarkers to predict responses. In this study, we show that Snail1 is a driver of CAFs-induced immunosuppression and pro-tumour immunity in melanoma, that its expression correlates with impaired responses to immune checkpoint inhibitors and therefore, we confirm its potential as a therapeutic target.

## METHODS

### Mice

All experiments involving animals were performed in accordance with the European Community Council Directive (2010/63/EU) and Spanish legislation. The protocols were approved by the CSIC Ethics Committee and the Animal Welfare Committee at the Instituto de Neurociencias CSIC-UMH. Mice were hosted in a pathogen-free facility under controlled temperature,

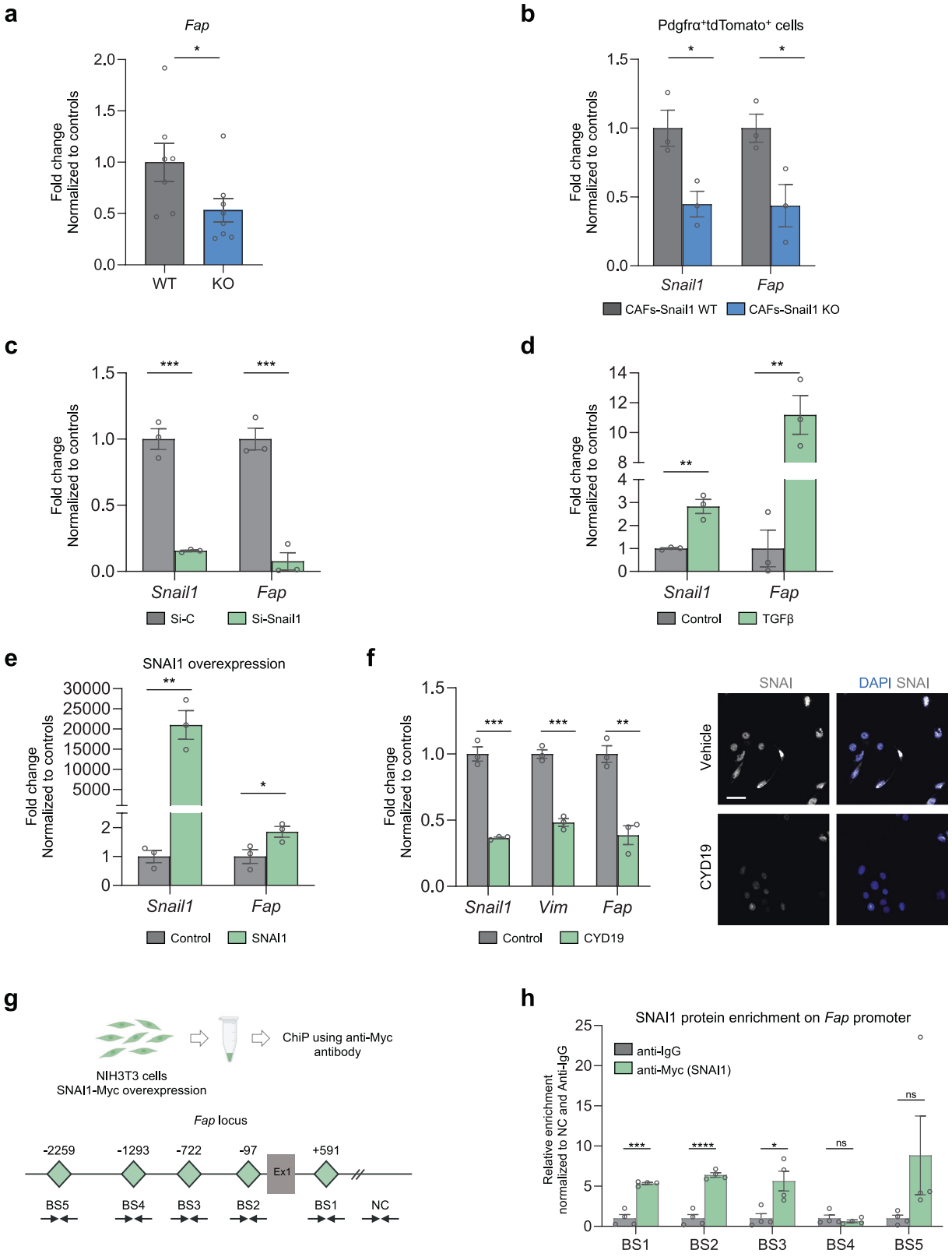


humidity, and 12 h light/dark cycle. All experiments were performed in 7–8-week-old mice C57BL/6. To analyse Snail1 in melanomas we crossed the inducible BRAF-driven mouse melanoma model $Braf^{CA}$,$Pten^{loxP}$,Tyr::-CreERT2 ($BRAF^{V600E}$/$Pten^{loxP}$) [26] (RRID:IMSR_JAX:013590) with Rosa-LSL-tdTomato (RRID:IMSR_JAX:007909) mice (referred as $Braf^{V600E}$/$Pten^{loxP}$/tdTomato). To investigate Snail1 in the TME we crossed UBC-Cre-ERT2 mice [29] (RRID:IMSR_JAX:008085) or PDGFRα-CreERT2 mice [61] with Rosa-LSL-tdTomato (tdTomato) (RRID:IMSR_JAX:007909) and $Snai1^{fl/fl}$ mice [30]. To analyse myeloid populations in tumours, we used Cx3cr1CreERT2-YFP mice (RRID: IMSR_JAX:021160).

**Fig. 4 Fap is a direct target of Snail1 in fibroblasts. a** *Fap* mRNA levels detected by RT-qPCR in $Braf^{V600E}$-5555 tumours from $Snail1^{ME}$-WT (WT) and $Snail1^{ME}$-KO (KO) mice ($n = 7$ WT and $n = 8$ KO). **b** *Fap* mRNA levels detected by RT-qPCR in Snail1-WT and Snail1-KO PDGFRα$^{+}$/tdTomato$^{+}$ isolated fibroblasts ($n = 3$ WT and $n = 3$ KO) (**c**) *Snail1* and *Fap* mRNA levels detected by RT-qPCR upon Snail1 silencing using a siRNA in TGFβ treated NIH3T3 cells. Transfected cells were collected 48 h after transfection ($n = 3$). **d** *Snail1* and *Fap* mRNA levels increase detected by RT-qPCR upon TGFβ treatment in NIH3T3 cells. Cells were collected 48 h after TGFβ treatment ($n = 3$). **e** *Snail1* and *Fap* mRNA levels increase detected by RT-qPCR after SNAI1 transfection in NIH3T3 cells ($n = 3$). **f** *Snail1*, *Vimentin* and *Fap* mRNA levels detected by RT-qPCR in NIH3T3 cells treated with TGFβ (2 ng/ml) for 24 h and then with vehicle or CYD19 (5 nM) in the presence of TGFβ for another 48 h (left panel). Representative IF of SNAI in cells from (**f**), scale bar: 50 µm (right panel). **g** SNAI1 enrichment on the *Fap* promoter shown by ChiP assay in NIH3T3 cells, using an anti-Myc antibody (for SNAI1-Myc overexpression). Schematic representation of the mouse *Fap* locus is shown. SNAI1 potential binding sites (E-boxes; CANNTG) on the *Fap* promoter are represented as green diamonds (BS1: +591 bp, BS2: −97bp, BS3: −722bp, BS4: −1293bp, BS5 −2259bp). An intergenic region without SNAI1 binding sites was used as a negative control (NC). Ex1: SNAI1 exon 1. **h** Relative enrichment of SNAI1 binding to the five potential sites, normalised to the NC region and the anti-IgG controls ($n = 4$). Data are represented by Mean ± SEM and statistically significant differences are tested by unpaired two-tailed Student *t*-test. Each dot represents one animal (**a**) or independent experiments (**c**–**f**) (ns = not significant, * = $p < 0.05$, ** = $p < 0.01$, ***$p < 0.001$, ****$p < 0.0001$).

## Cell culture

Murine melanoma cell line $Braf^{V600E}$-5555 [27, 28] was originally obtained from Richard Marais laboratory and luciferase-expressing $Braf^{V600E}$-5555 cells (5555-Luc) were kindly given by Imanol Arozarena´s lab (NavarraBiomed). $BRAF^{WT}NRAS^{WT}$-B16F10 (CRL-6475) and $BRAF^{V600E}$-YUMM1.7 (CRL-3362) cells were obtained from ATCC, and the FCT1 cell line was isolated from a tumour arising in $Braf^{V600E}/Pten^{loxP}$/tdTomato transgenic mouse in our laboratory. NIH3T3 fibroblasts (CRL1658) were purchased from ATCC. All cell lines were maintained in DMEM (Sigma) supplemented with 10% FBS (Sigma) and 1% penicillin/streptomycin (Sigma). Cells were kept at 37 °C in a humid atmosphere containing 5% $CO_2$ and the media was replaced every 2/3 days. Melanoma cells were passaged when they reached 80% confluency 1:10 every 72 h, while NIH3T3 cells were passaged when they reached 60–70% confluency 1:20 every 72 h. Cells were discarded up to seven consecutive passages and replaced by fresh stocks. All cell lines were tested and confirmed negative for mycoplasma monthly at the host institution.

## Inducible melanoma reporter model

Tumours were induced topically in 6–8 weeks $Braf^{V600E}/Pten^{loxP}$/tdTomato mice. Treatment with 1.5 µl 4 hydroxy tamoxifen (4-HT) (Sigma) (8 mg/ml), dissolved in ethanol:DMSO (80:20), was applied on the shaved skin of the back. Mice were immobilised until 4-HT dried completely. Tumours were collected when reaching approximately 1200 $mm^3$ (formula: length × width × depth × 0.562).

## Melanoma subcutaneous allografts

5555 melanoma cells ($5 \times 10^6$ in 100ul in sterile PBS $Ca^{2+}Mg^{2}$-free) were subcutaneously injected in the dorsal area of $Snail1^{ME}$-WT and $Snail1^{ME}$-KO or PDGFRα-CreERT2/tdTomato and PDGFRα-CreERT2/tdTomato $Snail1^{fl/fl}$ 7–8 weeks old mice. Treatment with tamoxifen (Sigma) (intraperitoneally, 100 mg/kg body weight), dissolved in corn oil:ethanol (90:10), was carried out to induce recombination. Tamoxifen administration began once tumours reached a volume of 80–100 $mm^3$. Tumour volume was recorded with a calliper every 2/3 days. When the tumours reached the limit size the mice were sacrificed, and tumours were collected for histological analysis.

For CAFs isolation by FACS $Snail1^{ME}$-WT and $Snail1^{ME}$-KO mice were injected with GFP-expressing 5555 cells as previously described. Four doses of tamoxifen were injected intraperitoneally on alternate days before collection and processing of the tumours. To study the myeloid populations in melanoma tumours, $Braf^{V600E}$-5555 melanoma cells were injected as described previously in Cx3cr1CreERT2-YFP mice.

## Experimental metastasis assay

To evaluate metastatic progression in vivo, $Braf^{V600E}$-5555 -Luc ($1 \times 10^4$ cells in 100 µl of sterile PBS $Ca^{2+}Mg^{2}$-free) were intravenously injected into the lateral tail vein, using a 27-gauge needle. Lung colonisation was analysed in vivo and ex vivo by BLI. Anaesthetised mice (isoflurane) were injected intraperitoneally with D-luciferin (Perkin Elmer) (150 mg/kg body weight) and imaged with an IVIS Lumina XR imaging system (PerkinElmer). The lung BLI of every mouse was determined using Living Image software (PerkinElmer). Tamoxifen treatment (intraperitoneally, 100 mg/kg body weight) was started once experimental metastases were established and detected by BLI imaging. Tamoxifen was administered three days a week until the end of the experiment. Mice were sacrificed after 3 weeks, and tissues were collected for histological analysis.

## Tumour processing

Tumours and lungs were fixed in 4% PFA for 4 h or ON respectively at 4 °C. After fixation, tumours and lungs were washed three times with PBS and incubated in 30% sucrose for three days at 4 °C before embedding in OCT. Embedded samples were kept in dry ice and transferred to −80 °C before sectioning. Finally, OCT-embedded lungs and tumours were sectioned in a cryostat (Leica) at 8 µm-thick sections and dried for 2 h at room temperature (RT) before being used for immunolabelling or stored at −80 °C.

## Immunofluorescence (IF) stainings

Sections were blocked in 5% NGS, 1% BSA and 0.2% Triton x-100 for 1 h at RT and incubated with the primary antibodies O/N at 4 °C in blocking solution and the following day for 30 min at RT. After extensive washing in PBS, slices were incubated with the secondary antibodies and DAPI in a blocking solution for 1 h at RT. After washing the secondary antibody with PBS, slices were mounted in Dako Fluorescence Mounting Medium (Dako). Information and dilution of antibodies are listed in Supplementary Table 1. For IF in fibroblasts, FAC isolated cells were cultured and treated on poly-lysine (Sigma) glass coverslips in 12-well plates and fixed with 4% PFA for 15 min at RT. Afterwards, cells were washed three times with PBS, permeabilized with 0.1% Triton x-100 in PBS for 15 min and blocked in a 0.1% Triton x-100 1% BSA solution for 1 h at RT. Then, cells were incubated with the primary antibodies O/N at 4 °C in 1% BSA solution and the following day for 30 min at RT. After washing three times with PBS, cells were incubated with the secondary antibodies and DAPI 1 h at RT in 1% BSA solution. After washing the secondary antibody with PBS, cells were imaged.

Immunostainings were conducted using the primary and secondary antibodies listed in Supplementary Table 1. Pictures were taken with an Olympus FV1200 confocal microscope with 20× or 40× objectives.

## Quantification of Ki-67 and cleaved Caspase-3

Proliferation and apoptosis were evaluated after IF staining by imaging sections and processing them with the ImageJ software. To analyse tumour proliferation and apoptosis, cell counts were obtained in three random fields from the tumour invasive front, three random fields from the tumour centre and three random fields from the tumour edge in each tumour slice. The same number of pictures were performed in every tumour slice. Four different tumours were analysed per condition. To analyse experimental lung metastases proliferation and apoptosis, representative pictures of different metastases were taken from each lung slice. Four different lungs were analysed per condition. The number of proliferating and apoptotic cells was determined as number of apoptotic or proliferating tumours cells/$mm^2$.

## Histological analysis of melanoma lung metastases

8 µm-thick lung sections were prepared and stained with Haematoxylin and Eosin (H&E) (Sigma) and documented with a Leica DFC700T digital camera. To quantify lung metastatic burden, 9 serial H&E stained lung sections were collected every 150 µm, spanning a total of 1200 microns of lung tissue. Total metastatic area (metastasis area/total lung area *100), number of metastases (number of metastases/lung) and average metastasis size (total metastatic area/number of metastases) were measured using Image J software.

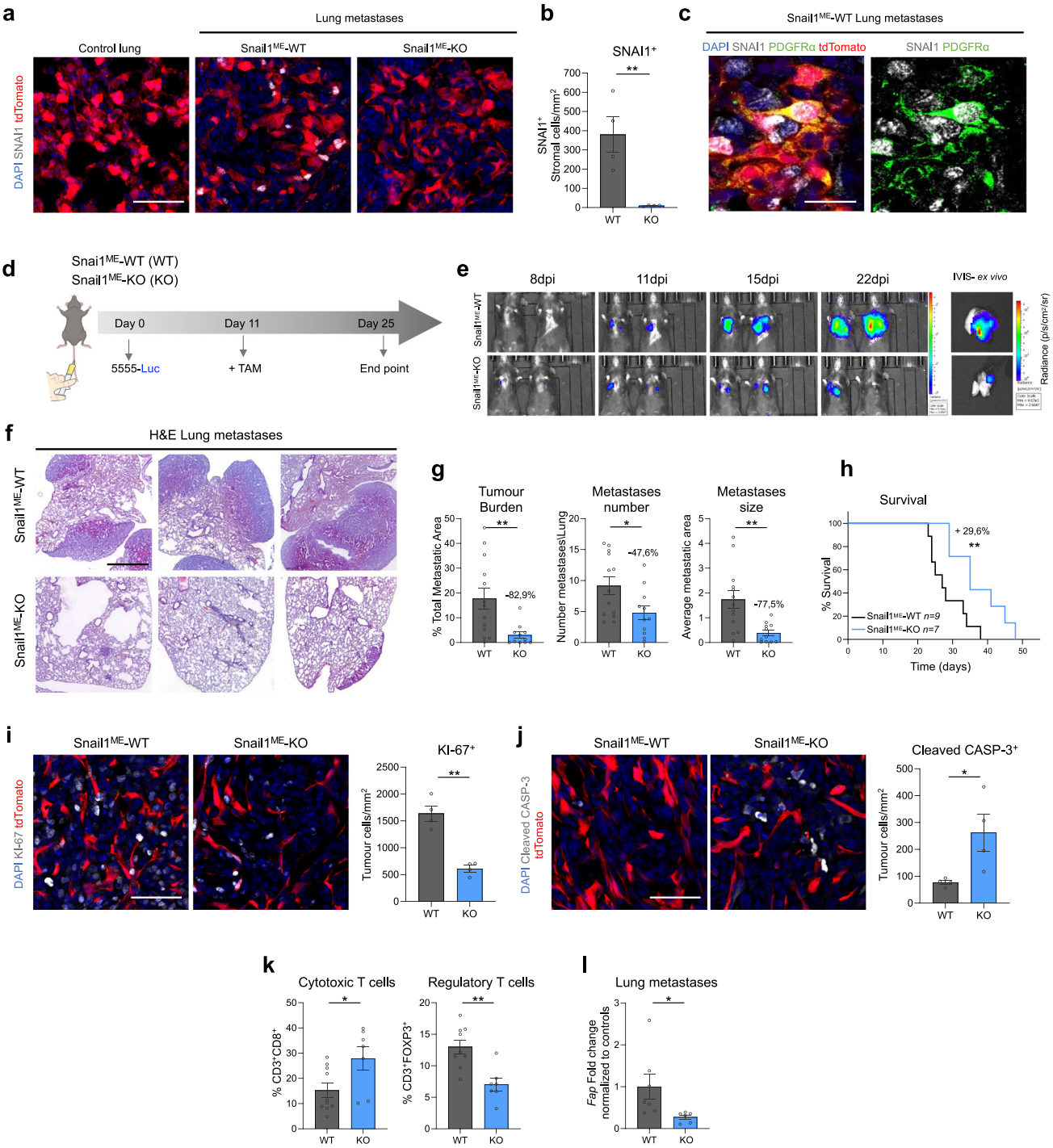


**Fig. 5 Microenvironmental Snail1 depletion reduces melanoma metastatic burden and improves mice survival. a** Representative images of immunolabelling for SNAI1 in control lung tissue and Braf$^{V600E}$-5555 lung metastases from Snail1$^{ME}$-WT and Snail1$^{ME}$-KO mice. Scale bar: 50 µm. **b** SNAI1 quantification after TAM administration in lung metastases from (**a**). **c** Representative images of double immunolabelling of SNAI1 (white) and PDGFRα (green) in Braf$^{V600E}$-5555 lung metastases from Snail1$^{ME}$-WT. Scale bar: 25 µm. **d** Experimental set-up of the in vivo strategy design to study the contribution of Snail1 to lung metastases progression in Snail1$^{ME}$-WT (WT) and Snail1$^{ME}$-KO (KO) mice. Created with BioRender.com. **e** Bioluminescent signal in mice from (**d**). The BLI scale is represented next to each panel. Units: p/s/cm2/sr ($n = 13$ WT and $n = 11$ KO). **f** Representative H&E-stained lung sections 25 days post-injection. Scale bar: 2 mm. **g** Tumour burden, number of metastases and metastases size, quantified in lungs from (**d**) ($n = 13$ WT and $n = 11$ KO). **h** Overall survival of Snail1$^{ME}$-WT and Snail1$^{ME}$-KO mice with melanoma lung metastases after Snail1-silencing compared to controls ($n = 9$ WT and $n = 7$ KO). **i** Representative images of immunolabelling for KI-67 and quantification ($n = 4$ per condition) in melanoma lung metastases from (**d**). Scale bar: 50 µm. **j** Representative images of immunolabelling for Cleaved-CASP3 and quantification ($n = 4$ per condition) in lung metastases from (**d**). Scale bar: 50 µm. **k** Graphs showing percentages of Cytotoxic T cells (CD3$^+$CD8a$^+$) and Regulatory T cells (CD3$^+$FOXP3$^+$) in lungs from (**d**) ($n = 10$ WT and $n = 7$ KO) assessed by flow cytometry. **l** *Fap* mRNA levels assessed by RT-qPCR in Snail1$^{ME}$-WT (WT) and Snail1$^{ME}$-KO (KO) lung metastases. Data are represented by Mean ± SEM and statistically significant differences are tested by unpaired two-tailed Student *t*-test. Each dot represents one animal (*=$p < 0.05$ and **=$p < 0.01$).

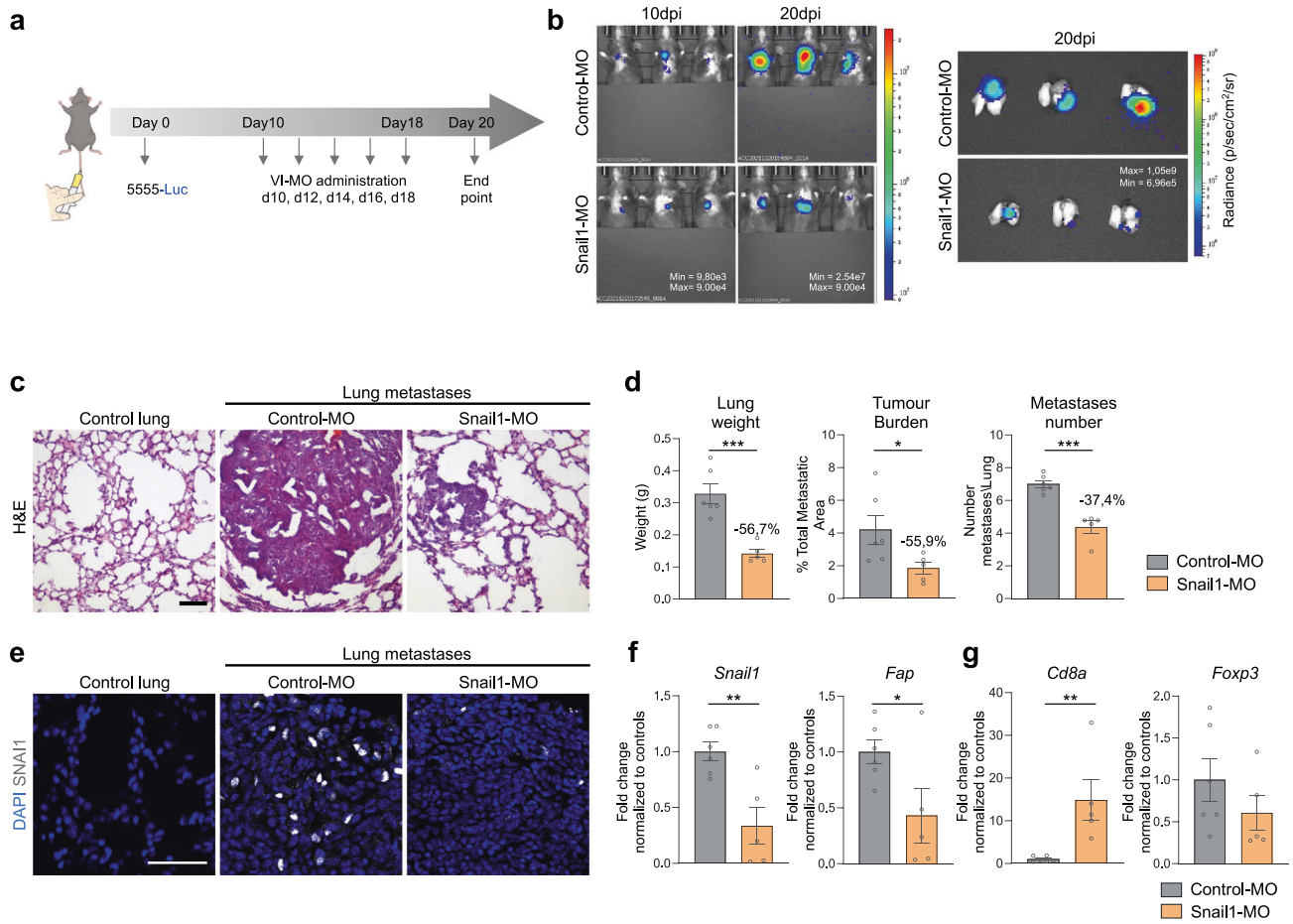


**Fig. 6 Snail1 systemic targeting significantly reduces melanoma lung metastases in mice. a** Scheme of the experimental approach. Nine days after tail vein injection of $Braf^{V600E}$-5555 cells, C57BL/6 mice were injected with vivo-morpholino (VI-MO) control (Control-MO) or Snail1 morpholino (Snail1-MO) every other day. Created with BioRender.com. **b** Bioluminescent signal in mice and lungs from (**a**). The BLI scale is represented in each panel. Units: p/s/cm2/sr. **c** Representative H&E-stained lung sections after VI-MO treatment. Scale: 100 µm. **d** Final lung weight, tumour burden and number of metastases from mice in (**a**) were quantified at the end of the experiment. **e** Representative images of immunolabelling for SNAI1 in lung sections after VI-MOs treatment. Scale bar: 50 µm. **f, g** *Snail1, Fap, Cd8a* and *Foxp3* mRNA expression assessed by RT-qPCR lung metastases from mice treated with Snail1-MO ($n = 6$ Control-MO and $n = 5$ Snail1-MO). Data are normalised to samples treated with Control-MO. Data are represented by Mean ± SEM and statistically significant differences are tested by unpaired two-tailed Student *t*-test. Each dot represents one animal (ns = not significant, * = $p < 0.05$, ** = $p < 0.01$, ***$p < 0.001$).

## Tissue processing for flow cytometry

Tumours and lungs were mechanically dissociated using a scalpel blade followed by a cold and slow enzymatic digestion (2.5 mg/ml Collagenase A and 0.2 mg/ml DNAse I) (all from Roche) in PBS at 4 °C for 1 h using constant gentle orbital agitation. After the incubation, the cell suspension was filtered through a 40 µm cell strainer using a 2 ml syringe plunger. The content was centrifuged (5 min 350 g and 1 min 10.000 rpm) and pellets were resuspended in 1 ml of RBC lysis buffer for 4 min at RT. Subsequently, cells were centrifuged and resuspended in fluorescence-activated cell sorting (FACS) buffer.

## FACS and flow cytometry

Prior to antibody staining, samples were blocked with Fc-block CD16/CD32 (Biolegend, 101320, 1:50) in FACS buffer for 10 min on ice to block nonspecific binding. For cell surface staining, cells were resuspended in the appropriate antibody cocktail and incubated for 30 min on ice protected from light. Samples were centrifuged and washed with a FACS buffer. For intracellular staining, cells were then collected and centrifuged for 5 min 350 g. Cells were fixed, permeabilized and stained for transcription factors using the True-Nuclear Transcription Factor Buffer Set (Biolegend, Cat# 424401) according to the manufacturer's instructions. Viability was assessed by staining with DAPI. Information and dilution for antibodies used for flow cytometry are listed in Supplementary Table 1. For fibroblast sorting cells, $PDGFR\alpha^{+}$ $GFP^{-}$ $tdTomato^{+}$ were selected and sorted directly into a lysis solution from Arcturus PicoPure RNA Isolation Kit (Thermofisher). For sample validation, cells were plated in poly-L-lysine treated (Sigma) glass coverslips in 12-well plates and cultured for 24 h prior to IF. Immune cell profiling by flow cytometry was carried out by analysing 50.000 live singlets in each sample. All fluorescent data were analysed using BD FACSDiva Software (BD Bioscience).

## Total RNA extraction cDNA synthesis and qPCR analysis

RNA extraction from FACS-isolated samples was performed following the instructions in the Arcturus PicoPure RNA Isolation Kit (Thermo Fisher). The RNA was collected in 15 µl of elution buffer (TE) and 1 µl was used for quantification and quality control using the Bioanalyzer High Sensitivity RNA chip. RNA extraction from bulk tumour or metastases samples was performed using the Illustra RNAspin Mini isolation kit (GE healthcare), following manufacturer's instructions. For cDNA synthesis, Maxima First Strand cDNA Synthesis kit (Thermo Fisher) was used, following the manufacturer's instructions. RT-qPCR was done using the Fast SYBR Green Mastermix (Applied Biosystems) and the primers listed in Supplementary Table 2. Relative levels of expression were calculated using a housekeeping gene and then experimental samples were normalised to their respective control.

## RNA sequencing

RNA degradation and purity were assessed using the RNA Nano 6000 Assay for the Bioanalyzer 2100 (Agilent). Samples were sent to Novogene

Co. Sequencing libraries were generated using NEBNext® Single Cell/Low Input RNA Library Prep Kit for Illumina (NEB) following the manufacturer's recommendations. Sequencing was performed using a cBot Cluster Generation Sequencing using PE Cluster Kit cBot-HS (Illumina) according to the manufacturer's recommendation. After cluster generation, the library preparations were sequenced on an Illumina platform and 250 bp paired-end reads were generated.

### RNA sequencing analysis

Raw data (raw reads) of FASTQ format were mapped to a mouse reference transcriptome (Mus_musculus.GRCm38.cdna.all.fa) built with Kallisto v.0.46.1. Read quantification to reference transcriptome was performed with Kallisto as well. The following steps were performed using R and RStudio. Tximport was used to import abundance.tsv files to R environment. EdgeR was used for differential expression analysis to obtain DEGlist objects and normalisation. The MatrixStats package was used to determine the statistics on the data. Data was filtered by choosing transcripts with at least 10 reads and later, at least one CPM in at least three samples. Normalisation factor TMM (trimmed mean of M-values) was applied. Limma and edgeR were used to obtain a final DEG list adjusted by BH (Benjamini-Hochberg) and sorted by $p$ value < 0.05 and LFC > 1. The graphical constructs of the RNAseq data were performed using gplots, plotly, gprofiler2, clusterprofiler, GSEABase and GSEA software v4.3.2 [35, 62].

### Transfection of plasmids and interfering RNAs

For RNA interference in NIH3T3 cells, siRNA obtained from Silencer® predesigned (Ambion) was used for Snail1 (Snail1 siRNA (antisense): AUAUUUGCAGUUGAAGAUCtt). Snai1-Myc plasmid was transfected in NIH3T3 cells seeded in six-well plates and 48 h after transfection cells were lysed for RNA extraction.

### CYD19 drug administration

NIH3T3 cells were initially treated with TGFβ (2 ng/ml) for 24 h. Subsequently, the cells were exposed to either the vehicle or 5 nM of CYD19 (Cat#AOB11460, Aobious) in the presence of TGFβ for an additional 48 h. Following the treatment, NIH3T3 cells were subjected to IF or gene expression analysis.

### Chromatin immunoprecipitation (ChIP) assay

NIH3T3 cells transfected with SNAI1-Myc were fixed at 80% confluency from 10 cm culture dish by adding 1% PFA for 10 min and subsequently quenched with glycine solution 0.125 M for 5 min. Then, the cells were harvested and pooled together from four plates, and the chromatin was isolated using the Pierce™ Magnetic ChIP Kit (Thermo Fisher) following the manufacturer's instructions. The sonication was performed in 15 cycles of 30-s on/off intervals in a Bioruptor® Pico sonication device (Diagenode). Finally, the immunoprecipitation and DNA isolation were performed using the same Pierce™ Magnetic ChIP Kit and the anti-Myc antibody listed in Supplementary Table 1. The isolated DNA was used for direct qPCR reaction.

### Vivo-morpholino treatment

Snail1 Vivo-morpholino (Snail1-MO) (5′-TGAACTCTGCGGGAAGAGAAGA-GAC-3′) against the boundary sequences of the intron 1 and exon 2 of Snail1 gene and standard control morpholino (Control-MO) that targets human β-globin intron mutation (5′-CCTCTTACCTCATTACAATTTATA-3′) were designed (by Gene Tools). C57BL/6 mice aged 7 weeks were injected in the tail vein with $Braf^{V600E}$-5555 -Luciferase cells. 10 dpi, a solution containing Snail1-MO or Control-MO in saline (100 µl; 6 mg MO per kg) was injected in the tail vein of the corresponding mice every other day. After 20 days mice were sacrificed and lungs were processed, sectioned, and subjected to analysis.

### Statistical analysis

All statistical tests were performed using GraphPad Prism 8 software. Student's $t$-test or One-way ANOVA with Bonferroni's multiple comparison test were performed to determine the significant values of the data. Kaplan-Meier data were analysed with the comparison of survival curves using the Long-rank (Mantel-Cox) test. All the values were shown as Mean values ± SEM (Standard Error of the Mean). Significant difference between groups were represented as follows: * = $p \le 0.05$, ** = $p \le 0.01$, *** = $p \le 0.001$ and **** = $p \le 0.0001$.

## DATA AVAILABILITY

Single Cell RNAseq data from [42] are accessible via supplementary information or ArrayExpress: E-MTAB-7427. Bulk RNAseq data of sorted fibroblasts from [43] were accessed via EGAS00001002508. The datasets generated during the current study are available from the corresponding author on reasonable request.

## REFERENCES

1. Davis LE, Shalin SC, Tackett AJ. Current state of melanoma diagnosis and treatment. Cancer Biol Ther. 2019;20:1366–79. https://doi.org/10.1080/15384047.2019.1640032.
2. Postovit LM, Seftor EA, Seftor REB, Hendrix MJC. Influence of the microenvironment on melanoma cell fate determination and phenotype. Cancer Res. 2006;66:7833–6.
3. Nieto MA, Huang RYYJ, Jackson RAA, Thiery JPP. Emt: 2016. Cell. 2016;166:21–45.
4. Nieto MA. Epithelial plasticity: a common theme in embryonic and cancer cells. Science. 2013;342:1234850.
5. Lu W, Kang Y. Epithelial-mesenchymal plasticity in cancer progression and metastasis. Dev Cell. 2019;49:361–74.
6. Hanahan D. Hallmarks of cancer: new dimensions. Cancer Discov. 2022;12:31–46.
7. Nieto MA. Context-specific roles of EMT programmes in cancer cell dissemination. Nat Cell Biol . 2017;19:416–8. https://doi.org/10.1038/ncb3520.
8. Dongre A, Rashidian M, Reinhardt F, Bagnato A, Keckesova Z, Ploegh HL. et al. Epithelial-to-mesenchymal transition contributes to immunosuppression in breast carcinomas. Cancer Res. 2017;77:3982–9.
9. Dongre A, Weinberg RA. New insights into the mechanisms of epithelial–mesenchymal transition and implications for cancer. Nat Rev Mol Cell Biol. 2019;20:69–84. https://doi.org/10.1038/s41580-018-0080-4.
10. Stanisavljevic J, Loubat-Casanovas J, Herrera M, Luque T, Peña R, Lluch A, et al. Snail1-expressing fibroblasts in the tumor microenvironment display mechanical properties that support metastasis. Cancer Res. 2015;75:284–95.
11. Alba-Castellón L, Olivera-Salguero R, Mestre-Farrera A, Peña R, Herrera M, Bonilla F, et al. Snail1-dependent activation of cancer-associated fibroblast controls epithelial tumor cell invasion and metastasis. Cancer Res. 2016;76:6205–17.
12. Cortés M, Sanchez-Moral L, de Barrios O, Fernández-Aceñero MJ, Martínez-Campanario M, Esteve-Codina A, et al. Tumor-associated macrophages (TAMs) depend on ZEB1 for their cancer-promoting roles. EMBO J. 2017;36:3336–55.
13. Blanco-Gomez A, Hontecillas-Prieto L, Corchado-Cobos R, García-Sancha N, Salvador N, Castellanos-Martín A, et al. Stromal SNAI2 is required for ERBB2 breast cancer progression. Cancer Res. 2020;80:5216–30.
14. Lee K-W, Yeo S-Y, Gong J-R, Koo O-J, Sohn I, Lee WY, et al. PRRX1 is a master transcription factor of stromal fibroblasts for myofibroblastic lineage progression. Nat Commun. 2022;13:1–23.
15. Sahai E, Astsaturov I, Cukierman E, DeNardo DG, Egeblad M, Evans RM, et al. A framework for advancing our understanding of cancer-associated fibroblasts. Nat Rev Cancer. 2020;20:174–86. https://doi.org/10.1038/s41568-019-0238-1.
16. Lavie D, Ben-Shmuel A, Erez N, Scherz-Shouval R. Cancer-associated fibroblasts in the single-cell era. Nat Cancer. 2022;3:793–807.
17. Vandamme N, Denecker G, Bruneel K, Blancke G, Akay O, Taminau J, et al. The EMT transcription factor ZEB2 promotes proliferation of primary and metastatic melanoma while suppressing an invasive, mesenchymal-like phenotype. Cancer Res. 2020;80:2983–95.
18. Caramel J, Papadogeorgakis E, Hill L, Browne GJ, Richard G, Wierinckx A, et al. A Switch in the expression of embryonic EMT-inducers drives the development of malignant melanoma. Cancer Cell. 2013;24:466–80.
19. Denecker G, Vandamme N, Akay Ö, Koludrovic D, Taminau J, Lemeire K, et al. Identification of a ZEB2-MITF-ZEB1 transcriptional network that controls melanogenesis and melanoma progression. Cell Death Differ. 2014;21:1250–61.
20. Vandamme N, Berx G. Melanoma cells revive an embryonic transcriptional network to dictate phenotypic heterogeneity. Front Oncol. 2014;4:1–6.
21. Karras P, Bordeu I, Pozniak J, Nowosad A, Pazzi C, Raemdonck N, et al. A cellular hierarchy in melanoma uncouples growth and metastasis. Nature. 2022;610:190–8.
22. Kudo-Saito C, Shirako H, Takeuchi T, Kawakami Y. Cancer metastasis is accelerated through immunosuppression during snail-induced EMT of cancer cells. Cancer Cell. 2009;15:195–206. http://ac.els-cdn.com/S1535610809000324/1-s2.0-S1535610809000324-main.pdf?_tid=ee389d7c-c684-11e5-bb54-00000aacb361&acdnat=1454071174_e8bca0dd8025cf245a3948d1a9866a01.
23. Brenot A, Knolhoff BL, Denardo DG, Longmore GD. SNAIL1 action in tumor cells influences macrophage polarization and metastasis in breast cancer through altered GM-CSF secretion. Oncogenesis. 2018;7:32. https://doi.org/10.1038/s41389-018-0042-x.
24. Cheng H-Y, Hsieh C-H, Lin P-H, Chen Y-T, Hsu DS, Tai S-K. et al. Snail- regulated exosomal microRNA- 21 suppresses NLRP3 inflammasome activity to enhance cisplatin resistance. J Immunother Cancer. 2022;10:1–16.

25. Cano A, Pérez-Moreno MA, Rodrigo I, Locascio A, Blanco MJ, Del Barrio MG, et al. The transcription factor Snail controls epithelial-mesenchymal transitions by repressing E-cadherin expression. Nat Cell Biol. 2000;2:76–83.
26. Dankort D, Curley DP, Cartlidge RA, Nelson B, Karnezis AN, Damsky WE, et al. BrafV600E cooperates with Pten loss to induce metastatic melanoma. Nat Genet. 2009;41:544–52.
27. Dhomen N, Reis-filho JS, Dias R, Hayward R, Savage K, Delmas V, et al. Oncogenic braf induces melanocyte senescence and melanoma in mice. Cancer Cell. 2009;15:294–303. https://doi.org/10.1016/j.ccr.2009.02.022.
28. Hirata E, Girotti MR, Viros A, Hooper S, Spencer-Dene B, Matsuda M, et al. Intravital imaging reveals how BRAF inhibition generates drug-tolerant microenvironments with high integrin β1/FAK signaling. Cancer Cell. 2015;27:574–88. https://doi.org/10.1016/j.ccell.2015.03.008.
29. Ruzankina Y, Pinzon-Guzman C, Asare A, Ong T, Pontano L, Cotsarelis G, et al. Deletion of the developmentally essential gene ATR in adult mice leads to age-related phenotypes and stem cell loss. Cell Stem Cell. 2007;1:113–26.
30. Rowe RG, Li X, Hu Y, Saunders TL, Virtanen I, Garcia de Herreros A, et al. Mesenchymal cells reactivate Snail1 expression to drive three-dimensional invasion programs. J Cell Biol. 2009;184:399–408.
31. Jung S, Aliberti J, Graemmel P, Sunshine MJ, Kreutzberg GW, Sher A, et al. Analysis of fractalkine receptor CX 3 CR1 function by targeted deletion and green fluorescent protein reporter gene insertion. Mol Cell Biol. 2000;20:4106–14.
32. Geissmann F, Jung S, Littman DR. Blood monocytes consist of two principal subsets with distinct migratory properties. Immunity. 2003;19:71–82.
33. Nieto MA, Bennett MF, Sargent MG, Wilkinson DG. Cloning and developmental expression of Sna, a murine homologue of the drosophila snail gene. Development. 1992;116:227–37.
34. Carver EA, Jiang R, Lan Y, Oram KF, Gridley T. The mouse snail gene encodes a key regulator of the epithelial-mesenchymal transition. Mol Cell Biol. 2001;21:8184–8.
35. Subramanian A, Tamayo P, Mootha VK, Mukherjee S, Ebert BL, Gillette MA, et al. Gene set enrichment analysis: a knowledge-based approach for interpreting genome-wide expression profiles. Proc Natl Acad Sci USA. 2005;102:15545–50.
36. Wiedemann GM, Knott MML, Vetter VK, Rapp M, Haubner S, Fesseler J, et al. Cancer cell-derived IL-1α induces CCL22 and the recruitment of regulatory T cells. Oncoimmunology. 2016;5:e1175794. https://doi.org/10.1080/2162402X.2016.1175794.
37. Ren J, Lan T, Liu T, Liu Y, Shao B, Men K. et al. CXCL13 as a novel immune checkpoint for regulatory B cells and its role in tumor metastasis. J Immunol. 2022;208:2425–35.
38. Weber R, Riester Z, Hüser L, Sticht C, Siebenmorgen A, Groth C, et al. IL-6 regulates CCR5 expression and immunosuppressive capacity of MDSC in murine melanoma. J Immunother Cancer. 2020;8:1–13.
39. Kuehnemuth B, Piseddu I, Wiedemann GM, Lauseker M, Kuhn C, Hofmann S, et al. CCL1 is a major regulatory T cell attracting factor in human breast cancer. BMC Cancer. 2018;18:1–6.
40. Martinenaite E, Munir Ahmad S, Hansen M, Met Ö, Westergaard MW, Larsen SK, et al. CCL22-specific T Cells: Modulating the immunosuppressive tumor microenvironment. Oncoimmunology. 2016;5:e1238541.
41. Erez N, Truitt M, Olson P, Hanahan D. Cancer-associated fibroblasts are activated in incipient neoplasia to orchestrate tumor-promoting inflammation in an NF-κB-dependent manner. Cancer Cell. 2010;17:135–47. https://doi.org/10.1016/j.ccr.2009.12.041.
42. Davidson S, Efremova M, Riedel A, Mahata B, Pramanik J, Huuhtanen J, et al. Single-Cell RNA sequencing reveals a dynamic stromal niche that supports tumor growth. Cell Rep. 2020;31:107628 https://doi.org/10.1016/j.celrep.2020.107628.
43. Costa A, Kieffer Y, Scholer-Dahirel A, Pelon F, Bourachot B, Cardon M, et al. Fibroblast heterogeneity and immunosuppressive environment in human breast cancer. Cancer Cell. 2018;33:463–479.e10.
44. Jenkins RW, Barbie DA, Flaherty KT. Mechanisms of resistance to immune checkpoint inhibitors. Br J Cancer. 2018;118:9–16. https://doi.org/10.1038/bjc.2017.434.
45. Kovács SA, Győrffy B. Transcriptomic datasets of cancer patients treated with immune-checkpoint inhibitors: a systematic review. J Transl Med. 2022;20:1–15. https://doi.org/10.1186/s12967-022-03409-4.
46. Lánczky A, Győrffy B. Web-based survival analysis tool tailored for medical research (KMplot): development and implementation. J Med Internet Res. 2021;23:1–7.
47. Yang X, Lin Y, Shi Y, Li B, Liu W, Yin W, et al. FAP Promotes immunosuppression by cancer-associated fibroblasts in the tumor microenvironment via STAT3-CCL2 Signaling. Cancer Res. 2016;76:4124–35.
48. Takahashi H, Sakakura K, Kawabata-Iwakawa R, Rokudai S, Toyoda M, Nishiyama M, et al. Immunosuppressive activity of cancer-associated fibroblasts in head and neck squamous cell carcinoma. Cancer Immunol Immunother. 2015;64:1407–17.
49. Cremasco V, Astarita JL, Grauel AL, Keerthivasan S, MacIsaac K, Woodruff MC, et al. FAP delineates heterogeneous and functionally divergent stromal cells in immune-excluded breast tumors. Cancer Immunol Res. 2018;6:1472–85.
50. Zhang Y, Ertl HCJ. Depletion of FAP+ cells reduces immunosuppressive cells and improves metabolism and functions CD8.T cells within tumors. Oncotarget. 2016;7:23282–99.
51. Cohen N, Shani O, Raz Y, Sharon Y, Hoffman D, Abramovitz L, et al. Fibroblasts drive an immunosuppressive and growth-promoting microenvironment in breast cancer via secretion of Chitinase 3-like 1. Oncogene. 2017;36:4457–68. https://doi.org/10.1038/onc.2017.65.
52. Li HM, Bi YR, Li Y, Fu R, Lv WC, Jiang N, et al. A potent CBP/p300-Snail interaction inhibitor suppresses tumor growth and metastasis in wild-type p53-expressing cancer. Sci Adv. 2020;6:eaaw8500.
53. Villarejo A, Cortés-Cabrera Á, Molina-Ortíz P, Portillo F, Cano A. Differential role of snail1 and snail2 zinc fingers in E-cadherin repression and epithelial to mesenchymal transition. J Biol Chem. 2014;289:930–41.
54. Grande MT, Sánchez-Laorden B, López-Blau C, De Frutos CA, Boutet A, Arévalo M, et al. Snail1-induced partial epithelial-to-mesenchymal transition drives renal fibrosis in mice and can be targeted to reverse established disease. Nat Med. 2015;21:989–97.
55. Chen J, Hu S, Wang H, Zhao T, Song Y, Zhong X, et al. Integrated analysis reveals the pivotal interactions between immune cells in the melanoma tumor microenvironment. Sci Rep. 2022;12:1–16. https://doi.org/10.1038/s41598-022-14319-2.
56. Boutet A, De Frutos CA, Maxwell PH, Mayol MJ, Romero J, Nieto MA. Snail activation disrupts tissue homeostasis and induces fibrosis in the adult kidney. EMBO J. 2006;25:5603–13.
57. Luo H, Xia X, Huang L-B, An H, Cao M, Kim GD. et al. Pan-cancer single-cell analysis reveals the heterogeneity and plasticity of cancer- associated fibroblasts in the tumor microenvironment. Nat Commun. 2022;13:6619.
58. Hsu DSS, Wang HJ, Tai SK, Chou CH, Hsieh CH, Chiu PH, et al. Acetylation of snail modulates the cytokinome of cancer cells to enhance the recruitment of macrophages. Cancer Cell. 2014;26:534–48. https://doi.org/10.1016/j.ccell.2014.09.002.
59. Rembold M, Ciglar L, Omar Yáñez-Cuna J, Zinzen RP, Girardot C, Jain A, et al. A conserved role for Snail as a potentiator of active transcription. Genes Dev. 2014;28:167–81.
60. Carlino MS, Larkin J, Long GV. Immune checkpoint inhibitors in melanoma. Lancet. 2021;398:1002–14. https://doi.org/10.1016/S0140-6736(21)01206-X.
61. Rivers LE, Young KM, Rizzi M, Jamen F, Psachoulia K, Wade A, et al. PDGFRA/NG2 glia generate myelinating oligodendrocytes and piriform projection neurons in adult mice. Nat Neurosci. 2008;11:1392–401.
62. Mootha VK, Lindgren CM, Eriksson KF, Subramanian A, Sihag S, Lehar J, et al. PGC-1α-responsive genes involved in oxidative phosphorylation are coordinately downregulated in human diabetes. Nat Genet. 2003;34:267–73.

## ACKNOWLEDGEMENTS

We thank members of Berta Sanchez-Laorden and Angela Nieto's labs for helpful discussions and comments along the project. We thank Joan Galceran and Khalil Kass Youssef for advice and help with the ChIP experiments and Jose Vicente Sanchez-Mut for advice with the data analysis. We also thank Isabel Perez Otaño for the PDGFRα-CreERT2 mice and the Imaging (Verona Villar and Giovanna Exposito) and OMICS (Antonio Caler) facilities for the technical support. This work was supported by grants SAF2016-75702-R and PID2019-106852-RBI00 (to BS-L), RTI2018-096501-B-I00 and PID2021-125682NB-I00 (to MAN) funded by MCIN/AEI/ 10.13039/501100011033 and ERDF, the Melanoma Research Alliance (https://doi.org/10.48050/pc.gr.91574 to B.S-L), the FERO Foundation (to B.S-L) and the AECC Scientific Foundation (FC_AECC PROYE19073NIE to MAN). MA-P and FC-T were recipients of a FPI predoctoral contract. FJR-B and FG hold contracts from the Generalitat Valenciana (APOSTD and ACIF, respectively). We also acknowledge financial support from the Spanish State Research Agency, through the 'Severo Ochoa Programme' for Centres of Excellence in R&D (SEV-2017-0273) and the Generalitat Valenciana through the 'Prometeo Programme' for Groups of Excellence (CIPROM/2021/045).

## AUTHOR CONTRIBUTIONS

MA-P performed most experiments, analysed, and interpreted the data, and contributed to writing the manuscript. FJR-B analysed and interpreted the transcriptomic data and performed some experiments, FC-T, FG and CL-B performed experiments. MAN provided the UBC-Cre-Snail1$^{loxp}$ mice and helped in the interpretation of data. BS-L conceived the project, interpreted the data, and wrote the manuscript.

## COMPETING INTERESTS

The authors declare no competing interests.

## ADDITIONAL INFORMATION

**Supplementary information** The online version contains supplementary material available at https://doi.org/10.1038/s41388-023-02793-5.

**Correspondence** and requests for materials should be addressed to Berta Sanchez-Laorden.

**Reprints and permission information** is available at http://www.nature.com/reprints

**Publisher's note** Springer Nature remains neutral with regard to jurisdictional claims in published maps and institutional affiliations.

# SUPPLEMENTARY FIGURES AND LEGENDS

## Supplementary Figure 1 (Related to Figure 1)

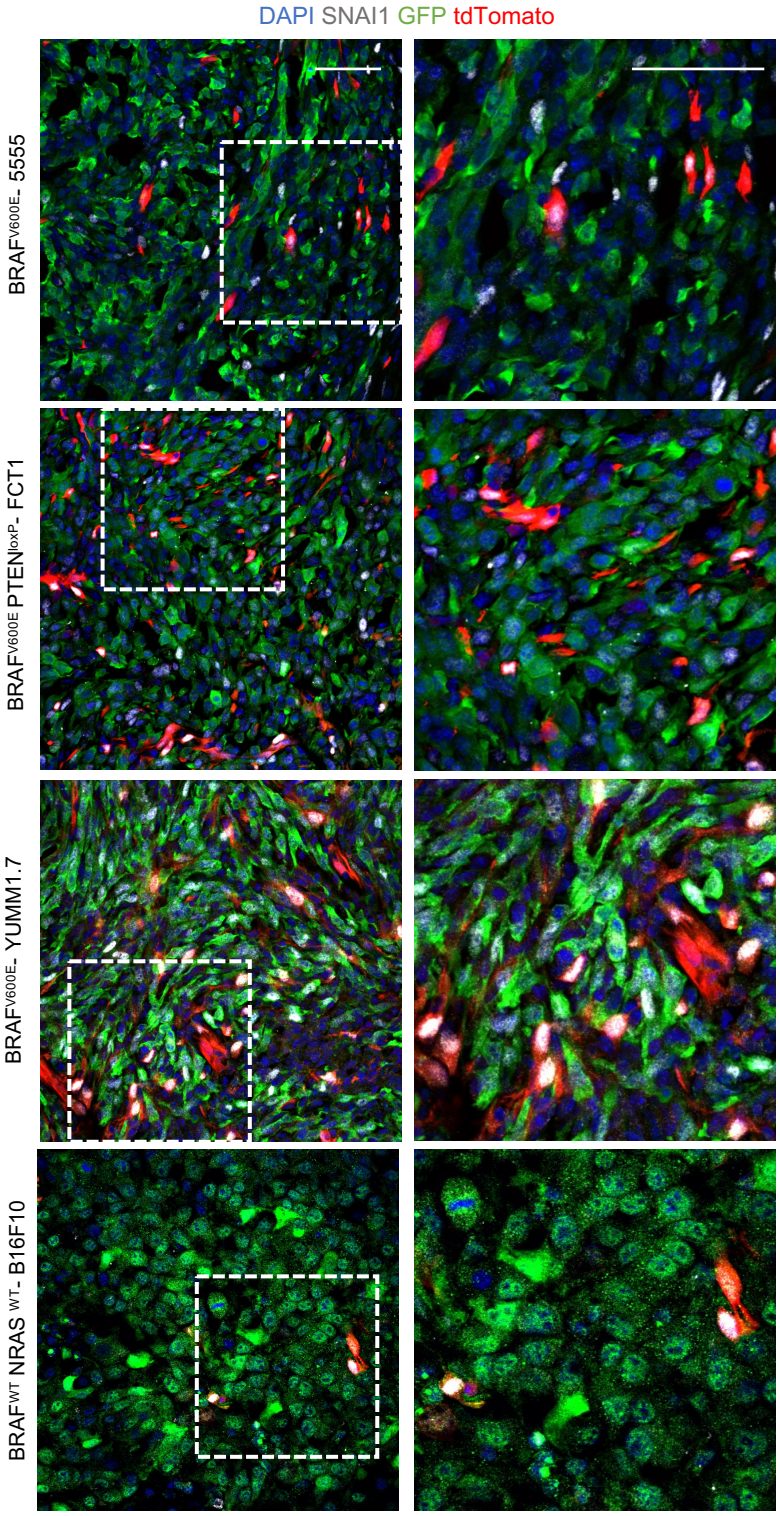

# Supplementary Figure 2 (Related to Figure 2)

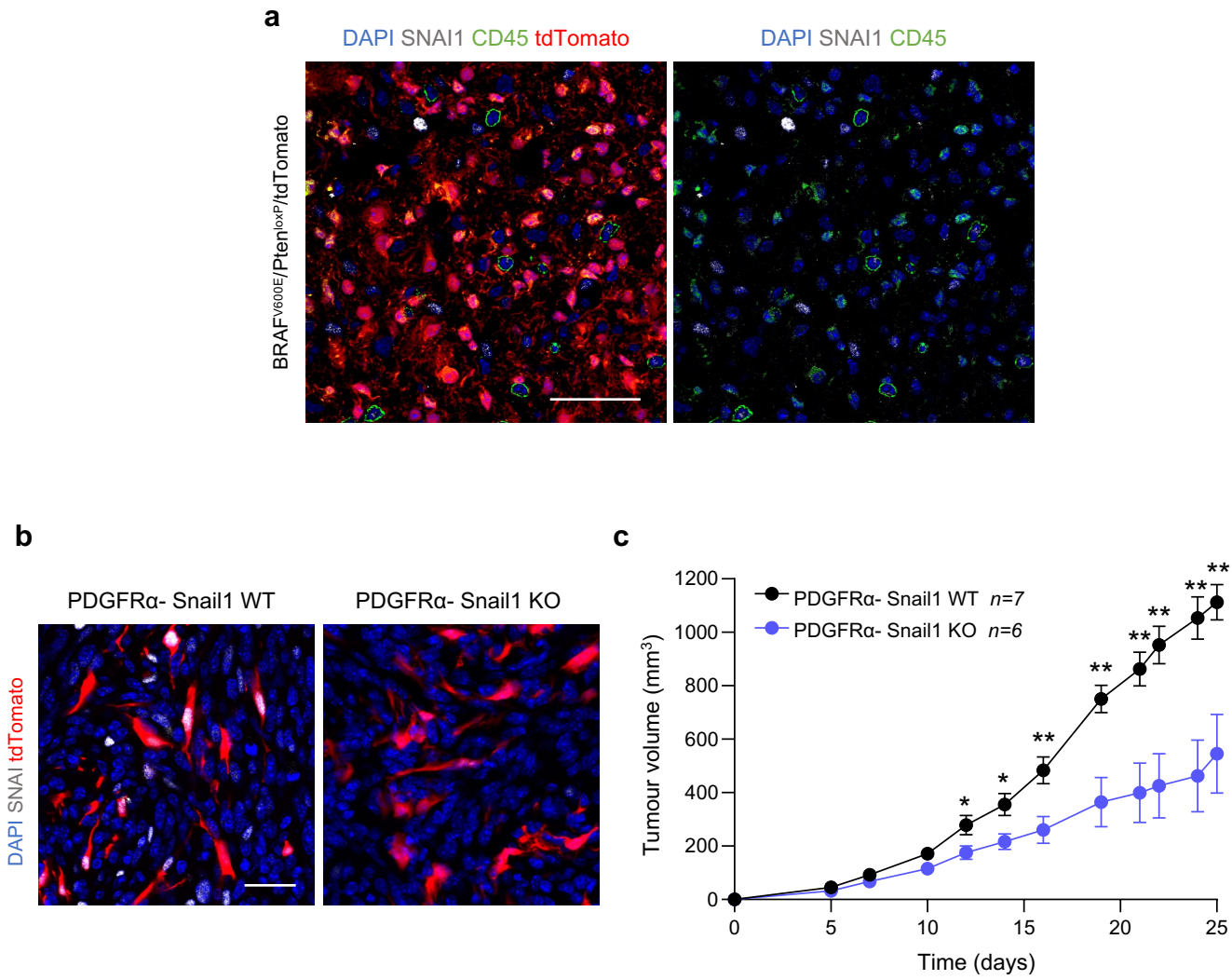

# Supplementary Figure 3 (Related to Figure 2)

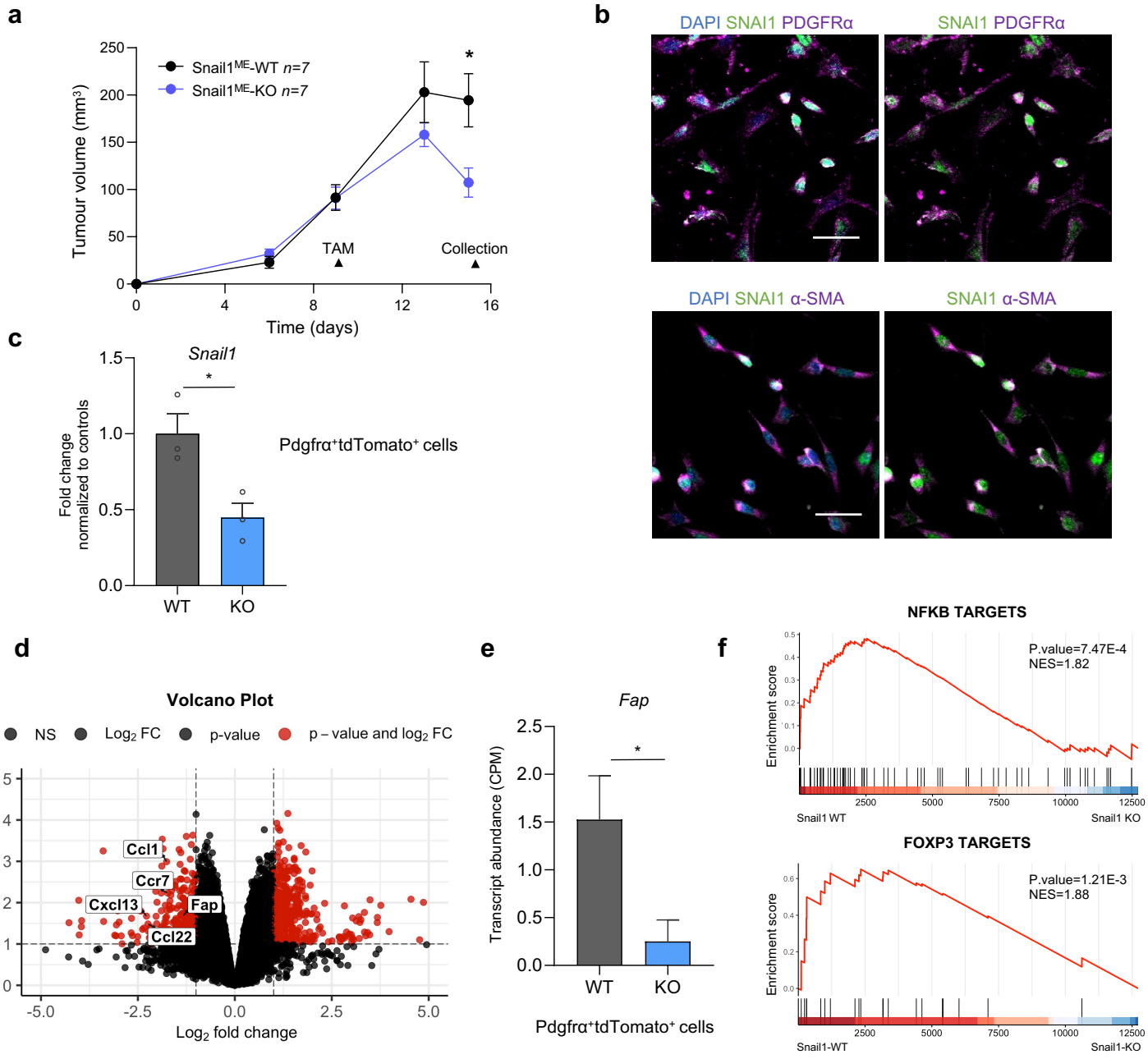

# Supplementary Figure 4 (Related to Figure 4)

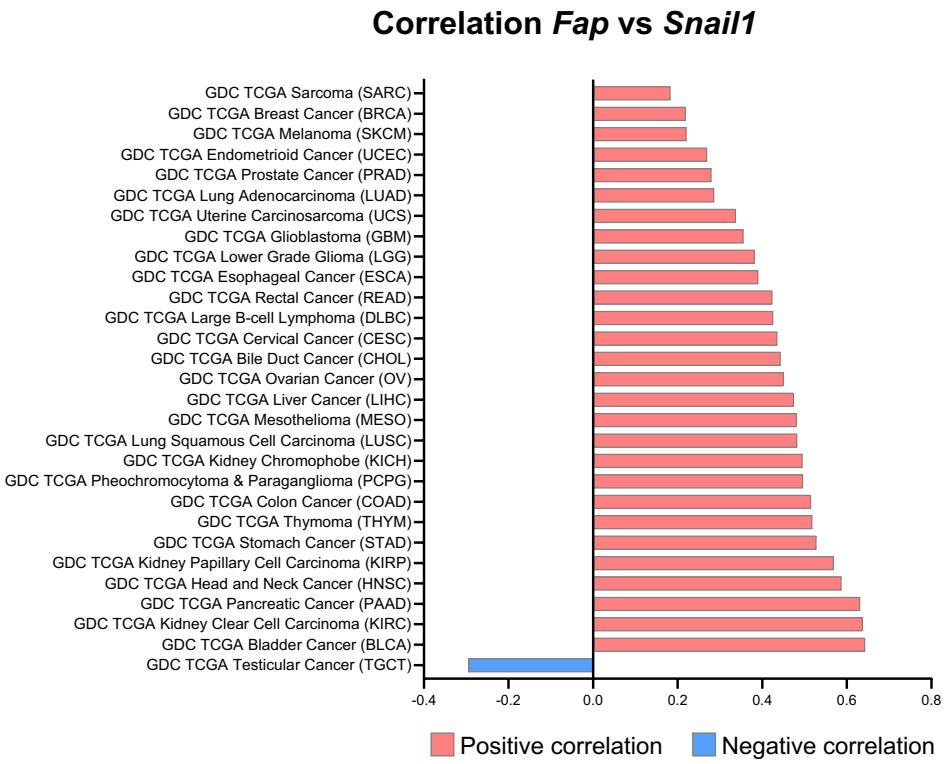

## Supplementary Figure 5 (Related to Figure 5)

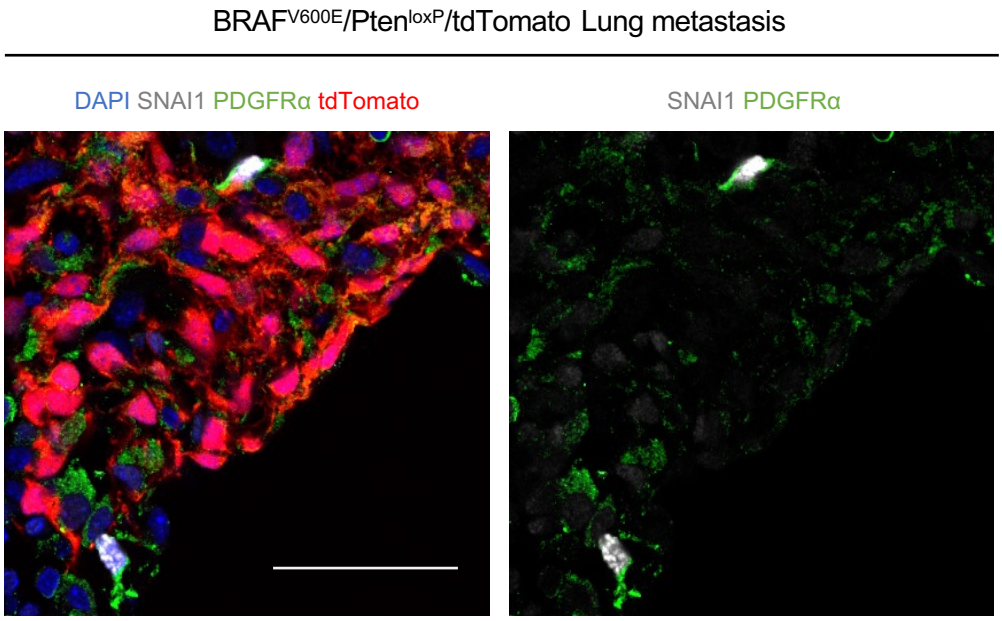

## SUPPLEMENTARY FIGURE LEGENDS

**Supplementary Figure 1 (Related to Figure 1). Snail1 expression in different syngeneic melanoma models.**

Representative images of double immunolabeling for SNAI1 (white) and GFP (green, melanoma cells) in subcutaneous tumours in tamoxifen-treated Snail1$^{ME}$-WT (stromal cells in red) upon injection of different mouse melanoma cell lines tagged with GFP: 5555 (BRAF$^{V600E}$); FCT1 (BRAF$^{V600E}$PTEN$^{flox/+}$); YUMM1.7 (BRAF$^{V600E}$PTEN$^{flox/flox}$Cdkn2a$^{-/-}$); B16F10 (BRAF$^{WT}$NRAS$^{WT}$). Scale bars: 50µm.

**Supplementary Figure 2 (Related to Figure 2). Snail1 targeting in PDGFRα$^{+}$ fibroblasts reduces melanoma growth.**

**(a)** Representative images of double immunolabeling for SNAI1 (white) and CD45 (green, immune cells) in BRAF$^{V600E}$/Pten$^{loxP}$/tdTomato melanoma model. tdTomato indicates melanoma cells (red). **(b)** Representative images of immunolabelling for SNAI1 (white) in PDGFRα-CreERT2-tdTomato (PDGFRα-Snail1 WT) (left) and PDGFRα-CreERT2-tdTomato-Snail1$^{fl/fl}$ (PDGFRα-Snail1 KO) (right) tumours upon tamoxifen administration. tdTomato indicates PDGFRα$^{+}$ cells (red). **(c)** Braf$^{V600E}$-5555 tumour growth curves in PDGFRα-Snail1 WT and PDGFRα-Snail1 KO mice (n=7 WT and n=6 KO). Data are represented by Mean±SEM and statistically significant differences are tested by unpaired two-tailed Student t-test (*=p<0.05 and **=p<0.01). Scale bar: 50µm.

**Supplementary Figure 3 (Related to Figure 2). Isolation strategy and transcriptomic analysis of Pdgfrα$^{+}$ CAFs from Snail1$^{ME}$-WT and Snail1$^{ME}$-KO mice.**

**(a)** *In vivo* experiment designed to isolate fibroblast from Braf$^{V600E}$-5555 melanomas grown subcutaneously in Snail1$^{ME}$-WT and Snail1$^{ME}$-KO mice. Tumour growth graph of an experiment showing the selected time point for the CAFs isolation (Snail1$^{ME}$-WT=7 and Snail1$^{ME}$-KO=7). **(b)** Representative images of double immunolabeling for SNAI1 (green) and different CAFs markers (magenta), in cells isolated from tumours in (a) after FACS-sorting (Pdgfrα$^{+}$tdTomato$^{+}$GFP$^{-}$). Scale bars: 50µm. **(c)** *Snail1* mRNA levels assessed by RT-qPCR to validate the fibroblasts population isolated by FACS (Pdgfrα$^{+}$tdTomato$^{+}$GFP$^{-}$) from tumours in (a) (samples from 3 animals with the same genotype were pooled for each condition). **(d)** Volcano plot of $Log_2$ fold change of DEGs between Snail1-WT and Snail1-KO fibroblast samples. The red dots on the right represent the upregulated genes and the red dots on the left the downregulated genes. **(e)** Transcript quantification in Pdgfrα$^{+}$tdTomato$^{+}$ fibroblasts subjected to RNA-Seq (Fig. 2d, e) (counts per million, CPM) from melanomas growing in Snail1-WT (WT) and Snail1-KO (KO) mice. **(f)** Gene set enrichment analysis (GSEA) showing enrichment of the indicated signatures in the Snail1$^{ME}$-WT and Snail1$^{ME}$-KO CAFs from tumours. NES, normalized enrichment score. Data are represented by Mean±SEM and statistically significant differences are tested by unpaired two-tailed Student t-test (*=p<0.05).

**Supplementary Figure 4 (Related to Figure 4). *Fap* and *Snail1* correlation across cancer types.**

Pearson correlation analysis between *Fap* and *Snail1* expression using all cancer types from The Cancer Genome Atlas program (TCGA) database. The graph includes cancer types with a significant correlation (p-value <0.05). Positive correlation is represented in red and negative correlation in blue.

**Supplementary Figure 5 (Related to Figure 5). Snail1 is expressed in Pdgfrα$^{+}$CAFs in lung metastases from an inducible BRAF$^{V600E}$/Pten$^{loxP}$/tdTomato melanoma model.**

Representative images of double immunolabeling for SNAI1 (white) and PDGFRα (green, fibroblasts) in BRAF$^{V600E}$/Pten$^{loxP}$/tdTomato melanoma lung metastases. tdTomato indicates melanoma cells (red). Scale bar: 50µm.

## Supplementary Table 1. Antibodies

| Antibody | Concentration | Species and type | Provider (Cat #) |
|---|---|---|---|
| Myc-tag (ChiP) | 1:500 | Goat pAb | Abcam (ab9132) |
| IgG (ChiP) | 1:500 | Rabbit | Thermo Fisher kit (1862739) |
| Snail1 | 1:50 | Rabbit monoclonal | Cell Signalling (C15D3, 3879) |
| GFP | 1:500 | Chicken polyclonal | Aveslab (2BScientific, GFP-1020) |
| PDGFRα | 1:100 | Rat monoclonal | Invitrogen (CD140a, 14-1401-82) |
| KI-67 | 1:1000 | Rabbit polyclonal | Abcam (ab15580) |
| Cleaved-CASPASE 3 | 1:500 | Rabbit monoclonal | Cell signalling (5A1E, 9664) |
| α-SMA | 1:1000 | Mouse monoclonal | Sigma (A2547) |
| CD45 | 1:350 | Rat monoclonal | BD Pharmingen™ (550539) |
| PDGFRα-APC | 1:50 | Rat monoclonal | Biolegend (135908) |
| CD11b-APC | 1:50 | Rat monoclonal | Biolegend (101211) |
| Ly6C-FITC | 1:50 | Rat monoclonal | Biolegend (128005) |
| Ly6G-APC/Fire | 1:50 | Rat monoclonal | Biolegend (127651) |
| CD3-APC | 1:50 | Rat monoclonal | Biolegend (100235) |
| CD4-APC/Fire | 1:50 | Rat monoclonal | Biolenged (100459) |
| CD8a-FITC | 1:50 | Rat monoclonal | Biolegend (100705) |
| CD45-APC | 1:50 | Rat monoclonal | Biolegend (103112) |
| CD11c-APC/Fire | 1:50 | Armenian Hamster monoclonal | Biolegend (117352) |
| CD22-FITC | 1:50 | Rat monoclonal | Biolegend (126106) |
| CD335-FITC | 1:50 | Rat monoclonal | Biolegend (137606) |
| FOXP3-AF488 | 1:50 | Rat monoclonal | Biolegend (126406) |
| Alexa Fluor 488 | 1:500 | Goat anti-rabbit | Invitrogen (A11008) |
| Alexa Fluor 488 | 1:500 | Goat anti-chicken | Life Technologies (A11039) |
| Alexa Fluor 488 | 1:500 | Goat anti-rat | Invitrogen (A11006) |
| Alexa Fluor 647 | 1:500 | Goat anti-rabbit | Life Technologies (A27040) |
| Alexa Fluor 647 | 1:500 | Goat anti-rat | Invitrogen (A21247) |
| Alexa Fluor 647 | 1:500 | Donkey anti-mouse | Invitrogen (A31571) |

**Supplementary Table 2. Primer Sequences**

| Gene | Primer Sequence (5'->3') |
|---|---|
| mTBP Fw | CCTTGTACCCTTCACCAATGAC |
| mTBP Rv | ACAGCCAAGATTCACGGTAGA |
| mSnail1 Fw | CAGCTGCTTCGAGCCATAGA |
| mSnail1 Rv | TGAGGGAGGTAGGGAAGTGG |
| mSnail1-e2 Fw (VM experiment) | CACGCTGCCTTGTGTCT |
| mSnail1-e3 Rv (VM experiment) | GAATGGCTTCTCACCAGTGT |
| mSnail1-exon1 Fw (RT-PCR) | AGTTGACTACCGACCTTGCG |
| mSnail1-exon3 Rv (RT-PCR) | TGGTATCTCTTCACATCCGAG |
| mFAP Fw | GGCTGGGGCTAAGAATCCG |
| mFAP Rv | GCATACTCGTTCACTGGACAC |
| mPDGFRα Fw | GGCACAGGTCACCACGAT |
| mPDGFRα Rv | GCGAGTTTAATGTTTATGCCTTG |
| mCol1a1 Fw | TAAGGGTCCCCAATGGTGAGA |
| mCol1a1 Rv | GGGTCCCTCGACTCCTACAT |
| mCol1a2 Fw | GCTCCTCTTAGGGGCCACT |
| mCol1a2 Rv | ATTGGGGACCCTTAGGCCAT |
| mCD3 Fw | CAGTCAAGAGCTTCAGACAAG |
| mCD3 Rv | GATGGCTGTACTGGTCATATTC |
| mArg1 Fw | CCGATTCACCTGAGCTTTGA |
| mArg1 Rv | AAAGGAGCCCTGTCTTGTAAAT |
| mCD8 Fw | CCATGAGGGACACGAATAATAA |
| mCD8 Rv | GAGTTCACTTTCTGAAGGACTG |
| mFOXP3 Fw | CAATAGTTCCTTCCCAGAGTTC |
| mFOXP3 Rv | TCGGATAAGGGTGGCATAG |
| BS1 Fw (ChiP) | GCGCTTGCTTTAGTGGTGAT |
| BS1 Fw (ChiP) | TTTGGAAAATAGGCACTTAGGA |
| BS2 Fw (ChiP) | ATTTGGCTCCACTGTTCTTCC |
| BS2 Fw (ChiP) | CCGTTTTATTTCACCTTTTTGTT |
| BS3 Fw (ChiP) | TGGAGACACCATATTCTAGCAAC |
| BS3 Fw (ChiP) | TTCATTTTGGCTAAGTCCACATA |
| BS4 Fw (ChiP) | TTTCTCTCGGATTGACGCCT |
| BS4 Rv (ChiP) | CAAATTGAAGCAGTACCAGGCA |
| BS5 Fw (ChiP) | TGGATCAATGTCATTCTGTCTG |
| BS5 Fw (ChiP) | TCTTGGAGCTCCTGCTGAGT |
| NC Fw (ChiP) | ATTTTGTGCTGCATAACCTCCT |
| NC Rv (ChiP) | TAGCAACATCCTAAGCTGGACA |

# ACKNOWLEDGMENTS

Quiero aprovechar este apartado de la tesis para agradecer a todas las personas que me han acompañado durante este tiempo, haciendo posible que me encuentre ahora mismo muy cerca de cerrar este capítulo. Todos vosotros habéis sido un pilar fundamental en este viaje lleno de retos a nivel personal y profesional.

En primer lugar, quiero agradecer a mi directora de tesis, **Berta Sánchez-Laorden**, por haberme brindado la oportunidad de realizar este proyecto en su laboratorio, por la orientación, apoyo y confianza a lo largo de todo el proceso. Gracias por haberme guiado en el desarrollo de los experimentos y, al mismo tiempo, por haberme dado la libertad necesaria para investigar, proponer ideas y explorar nuevos enfoques. Además, me alegra mucho haber presenciado el crecimiento del laboratorio desde mis inicios hasta hoy; estoy convencida que os espera un futuro lleno de éxitos.

También quiero agradecer a **Angela Nieto**, por el amplio conocimiento e inspiración que transmite en cada reunión. A **Joan Galceran**, por ayudarme en el diseño de experimentos y técnicas nuevas siempre que lo he necesitado. Todas vuestras sugerencias y aportaciones han sido de gran ayuda.

Además, quiero agradecer también a todos los miembros del laboratorio de Berta y Angela, por el apoyo que me han dado durante estos años y por crear un ambiente tan agradable en el laboratorio. Estoy agradecida por haber tenido la oportunidad de formar parte de este equipo.

Quiero empezar dando las gracias a **Javi**. Me has ayudado desde el momento en el que aterricé en Alicante. A pesar de estar siempre inmerso en múltiples tareas, siempre has encontrado un momento para escuchar mis dudas. Tu experiencia y conocimientos han sido fundamentales para superar los desafíos a los que me he enfrentado en esta etapa. Todas tus sugerencias han sido de gran importancia y tu apoyo y motivación han sido una fuente constante de inspiración a lo largo de estos años. Aprecio enormemente todo el tiempo que me has dedicado. Deseo que tengas mucho éxito en todo lo que te propongas, y estoy convencida de que así será.

A **Fran Cabello**. Has sido mi compañero de batallas desde que entré en el laboratorio. Gracias por el apoyo mutuo a lo largo de este camino, los días interminables en cultivos juntos no los olvidaré. Gracias por enseñarme a ver la vida con perspectiva, a apuntarte a todo conmigo para conseguir los deseados “papelitos”. Gracias por tu risa contagiosa, por echarme una mano en los experimentos y por tener siempre un sí por respuesta

(menos cuando te preguntaba si salías a comer y me decías que no, que hoy te tocaba batido jaja). Te voy a echar muchísimo de menos cuando me vaya. Gracias por todo.

A **Fran Quiles**, mi "*soulmate*" del laboratorio. Qué surte tuve cuando entraste a trabajar en el laboratorio de Berta. Siempre recordaré esos experimentos complicados que empezaban a las 6 de la mañana, en chándal, claro, y terminaban casi de noche. Trabajar mano a mano contigo en tantos experimentos nos ha unido muchísimo, hasta el punto de entendernos sin necesidad de palabras (a veces asusta el nivel de complicidad, ¿verdad?). Hemos dividido las derrotas, muchas de ellas durante el período del "*afternoon shift*", y multiplicado las victorias, manteniendo siempre una actitud positiva, tomándonoslo con "*flow*" y buen humor. Ha sido un placer coincidir contigo en esta aventura y sin duda eres una de las personas más especiales que me llevo de esta experiencia. Espero que siempre mantengas esa gran actitud que tienes y que tanto te caracteriza. Valoro enormemente nuestra amistad, y estoy segura de que, donde sea que nos lleve la vida, nuestra amistad será para siempre. Gracias por todo, Fran.

A **Cristina**. Me has ayudado muchísimo en el laboratorio. Sin tu ayuda, la gestión de los ratones habría sido mucho más complicada. Gracias por todo el tiempo que me has dedicado, sobre todo los días de nuestras estimadas "*tail vein*". Trabajar contigo siempre ha sido un placer. Muchas gracias por dejarme aprender de ti, por ser una persona tan alegre, amable y divertida.

A **Marilyn**. Me has enseñado a valorar y priorizar el tiempo y las cosas verdaderamente importantes. Espero coincidir más contigo; tenemos pendiente una salida de fiesta juntas y una cata de brownies.

A **Pablo**. Aunque apareciste más tarde en el laboratorio, has sido una parte esencial en esta etapa. Gracias por ayudarme siempre que lo he necesitado, y por esas cervezas sorpresa que aparecían y compartías con todos nosotros al final de un día duro (una recompensa muy merecida). Me encantan tus mensajes de voz que empiezan con un "simplemente" o "te quiero pedir una pequeña cosita" y luego se extienden por cinco minutos. Por favor, sigue enviándolos.

A **Anna Miralles** y a **Gema**, disfruté mucho el tiempo que compartimos juntas en el laboratorio. Era un placer llegar por las mañanas y veros allí, siempre radiantes de energía positiva. Gracias por vuestra ayuda y consejos, tanto profesionales como personales. Sois extraordinarias. Siempre nos encontraremos en el S*pring Festival*. A

**Alba.** Gracias por contribuir a un ambiente positivo en el laboratorio, por tu espíritu de equipo y consejos "*fit*". Mi vida es más saludable desde que te uniste a nosotros.

A **Noemi.** Hemos aprendido muchas juntas durante esta etapa. Te agradezco profundamente haber estado siempre dispuesta a echarme una mano. Me llevo divertidas sesiones y tutoriales de maquillaje juntas; aunque admito que todavía me queda mucho por mejorar. Te has convertido en una persona clave en mi vida y una de las amistades más valiosas que me llevo de Alicante. Te admiro y te quiero mucho. A **Andrea**, recuerdo con cariño el primer día que llegaste al laboratorio, tan simpática, amable y radiante. También recuerdo pensar que me llevaría bien contigo y seríamos buenas amigas, y no me equivoqué. Siempre te echo de menos, pero me alegra mucho saber que has alcanzado tus metas; siempre supe que lo lograrías. Recuerda que tienes un sitio en Barcelona siempre que quieras. A **Andrés**. Fuiste un compañero de trabajo y eres un amigo genial. Espero que me sigas dando envidia de la buena con tus viajes e historias. Sigo esperando tu tarta de queso. A **David**. Me ha encantado que nuestros caminos se hayan vuelto a juntar en la ciudad de Barcelona. Que ganas de seguir sumando momentos contigo.

También quiero agradecer a los miembros del laboratorio de Angela que me han ayudado de manera activa a llegar hasta aquí. A **Sonia**. Siempre estás dispuesta a solucionarnos todas nuestras dudas y ayudarnos en todo lo que necesitamos. Es un placer trabajar contigo. Gracias a **Khalil** y **Raúl**, vuestras aportaciones y comentarios siempre me han ayudado mucho. To **Sanjay** and **Nitin**. You are both very good people with excellent cooking skills. We need to repeat the Indian dinner someday. A **Ismael**. Aunque estuviste un año con nosotros, disfruté mucho el tiempo que compartimos. Siempre estabas tranquilo, sonriendo y de buen humor, y nunca te faltaba una caja de hielo en la mano, lo cual siempre nos sacaba una carcajada a Quiles y a mi jaja. Es genial tener a personas como tú cerca. Eché mucho de menos tus visitas al laboratorio vecino cuando te fuiste, pero me alegra mucho que sigamos en contacto. To **Angelita**. Thank you for introducing me to the Pilates reformer world, particularly during the manuscript preparation phase of this journey. I am so glad that our paths have crossed.

**Anna Prieto**. Quina sort vaig tenir de viure amb tu durant el meu últim període a Alacant, ja que així et vaig poder conèixer millor. Sempre he sentit que et coneixia d'abans, i és que, encara que ens haguem conegut aquí a Alacant, les dues venim de ciutats molt properes a Barcelona i els nostres objectius vitals són molt similars. M'ha encantat viure aquests anys tant intensos amb la teva complicitat. Compartir els moments de ball els

dimecres, els sopars al piset amb espelmes per fer-ho més "*cozy*" mentre ens explicàvem que tal havia anat el dia, i sessions de cine desconnectant de tot. Espero que la vida ens torni a unir en el futur i que ens tornem a trobar, ja sigui a Barcelona o a qualsevol altre lloc. Et recordo que tenim un viatge pendent. Seràs la pròxima doctora. Et desitjo el millor, gràcies per tot.

A **Lucía**. Eres una gran persona. Tu apoyo ha sido esencial, y me has enseñado la importancia de avanzar poco a poco. Contigo he aprendido a no concentrarme solo en la meta, sino a apreciar cada momento y desglosar los retos en pequeñas etapas más alcanzables. Sería mentirte si no admitiera que gracias a ti he desarrollado un cierto gusto por las películas de terror. Eres una persona encantadora y deseo que sigas siendo parte de mi vida para siempre.

A **Aysha**, eres realmente una persona vitamina, de esas que quiero siempre cerca. Tu positividad, tu energía inagotable y tu sonrisa son auténticos tesoros. Tu presencia enriquece la vida de quienes te rodean, y valoro enormemente cada momento que has dedicado a escucharme cuando más lo he necesitado. Las aventuras increíbles que hemos vivido juntas en Alicante son inolvidables, y me siento muy afortunada de tenerte como una amiga para toda la vida. Gracias por acogerme siempre en tu pisito y hacerme sentir en casa, donde sea que esté, contigo. A **Carmen**, aunque coincidimos más tarde, te has ganado un lugar muy especial en mi corazón. Agradezco mucho los momentos dulces que me has dado, ya sea con golosinas o en forma de abrazos. Además, tenemos pendiente explorar Huelva juntas mientras comemos muchas fresas. Descubrir que compartimos los mismos gustos en absolutamente todo fue muy gracioso. Estoy deseando seguir compartiendo experiencias y creando recuerdos contigo. A **Cristina**, mi catalana en Alicante. Desde que nos conocimos, supe que nuestras almas eran parecidas. Tu presencia siempre mejora cualquier plan. Gracias por demostrarme que la distancia no es un obstáculo, por estar siempre ahí con videollamadas cuando las necesitamos y por cuidarnos mutuamente. Confío en que seguiremos encontrándonos, ya sea en Barcelona, Alicante, Vic o donde sea, porque esto no termina aquí, apenas comienza. A **Juanjo**, ojalá te hubiera conocido antes, pero compartir este tiempo contigo ha sido genial. Tienes un don especial para alegrarme con tu sonrisa contagiosa y hacer que cada momento sea único. Reírnos juntos después de esos días duros, cuando los experimentos no salían y nos sentíamos frustrados, ha sido clave para recargarme las pilas y seguir adelante. Creo que hablo por todos cuando digo que apreciamos enormemente tu coordinación y paciencia (mucha paciencia), que han hecho posibles

viajes y actividades que, sin ti, habrían sido un caos por nuestra falta de organización. No cambies nunca, sumas mucho, de verdad. A **Ernesto**, has estado a mi lado casi desde el inicio de esta aventura. Pasamos de saludarnos en los pasillos con un simple "hola" a ser verdaderos amigos, y me has demostrado que puedo contar contigo, aunque nos separen 600 km. Me encanta que siempre te apuntes a cualquier bombardeo. Continuaré consultándote mis dudas sobre musculación y gym, jaja, no puedo evitarlo. Gracias de corazón por tu apoyo y por estar siempre disponible cuando más lo he necesitado; ha significado mucho. ¡Qué bonito "*Dream Team*" se ha unido en Alicante! Os quiero mucho, familia alicantina.

También quiero dar las gracias a **Alicia, Francesco, Edu, Bea, Sofia, Marina, Pablo A., Miguel, Oscar, Pablo C., Sergio, Bárbara, Andrea, Marta y Juan Paraíso**. Muchas gracias por todos los buenos recuerdos que me dejáis, por tantas risas en las "*happy hour*" y por formar parte de esta increíble familia alicantina que hemos construido.

También quiero dar las gracias a las personas que trabajan en las Unidades Comunes del centro. A **Antonio, Verona, Giovanna, Trini.** Muchas gracias por vuestra ayuda y amabilidad diaria. También a muchos otros trabajadores del Instituto de Neurociencias por hacer posible nuestro trabajo en este centro.

Llegar hasta aquí es fruto de un largo recorrido. Por eso, me gustaría no sólo agradecer a la gente que ha colaborado directamente en esta tesis, dentro del Instituto de Neurociencias, sino también a las personas que han participado indirectamente desde fuera facilitándome el equilibrio personal y la paz interior que me ha permitido disfrutarla.

A les meves amigues de Calldetenes **Anna, Laura, Ari, Sandra, Alba, Bruna, Cristina, Gina, Aina i Ivet**. Gràcies per ser-hi sempre malgrat la distància. Quan estic amb vosaltres em sento a casa. Agreixo el fet d'haver-nos cuidat mútuament durant tots aquests anys i que hagueu contribuït tant al meu creixement personal. Gràcies per la vostra amistat incondicional. A l'**Ariadna Vilarrasa,** sempre tant positiva i divertida. M'has motivat, ajudat i acompanyat en aquest trajecte. Espero tenir-te al meu costat sempre.

A la **Laura Llinàs**, mai has deixat que em rendeixi. Gràcies per haver compartit tants moments especials amb mi, tant de dia com de nit, al costat del mar. Els estius a la Costa Brava són teràpia i una font de renovació gràcies a tu. També et vull agrair les videotrucades i els missatges plens d'energia que m'has fet durant els moments més intensos d'aquesta recta final. Em coneixes molt bé i saps perfectament quines són les

paraules que necessito per fer un ''*reset*''. Espero que a partir d'ara, amb més temps lliure i vivint més a prop, puguem compartir molts més estius juntes a la costa.

Quiero dedicar un espacio especial en estos agradecimientos también a mis amigos del Erasmus: **Roge, Jesús, Laura M., Javi, Laura L.** e **Inés**. A pesar de estar cada uno en un rincón del mundo, siempre hemos conseguido mantener nuestro vínculo, organizando encuentros y escapadas para ponernos al día a lo largo de estos años. Hace ocho años me enseñasteis lo que significa tener una familia elegida, esa que no te viene dada, pero que cuidas porque te importa. Esa familia que, aunque pasen años sin verse, siempre está ahí. Agradezco cada consejo y cada momento de diversión que hemos compartido. Las conversaciones intensas, tanto sobre ciencia como sobre otros temas, han sido un verdadero chute de energía. Espero que, ahora que casi todos –o todos– hemos terminado nuestras respectivas tesis (¡por fin!), podamos vernos más a menudo.

A ti, **Fran**, mi apoyo incondicional. Has sido, sin duda, un pilar fundamental durante mi doctorado. Has estado presente en esta tesis desde el principio hasta el fin, siempre dispuesto a respaldarme, orientarme y aconsejarme cuando lo he necesitado. Qué suerte habernos conocido en el laboratorio y contar contigo; gracias a ti, cada paso ha sido un poco más fácil. Aunque no ha sido sencillo, has logrado que siempre te sienta cerca, incluso a pesar de los miles de kilómetros que nos han separado estos últimos años. Estoy inmensamente agradecida por toda tu entrega y cariño; sinceramente, sin ti, todo habría sido mucho más difícil. Te quiero.

Tot i que mai hauria arribat fins aquí si no fos per la meva estimada família. A tu, **mare**, gràcies per tots els sacrificis que has fet perquè jo pogués arribar fins aquí i aconseguir les meves metes, encara que això suposés estar lluny l'una de l'altra. Estic eternament agraïda per tot el que fas i has fet per mi cada dia, i et prometo treballar per fer-te sentir sempre orgullosa. El teu amor incondicional, suport, ajuda i comprensió han estat essencials per aconseguir-ho. Gràcies per haver creat un entorn segur al qual sempre he pogut tornar per trobar pau i calma. A les meves germanes, **Alba** i **Cristina**, el vostre suport durant aquesta etapa ha estat fonamental. Malgrat la distància, sempre us he tingut molt presents. Moltes gràcies per les infinites videotrucades, on les vostres paraules d'ànim i confiança m'han donat la força necessària per superar tots els obstacles que m'he anat trobant pel camí. També vull expressar el meu agraïment al meu **pare** per creure i confiar en mi, així com als meus **tiets** i **cosins** pel seu suport constant. Sense la vostra ajuda i empatia, res d'això hauria estat possible. Finalment,

amb molt d'afecte, recordo aquells qui ja no hi són; el vostre record és present en el meu cor i m'acompanya en cada pas. Moltes gràcies per ser-hi sempre i no deixar-me caure.

Para cerrar este capítulo tan importante, quiero hacer algo que rara vez hago: darme las gracias. Este año ha sido una montaña rusa, llena de retos que, en algún momento, parecían insuperables. Gracias por no dejarte vencer, por tomar las riendas de tu propio camino y por no conformarte cuando sabías que podías dar más. Gracias por apoyarte en quienes te rodean cuando sentías que sola no podrías, y por tener el coraje de pedir ayuda. Pero, sobre todo, gracias por la determinación de seguir adelante y por superar los desafíos de esta tesis, de los cuales has aprendido y crecido de maneras que ni imaginabas. Hoy, puedo decir que estoy realmente orgullosa de ti.

En resumen, este logro no es solo el resultado de mi esfuerzo personal, sino también del increíble apoyo de todas las personas que he mencionado anteriormente. Sin vuestro apoyo incondicional, no habría sido posible llegar hasta aquí. Aunque he intentado ser breve, es difícil expresar lo privilegiada y afortunada que me siento al contar con vuestro respaldo. La palabra "gracias" se queda corta para expresar lo que realmente siento. Cada uno de vosotros ha dejado una huella única en mí, y os quiero mucho.

**¡Gracias de corazón! <3**